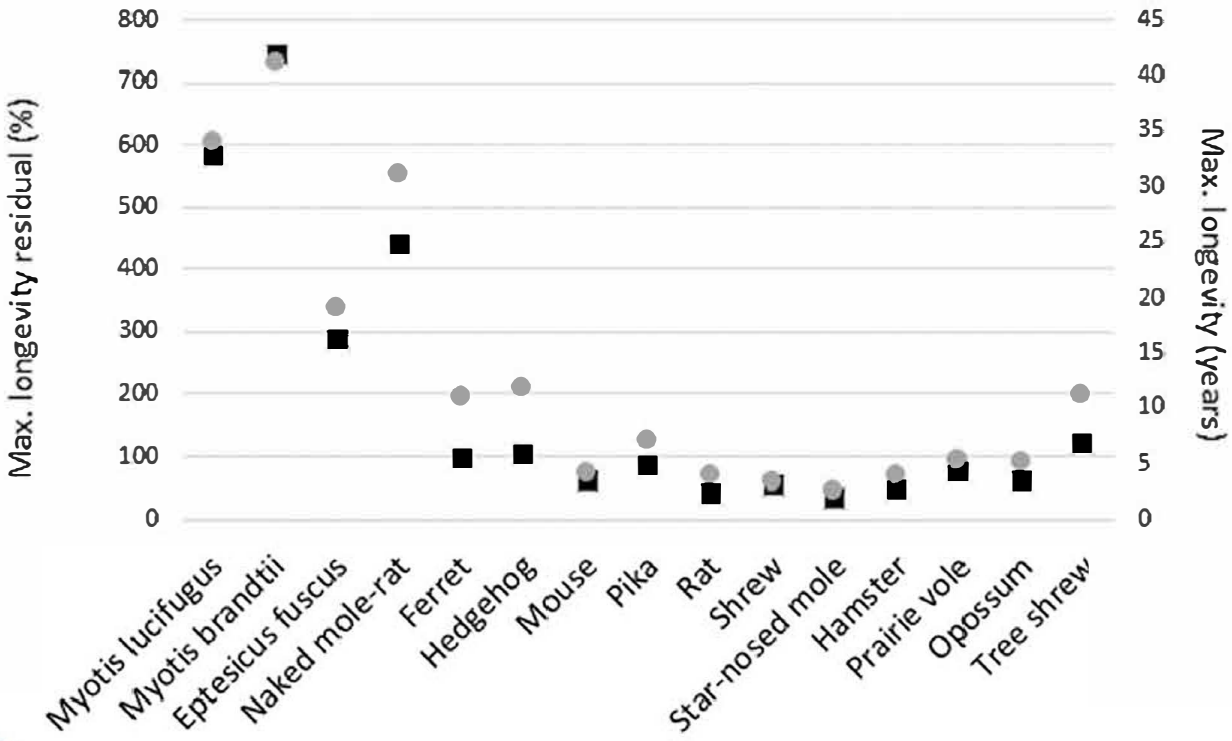

Special Collection on Tumor Suppressors

Small-bodied mammals that display exceptional longevity, see Lambert et al. - "Adaptive sequence convergence of the tumor suppressor ADAMTS9 between small-bodied mammals displaying exceptional longevity."

Tumor Suppressors

AGING

ONLINE ISSN: 1945-4589

AGING

www.aging-us.com

EDITORIAL BOARD

EDITORIAL BOARD

Table of Contents

Research Paper

Adaptive sequence convergence of the tumor suppressor ADAMTS9 between small-bodied mammals displaying exceptional longevity

Matthew J. Lambert[1] and Christine V. Portfors[1]

[1]School of Biological Sciences, Washington State University, Vancouver, WA 98686, USA

Correspondence to: Matthew J. Lambert; **email:** Matthew.Lambert@wsu.edu
Keywords: ADAMTS9; convergent evolution, longevity, naked mole-rat, microbats **doi:** 10.18632/aging.101180
Received: January 6, 2017 **Accepted:** February 11, 2017 **Published:** February 26, 2017

ABSTRACT

Maximum lifespan varies by two orders of magnitude across mammals. How such divergent lifespans have evolved remains an open question, with ramifications that may potentially lead to therapies for age-related diseases in humans. Several species of microbats as well as the naked mole-rat live much longer than expected given their small sizes, show reduced susceptibility to neoplasia, and largely remain healthy and reproductively capable throughout the majority of their extended lifespans. The convergent evolution of extreme longevity in these two groups allows for the opportunity to identify potentially important aging related genes that have undergone adaptive sequence convergence in these long-lived, yet small-bodied species. Here, we have tested 4,628 genes for evidence of convergence between the microbats and naked mole-rat. We find a strong signal of adaptive sequence convergence in the gene A disintegrin-like and metalloprotease with thrombospondin type 1 motifs 9 (ADAMTS9). We also provide evidence that the shared substitutions were driven by selection. Intriguingly, ADAMTS9 is a known inhibitor of the mTor pathway and has been implicated in several aging related processes.

INTRODUCTION

For several decades, it has been well recognized that there is strong correlation between lifespan and body mass [1,2], with larger species typically living longer than smaller species. There are, however, several species that violate this general rule, living much longer than expected given their small size and high metabolic rates. Of particular interest are the microbats, several species of which demonstrate longer maximum life-spans than any other mammals when controlling for body size [3]. In addition to their exceptional longevity, microbats appear to be resistant to neoplasia [4, 5] and remain healthy and reproductively capable throughout the majority of their lives [6].

Much like the microbats, *Heterocephalus glaber* (naked mole-rat) lives approximately three times longer than expected given its small size [7], is remarkably resistant to neoplasia [8-10] and displays no symptoms of aging well into its second decade [11].

Although once thought to be rare, there have been numerous recent studies demonstrating adaptive sequence convergence between a variety of species displaying convergent traits. These studies have highlighted genes that have been repeatedly targeted during the evolution of a given trait. For example, the evolution of echolocation in bats and toothed whales appears to be driven, in part, by common mutations in the genes *Prestin* [12, 13] and *Cdh23* [14, 15]; cardiac glycoside toxin resistance in numerous disparate vertebrates and invertebrates can be explained by identical amino acid substitutions in the enzyme Na+/K+-ATPase [16]; and the repeated convergent evolution of the sodium ion transporter NaV1.7 in hibernating mammals and mole-rats is believed to impart insensitivity to the accumulation of CO2 [17]. These studies, and many others, demonstrate that common selective pressures can drive common mutations in relevant genes.

The evolution of extreme longevity in microbats and the naked mole-rat is likely attributable to a lack of

extrinsic sources of mortality in these species. Bats, being nocturnal and capable of flight, generally contend with few predators. Likewise, the naked mole-rat lives in subterranean burrows where the risk of predation is low. Several theories of aging suggest that a lack of extrinsic sources of mortality will result in selection for longer lifespan [8, 18]. For example, according to the antagonistic pleiotropy (AP) theory of aging, a mutation can be beneficial during development, but have late-onset deleterious effects [19]. AP is expected to be more prevalent in species with high levels of extrinsic mortality since most individuals are unlikely to survive long after reaching sexual maturity, therefore there will be little pressure to select against the deleterious effects that manifest later in life. Also, the disposable soma theory of aging suggests that there exists a trade-off between growth/development and repair/maintenance [20]. In species that contend with many predators, it should be beneficial to allocate resources to grow and develop as quickly as possible rather than to invest in repair and maintenance since longevity is already unlikely. According to both theories, for species that contend with numerous extrinsic sources of mortality, the decline in fitness due to aging is minimal, so selection is inefficient at promoting mutations that increase longevity. However, for species that exist in relatively safe niches, like microbats and the naked mole-rat, the strength of selection to delay senescence will be much stronger, as individuals that live longer will have higher lifetime reproductive fitness. We hypothesize that the pressure to delay senescence shared by microbats and naked mole-rat may have led to convergent sequence evolution in key longevity promoting genes. The identification of genes that have undergone convergent evolution in these long-lived species would provide a better understanding of the genetics of longevity and could potentially identify therapeutic targets for cancer and other age-related illnesses.

Here we tested for adaptive convergent sequence evolution between microbats and the naked mole-rat in almost 5,000 genes conserved across a wide-range of mammals. We found that A disintegrin-like and metalloprotease with thrombospondin type 1 motifs 9 (ADAMTS9) displays numerous convergent substitutions between the long-lived species that were likely driven by positive selection.

RESULTS

The goal of this study was to determine if any genes display evidence of adaptive sequence convergence between long-lived microbats and the naked mole-rat. We tested for convergence in 4,628 1:1 ortholog groups between 3 microbat species (*Myotis lucifugus, Myotis brandtii* and *Eptesicus fuscus*), and the naked mole-rat. Additionally, as outgroup species, we included sequences from 11 small-bodied rodents and laurasiatherian mammals with at least acceptable longevity data curated in the AnAge database [21]. The relationship between the 15 species is shown in the phylogeny in Figure 1a. Importantly, none of these additional species demonstrate exceptional longevity (Fig. 1b). The requirement that sister species to microbats and naked mole-rat be small-bodied and not long-lived allowed us to control for body size and phylogeny while giving us the opportunity to test for convergence in the long-lived species as compared to normal aging species.

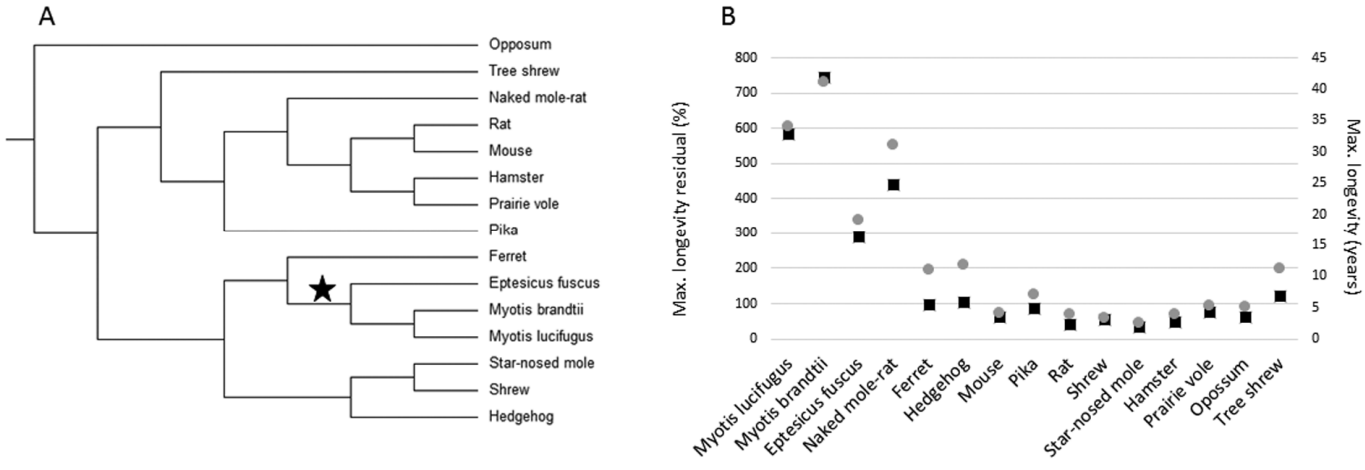

Figure 1. Small-bodied mammals that display exceptional longevity. (**A**) The accepted tree topology for the 15 species included in this study. (**B**) Maximum longevity residual (left axis, black boxes) and maximum longevity (right axis, grey circles) of the 15 species. Maximum longevity residual (tmax) is the percentage of the expected maximum longevity given adult body size (*M*), derived from the mammalian allometric equation: $tmax = 4.88M^{0.153}$ [30].

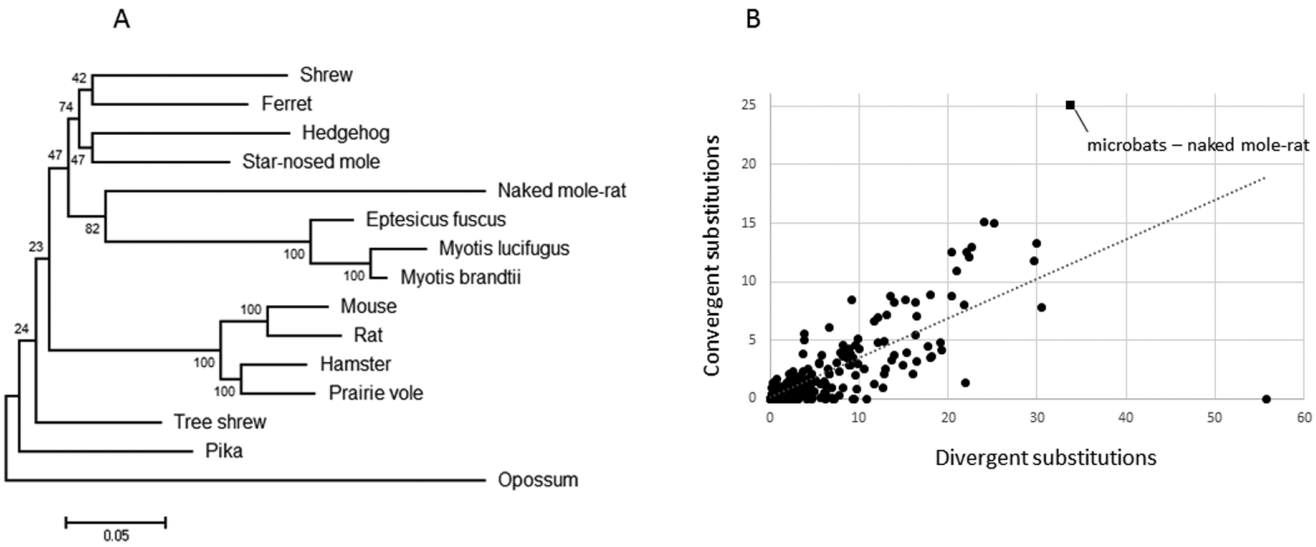

Figure 2. Evidence for ADAMTS9 sequence convergence in long-lived mammals. (**A**) Maximum-likelihood gene tree constructed using the best fitting nucleotide substitution model (GTR+G) demonstrates a monophyletic grouping of the long-lived mammals. (B) Plot of the numbers of divergent versus convergent substitutions occurring between all independent pairs of branches of the species tree. The microbat-naked mole-rat comparison has the highest level of convergence as well as the largest distance from the trendline.

Initially, we constructed maximum likelihood gene trees based on nucleotide alignments for each of the 4,628 ortholog groups. These trees were then parsed programmatically, searching for instances in which the long-lived mammals (naked mole-rat, *Myotis davidii*, *Myotis lucifugus* and *Eptesicus fuscus*) formed a monophyletic group, to the exclusion of their true closest relatives (rodents and carnivores/insectivores for the naked mole-rat and microbats, respectively). We found that only one gene, ADAMTS9, violated the known species tree in such a manner (Fig. 2a), suggesting sequence convergence between the naked mole-rat and microbats occurred during the evolution of this gene. To determine which sites were responsible for the observed grouping of the long-lived species, we used a maximum likelihood approach to reconstruct all ancestral amino acid sequences at interior nodes of the accepted phylogeny. These ancestral sequences were used to map and count all pairwise convergent substitutions (mutations from the ancestral state that lead to identical amino acids) shared between the microbats and naked mole-rat. Although, the microbats and naked mole-rat share 21 convergent substitutions in this gene (Table 1), which is far more than any other instance of sequence convergence described to date, it may be possible that this represents a normal level of background convergence if for example ADAMTS9 is rapidly evolving. However, Castoe et al. [22] developed a method to generate an empirical null distribution for the expected level of convergence for a given gene, provided a sufficient number of taxa are included. Briefly, the number of divergent (mutations that lead to different amino acids at homologous sites in the species being compared) and convergent substitutions are estimated for every pair of branches in a phylogeny. It has previously been demonstrated that the number of divergent substitutions reliably predict the number of convergent substitutions, therefore excess convergence between any two branches would appear as an outlier with a higher convergent to divergent substitution ratio than all other pairwise comparisons between branches [22]. This method allowed us to distinguish between rapid evolution and potential adaptive convergence. To test this, we used the program Grand-conv [23, 24], which estimates the posterior numbers of convergent and divergent substitutions shared between all pairs of branches in the given phylogeny. We found that the convergence between the naked mole-rat and microbats exceeded expectations given the phylogeny (Fig. 2b), again suggesting sequence convergence between the long-lived species. In addition, using the methods of Zhang and Kumar [25], we found that the level of convergence between microbats and naked mole-rat exceeds random expectations ($p < .001$), indicating a significant amount of convergence.

Table 1. ADAMTS9 convergent sites. The numbers at the top of each column indicate the amino acid position in the alignment.

	54	236	244	324	362	512	558	565	775	838	884	890	1110	1314	1319	1489	1497	1597	1675	1765	1933
Naked mole-rat	V	R	R	V	P	S	D	Q	A	K	V	R	Q	R	R	R	E	R	A	S	T
Eptesicus fuscus	V	R	R	V	P	S	D	Q	A	K	V	R	Q	R	R	R	E	R	A	S	T
Myotis brandtii	V	R	R	V	P	S	D	Q	A	K	V	R	Q	R	R	-	-	R	A	S	T
Myotis lucifugus	V	V	Q	V	P	S	D	Q	A	K	V	R	Q	R	R	R	E	R	A	S	T
Rat	I	K	K	I	S	P	-	-	T	S	I	R	E	Q	T	K	D	Q	T	N	L
Mouse	I	K	K	I	Y	P	H	R	T	S	I	K	E	Q	T	K	D	Q	T	N	K
Prairie vole	I	K	K	I	S	P	H	R	T	S	I	K	E	Q	T	K	D	Q	T	N	K
Hamster	I	K	K	I	S	P	H	R	T	N	I	K	E	Q	R	K	D	Q	T	N	K
Star-nosed mole	I	K	K	I	S	S	P	R	T	N	V	K	E	Q	S	K	D	K	T	K	K
Shrew	-	K	K	I	S	X	L	R	T	N	V	K	E	Q	S	X	X	K	T	L	K
Ferret	I	K	K	I	S	P	-	R	T	N	I	K	E	Q	S	K	D	K	T	E	K
Tree shrew	V	K	K	I	X	P	X	X	T	X	-	K	E	Q	S	K	E	K	X	X	K
Hedgehog	-	S	K	I	S	Y	H	R	X	N	V	K	E	Q	D	K	D	K	T	N	K
Opossum	-	K	R	V	A	P	H	R	T	N	I	S	A	R	R	K	D	K	T	K	K
Pika	I	S	K	V	S	P	H	R	T	N	I	K	E	Q	M	K	D	K	A	Q	K

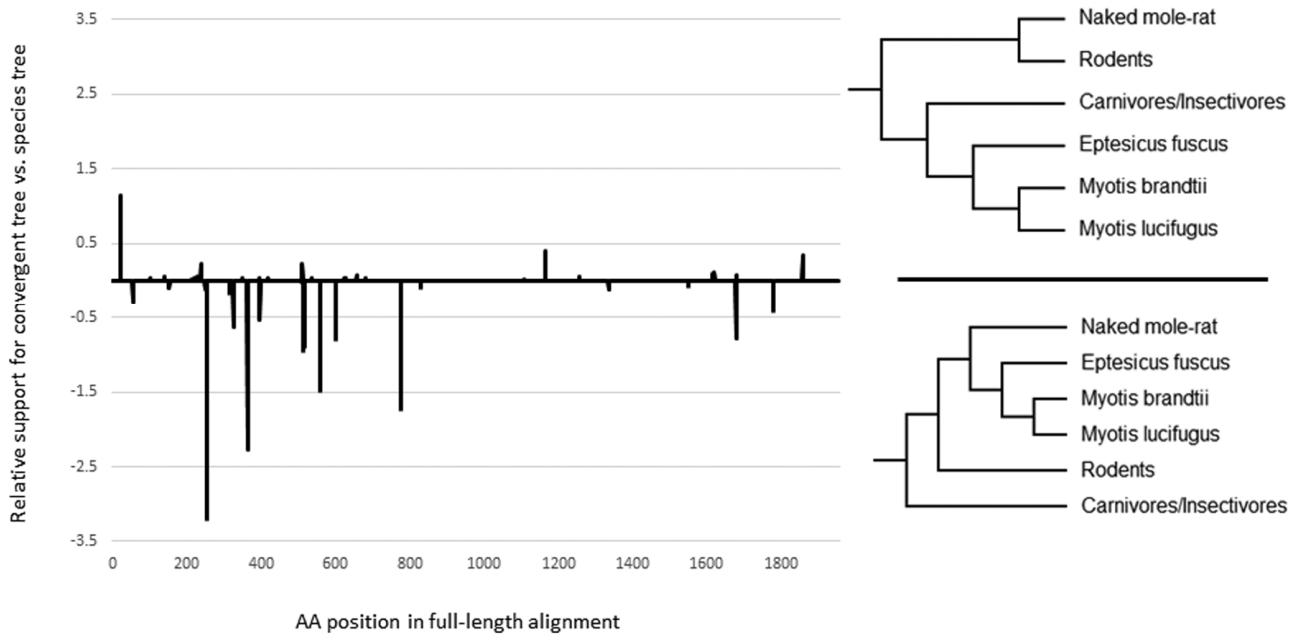

Figure 3. The relationship between sequence convergence and positive selection. Relative support for convergent tree and species tree topologies for all positively selected sites along the *ADAMTS9* gene sequence. The values are the difference between site-wise log likelihood scores for the species tree and the convergent tree. Negative values indicate more support for the convergent tree.

Notably, the addition of the moderately long-lived rodent, Cavia porcellus (guinea pig), and megabats, Pteropus alecto and Pteropus vampyrus, disrupted the monophyletic grouping of the naked mole-rat and microbats in maximum-likelihood gene trees based on amino acid alignments (Not shown). However, even with the inclusion of these moderately long-lived mammals we still found that the naked mole-rat and microbats share

16 convergent substitutions (Supplemental Table 1), which remains significant using the method of Zhang and Kumar [25]. Furthermore, estimates of posterior numbers of divergent versus convergent changes still suggest sequence convergence between the naked mole-rat and microbats even when the megabats and guinea pig were included (Supplemental Fig. 1).

Lastly, to test if the observed sequence convergence may be due to positive selection, we employed a unique multistep approach. First, all sites with significant evidence for positive selection along the ancestral microbat branch (indicated by a star in Fig. 1a) were identified with the program TreeSAAP [26], producing a list of 77 sites. These 77 sites were then extracted from the original alignment and used to create a new alignment that consisted only of the sites with evidence of positive selection in microbats. Next, we calculated site-wise log-likelihood values for the convergent gene tree (Fig. 2a) and compared these to site-wise log likelihood values for the accepted species tree (Fig. 1a), using the positively selected sites alignment. If the observed convergence was due to chance, we would expect the positively selected sites to support the accepted species topology. However, we found that the opposite is true, the sites with evidence of positive selection strongly favored the convergent topology (Fig. 3). Indeed, an approximately unbiased test suggests that the convergent tree was much more likely than the accepted species tree ($P = .886$ and $P = .114$, respectively), suggesting that the convergence between the long-lived species was driven by selection.

DISCUSSION

We tested 4,628 genes for evidence of adaptive sequence convergence between long-lived, small-bodied mammals. We found evidence for an enrichment of convergent substitutions between the microbats and the naked mole-rat in the gene ADAMTS9. ADAMTS9 is the most widely conserved member of the ADAMTS family and has recently been reported to be a novel tumor suppressor that is downregulated in several varieties of human cancer [27]. Intriguingly, ADAMTS9 inhibits tumor growth by blocking the mTOR pathway [28], which has long been known to be associated with aging [29]. In addition to its role in tumor suppression, ADAMTS9 has also been implicated in several age-related conditions including arthritis [30], type 2 diabetes [31, 32], age-related macular degeneration [33, 34] and menopause [35]. Furthermore, in C. elegans the loss of GON-1, the roundworm homolog of ADAMTS9, alters lifespan and promotes dauer formation [36]. These effects are likely due to modified insulin and insulin-like ortholog secretion and altered insulin/IGF-1 signaling, which is also known to contribute to aging [37].

Although, it may be possible that the observed convergent changes shared by microbats and the naked mole-rat may be the product of some non-adaptive force rather than selection for increased longevity, several lines of evidence suggest otherwise. First, the convergent substitutions are distributed along the length of the coding sequence, eliminating gene conversion or alternate exon usage as possible causes. Second, the convergent topology was strongly favored when only sites with evidence of positive selection occurring on the long-lived microbat branch were considered, suggesting that the convergence was indeed driven by selection. Finally, ADAMTS9 has previously been implicated in several aging processes and age-related diseases [27, 30-37], supporting the hypothesis that modulation of ADAMTS9 function alters lifespan. Together, this evidence suggests that ADAMTS9 has been repeatedly targeted by selection for increased longevity in microbats and the naked mole-rat.

As yet, we can provide no explanation for how the convergent evolution of ADAMTS9 has promoted longevity in microbats and the naked mole-rat. However, it is rather intriguing that ADAMTS9 is a known inhibitor of the mTor pathway. The hyperfunction theory of aging posits that aging is due to the prolonged activity of growth-promoting pathways, such as mTor [38]. According to this theory, aging itself is not a program, but rather aging is a harmful continuation of developmental programs after growth has ended [39]. This hypothesis is supported by several lines of evidence that have identified mTor activity as a driver of senescence [29, 40-43]. Therefore, it is a distinct possibility that the convergent evolution of ADAMTS9 in long-lived species may have altered this gene's function such that it now serves to slow the effects of mTor, preventing the declines normally associated with aging. Indeed, the author of the hyperfunction theory has recently speculated that the extraordinary longevity of microbats and the naked mole-rat may be due to selection for a "decelerator of mTor" [44].

Given the role of ADAMTS9 in such a wide range of age-related conditions, its direct effect on lifespan in C. elegans and its ability to modulate mTOR and insulin/IGF-1 signaling, it is likely that the convergent evolution of ADAMTS9 may be, in part, responsible for the exceptional longevity and resistance to neoplasia found in microbats and the naked mole-rat.

MATERIALS AND METHODS

Ensembl Compara [45] was used to identify all 1:1 orthologs from the species Myotis lucifugus, Pteropus vampyrus, Erinaceus Europaeus, Mustela putorius, Sorex araneus, Mus musculus, Rattus norvegicus, Ochotona princeps, Cavia porcellus and Monodelphis domesticus. This generated a list of 5109 1:1 ortholog groups from these species. Amino acid and coding sequences for the species listed above were downloaded from Ensembl version 84. For the species Myotis brandtii, Eptesicus fuscus, Miniopterus natalensis, Pteropus alecto, Condylura cristata, Mesocricetus auratus, Microtus ochrogaster and Heterocephalus glaber, orthologs were identified with a recriprocal best hit approach. For example, the naked mole-rat orthologs were identified by first using blastp to align the 5,109 Cavia porcellus protein sequences from Ensembl against all naked mole-rat refSeq sequences. The top naked mole-rat hits were then aligned against all Cavia porcellus protein sequences from Ensembl. All instances in which the reciprocal blast alignments identified the same sequences were included for further study, all others were discarded. This reduced the number of 1:1 ortholog groups to 4,978.

Amino acid sequences for each of the 4,978 1:1 ortholog groups were aligned with Muscle [46]. TrimAl [47] was used to filter alignments with mean percentage identity below 60%. This left 4,628 high quality multiple sequence alignments. Pal2Nal [48] was then used to create codon oriented nucleotide alignments for the 4,628 ortholog groups. We then constructed Maximum-likelihood gene trees in PhyML 3.0 [49] using the best fitting nucleotide substitution model for each gene as indicated by jModelTest 2 [50]. A custom perl script was used to analyze the resulting Newick files, searching for monophyletic groupings of the long-lived species.

PAML, specifically the program CodeML, [51] was used to reconstruct ancestral amino acid sequences at all interior nodes of the species tree for ADAMTS9. We then used custom Perl scripts to map and count all convergent substitutions occurring between the naked mole-rat and microbat branches. Since detection of convergent and divergent substitutions is critically dependent upon alignment quality we used PRANK [52], a phylogeny aware alignment tool, to generate a second ADAMTS9 multiple sequence alignment. Differences between the Muscle and PRANK alignments were minimal and both recovered the same 21 convergent substitutions between microbats and naked mole-rat.

Both the Muscle and PRANK ADAMTS9 amino acid multiple sequence alignments, the accepted tree topology and the program Grand-conv were used to estimate the posterior numbers of convergent and divergent substitutions. The two alignments produced identical results. To determine which sites were subject to positive selection along the microbat lineage we used the program TreeSAAP. The ADAMTS9 nucleotide multiple sequence alignment and the accepted species tree were used as input. We only considered radical substitutions (categories 6-8) with Z-scores greater than 3.09. PhyML was used to calculate site-wise log likelihood values for both the convergent tree and a constrained species tree using a multiple sequence alignment containing only sites with evidence of positive selection as indicated by TreeSAAP. An approximately unbiased test comparing the likeliness of the convergent and species trees was conducted in Consel [53].

AUTHOR CONTRIBUTIONS

MJL and CVP conceived of the study. MJL performed all analyses. MJL and CVP wrote the manuscript.

CONFLICTS OF INTEREST

The authors declare that there are no conflicts of interest.

FUNDING

Funding provided by Washington State University from the Herbert L. Eastlick Distinguished Professorship to CVP.

REFERENCES

1. Promislow DE. On size and survival: progress and pitfalls in the allometry of life span. J Gerontol. 1993; 48:B115–23. doi: 10.1093/geronj/48.4.B115

2. de Magalhães JP, Costa J, Church GM. An analysis of the relationship between metabolism, developmental schedules, and longevity using phylogenetic independent contrasts. J Gerontol A Biol Sci Med Sci. 2007; 62:149–60. doi: 10.1093/gerona/62.2.149

3. Podlutsky AJ, Khritankov AM, Ovodov ND, Austad SN. A new field record for bat longevity. J Gerontol A Biol Sci Med Sci. 2005; 60:1366–68. doi: 10.1093/gerona/60.11.1366

4. Buckles EL. Chiroptera (bats). In: Fowler ME, Miller RE (eds.). Zoo and wildlife medicine, Volume 8. St. Louis (MO): Elsevier; 2014. p. 285–286.

5. Chu P, Shuo Y, Wang F, Jeng C, Pang V, Chang P, Chin S, Liu C. Spontaneous neoplasms in zoo mammals, birds, and reptiles in Taiwan—a 10 year survey. Anim

Biol. 2012; 62:95–110.
doi: 10.1163/157075611X616941

6. Brunet-Rossinni A, Wilkinson G. Methods for age estimation and the study of senescence in bats. T. Kunz, S. Parsons (Eds.), Ecological and Behavioral Methods for the Study of Bats, The Johns Hopkins University Press, Baltimore, MD, USA. 2009; pp. 315–325.

7. Buffenstein R, Jarvis JU. The naked mole rat--a new record for the oldest living rodent. Sci SAGE KE. 2002; 2002:pe7. doi: 10.1126/sageke.2002.21.pe7

8. Buffenstein R. The naked mole-rat: a new long-living model for human aging research. J Gerontol A Biol Sci Med Sci. 2005; 60:1369–77.
doi: 10.1093/gerona/60.11.1369

9. Liang S, Mele J, Wu Y, Buffenstein R, Hornsby PJ. Resistance to experimental tumorigenesis in cells of a long-lived mammal, the naked mole-rat (Heterocephalus glaber). Aging Cell. 2010; 9:626–35. doi: 10.1111/j.1474-9726.2010.00588.x

10. Delaney MA, Nagy L, Kinsel MJ, Treuting PM. Spontaneous histologic lesions of the adult naked mole rat (Heterocephalus glaber): a retrospective survey of lesions in a zoo population. Vet Pathol. 2013; 50:607–21. doi: 10.1177/0300985812471543

11. Edrey YH, Hanes M, Pinto M, Mele J, Buffenstein R. Successful aging and sustained good health in the naked mole rat: a long-lived mammalian model for biogerontology and biomedical research. ILAR J. 2011; 52:41–53. doi: 10.1093/ilar.52.1.41

12. Liu Y, Cotton JA, Shen B, Han X, Rossiter SJ, Zhang S. Convergent sequence evolution between echolocating bats and dolphins. Curr Biol. 2010; 20:R53–54. doi: 10.1016/j.cub.2009.11.058

13. Liu Z, Qi FY, Zhou X, Ren HQ, Shi P. Parallel sites implicate functional convergence of the hearing gene prestin among echolocating mammals. Mol Biol Evol. 2014; 31:2415–24. doi: 10.1093/molbev/msu194

14. Shen YY, Liang L, Li GS, Murphy RW, Zhang YP. Parallel evolution of auditory genes for echolocation in bats and toothed whales. PLoS Genet. 2012; 8:e1002788. doi: 10.1371/journal.pgen.1002788

15. Lambert M, Nevue A, Portfors C. Contrasting patterns of adaptive sequence convergence among echolocating mammals. Gene. 2017; 605:1-4. doi: 10.1016/j.gene.2016.12.017.

16. Ujvari B, Casewell NR, Sunagar K, Arbuckle K, Wüster W, Lo N, O'Meally D, Beckmann C, King GF, Deplazes E, Madsen T. Widespread convergence in toxin resistance by predictable molecular evolution. Proc Natl Acad Sci USA. 2015; 112:11911–16.
doi: 10.1073/pnas.1511706112

17. Liu Z, Wang W, Zhang TZ, Li GH, He K, Huang JF, Jiang XL, Murphy RW, Shi P. Repeated functional convergent effects of NaV1.7 on acid insensitivity in hibernating mammals. Proc Biol Sci. 2013; 281:20132950. doi: 10.1098/rspb.2013.2950

18. Ricklefs RE. Evolutionary theories of aging: confirmation of a fundamental prediction, with implications for the genetic basis and evolution of life span. Am Nat. 1998; 152:24–44. doi: 10.1086/286147

19. Williams GC. Pleiotropy, natural selection and the evolution of senescence. Evolution. 1957; 11:398–411. doi: 10.2307/2406060

20. Kirkwood TB. Evolution of ageing. Nature. 1977; 270:301–04. doi: 10.1038/270301a0

21. Tacutu R, Craig T, Budovsky A, Wuttke D, Lehmann G, Taranukha D, Costa J, Fraifeld VE, de Magalhães JP. Human Ageing Genomic Resources: integrated databases and tools for the biology and genetics of ageing. Nucleic Acids Res. 2013; 41:D1027–33. doi: 10.1093/nar/gks1155

22. Castoe TA, de Koning AP, Kim HM, Gu W, Noonan BP, Naylor G, Jiang ZJ, Parkinson CL, Pollock DD. Evidence for an ancient adaptive episode of convergent molecular evolution. Proc Natl Acad Sci USA. 2009; 106:8986–91. doi: 10.1073/pnas.0900233106

23. Qian C, de Koning AP. Rapid Discovery of Convergent Molecular Evolution Across Entire Phylogenies. 2015. University of Calgary. http://lab.jasondk.io.

24. Qian C, Bryans N, Kruykov I, de Koning AP. Visualization and analysis of statistical signatures of convergent molecular evolution. 2015. University of Calgary. http://lab.jasondk.io.

25. Zhang J, Kumar S. Detection of convergent and parallel evolution at the amino acid sequence level. Mol Biol Evol. 1997; 14:527–36.
doi: 10.1093/oxfordjournals.molbev.a025789

26. Woolley S, Johnson J, Smith MJ, Crandall KA, McClellan DA. TreeSAAP: selection on amino acid properties using phylogenetic trees. Bioinformatics. 2003; 19:671–72. doi: 10.1093/bioinformatics/btg043

27. Peng L, Yang Z, Tan C, Ren G, Chen J. Epigenetic inactivation of ADAMTS9 via promoter methylation in multiple myeloma. Mol Med Rep. 2013; 7:1055–61.

28. Du W, Wang S, Zhou Q, Li X, Chu J, Chang Z, Tao Q, Ng EK, Fang J, Sung JJ, Yu J. ADAMTS9 is a functional tumor suppressor through inhibiting AKT/mTOR pathway and associated with poor survival in gastric cancer. Oncogene. 2013; 32:3319–28. doi: 10.1038/onc.2012.359

29. Vellai T, Takacs-Vellai K, Zhang Y, Kovacs AL, Orosz L, Müller F. Genetics: influence of TOR kinase on lifespan in C. elegans. Nature. 2003; 426:620. doi: 10.1038/426620a

30. Yaykasli KO, Hatipoglu OF, Yaykasli E, Yildirim K, Kaya E, Ozsahin M, Uslu M, Gunduz E. Leptin induces ADAMTS-4, ADAMTS-5, and ADAMTS-9 genes expression by mitogen-activated protein kinases and NF-κB signaling pathways in human chondrocytes. Cell Biol Int. 2015; 39:104–12. doi: 10.1002/cbin.10336

31. Keaton JM, Cooke Bailey JN, Palmer ND, Freedman BI, Langefeld CD, Ng MC, Bowden DW. A comparison of type 2 diabetes risk allele load between African Americans and European Americans. Hum Genet. 2014; 133:1487–95. doi: 10.1007/s00439-014-1486-5

32. Kong X, Zhang X, Xing X, Zhang B, Hong J, Yang W. The Association of Type 2 Diabetes Loci Identified in Genome-Wide Association Studies with Metabolic Syndrome and Its Components in a Chinese Population with Type 2 Diabetes. PLoS One. 2015; 10:e0143607. doi: 10.1371/journal.pone.0143607

33. Whitmore SS, Braun TA, Skeie JM, Haas CM, Sohn EH, Stone EM, Scheetz TE, Mullins RF. Altered gene expression in dry age-related macular degeneration suggests early loss of choroidal endothelial cells. Mol Vis. 2013; 19:2274–97.

34. Helisalmi S, Immonen I, Losonczy G, Resch MD, Benedek S, Balogh I, Papp A, Berta A, Uusitupa M, Hiltunen M, Kaarniranta K. ADAMTS9 locus associates with increased risk of wet AMD. Acta Ophthalmol. 2014; 92:e410. doi: 10.1111/aos.12341

35. Pyun JA, Kim S, Cho NH, Koh I, Lee JY, Shin C, Kwack K. Genome-wide association studies and epistasis analyses of candidate genes related to age at menarche and age at natural menopause in a Korean population. Menopause. 2014; 21:522–29. doi: 10.1097/GME.0b013e3182a433f7

36. Yoshina S, Mitani S. Loss of C. elegans GON-1, an ADAMTS9 Homolog, Decreases Secretion Resulting in Altered Lifespan and Dauer Formation. PLoS One. 2015; 10:e0133966. doi: 10.1371/journal.pone.0133966

37. Tatar M, Bartke A, Antebi A. The endocrine regulation of aging by insulin-like signals. Science. 2003; 299:1346–51. doi: 10.1126/science.1081447

38. Blagosklonny MV. Answering the ultimate question "what is the proximal cause of aging?". Aging (Albany NY). 2012; 4:861–77. doi: 10.18632/aging.100525

39. Blagosklonny MV. Aging is not programmed: genetic pseudo-program is a shadow of developmental growth. Cell Cycle. 2013; 12:3736–42. doi: 10.4161/cc.27188

40. Demidenko ZN, Blagosklonny MV. Growth stimulation leads to cellular senescence when the cell cycle is blocked. Cell Cycle. 2008; 7:3355–61. doi: 10.4161/cc.7.21.6919

41. Demidenko ZN, Zubova SG, Bukreeva EI, Pospelov VA, Pospelova TV, Blagosklonny MV. Rapamycin decelerates cellular senescence. Cell Cycle. 2009; 8:1888–95. doi: 10.4161/cc.8.12.8606

42. Demidenko ZN, Shtutman M, Blagosklonny MV. Pharmacologic inhibition of MEK and PI-3K converges on the mTOR/S6 pathway to decelerate cellular senescence. Cell Cycle. 2009; 8:1896–900. doi: 10.4161/cc.8.12.8809

43. Wesierska-Gadek J. mTOR and its link to the picture of Dorian Gray - re-activation of mTOR promotes aging. Aging (Albany NY). 2010; 2:892–93. doi: 10.18632/aging.100240

44. Blagosklonny MV. Big mice die young but large animals live longer. Aging (Albany NY). 2013; 5:227–33. doi: 10.18632/aging.100551

45. Vilella AJ, Severin J, Ureta-Vidal A, Heng L, Durbin R, Birney E. EnsemblCompara GeneTrees: Complete, duplication-aware phylogenetic trees in vertebrates. Genome Res. 2009; 19:327–35. doi: 10.1101/gr.073585.107

46. Edgar RC. MUSCLE: multiple sequence alignment with high accuracy and high throughput. Nucleic Acids Res. 2004; 32:1792–97. doi: 10.1093/nar/gkh340

47. Capella-Gutiérrez S, Silla-Martínez JM, Gabaldón T. trimAl: a tool for automated alignment trimming in large-scale phylogenetic analyses. Bioinformatics. 2009; 25:1972–73. doi: 10.1093/bioinformatics/btp348

48. Suyama M, Torrents D, Bork P. PAL2NAL: robust conversion of protein sequence alignments into the corresponding codon alignments. Nucleic Acids Res. 2006; 34:W609-12. doi: 10.1093/nar/gkl315

49. Guindon S, Dufayard JF, Lefort V, Anisimova M, Hordijk W, Gascuel O. New algorithms and methods to estimate maximum-likelihood phylogenies: assessing the performance of PhyML 3.0. Syst Biol. 2010; 59:307–21. doi: 10.1093/sysbio/syq010

50. Darriba D, Taboada GL, Doallo R, Posada D. jModelTest 2: more models, new heuristics and parallel computing. Nat Methods. 2012; 9:772. doi: 10.1038/nmeth.2109

51. Yang Z. PAML 4: phylogenetic analysis by maximum likelihood. Mol Biol Evol. 2007; 24:1586–91. doi: 10.1093/molbev/msm088

52. Löytynoja A. Phylogeny-aware alignment with PRANK. Methods Mol Biol. 2014; 1079:155–70. doi: 10.1007/978-1-62703-646-7_10

53. Shimodaira H, Hasegawa M. CONSEL: for assessing the confidence of phylogenetic tree selection. Bioinformatics. 2001; 17:1246–47. doi: 10.1093/bioinformatics/17.12.1246

SUPPLEMENTARY MATERIAL

Supplemental Table 1. ADAMTS9 convergent sites. The numbers at the top of each column indicate the amino acid position in the alignment.

	54	236	244	362	512	775	838	890	1110	1342	1489	1497	1597	1675	1765	1933
Naked mole-rat	V	R	R	P	S	A	K	R	Q	G	R	E	R	A	S	T
Eptesicus fuscus	V	R	R	P	S	A	K	R	Q	G	R	E	R	A	S	T
Myotis brandtii	V	R	R	P	S	A	K	R	Q	G	-	-	R	A	S	T
Myotis lucifugus	V	V	Q	P	S	A	K	R	Q	G	R	E	R	A	S	T
Pteropus vampyrus	I	K	K	S	P	T	N	K	E	S	K	D	K	T	N	K
Pteropus alecto	I	K	K	S	P	T	N	K	E	S	K	D	K	T	N	K
Guinea pig	Q	D	F	L	P	T	N	K	E	S	K	D	Q	T	N	K
Mouse	I	K	K	Y	P	T	S	K	E	S	K	D	Q	T	N	K
Rat	I	K	K	S	P	T	S	R	E	S	K	D	Q	T	N	L
Hamster	I	K	K	S	P	T	N	K	E	S	K	D	Q	T	N	K
Prairie vole	I	K	K	S	P	T	S	K	E	S	K	D	Q	T	N	K
Pika	I	S	K	S	P	T	N	K	E	G	K	D	K	A	Q	K
Shrew	-	K	K	S	X	T	N	K	E	N	X	X	K	T	L	K
Ferret	I	K	K	S	P	T	N	K	E	G	K	D	K	T	E	K
Tree shrew	V	K	K	X	P	T	X	K	E	S	K	E	K	X	X	K
Hedgehog	-	S	K	S	Y	X	N	K	E	S	K	D	K	T	N	K
Star-nosed mole	I	K	K	S	S	T	N	K	E	N	K	D	K	T	K	K
Opossum	-	K	R	A	P	T	N	S	A	N	K	D	K	T	K	K

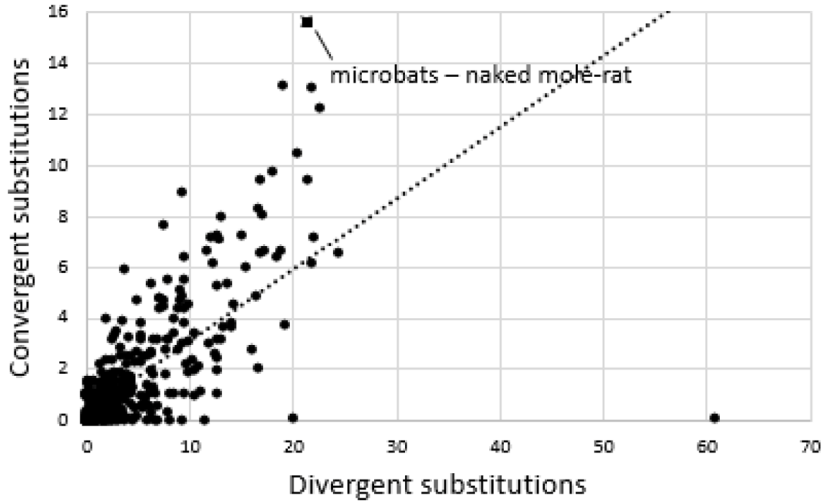

Supplemental Figure 1. Evidence for ADAMTS9 sequence convergence in long-lived mammals. Plot of the numbers of divergent versus convergent substitutions occurring between all independent pairs of branches of the species tree.

Mir 145/143: tumor suppressor, oncogenic microenvironmental factor or …both?

Mario Cioce, Sabrina Strano, Paola Muti, and Giovanni Blandino doi: 10.18632/aging.100965

An interesting debate is emerging from the recent literature regarding the role of mir-143/145 in tumor initiation/progression. Herein, we aim to contribute our experience and observations to this ongoing debate. We will start from the experimental data presented in the outstanding work of the Tyler Jacks lab, by Dimitrova, Gocheva and colleagues [6]. They show, in a kRAS/p53 murine model of lung adenocarcinoma, that the contribution of the microRNA 143/145 cluster to lung cancer development is non-cell autonomous with the expression of mir143/145 from the tumor micro-environment resulting protumorigenic. More specifically, higher expression of microRNA 143/145 by endothelial cells would be pivotal in tumor progression by favoring tumor angiogenesis in a lung tissue specific fashion. The authors conclude, and their conclusion is shared by Almeida and Calin in a commentary on Genome Biology [1], that mir-143/145 is a non-cell autonomous oncogenic factor rather than a tumor suppressor, with their speculation further supported by the absence of tumor development in mice devoid of such microRNAs and by their lack of expression in murine epithelial cell lines [6]. This is in apparent contrast to what was published by our group and by many others, who provided evidence for the roles that mir-143/145 play as tumor suppressors in human tumors of epithelial origin, including and not limited to cervical, colon, gastric, breast and pancreatic carcinomas, NSCLC and malignant pleural mesothelioma (reviewed in Das and Pillai, 2015) [5].

In their commentary, Almeida and Calin claim that the "heterogeneity" of the human tumors collected for the human studies has prevented to provide a precise definition of the mir143/145 role. They basically substantiate such observation with the possibility that, in unfractionated human tumor tissues, residual expression of mir-143/145 by stromal component may escape the analysis of unfractionated human tumors. Even though this is certainly possible, we will try to provide a "parallel" and not mutually exclusive vision to integrate the ongoing discussion, starting from the work by Dimitrova et al. [6].

First, the data supporting a non-cell autonomous oncogenic role for the mir143/145 derive from a murine system. Dimitrova and coworkers employed an excellent albeit limited experimental system. In fact, while mice were engineered to express/not express specific tumor suppressors or oncogenes, represent an invaluable tool to study tumor progression, however there is little doubt left that such a system may reflect, at its best, one or few subtypes of its human counterparts of which it may recapitulate a gross history. Second, the mentioned data stem from the use of transgenic mice ($Kras^{G12D/+,}$ $p53^{-/-}$). Such a model basically represents a "frozen status", again, corresponding only to a specific subset of the modeled tumors and "addicted" to the absence or expression of specific molecular lesions. Thus, engineered mice may not adequately represent the interpatient heterogeneity of human lung tumors. From this perspective, heterogeneity, more than representing an "Achille's Heel" of the mir-143/145 studies in human tumors, may represent an added welcome level of complexity toward understanding the "real life" modulation of such a miRNA locus. Third, by manipulating the levels of microRNA 143/145 into MEFs (Mouse Embryo Fibroblasts), Dimitrova and coworkers conclude that no tumor suppressor activity can be ascribed to the microRNA 143/145 in such cells. Now, it is pleonastic to note that MEFs represent a totally different experimental system from the human epithelial tumors, in terms of embryonal origin and histotype. Thus, it is far from appropriate to draw conclusions regarding functions of the microRNA143/145 locus in human epithelial tumors from experiments performed by inducing deletion of the microRNAs into murine cells of non–epithelial origin. Fourth, and here we come to addressing the system we and many others have employed recently, where matched human specimens have been used. In all the cases, deep downregulation of the miRNA-143-145 expression as compared to normal matched tissues was observed. This occurred in extremely different tumors in terms of history, tissue of origin, and aggressiveness. In fact, both miR-143 and miR-145 were broadly described as downregulated in a plethora of solid tumors, including and not limited to breast, lung, colon (n=43 matched tissues), prostate, the gastrointestinal system, ovary, cervix, head and neck, bladder, thyroid, pituitary and gonads, germ-cell tumors (GCTs), gallbladder cancer, renal cell carcinoma,

osteosarcoma, and neuroblastoma, mesothelioma (reviewed in Das and Pillai, 2015) [5] and thymic epithelial tumors [9]. Notably in most of the work mentioned, matched normal vs tumor samples were analyzed and, despite the fact that the analyzed tumors were very different in terms of history, tissue of origin, aggressiveness, mir143/145 levels, were invariably lower in the transformed tissues.

Rather convincing evidence supporting the tumor suppressor role of mir-143/145 in human malignancies comes from data showing that the downregulation of mir-143/145 is dynamic and correlates with the history of the disease. For example, Slaby et al. showed that downregulation of mir-145 was deeper in relapsing ccRCC as compared to the primary tumor, and, even deeper, in their metastatic counterparts [16]. Along the same line, reduced expression of mir-145 strongly correlated with shorter disease-free survival in prostate and small cell carcinoma of the cervix [2, 10]. Interestingly, by using in situ hybridization of >100 formalin fixed matched breast cancer specimens, Sempere and coworkers found that mir-145 was strongly downregulated in breast tumor tissues with its expression higher in the vessels and myoepithelial compartment of normal breast tissues but strongly reduced in the same compartments within the transformed tissues. However, there are not in enough samples to draw statistical conclusions [14]. On an even broader perspective, a relatively large study on postmenopausal women has recently been published where lower levels of mir-145 in circulating leukocytes were clearly shown to represent prognostic indicators linked to breast cancer progression [12]. Furthermore, dynamic reduction of mir-143/145 staining was observed upon exposure of rats to cigarette smoke [11]. Now, if increased expression of the mir-145 in stromal/endothelial human components would be oncogenic, as shown by Dimitrova et al. in the murine experimental system, it appears slightly counterintuitive that its levels were progressively downregulated in relapsing disease, metastatic disease, or upon stress stimuli conferring clear protumorigenic properties. Indeed, all these processes require a dynamic rearrangement of stromal cell subpopulations and neo-angiogenesis and this may likely lead to detectable changes of microRNA 143/145 expression. Thus, there generally appears to be a profound difference between human and murine tissues.

On a different note, other evidence point to active control of mir-143/145 levels within epithelial tumors and cell lines, in a protumorigenic direction. For example, we have shown that the mir-143/145 promoter is actively hyper-methylated in mesothelioma cancer cell lines4 and that hyper-methylation of this promoter correlates with the progressive downregulation of the mir-143/145 in brain metastases of lung tumors, as opposed to primary lung tumors and, lastly, to normal lung tissue [7]. Furthermore, treatment with histone deacetylase inhibitors and de-methylating agents or ectopic restoration of the miRNA levels correlates with lack of tumorigenicity in vivo [7] and similar results were shown in Burkitt's lymphoma cells [8]. The tumor specimens used in the mentioned studies were composed for a large portion of tumor tissue (typically 85-90% of the total tissue) and represented the results of the analysis from many different institutions. Notably, in most of the mentioned studies, the levels of mir-143-145 were in no case undetectable but rather significantly lower than their matched normal tissues. In regards to the cell lines, it may be interesting to note that in vitro grown human cell lines are virtually devoid of any significant stroma component, due to the long adaptation to in vitro growth. Thus, the described dynamic downregulation of the mir-143-145 taking place in the cell lines of the mentioned work may represent an intrinsic property of the transformed epithelial cells.

On the other hand, Almeida and Calin suggest the use of FACS-sorted cell subpopulations and/or the use of laser microdissection to better study the function of microRNAs, in order to ensure cell subpopulations homogeneity. In support of the latter, it is worth mentioning that, in head and neck cancer, ALDH+ve/CD44^{+ve} cancer stem cells exhibited low levels of miR-145 [18]. Similarly, chemoresistant ABCG2 expressing glioma with decreased levels of the microRNAs 143/145 positively correlated with poor prognosis [15]. Thus, there is increasing evidence for a cell-subpopulation restricted expression of the microRNAs, possibly modulated by external stimuli affecting the progression of the disease. However, the current repertoire of cell surface markers generally used to purify cell subpopulations is still very limited in terms of specificity, and to be able to narrow down a pure, functionally homogeneous cell subpopulations with absolute specificity and enough sensitivity. Thus we note that, the purification of cell subpopulations based on the current repertoire of cell surface markers and/or functional assays may not favorably deal with the intrinsic tumor heterogeneity of the cell subpopulations composing the tumor, which takes place at a single cell level, as shown by single-cell RNAseq studies [3, 13].

Finally, the observation that increased miR-145 could force [17] differentiation of ES cells into the mesoderm and ectoderm lineages may reconcile with the observed

expression of mir-145 into the lung endothelial cells of the vessels of the transgenic kRAS/p53 mice, given the mesodermal derivation of endothelial cells in mouse. We are of the opinion that the use of matched human tissues may constitute an experimental system capable of capturing the complex modulation of the miRNA 143/145 in human tumors and may complement the observations performed in a single mouse strain, engineered to express frequent mutations in a time- and space- restricted manner. Therefore, the precise definition of the mir-143/145 contribution to oncogenesis is still ongoing…

REFERENCES

1. Almeida MI and Calin GA. Genome medicine. 2016;8:29.
2. Avgeris M, et al. British journal of cancer. 2013; 108:2573-2581.
3. Buettner F, et al. Nature biotechnology. 2015; 33:155-160.
4. Cioce M, et al. Oncogene. 2014; 33:5319-5331.
5. Das AV and Pillai RM. Cancer cell international. 2015; 15:92.
6. Dimitrova N, et al. Cancer discovery. 2016; 6:188-201.
7. Donzelli S, et al. Oncotarget. 2015; 6:35183-35201. doi: 10.18632/oncotarget.5930.
8. Ferreira AC, et al. Annals of hematology. 2014;93:983-993.
9. Ganci F, et al. Lung cancer. 2014;85:197-204.
10. Huang L, et al. PloS one. 2012; 7:e33762.
11. Izzotti A, et al. FASEB journal. 2009; 23:806-812.
12. Muti P, et al. Cancer Epidemiol Biomarkers Prev. 2014; 23: 2471-2481.
13. Patel AP, et al. Science. 2014; 344:1396-1401.
14. Sempere LF, et al. Cancer research. 2007; 67:11612-11620.
15. Shi L, et al. Neuromolecular Med. 2014;16:517-528.
16. Slaby O, et al. Genes, chromosomes & cancer. 2012; 51: 707-716.
17. Xu N, et al. Cell. 2009; 137:647-658.
18. Yu CC, et al. Cancer research. 2013; 73:3425-3440.

Giovanni Blandino: Oncogenomic and Epigenetic Unit, Regina Elena, National Cancer Institute, Rome, 00144 Italy

Correspondence: *Giovanni Blandino*
Email: *blandino@ifo.it*

Acknowledgements: *We thank all the authors and collaborators whose work was mentioned here and we also apologize for the ones not mentioned here, for brevity. We thankfully acknowledge the help of Ms Tania Merlino (Regina Elena Cancer Institute) for proofreading the present manuscript.*
Keywords: *miR-143/145, cancer, tumor suppressor, microenvironment*

Received: May 15, 2016
Published: May 18, 2016

Research Paper

p63 expression confers significantly better survival outcomes in high-risk diffuse large B-cell lymphoma and demonstrates p53-like and p53-independent tumor suppressor function

Zijun Y. Xu-Monette[1*], Shanxiang Zhang[2*], Xin Li[1*], Ganiraju C. Manyam[3], Xiao-xiao Wang[1], Yi Xia[1], Carlo Visco[4], Alexandar Tzankov[5], Li Zhang[3], Santiago Montes-Moreno[6], Karen Dybkaer[7], April Chiu[8], Attilio Orazi[9], Youli Zu[10], Govind Bhagat[11], Kristy L. Richards[12], Eric D. Hsi[13], William W.L. Choi[14], J. Han van Krieken[15], Jooryung Huh[16], Maurilio Ponzoni[17], Andrés J.M. Ferreri[17], Xiaoying Zhao[18], Michael B. Møller[19], Ben M. Parsons[20], Jane N. Winter[21], Miguel A. Piris[6], L. Jeffrey Medeiros[1], and Ken H. Young[1,22]

[1]Department of Hematopathology, The University of Texas MD Anderson Cancer Center, Houston, TX 77030, USA
[2]University of Indiana School of Medicine, Indianapolis, IN 46202, USA
[3]Department of Bioinformatics and Computational Biology, The University of Texas MD Anderson Cancer Center, Houston, TX 77030, USA
[4]San Bortolo Hospital, Vicenza, Italy
[5]University Hospital, Basel, Switzerland
[6]Hospital Universitario Marques de Valdecilla, Santander, Spain
[7]Aalborg University Hospital, Aalborg, Denmark
[8]Memorial Sloan-Kettering Cancer Center, New York, NY 10065, USA
[9]Weill Medical College of Cornell University, New York, NY 10065, USA
[10]The Methodist Hospital, Houston, TX 77030, USA
[11]Columbia University Medical Center and New York Presbyterian Hospital, New York, NY 10032, USA
[12]University of North Carolina School of Medicine, Chapel Hill, NC 27513, USA
[13]Cleveland Clinic, Cleveland, OH 44195, USA
[14]University of Hong Kong Li Ka Shing Faculty of Medicine, Hong Kong, China
[15]Radboud University Nijmegen Medical Centre, Nijmegen, Netherlands
[16]Asan Medical Center, Ulsan University College of Medicine, Seoul, Korea
[17]San Raffaele H. Scientific Institute, Milan, Italy
[18]Zhejiang University School of Medicine, Zhejiang, China
[19]Odense University Hospital, Odense, Denmark
[20]Gundersen Medical Foundation, La Crosse, WI 54601, USA
[21]Feinberg School of Medicine, Northwestern University, Chicago, IL 60611, USA
[22]The University of Texas School of Medicine, Graduate School of Biomedical Sciences, Houston, TX 77030, USA
*These authors contributed equally to this work.

Key words: p63, DLBCL, p53, TP53 mutation, MDM2
Received: 01/15/16; Accepted: 01/26/16; Published: 02/14/16 **doi:** 10.18632/aging.100898
Correspondence to: Ken H. Young, MD; **E-mail:** khyoung@mdanderson.org

Abstract: **The role of p53 family member, p63 in oncogenesis is the subject of controversy. Limited research has been done on the clinical implications of p63 expression in diffuse large B-cell lymphoma (DLBCL). In this study, we assessed p63 expression in *de novo* DLBCL samples (n=795) by immunohistochemistry with a pan-p63-monoclonal antibody and correlated it with other clinicopathologic factors and clinical outcomes. p63 expression was observed in 42.5% of DLBCL, did not correlate with p53 levels, but correlated with p21, MDM2, p16^{INK4A}, Ki-67, Bcl-6, IRF4/MUM-1 and CD30 expression, *REL* gains, and *BCL6* translocation. p63 was an independent favorable prognostic factor in DLBCL, which was most significant in patients with International Prognostic Index (IPI) >2, and in activated-B-cell–like DLBCL patients with wide-type *TP53*. The prognostic impact in germinal-center-B-cell–like DLBCL was not apparent, which was likely due to the association of p63 expression with high-risk IPI, and potential presence of ΔNp63 isoform in *TP63* rearranged patients (a mere speculation). Gene expression profiling suggested that p63 has both overlapping and distinct functions compared with p53, and that p63 and mutated p53 antagonize each other. In summary, p63 has p53-like and p53-independent functions and favorable prognostic impact, however this protective effect can be abolished by *TP53* mutations.**

INTRODUCTION

TP63, a member of the *TP53* gene family, encodes p63 with 2 types of isoforms: a form with the N-terminal transactivation (TA) domain (TAp63) and a truncated form without the N-terminus (ΔNp63). Both TAp63 and ΔNp63 have isoforms α, β, γ, δ, and ε owing to alternative splicing at the 3' end [1-5]. p63 shares structural and sequence homology with p53 and p73, the third member of the p53 family [1, 6]. Like p53, TAp63 has been implicated in cell cycle arrest and apoptosis in response to DNA damage, ectoderm development, maternal reproduction and metabolism, dependent or independent of p53-functions [1, 7-13]. For example, TAp63 can transactivate some well-known p53 target genes including *CDKN1A*, *BAX* and *MDM2* [1, 14]. Moreover, p53-dependent apoptosis in response to DNA damage required p63 and p73 in mouse developing brain and embryonic fibroblasts [7]. However, in a mouse model p63 and p73 did not contribute to p53 tumor suppression function in lymphoma development [15]. ΔNp63, on the other hand, interacts with p53, TAp63, and TAp73 in a dominant-negative fashion to inhibit their tumor-suppressive functions [3]. It is generally believed that TAp63, like p53, is a tumor suppressor, whereas ΔNp63 has a critical role in epidermal development and functions as an oncogene in a mouse model [16-19]. Furthermore, the α, β, γ, δ, and ε isoforms of TAp63 and ΔNp63 have differential functions [5, 14, 20-24].

In normal human tissues, p63 expression is tissue-specific and restricted to epithelial cells, certain subpopulations of basal cells, and occasionally cells in the germinal centers of lymph nodes [1, 25, 26]. Accordingly, in tumors structural disruption of *TP63* and aberrant p63 expression are commonly seen in squamous cell and transitional cell carcinomas, but are also observed in non-Hodgkin lymphomas, predominantly in basal epithelial cells and squamous cell carcinomas, the ΔNp63 isoform, especially ΔNp63α, is predominantly expressed, possibly due to the increased ΔNp63 stability caused by the lack of the transactivation domain which is indispensable for proteasome-dependent MDM2-independent degradation of p63 [24, 31]. In contrast, TAp63 is present mostly in epithelial lining cells at lower levels under normal physiological conditions, and in adenocarcinoma, thymoma and lymphoma cells; TAp63 accumulates in response to genotoxic stress [24, 26]. Although p63 expression has been shown in a few studies to indicate a poor prognosis in some carcinomas [32-34], its prognostic significance in DLBCL is unclear.

DLBCL is the most common type of non-Hodgkin lymphoma and can be divided into germinal center B-cell–like (GCB) and activated B-cell–like (ABC) subgroups by gene expression profiling [35]. Numerous genetic factors affecting the prognosis of DLBCL have been identified [36]. In our previous study, *TP53* mutations were detected in approximately 20% of *de novo* DLBCL cases and conferred a worse prognosis among DLBCL patients treated with rituximab, cyclophosphamide, doxorubicin, vincristine, and prednisolone (R-CHOP) [37]. Overexpression of mutated but not wild-type p53 (WT-p53) protein is also associated with a poor prognosis in DLBCL patients [38]. The dysregulation, expression, and clinical implications of p63 in DLBCL are less clear than those of p53; likewise, p63's role in tumorigenesis and its functional relationship with p53 are not well understood. p63, predominantly TAp63 (likely TAp63β and/or TAp63γ) but not ΔNp63 or p63α, was found expressed in 15.1% to 52.5% of DLBCLs at higher levels than in normal lymphoid tissues [21, 25-27, 39]. Truncated p63 homologous to ΔNp63 due to *TP63* gene rearrangements was also reported in 1.2%-5% of DLBCL, exclusive of GCB subtype [40, 41].

Conflicting results showing the effect of p63 expression on patients' prognosis have been reported [21, 27, 39, 42, 43], likely owing to small number of patients (fewer than 100) in each study, the use of different cutoffs for p63 positivity, the differential functions and complicated interactions of multiple p63 isoforms [23, 43].

To fill this knowledge gap, we studied the prognostic effects of p63 expression correlating with *TP53* status in a multicenter cohort of patients with well-characterized *de novo* DLBCL treated with R-CHOP. We found that p63 expression conferred better clinical outcomes in DLBCL which however could be compromised or abolished by the difference in International Prognostic Index (IPI) scores and/or the presence of *TP53* mutations. We further investigated p63-associated biology to understand possible underlying molecular mechanisms.

RESULTS

p63 expression in DLBCL

We observed nuclear expression of p63 at variable levels in tumor cells of 317 (61%) of 520 samples from patients in the training set and 180 (65%) of 275 samples from patients in the validation set. Representative immunohistochemical stains are shown in Fig 1A, B and the histograms of p63 expression by immunohistochemistry are shown in Fig 1C, D. The mean number of p63 positive tumor cells in the training set was 18%, which was significantly higher than that of WT-p53 (P=0.017) but significantly lower than that of mutated p53 (MUT-p53, P<0.0001, Fig 1E) (Supplemental Fig 1A, B) [37, 38], although the *TP63* mRNA levels were significantly lower than the *TP53*

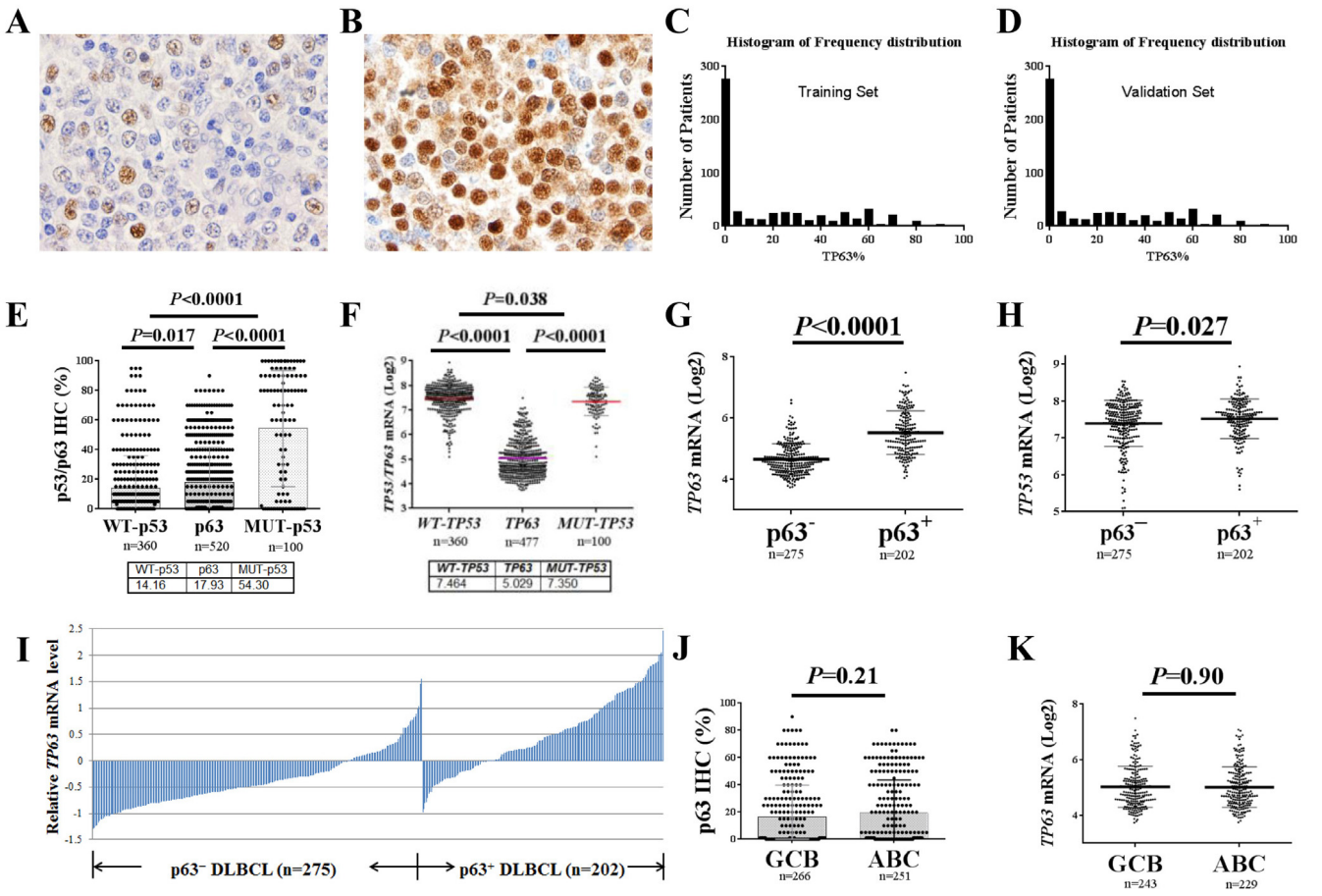

Figure 1. p63 expression in diffuse large B-cell lymphoma (DLBCL) in comparison with p53 expression. (**A-B**) Representative immunohistochemistry staining for p63 (10% and 95%) in DLBCL. (**C-D**) Histograms of p63 expression in the training and validation sets. (**E**) Comparisons between p63 and p53 expression levels in DLBCL. (**F**) Comparisons between *TP63* and *TP53* mRNA levels in DLBCL. (**G**) $p63^+$ DLBCL had significantly higher levels of *TP63* mRNA compared with $p63^-$ DLBCL. (**H**) $p63^+$ DLBCL had significantly higher *TP53* mRNA levels compared with $p63^-$ DLBCL. (**I**) Expression of p63 protein correlated with *TP63* mRNA levels. The *TP63* mRNA expression levels (Log2 values) were retrieved from the gene expression profiling data. The mean values of 3 probe-sets (1555581_a_at, 207382_at, 209863_s_at) for each patient were used. The relative mRNA level refers to the difference between the *TP63* mRNA level for each patient and the mean *TP63* mRNA level for the entire cohort. (**J-K**) Comparisons of p63 protein and *TP63* mRNA expression levels between germinal center B-cell–like (GCB) and activated B-cell–like (ABC) subtypes of DLBCL patients.

mRNA levels (P<0.0001, Fig 1F). p63 protein expression significantly correlated with *TP63* mRNA (Spearman rank correlation: r=0.596, P<0.0001).

Owing to the significantly lower level of p63 compared with MUT-p53 expression in DLBCL and the exclusion of potential false-positive cases, we used a cutoff value of 5% of tumor cells being p63-positive for p63 expression in DLBCL ($p63^+$: >5%). Using this cutoff, 221 patients (42.5%) in the training set, and 130 (47%) of 275 patients in the validation set had $p63^+$ DLBCL. The $p63^+$ group showed a significantly higher mean *TP63* mRNA level compared with the $p63^-$ group (unpaired t test, P<0.0001, Fig 1G) and *TP53* mRNA level (Fig 1H). Transcriptional activation appeared to be the most common mechanism for p63 expression in this study of DLBCL (Fig 1I). No significant difference in the expression levels of p63/*TP63* was observed between the GCB and ABC subtypes of tumor samples, either at the protein (16.66% *vs.* 19.26%, P=0.21) or mRNA (P=0.90) levels (Fig 1J, K).

Clinical and pathobiological features of $p63^+$ DLBCL

We compared the clinicopathologic features of patients with $p63^+$ and $p63^-$ DLBCL. The $p63^+$ group more often had male (P=0.0056) and patients with small (< 5 cm) tumors (P=0.05) than did the $p63^-$ group. In addition, a higher proportion (41.9%) of $p63^+$ patients had an IPI score >2 compared with $p63^-$ patients (34.4%), but this difference was not significant (P=0.086); however, by unpaired t test, patients with IPI scores >2 showed significantly higher mean levels of p63 (P=0.05, Fig 2A) and MUT-p53 (P=0.011, figure not shown) than did patients with IPI scores ≤ 2. When DLBCL cases were stratified into the GCB and ABC subtypes, in GCB-DLBCL $p63^+$ compared with $p63^-$ patients was associated with IPI scores >2, small tumors, and possibly stage III/IV disease (P=0.06), whereas in ABC-DLBCL $p63^+$ patients had higher percentages of male gender and extranodal DLBCL (44% compared with the 31% in $p63^-$ ABC-DLBCL) (Table 1). In contrast, WT-p53 overexpression was more common in nodal DLBCL (data not shown).

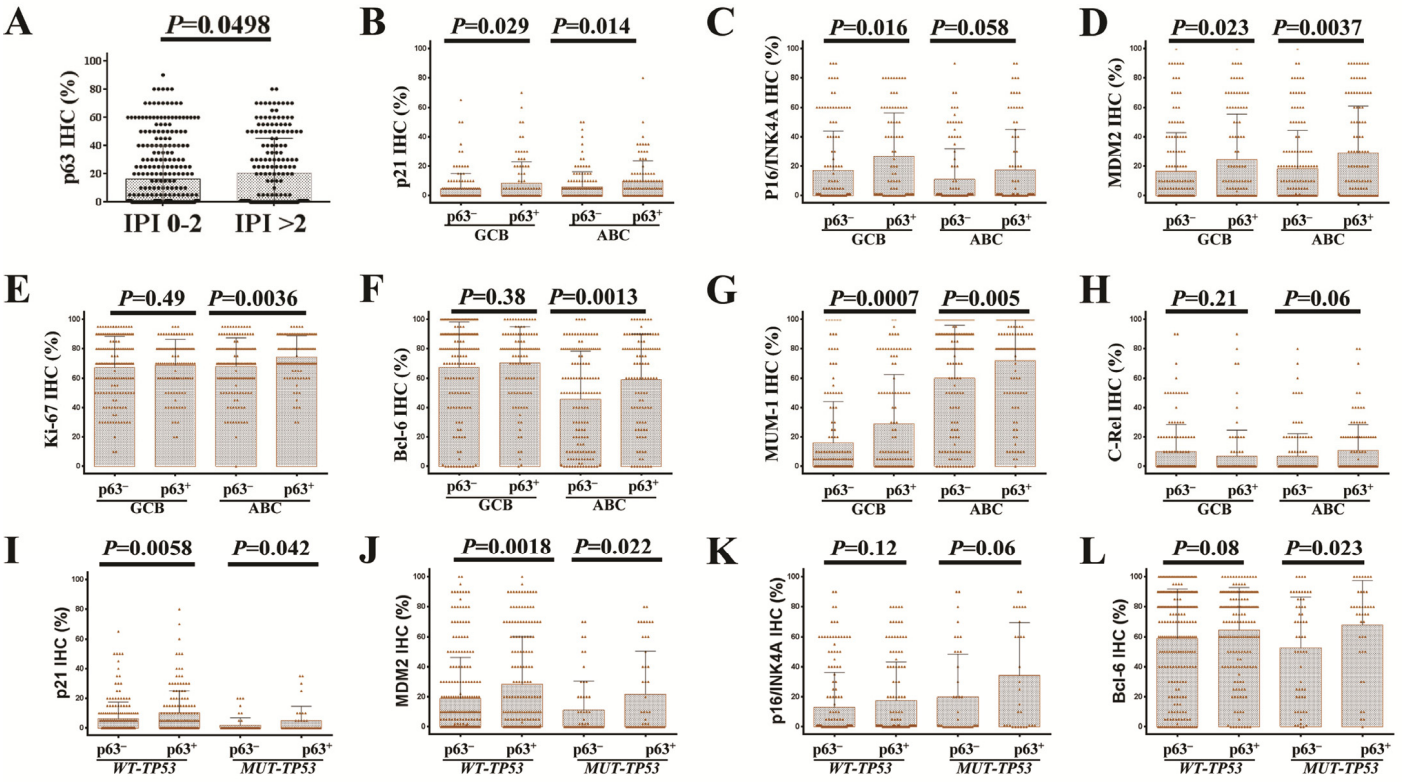

Figure 2. Correlations between p63 expression and other tumor associated factors. (**A**) The group with high International Prognostic Index (IPI) scores had a significantly higher mean level of p63 expression. (**B-D**) p63 expression was associated with significantly higher levels of p21, MDM2, and p16-INK4a in both germinal center B-cell like (GCB) and activated B-cell like (ABC) subtypes of DLBCL patients. (**E-F**) p63 expression was associated with significantly higher levels Ki-67 and Bcl-6 in ABC-DLBCL. (**G**) p63 expression was associated with significantly higher levels of IRF4/MUM-1 in both GCB and ABC subtypes of DLBCL patients. (**H**) $p63^+$ ABC-DLBCL was associated with a trend toward higher c-Rel level. (**I-J**) The association of p63 expression with p21 and MDM2 is independent of p53 mutation status. (**K-L**) p53 mutation status did not impact the association with increased p16-INK4a, Bcl-6 and IRF4/MUM-1(figure not shown) levels.

Table 1. Clinical characteristics of patients with *de novo* DLBCL in the training cohort.

	DLBCL			GCB-DLBCL			ABC-DLBCL			
	$p63^+$	$p63^-$		$p63^+$	$p63^-$		$p63^+$	$p63^-$		
	N (%)	N (%)	*P1*	N (%)	N (%)	*P2*	N (%)	N (%)	*P3*	*P4*
Patients	221	299		110	156		110	141	.59	
Age (yr)										
< 60	92 (42)	133 (45)	.52	52 (47)	84 (54)	.29	39 (35)	47 (33)	.73	.075
≥ 60	129 (58)	166 (55)		58 (53)	72 (46)		71 (65)	94 (67)		
Sex										
Female	76 (34)	139 (46)	**.0056**	41 (37)	68 (44)	.30	34 (31)	70 (50)	**.0028**	.32
Male	145 (66)	160 (54)		69 (63)	88 (56)		76 (69)	71 (50)		
Stage										
I-II	94 (44)	141(49)	.30	50 (48)	89 (59)	**.06**	44 (41)	51 (37)	.54	.34
III-IV	119 (56)	148 (51)		55 (52)	61 (41)		63 (59)	86 (63)		
B symptoms										
No	136 (63)	183 (65)	.63	73 (67)	101 (70)	.67	62 (58)	81 (60)	.76	.17
Yes	79 (37)	97 (35)		35 (32)	43 (30)		44 (42)	53 (40)		
Serum LDH										
Normal	79 (39)	107 (39)	.97	42 (42)	56 (39)	.70	37 (36)	51 (39)	.71	.40
Elevated	124 (61)	169 (61)		58 (58)	86 (61)		65 (64)	81 (61)		
No. of extranodal sites										
0-1	156 (75)	228 (79)	.27	79 (78)	121 (81)	.56	76 (71)	106 (77)	.30	.23
≥ 2	53 (25)	61 (21)		22 (22)	28 (19)		31 (29)	32 (23)		
Performance status										
0-1	164 (85)	225 (83)	.66	78 (85)	119 (86)	.76	85 (84)	104 (79)	.35	.90
≥ 2	30 (15)	46 (17)		14 (15)	19 (14)		16 (16)	27 (21)		
Size of largest tumor										
< 5cm	106 (65)	120 (55)	**.05**	56 (70)	62 (55)	**.04**	49 (59)	58 (54)	.51	.14
≥ 5cm	58 (35)	99 (45)		24 (30)	50 (45)		34 (41)	49 (46)		
IPI score										
0-2	125 (58)	189 (66)	.086	65 (61)	111 (75)	**.025**	59 (55)	76 (56)	.90	.32
3-5	90 (42)	99 (34)		41 (39)	38 (25)		49 (45)	61 (44)		
Therapy response										
CR	178 (81)	227 (76)	.21	87 (79)	118 (76)	.51	90 (82)	104 (74)	.13	.61
PR	24	43		13	19		11	24		
SD	8	13		6	7		2	6		
PD	11	16		4	12		7	7		
Primary origin										
Nodal	131 (60)	193 (66)	.16	69 (64)	97 (64)	1.0	62 (56)	95 (69)	**.048**	.27
Extranodal	88 (40)	99 (34)		39 (36)	55 (36)		48 (44)	43 (31)		
Ki-67										
< 70%	66 (30)	119 (40)	**.0016**	41 (37)	64 (42)	.45	24 (22)	55 (39)	**.004**	**.018**
≥ 70%	155 (70)	175 (60)		69 (63)	88 (58)		86 (78)	86 (61)		
***TP53* mutations**										
WT-TP53	154 (80)	206 (77)	.65	70 (74)	105 (76)	.76	83 (85)	100 (79)	.38	.059
MUT-TP53	40 (21)	60 (23)		25 (26)	34 (24)		15 (15)	26 (21)		
***MYC* translocation**										
No	138 (89)	158 (88)	.86	62 (89)	73 (80)	.20	75 (89)	85 (95)	.15	1
Yes	17 (11)	22 (12)		8 (11)	18 (20)		9 (11)	4 (5)		
***BCL2* translocation**										
No	159 (84)	187 (81)	.44	68 (74)	74 (64)	.18	90 (94)	113 (97)	.31	**.0002**
Yes	30 (16)	44 (19)		24 (26)	41 (36)		6 (6)	3 (3)		
***BCL6* translocation**										
No	98 (60)	145 (74)	**.0041**	54 (69)	83 (78)	.16	43 (51)	61 (69)	**.0016**	**.016**
Yes	66 (40)	51 (26)		24 (31)	23 (22)		42 (49)	28 (31)		
***REL* gains**										
Normal	140 (86)	216 (92)	**.068**	62 (77)	118 (92)	**.003**	77 (94)	98 (92)	**.036**	**.0001**
Amplification/ polysomy	23 (14)	19 (8)		18 (23)	10 (8)		5 (6)	9 (8)		
***REL* amplification**										
No	156 (95)	227 (97)	.60	72 (91)	121 (95)	.40	83 (99)	106 (99)	1.0	**.03**
Yes	8 (5)	8 (3)		7 (9)	7 (5)		1 (1)	1 (1)		
CD30 expression										
–	175 (79)	259 (88)	**.0048**	86 (78)	133 (88)	**.06**	88 (80)	125 (89)	**.049**	.87
+	46 (21)	34 (12)		24 (22)	19 (12)		22 (20)	15 (11)		
p53 expression										
< 20%	116 (61)	172 (66)	.27	57 (61)	89 (66)	.40	59 (62)	83 (66)	.48	1.0
≥ 20%	74 (39)	87 (34)		37 (39)	45 (34)		37 (38)	42 (34)		

Abbreviations: DLBCL, diffuse large B-cell lymphoma; GCB, germinal center B-cell–like; ABC, activated B-cell–like; LDH, lactate dehydrogenase; IPI, International Prognostic Index; CR, complete remission; PR, partial response; SD, stable disease; PD, progressive disease.

Note: *P* values indicate the significance of differences in the positivity frequencies of listed parameters between 2 groups. *P1* values are for comparisons between overall $p63^+$ and $p63^-$ DLBCL patients; *P2* values are for comparisons between $p63^+$ and $p63^-$ GCB-DLBCL patients; *P3* values are for comparisons between $p63^+$ and $p63^-$ ABC-DLBCL patients; *P4* values are for comparisons between $p63^+$ GCB-DLBCL and $p63^+$ ABC-DLBCL patients. For therapy response, we calculated *P* values by comparing CR to other responses.

When correlating p63 expression with other genetic abnormalities and immunohistochemical biomarkers in DLBCL, we found that the $p63^+$ group had higher frequencies of *BCL6* translocation and CD30 positivity (21% compared with the 12% in $p63^-$ patients) (Table 1), as well as elevated expression levels of Bcl-6, IRF4/MUM-1, p21, MDM2, p16-INK4a, and Ki-67 (in ABC-DLBCL only); most of these associations were independent of *TP53* mutation status (Fig 2B-L). In addition, p63 expression was associated with *REL* gains (including amplification and polysomies) in both the GCB and ABC subsets. No significant differences in frequencies of *TP53* mutations, *MYC* or *BCL2* translocations, or the expression levels of p53, Myc, or Bcl-2, were observed between the $p63^+$ and $p63^-$ groups.

p63 expression confers better clinical outcomes, more apparently in high-risk DLBCL and ABC-DLBCL

Univariate survival analysis in the training set

With a median follow-up of 62 months, $p63^+$ DLBCL patients showed better progression-free survival (PFS, P=0.05) compared with $p63^-$ DLBCL patients (Fig 3a, b). When patients with low-risk (IPI score ≤ 2) and high-risk DLBCL (IPI score >2) were analyzed separately (Fig 3c, d), p63 expression showed prognostic significance only in the high-risk group and correlated with significantly better overall survival (OS) (P=0.006) and PFS (P=0.0043).

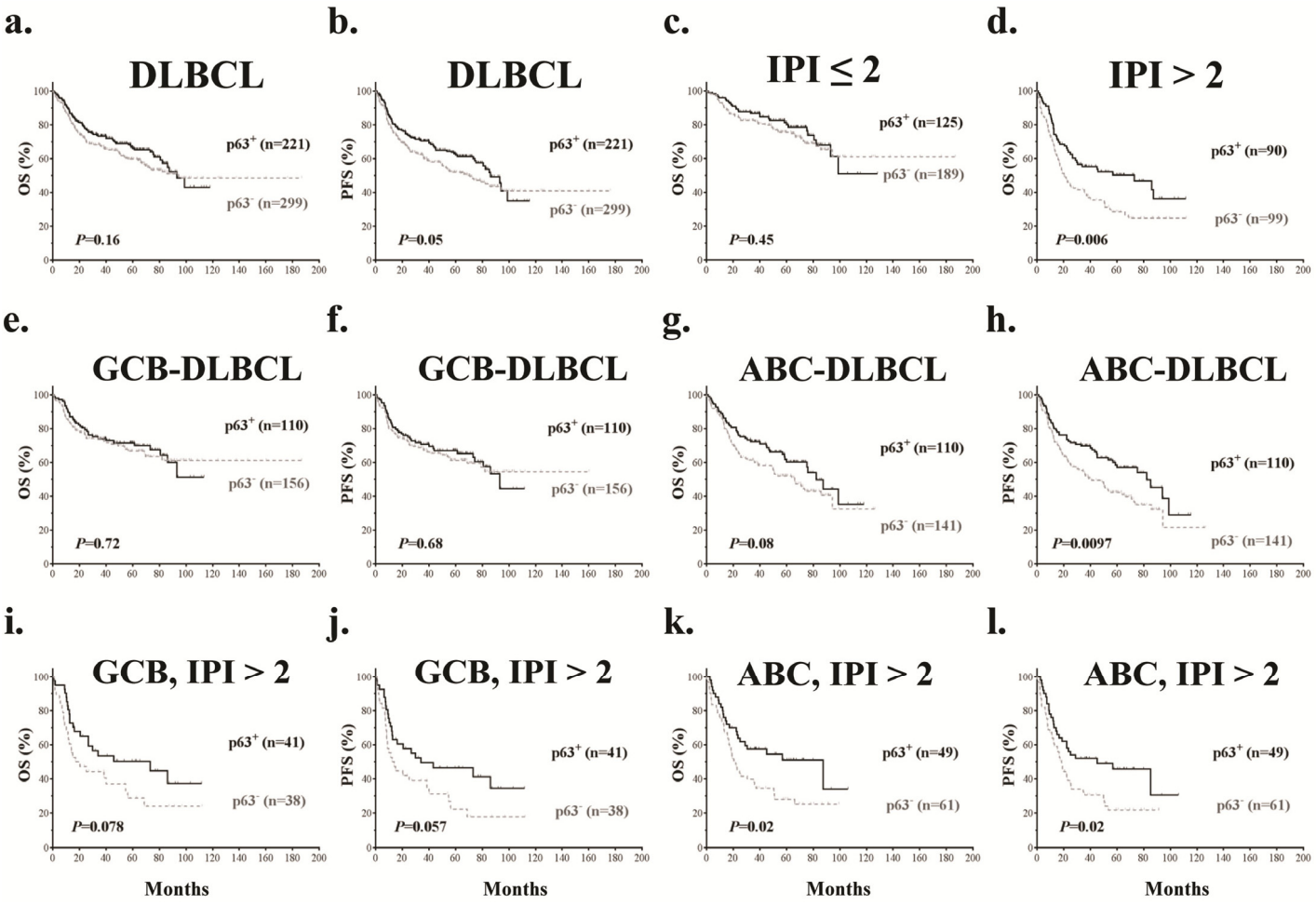

Figure 3. Prognostic analysis of p63 expression in DLBCL. (**a-b**) p63 expression correlated with significantly better progression-free survival (PFS) but not overall survival (OS) in DLBCL. (**c-d**) p63 expression correlated with significantly better overall survival in DLBCL patients with IPI scores > 2 but not in DLBCL patients with IPI scores ≤ 2. (**e-h**) p63 expression correlated with significantly better PFS in ABC- but not GCB-DLBCL patients. (**i-j**) p63 expression was associated with trends towards better survival outcomes in GCB-DLBCL patients with IPI scores > 2. (**k-l**) p63 expression correlated with significantly better survival outcomes in ABC-DLBCL patients with IPI scores > 2.

Table 2. Multivariate survival analysis.

	OS			PFS		
Variable	HR	95% CI	*P*	HR	95% CI	*P*
Overall DLBCL						
IPI >2	3.08	2.21-4.38	**< .0001**	2.84	2.08-3.89	**< .0001**
$p63^+$	.62	.45- .87	**.006**	.66	.48- .90	**.009**
Female sex	.86	.62-1.20	.37	.92	.67-1.26	.60
Tumor size ≥5 cm	1.30	.94-1.79	.11	1.26	.93-1.70	.14
B symptoms present	1.32	.95-1.85	.10	1.24	.90-1.71	.18
GCB-DLBCL						
IPI >2	4.00	2.36-6.79	**< .0001**	3.44	2.27-5.21	**< .0001**
$p63^+$	.64	.41- .99	**.045**	.67	.42-1.09	.11
Female sex	.94	.61-1.45	.78	1.00	.67-1.50	.99
Tumor size ≥5 cm	1.53	.92-2.54	.10	1.46	.92-2.34	.11
B symptoms present	1.08	.69-1.70	.74	1.21	.74-1.98	.44
ABC-DLBCL						
IPI >2	2.35	1.61-3.43	**< .0001**	2.23	1.57-3.16	**< .0001**
p63+	.56	.38- .83	**.004**	.58	.40- .83	**.003**
Female sex	.77	.52-1.15	.20	.78	.54-1.12	.17
Tumor size ≥5 cm	1.03	.58-1.56	.88	.99	.66-1.47	.94
B symptoms present	1.06	.72-1.58	.76	1.14	.79-1.64	.49
DLBCL with *WT-TP53*						
IPI >2	3.29	2.21-4.88	**< .0001**	3.21	2.18-4.72	**< .0001**
$p63^+$	.61	.40- .91	**.015**	.63	.43- .92	**.016**
$p53^+$	.97	.62-1.52	.90	.91	.60-1.40	.68
Female sex	.91	.61-1.36	.65	.85	.57-1.26	.42
Tumor size ≥5 cm	1.19	.81-176	.38	1.11	.76-1.62	.59
B symptoms present	1.45	.97-2.17	.07	1.48	1.00-2.20	**.049**
DLBCL with *MUT-TP53*						
IPI >2	2.43	1.17-5.05	**.017**	2.11	1.07-4.18	**.032**
$p63^+$	.70	.34-1.44	.33	.72	.36-1.44	.36
$p53^+$	3.16	1.17-8.52	**.023**	2.30	.97-5.45	.06
Female sex	1.02	.50-2.11	.96	1.12	.57-2.20	.75
Tumor size ≥5 cm	1.57	.77-3.20	.21	1.85	.95-3.63	.07
B symptoms present	1.19	.54-2.60	.67	1.03	.49-2.17	.93

Abbreviations: DLBCL, diffuse large B-cell lymphoma; ABC, activated B-cell–like; OS, overall survival; PFS, progression-free survival; HR, hazard ratio; CI, confidence interval; IPI, International Prognostic Index.

When analyzed in GCB- and ABC-DLBCL subsets separately, patients with $p63^+$ ABC-DLBCL showed significantly better PFS (*P*=0.0097) and a trend of better OS (*P*=0.08) compared with $p63^-$ ABC-DLBCL patients. In contrast, in GCB-DLBCL, p63 expression did not show significant impact on OS or PFS (Fig 3e-h). Consistently, survival analysis based on *TP63* mRNA levels showed that *TP63* mRNA expression correlated with favorable OS and significantly better PFS in ABC-DLBCL patients only (*P*=0.06 and *P*=0.036 respectively, Supplemental Fig S1D-G).

Since the $p63^+$ GCB-DLBCL group had a higher portion of patients with high-risk DLBCL (Table 1) which may have confounded the analysis [44], patients with low-risk and high-risk DLBCL were analyzed separately. In GCB-DLBCL patients with IPI scores >2, $p63^+$ GCB-DLBCL patients showed trends of better OS and PFS (*P*=0.078 and *P*=0.057 respectively) (Fig 3i-j). Similarly, the prognostic impact of p63 expression in ABC-DLBCL patients was more apparent in those with IPI scores >2 (Fig 3k-l); For ABC-DLBCL patients with IPI scores ≤ 2, OS and PFS rates were higher for $p63^+$

patients but not the differences were not significant (P=0.48 and P=0.12 respectively).

Multivariate survival analysis

We performed multivariate survival analysis for p63 expression adjustin g clinic al parameters including IPI score, sex, tumor size and B symptoms. p63 expression was found to be an independent prognostic factor for better OS in the overall DLBCL, GCB-DLBCL and ABC-DLBCL sets, and an independent prognostic factor for better PFS in the overall DLBCL and ABC-DLBCL sets but not in the GCB-DLBCL set (Table 2).

Validation set

Similar to the training set, no significant difference was observed in p63 expression between the GCB and ABC subtypes (P=0.68). These similar prognostic impacts as in the training set were all significant with a ≥5% cutoff value for p63 expression (P=0.02, P=0.047, and P=0.0007 for PFS in DLBCL, ABC-DLBCL and high-risk DLBCL respectively. Supplemental Fig S2). A multivariate survival analysis indicated that after adjusting clinical parameters, p63 expresssion ≥5% was an independent favorable prognostic factor in overall DLBCL and ABC-DLBCL but not in GCB-DLBCL (data not shown).

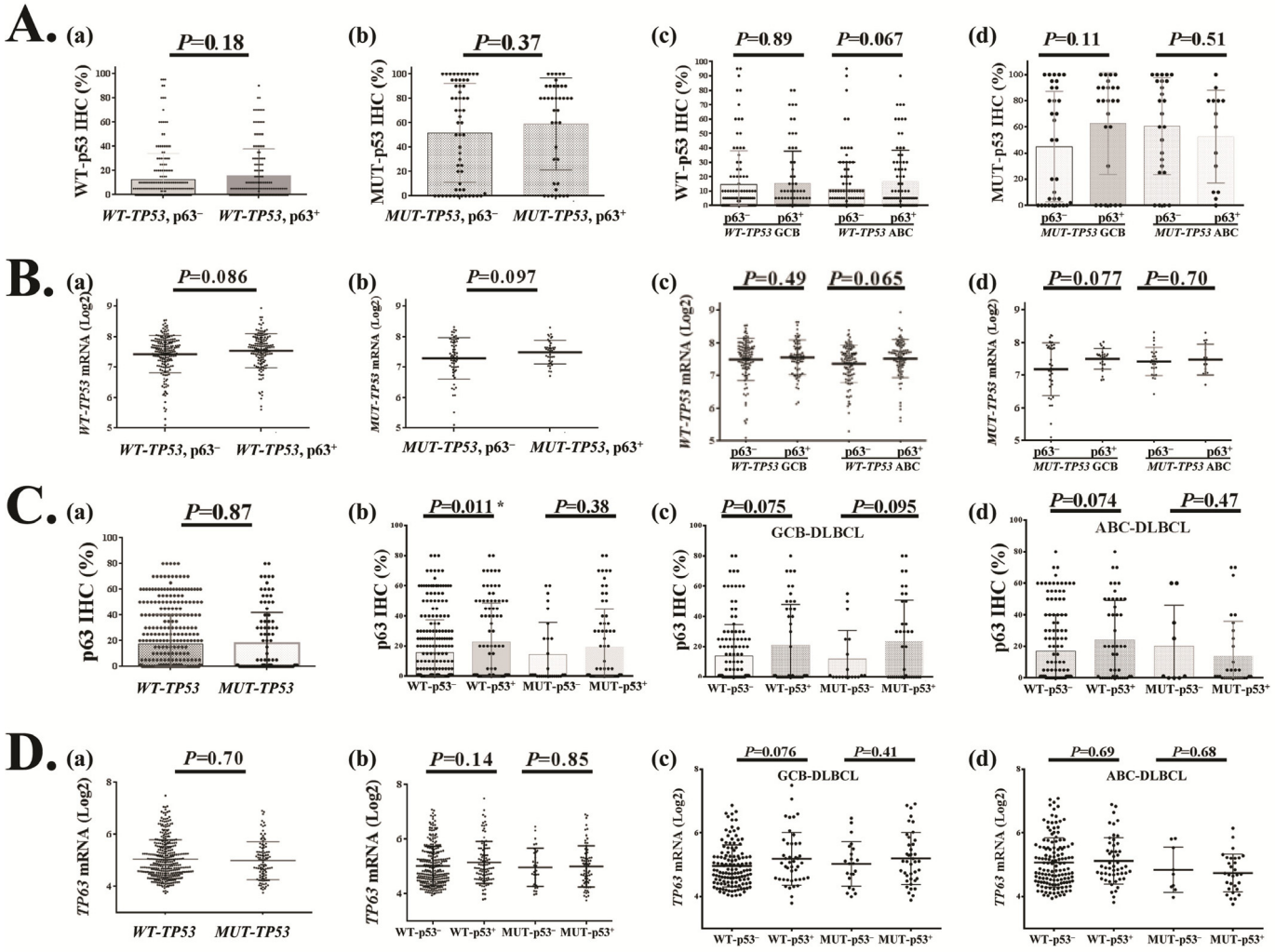

Figure 4. Relationship between *TP63*/p63 and *TP53*/p53 expression in DLBCL. (**A**) Comparison of wild-type (WT) or mutated (MUT) p53 protein expression between $p63^+$ and $p63^-$ patients with DLBCL or GCB/ABC subtypes of DLBCL. (**B**) Comparison of *TP53* mRNA expression between $p63^+$ and $p63^-$ patients with *WT-TP53* or *MUT-TP53* and GCB/ABC DLBCL. (**C**) Comparison of p63 protein expression between *WT-TP53* and *MUT-TP53* DLBCL, and between $p53^+$ and $p53^-$ patients with DLBCL or GCB/ABC subtypes of DLBCL. (**D**) Comparison of *TP63* mRNA expression between *WT-TP53* and *MUT-TP53* DLBCL, and between $p53^+$ and $p53^-$ patients with DLBCL or GCB/ABC subtypes of DLBCL.

Relationships with *TP53* mutations and p53 expression

Non-significant correlation with p53 expression and correlation with TP53 mRNA

By Spearman rank correlation *TP63* mRNA showed correlation with *TP53* mRNA levels in the overall DLBCL set (r=0.091, *P*=0.048) and *WT-TP53* subset (r=0.106, *P*=0.044) but not in the *MUT-TP53* subset. In contrast, p63 expression did not show significant correlation with overall p53 (r=0.071, *P*=0.132), WT-p53 (r=0.08, *P*=0.135), or MUT-p53 (r=0.072, *P*=0.481). Using unpaired *t*-tests, p63 expression did not correlate with p53 levels (Supplemental Fig S1C), but was associated with elevated *TP53* mRNA levels (Fig 1H). Analysis in GCB/ABC DLBCL subsets with WT-p53 or MUT-p53 showed no significant correlations between p63 positivity and WT-p53/MUT-p53 expression levels (Table 1, Fig 4A, B). However, the WT-p53$^+$ (≥20% [38]) compared with the WT-p53$^-$ DLBCL group had a significantly higher mean level of p63 protein (Fig 4C(b)) but not *TP63* mRNA (Fig 4D).

Prognostic impact of p63 expression in the presence of WT-TP53 or MUT-TP53

The clinicopathologic features of patients with p63$^+$ or p63$^-$ DLBCL with *WT-TP53* or *MUT-TP53* are shown in Table 3. p63 expression was associated with significantly better OS and PFS in patients with *WT-TP53* and IPI scores >2 (Fig 5A, B) and in ABC-DLBCL patients with *WT-TP53* (Fig 5C, D), and favorable trends in patients with MUT-p53$^+$ GCB-DLBCL (Fig 5G, H).

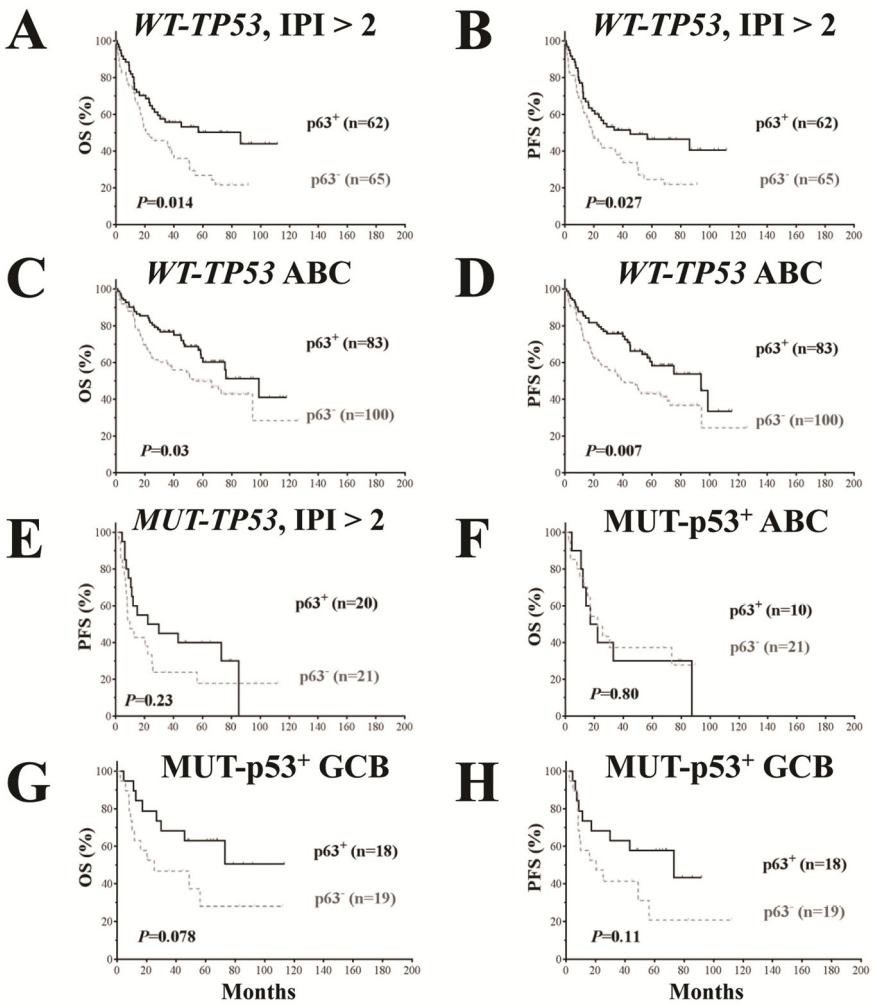

Figure 5. Prognostic analysis for p63 expression in DLBCL patients with wild- type and mutated *TP53*. (**A-B**) p63 expression correlated with significantly better survival outcomes in patients with high-risk (IPI > 2) DLBCL and *WT-TP53*. (**C-D**) p63 expression correlated with significantly better survival outcomes in patients with ABC-DLBCL and *WT-TP53*. (**E**) In patients with high-risk (IPI > 2) DLBCL and *MUT-TP53*, p63 expression did not correlate with survival outcomes although showed a trend toward better PFS. (**F**) p63 expression did not correlate with survival outcomes in patients with ABC-DLBCL and MUT-p53 overexpression. (**G-H**) p63 expression was associated with trends toward better survival outcomes in GCB-DLBCL patients with MUT-p53 overexpression (marginal *P* values).

Table 3. Clinical characteristics of DLBCL patients with wild-type *TP53* (*WT-TP53*) or mutated *TP53* (*MUT-TP53*).

	WT-TP53			*MUT-TP53*		
	$p63^+$	$p63^-$		$p63^+$	$p63^-$	
Characteristic	N (%)	N (%)	*P*	N (%)	N (%)	*P*
Patients	154	206		40	60	
Age (y)						
< 60	62 (40)	87 (42)	.75	16 (40)	25 (42)	1.0
≥ 60	92 (60)	119 (58)		24 (60)	35 (58)	
Gender						
Male	106 (69)	107 (52)	**.0013**	24 (60)	36 (60)	1.0
Female	48 (31)	99 (48)		16 (40)	24 (40)	
Stage						
I-II	62 (42)	97 (49)	.21	17 (43)	28 (47)	.68
III-IV	84 (58)	100 (51)		23 (58)	32 (53)	
B symptoms						
No	100 (67)	196 (66)	.92	23 (59)	38 (68)	.37
Yes	50 (33)	65 (34)		16 (41)	18 (32)	
LDH						
Normal	58 (41)	82 (44)	.66	12 (32)	19 (33)	.93
Elevated	82 (59)	105 (56)		25 (68)	38 (67)	
No. of extranodal sites						
0-1	105 (73)	155 (78)	.30	29 (74)	46 (78)	.68
≥ 2	38 (27)	43 (22)		10 (26)	13 (22)	
Performance status						
0-1	117 (87)	231 (85)	.62	30 (88)	50 (86)	.78
≥ 2	18 (13)	28 (15)		4 (12)	8 (14)	
Size of largest tumor						
< 5cm	81 (68)	90 (58)	.079	18 (58)	23 (48)	.38
≥ 5cm	38 (32)	66 (42)		13 (42)	25 (52)	
IPI risk group						
0-2	87 (58)	132 (67)	.10	19 (49)	38 (64)	.12
3-5	62 (42)	65 (33)		20 (51)	21 (36)	
Therapy response						
CR	126 (82)	163 (79)	.59	27 (68)	35 (58)	.40
PR	16	24		7	13	
SD	3	7		3	3	
PD	9	12		3	9	
Ki-67						
< 70%	50 (33)	83 (41)	.10	9 (22)	17 (29)	.64
≥ 70%	104 (67)	119 (59)		31 (78)	42 (71)	
Primary origin						
Nodal	91 (40)	134 (66)	.21	25 (37)	39 (70)	.54
Extranodal	61 (60)	68 (66)		15 (63)	17 (30)	
DLBCL subtypes						
GCB	70 (46)	105 (51)	.34	25 (62)	34 (57)	.68
ABC	83 (54)	100 (49)		15 (38)	26 (43)	
***BCL6* translocation**						
–	73 (63)	97 (70)	.21	17(57)	35 (85)	**.007**
+	43 (37)	41 (30)		13(43)	6 (15)	
CD30						
–	120 (78)	178 (89)	**.0085**	32 (80)	54 (92)	.13
+	34 (22)	23 (11)		8 (20)	5 (8.5)	
p53 expression						
< 20%	106 (70)	154 (77)	.18	10 (26)	18 (31)	.65
≥ 20%	45 (30)	47 (23)		29 (74)	40 (69)	

Abbreviations: DLBCL, diffuse large B-cell lymphoma; R-CHOP, rituximab with cyclophosphamide, doxorubicin, vincristine, and prednisone; LDH, lactate dehydrogenase; IPI, international prognostic index; CR, complete remission; PR, partial response; SD, stable disease; PD, progressive disease; GCB, germinal center B-cell–like; ABC, activated B-cell–like.

Table 4. Genes differentially expressed between patients with p63$^+$ and p63$^-$ DLBCL.

	p63$^+$ DLBCL FDR< 0.20		p63$^+$ DLBCL with *MUT-TP53* FDR< 0.05, fold change > 1.68		p63$^+$ ABC-DLBCL with *WT-TP53* FDR< 0.20	
Function categories	**Upregulated**	**Downregulated**	**Upregulated**	**Downregulated**	**Upregulated**	**Downregulated**
Signaling, immune response, inflammation	***FLJ23834***, ***TRAF1***	*SGPP1*			***FOXD1***, ***PDE7A***	*GABRR2*, *MS4A2*, *COMMD5*
Development, differentiation	***SOX4***, ***FOXC1***			*ZNF141*, *BACH2*	***SOX4***, ***EPHA4***	
Cell growth and proliferation, gene expression, metabolism	***H2AFB1/2/3***	*MSI2*, *TBC1D1*, *ZNF652*, *TOR1AIP1*, *ZMYM2*		*STRBP*, *CDC2L5*, *DDX18*, *MSI2*, *ZNF439*, *ZNF91*, *ZNF226*, *MTMR2*	***MEF2C***, ***DCN***, ***KDM2B***, ***RPS15***, ***NFYB***, ***DDX3Y***, ***FOXD1***, ***UTY***	*CCND2*
Apoptosis, cell death, DNA damage response	***TP63***, ***BCL2L1***, ***ZAK***, ***RFFL***, ***ATG4B***, ***MKL1***, ***HIPK2***	*C13orf15*	***TP63***		***TP63***, ***MKL1***	
Protein folding, protein translocation, heat shock	***PPIL6***	*HSF2*, *SEC62*				
Transport, mobility, cell adhesion	***KCNMA1***, ***ATP2B1***, ***KIF21A***, ***ANKH***, ***TRPM4***	*VAMP1*		*ITGB1*, *CXCR4*	***ECM2***, ***RHOBTB3***	
IncRNA and other unknown function	***COBLL1***, ***NCRNA00173***	*C17orf58*, *C8orf6*		*SETD5*, *SLMO2*	***DNAJC5B***, ***TMEM57***, ***ANUBL1***, ***IQCK***	*C10orf53*

Abbreviations: DLBCL, diffuse large B-cell lymphoma; FDR, false discovery rate; IncRNA, long noncoding RNA.

Multivariate survival analysis

We further performed multivariate survival analysis including p63 expression, p53 overexpression, and clinical parameters in the *WT-TP53* and *MUT-TP53* subsets individually. In the *WT-TP53* subset, p63 expression but not WT-p53 overexpression remained as an independent prognostic factor for better OS and PFS; in the *MUT-TP53* subset, MUT-p53 overexpression but not p63 expression was an independent prognostic factor for poorer PFS (borderline *P* value for OS) (Table 2).

Gene expression profiling signature of p63 expression

To gain insights into the potential molecular mechanisms underlying the prognostic observation, we performed a series of GEP analyses comparing p63$^+$ and p63$^-$ patients in the overall DLBCL group and various subsets stratified by GCB/ABC subtype, *TP53* mutation and p53 overexpression status (Fig 6A-H, Supplemental Fig S3A-D). Counts of significant differentially expressed genes (DEGs) between compared groups with different false discovery rate (FDR) thresholds are listed in Supplemental Table S1. Largely, whether p63 expression was associated with distinct GEP signatures did not correlated with whether p63 showed apparent prognostic effects, and the GEP signature of p63 expression in the *MUT-TP53* subset was much more prominent (Fig 6B, Table 4) than that in the *WT-TP53* subset (7 genes only with a FDR threshold of 0.30, figure not shown). However, after dividing the *WT-TP*53 subset into GCB and ABC subtypes of DLBCL patients, p63 expression showed GEP signatures, more distinctive in ABC than in GCB (Fig 6C, Supplemental Fig S3A), which was opposite to the pattern for overall

ABC and GCB (only few DEGs in ABC compared to the distinct GEP signature in GCB, Supplemental Table S1). The p63 GEP signatures in the *MUT-TP53* and *WT-TP53* subsets had both similarity (upregulated *ATP2A2* and downregulated *ZNF652*) and difference (three genes, *GABBR2*, *PDHA1* and *NFYB*, showed opposite up- or down-regulation). Reinforcing the idea that p63 GEP signatures are more highlighted in the absence of WT-p53 activities as shown in the *MUT-TP53* subset, we further found that in WT-p53$^-$ ABC-DLBCL but not in WT-p53$^+$ ABC-DLBCL, p63 expression was associated with significant DEGs (Supplemental Fig S3B, Supplemental Table S3).

To gain insights into the functional relationship between p53 and p63, we further analyzed the overlap and difference between the p53 [37, 38] and p63 GEP signatures. The results (Table 5) suggest p63 expression had a WT-p53-like GEP signature either in the context of *WT-TP53* (such as *CTAG2*, *SOX4* and *ELL2*, accounting for approximately 21% of the DEGs between *WT-TP53*/p63$^+$ and *WT-TP53*/p63$^-$) or *MUT-TP53* (such as *DSE*, *ATM*, *CDK13*, *CD47*, *ELF1*, *DYRK1A* [45], *PFDN4*, and *TMEM97*, accounting for approximately 4% of the DEGs between *MUT-TP53*/p63$^+$ and *MUT-TP53*/p63$^-$), yet remained some MUT-p53-like GEP signature mainly in the context of *MUT-TP53* (such as *CAMTA1* resembling the MUT-p53 GEP signature, and *ABHD11*, *KCNN3*, *MART3*, and *MRPL30* opposite to the WT-p53 GEP signature; accounting for approximately 1.4% of the DEGs between *MUT-TP53*/p63$^+$ and *MUT-TP53*/p63$^-$). Moreover, only in the p63$^+$ but not in the p63$^-$ subset, expression of WT-p53 or MUT-p53 was associated with distinct GEP signatures (Fig 6G, H), which may suggest that p63 is important for p53 activities.

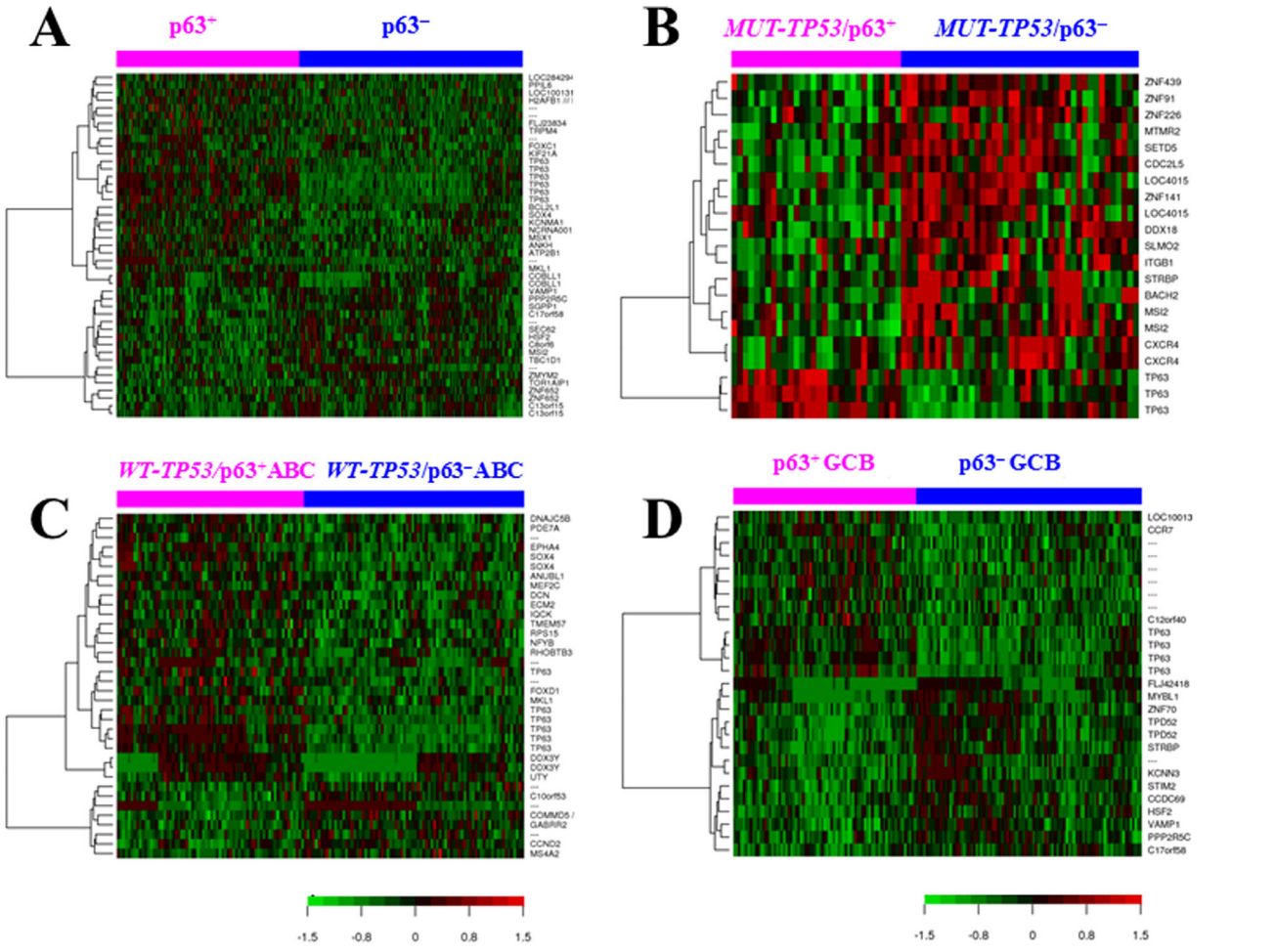

Figure 6. Gene expression profiling analysis. (**A**) Heatmap for comparison between p63$^+$ and p63$^-$ DLBCL patients (false discovery rate < 0.15). (**B**) Heatmap for comparison between p63$^+$ and p63$^-$ DLBCL patients with *MUT-TP53* (false discovery rate < 0.05, fold change >1.68). (**C**) Heatmap for comparison between p63$^+$ *versus* p63$^-$ patients with ABC-DLBCL and *WT-TP53* (false discovery rate < 0.20). (**D**) Heatmap for comparison between p63$^+$ *versus* p63$^-$ patients with GCB-DLBCL (false discovery rate < 0.05).

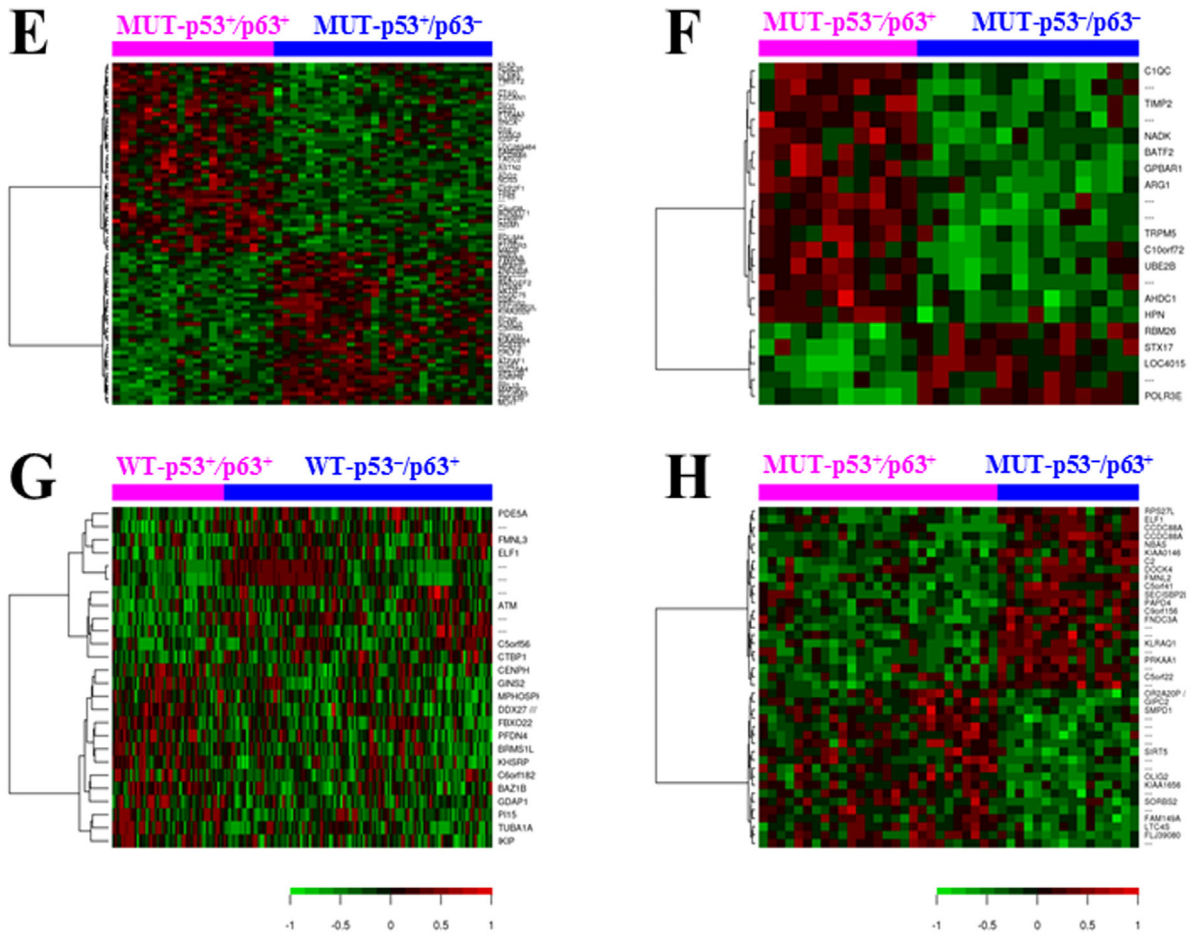

Figure 6. Gene expression profiling analysis. (**E**) Heatmap for comparison between $p63^+$ and $p63^-$ DLBCL patients with MUT-p53 overexpression (false discovery rate < 0.15). (**F**) Heatmap for comparison between $p63^+$ and $p63^-$ DLBCL patients with no or low (< 20%) expression levels of MUT-p53 (false discovery rate < 0.10). (**G**) Heatmap for comparison between WT-$p53^+$ (≥ 20%) and WT-$p53^-$ (< 20%) DLBCL patients with p63 expression (false discovery rate < 0.30). (**H**) Heatmap for comparison between MUT-$p53^+$ (≥ 20%) and MUT-$p53^-$ (< 20%) DLBCL patients with p63 expression (false discovery rate < 0.20).

We also compared the p63 GEP signature with the MDM2 GEP signature [38], and found 21 DEGs were common between the GEP signatures of p63 and MDM2 expression, among which 16 DEGs were not shared by the p53 GEP signature (Table 5).

Although the p53 and p63 GEP signatures overlapped, majority of the DEGs were not shared. Nonetheless, a p53-like tumor suppressor role of p63 was suggested by the p63 GEP signatures, including downregulation of *CCND2* (in *WT-TP53*/$p63^+$ ABC-DLBCL), *CDC27* and *MYCT1* (in *WT-TP53*/$p63^+$ GCB-DLBCL), *CDC2L5*/*CDK13* and *CXCR4* (in *MUT-TP53*/$p63^+$ DLBCL. *TP53* mutations were associated with increased CXCR4 levels especially in GCB- DLBCL as previously reported [46]), *ELF1* which encodes a transcription factor that activates *LYN* and *BLK* (in *MUT-TP53*/$p63^+$ GCB-DLBCL), *MYBL1* and *STRBP* which play roles in proliferation and growth (in *MUT-TP53*/$p63^+$ GCB-DLBCL), antiapoptotic *C9orf82* and *BCOR* (which encodes an interacting corepressor of BCL6 required for germinal center formation and may influence apoptosis) (in *MUT-TP53*/$p63^+$ ABC-DLBCL), as well as upregulation of *HIPK2* (which promotes apoptosis through the activation of p53/*TP53*) (in $p63^+$ DLBCL) and *WWOX* (which functions synergistically with p53/*TP53* to control genotoxic stress-induced cell death) (in *MUT-TP53*/$p63^+$ ABC-DLBCL) (Supplemental Fig S3C-D).

Table 5. Lists of differentially expressed genes between p63$^+$ and p63$^-$ DLBCL that are also in the p53 signatures and MDM2 signatures.

Common genes shared by the p63$^+$ and p53$^+$ signatures				
	WT-TP53 **WT-p53$^+$ *vs* WT-p53$^-$**		***MUT-TP53*** **MUT-p53$^+$ *vs* WT-p53$^-$** ***MUT-TP53 vs WT-TP53***	
		Same		Same
Up ↑	***DSE***	↑ in *MUT-TP53*/p63$^+$ *vs MUT-TP53*/p63$^-$ ↑ in MUT-p53$^+$/p63$^+$ *vs* MUT-p53$^+$/p63$^-$	***BCAS1***	↑ in p63$^+$ GCB *vs* p63$^-$ GCB
	ELL2	↑ in *WT-TP53*/p63$^+$ *vs WT-TP53*/p63$^-$		
	FDXR	↑ in WT-p53$^-$/p63$^+$ ABC *vs* WT-p53$^-$/p63$^-$ ABC		
	GRRP1	↑ in *MUT-TP53*/p63$^+$ *vs MUT-TP53*/p63$^-$		
	HPGD	↑ in *MUT-TP53*/p63$^+$ *vs MUT-TP53*/p63$^-$		
	PFDN4	↑ in *MUT-TP53*/p63$^+$ *vs MUT-TP53*/p63$^-$		
	SOX4	↑ in p63+ *vs* p63$^-$ ↑ in *WT-TP53*/p63$^+$ *vs WT-TP53*/p63$^-$ ↑ in WT-p53$^-$/p63$^+$ ABC *vs* WT-p53$^-$/p63$^-$ ABC		
Down ↓	***ATM***	↓ in *MUT-TP53*/p63$^+$ *vs MUT-TP53*/p63$^-$	***CAMTA1***	↓ in *MUT-TP53*/p63$^+$ *vs MUT-TP53*/p63$^-$ ↓ in *MUT-TP53*/p63$^+$ GCB *vs MUT-TP53*/p63$^-$ GCB
	C3orf63	↓ in MUT-p53$^+$/p63$^+$ *vs* MUT-p53$^+$/p63$^-$		
	CCDC69	↓ in p63$^+$ GCB *vs* p63$^-$GCB		
	CD47	↓ in MUT-p53$^+$/p63$^+$ *vs* MUT-p53$^+$/p63$^-$		
	CDC2L5/C	↓ in *MUT-TP53*/p63$^+$ *vs MUT-TP53*/p63$^-$		
	DK13	↓ in *MUT-TP53*/p63$^+$ GCB *vs MUT-TP53*/p63$^-$ GCB		
	DCLRE1C	↓ in *MUT-TP53*/p63$^+$ *vs MUT-TP53*/p63$^-$ ↓ in *MUT-TP53*/p63$^+$ GCB *vs MUT-TP53*/p63$^-$ GCB		
	DYRK1A	↓ in *MUT-TP53*/p63$^+$ *vs MUT-TP53*/p63$^-$		
	ELF1	↓ in *MUT-TP53*/p63$^+$ *vs MUT-TP53*/p63$^-$ ↓ in *MUT-TP53*/p63$^+$ GCB *vs MUT-TP53*/p63$^-$ GCB ↓ in p63$^+$ GCB *vs* p63$^-$ GCB		
	ESR2	↓ in p63$^+$ GCB *vs* p63$^-$GCB		
	HCG18	↓ in *WT-TP53*/p63$^+$ *vs WT-TP53*/p63$^-$		
	HERC4	↓ in *MUT-TP53*/p63$^+$ *vs MUT-TP53*/p63$^-$ ↓ in *MUT-TP53*/p63$^+$ GCB *vs MUT-TP53*/p63$^-$ GCB		
	ITCH	↓ in *MUT-TP53*/p63$^+$ *vs MUT-TP53*/p63$^-$		
	LOC645513	↓ in *MUT-TP53*/p63$^+$ *vs MUT-TP53*/p63$^-$		
	ORC4L	↓ in *MUT-TP53*/p63$^+$ *vs MUT-TP53*/p63$^-$		
	PPP1R2	↓ in *MUT-TP53*/p63$^+$ *vs MUT-TP53*/p63$^-$		
	TBC1D1	↓ in p63+ *vs* p63$^-$ ↓ in p63$^+$ GCB *vs* p63$^-$ GCB		
	PXK	↓ in p63$^+$ GCB *vs* p63$^-$GCB		
	TMCC1	↓ in *MUT-TP53*/p63$^+$ ABC *vs MUT-TP53*/p63$^-$ ABC		
	ZCCHC7	↓ in *MUT-TP53*/p63$^+$ *vs MUT-TP53*/p63$^-$		
	ZNF221	↓ in WT-p53$^-$/p63$^+$ ABC *vs* WT-p53$^-$/p63$^-$ ABC		
		Opposite		Opposite
Up ↑	***KCNN3***	↓ in p63$^+$ GCB *vs* p63$^-$GCB	***CTAG2***	↓ in WT-p53$^-$/p63$^+$ ABC *vs* WT-p53$^-$/p63$^-$ ABC
	KIAA0564	↓ in *MUT-TP53*/p63$^+$ *vs MUT-TP53*/p63$^-$ ↓ in MUT-p53$^+$/p63$^+$ *vs* MUT-p53$^+$/p63$^-$	***TMEM97***	↓ in *MUT-TP53*/p63$^+$ *vs MUT-TP53*/p63$^-$
	MATR3	↓ in *MUT-TP53*/p63$^+$ *vs MUT-TP53*/p63$^-$	***SLC16A1***	↓ in p63$^+$ GCB *vs* p63$^-$GCB
	MRPL30	↓ in *MUT-TP53*/p63$^+$ *vs MUT-TP53*/p63$^-$		
Down ↓	***ABHD11***	↑ in *MUT-TP53*/p63$^+$ ABC *vs MUT-TP53*/p63$^-$ ABC		

Common genes shared by the p63$^+$ and MDM2$^+$ signatures				
	WT-TP53 **MDM2$^+$ *vs* MDM2$^-$**		***MUT-TP53*** **MDM2$^+$ *vs* MDM2$^-$**	
		Same		Same
Up ↑	***FAM83A***	↑ in *MUT-TP53*/p63$^+$ ABC *vs* *MUT-TP53*/p63$^-$ ABC		
	FDXR	↑ in WT-p53$^-$/p63$^+$ ABC *vs* WT-p53$^-$/p63$^-$ ABC		
	MICAL2	↑ in *MUT-TP53*/p63$^+$ GCB *vs* *MUT-TP53*/p63$^-$ GCB		
	PCBP3	↑ in *MUT-TP53*/p63$^+$ *vs* *MUT-TP53*/p63$^-$		
	TCEB3	↑ in p63+ *vs* p63$^-$		
Down ↓	***ATM***	↓ in *MUT-TP53*/p63$^+$ *vs* *MUT-TP53*/p63$^-$		
	BPTF	↓ in *MUT-TP53*/p63$^+$ *vs* *MUT-TP53*/p63$^-$ ↓ in p63$^+$ GCB *vs* p63$^-$ GCB	***ATG7***	↓ in p63$^+$ GCB *vs* p63$^-$ GCB
	BRWD1	↓ in p63$^+$ GCB *vs* p63$^-$ GCB	***ATP5C1***	↓ in *MUT-TP53*/p63$^+$ *vs* *MUT-TP53*/p63$^-$ ↓ in *MUT-TP53*/p63$^+$ GCB *vs* *MUT-TP53*/p63$^-$ GCB
	CD22	↓ in p63$^+$ GCB *vs* p63$^-$ GCB	***EIF2A***	↓ in *MUT-TP53*/p63$^+$ *vs* *MUT-TP53*/p63$^-$
	DHX36	↓ in *MUT-TP53*/p63$^+$ *vs* *MUT-TP53*/p63$^-$	***PAK2***	↓ in *MUT-TP53*/p63$^+$ *vs* *MUT-TP53*/p63$^-$
	EIF2A	↓ in *MUT-TP53*/p63$^+$ *vs* *MUT-TP53*/p63$^-$	***PRICKLE4/ TOMM6***	↓ in *MUT-TP53*/p63$^+$ ABC *vs* *MUT-TP53*/p63$^-$ ABC
	NKTR	↓ in *MUT-TP53*/p63$^+$ *vs* *MUT-TP53*/p63$^-$ ↓ in MUT-p53$^+$/p63$^+$ *vs* MUT-p53$^+$/p63$^-$ ↓ in *MUT-TP53*/p63$^+$ GCB *vs* *MUT-TP53*/p63$^-$ GCB		
	RBM26	↓ in *MUT-TP53*/p63$^+$ *vs* *MUT-TP53*/p63$^-$ ↓ in MUT-p53$^-$/p63$^+$ *vs* MUT-p53$^-$/p63$^-$		
	RPL34	↓ in *MUT-TP53*/p63$^+$ *vs* *MUT-TP53*/p63$^-$		
	SLC35F5	↓ in *MUT-TP53*/p63$^+$ *vs* *MUT-TP53*/p63$^-$		
	WT-TP53 **MDM2$^+$ *vs* *MUT-TP53*** **MDM2$^+$**			
		Same		
Down ↓	***LPP***	↓ in p63$^+$ GCB *vs* p63$^-$ GCB		

On the other hand, some DEGs promoting tumor cell survival were also shown in the comparison between overall p63$^+$ and p63$^-$ DLBCL patients, which may be due to the oncogenic function provided by MUT-p53 or p63 isoforms in the p63$^+$ DLBCL subsets. For example, antiapoptotic *BCL2L1*, *RFFL* (which negatively regulates p53, CASP8 and CASP10 through proteasomal degradation), *ATG4B* (required for autophagy), and *MKL1* (which suppresses TNF-induced cell death by inhibiting caspase activation) were up-regulated in p63$^+$ DLBCL compared with p63$^-$ DLBCL, whereas *C13orf15/RGCC* (in response to DNA damage) was downregulated in p63$^+$ DLBCL patients (Table 4). Cytokine/receptor genes *IL17RC*, *IL4*, *IL4I1* and *IL8RB/CXCR2* which have been associated with poorer prognosis in cancers, were upregulated in *MUT-TP53*/p63$^+$ compared with *MUT-TP53*/p63$^-$ DLBCL (Supplemental Table S2); *MLL2* was upregulated in p63$^+$ patients with ABC-DLBCL and *MUT-TP53* (Supplemental Fig S3D).

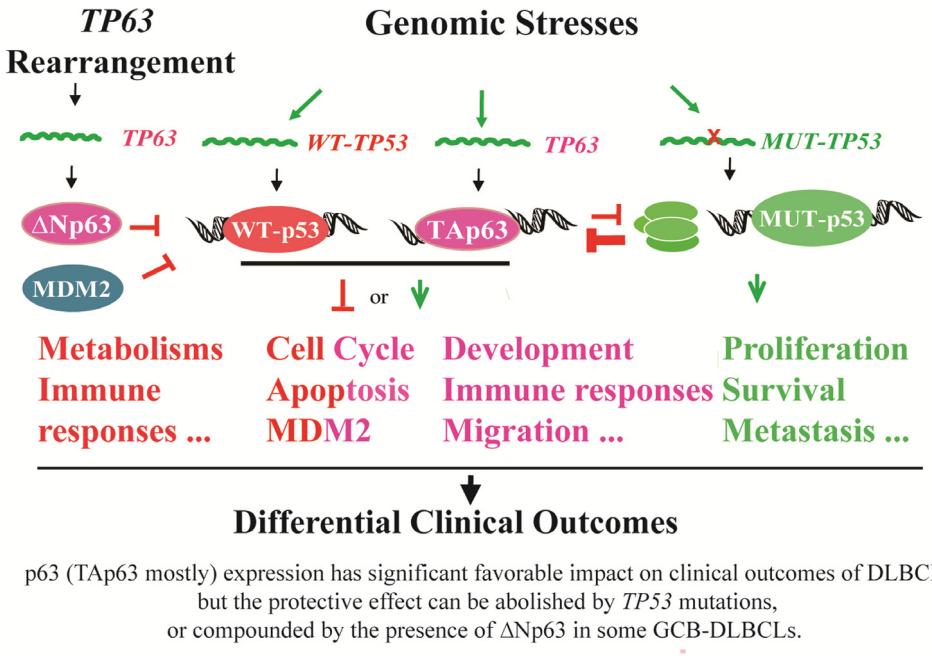

Figure 7. A hypothetical model illustrating the regulation and roles of p53 and p63 in DLBCL lymphomagenesis and clinical outcomes suggested by our clinical and biological data.

DISCUSSION

Abnormal p63 expression patterns instead of *TP63* mutations have been found to be important for tumorigenesis [5]. Little data are available with conflicting results regarding p63 expression and its prognostic role [27, 39, 43]. We found that p63 expression correlated with a superior survival in ABC-DLBCL with *WT-TP53* and in high-risk (IPI >2) DLBCL (regardless GCB or ABC), which is consistent with a previous study in high-intermediate and high risk DLBCL [27]. The association of p63 expression with high-risk IPI in GCB-DLBCL, and thus affecting its apparent prognostic effects in GCB and overall DLBCL, may contribute to the inconsistent findings from previous studies.

The prognostic effect of p63 expression suggests that p63 has a tumor suppressor role for DLBCL, although its protective effect can be antagonized or abolished by *TP53* mutations and high-risk DLBCL associated biology. In our cohort, p63 expression was associated with increased levels of IRF4/MUM-1, p21, MDM2, and p16-INK4a resembling that of WT-p53 yet independent of p53 mutation status. GEP analysis showed that compared to the prominent p63 GEP signature within the *MUT-TP53* subset, the comparison between $p63^+$ and $p63^-$ patients with *WT-TP53* had much fewer DEGs; DEGs were shown within the WT-$p53^-$ but not WT-$p53^+$ ABC-DLBCL subset. These results may suggest that the tumor suppressor function of p63 may overlap with (and is probably weaker than) that of WT-p53, and when *TP53* was mutated, p63 functions as a supplemental tumor suppressor alternative to WT-p53. However, MUT-p53 function remained or dominated p63 function in certain *MUT-TP53* cases (Table 5), likely due to the significantly higher levels of MUT-p53 than p63 [47]. In addition to the GEP results as above, p63 expression correlated with *MDM2* upregulation and *BCL2* and *MDM4* downregulation (P=0.0174, P=0.0487 and P=0.090 respectively) resembling WT-p53 expression GEP signature (although the FDRs for the comparison between $p63^+$ and $p63^-$ DLBCL were higher). In contrast, *CDKN1A/p21*, *MCL1*, *B2M*, and *FYB* showed great variation even opposite up/down regulation between the WT-$p53^+$ and the $p63^+$ GEP signature. These phenomena may be explained by the remained MUT-p53-like function in the *MUT-TP53*/$p63^+$ cases, whereas *TP63* mutations and expression of different p63 isoforms may not be significant factors as suggested by the previous studies [5, 25, 43] and our preliminary data of *TP63* mutations in DLBCL (unpublished data).

These observations in DLBCL may support previous functional studies, which showed that TAp63α and TAp63γ (but not ΔNp63) could induce apoptosis at lesser levels than WT-p53 [48]; TAp63, and also TAp73, together with p53, may transactivate a group of common target genes in response to DNA damage, including damage resulting from exposure to doxorubicin, a component of R-CHOP; [1] TAp63 and MUT-p53 antagonize each other mainly in the regulation of metastasis and tumor dissemination [5]; p53 mutants may bind directly to p63 and inhibit the p63-mediated transcription of p53 target genes [49, 50]. Strategies to overcome MUT-p53 interaction with p63, decrease MUT-p53 levels and enhance p63 levels may have therapeutic value [47]. On the other hand, in mouse embryonic fibroblasts, p63 and p73 are required for p53-dependent apoptosis in response to DNA damage [7]. This may explain why our GEP comparisons between $p53^+$ and $p53^-$ DLBCL showed DEGs within the $p63^+$ but not $p63^-$ subset. Moreover, our data suggested that p63 act together with p53 in some essential pathways yet also function independently in many processes such as development, immune response and chemokinesis. Large variations between p63 signatures in the overall DLBCL patient population and in the GCB and ABC subsets may also imply a wide range of p63 activities. These characteristics of p63 function compared with p53, as well as association with high Ki-67 (consistent with previous studies [21, 43]) and high IPI may explain the limitation of p63's apparent prognostic effect in DLBCL.

It is also possible that the correlation between p63 expression and better survival outcomes may be also influenced by the escape from MDM2-mediated degradation. In our cohort, the p63's protective effects on patient survival were independent of MDM2 expression, yet GEP signatures were only shown in $MDM2^{low}$ but not in $MDM2^{high}$ subsets (data not shown), suggesting that MDM2 may suppress p63 function but the suppression is not significant to the p63's protective effect. Conversely, p63 may have confounded the MDM2's prognostic effect in DLBCL just as that of WT-p53 [38], suggested by the common genes shared by the MDM2 and p63 GEP signatures (Table 5). Previous studies have suggested that p63 degradation is independent of MDM2 [24, 31] and that MDM2 increases the protein level and transcriptional activity of p63 [51]. The MDM2 inhibitor p14ARF directly interacts with and impairs p63 transcriptional activity [52]. On the other hand, it has also been shown that MDM2 transports p63 out of nucleus and inhibits its transcription function [53].

Yang *et al*. speculated that p63 expression in cancer cells was due to *TP63* gene amplification by genomic instability [3], and other researches showed that p63 expression was regulated via mRNA stability [4, 19]. *TP63* rearrangements have been reported in 1.2-5% of DLBCL (exclusive of GCB subtype) and also in 5.8% of peripheral T-cell lymphomas, which resulted in a truncated p63 protein lacking the TA domain [40, 41]. Our data showed the associations of p63 expression with *BCL6* (mapped to 3q27) translocations, which appears to suggest the possibility of concurrent translocation of *TP63* gene (mapped to 3q27-28) due to chromosomal proximity in $p63^+$ DLBCL subsets. In these cases it is possible that expressed p63 had oncogenic function like ΔNp63, which may explain the oncogenic DEGs in the p63 GEP signatures, and the lack of p63's prognostic significance in GCB-DLBCL. In addition, genomic stress similar to that inducing p53 may also be the cause of p63 expression in subsets of $p63^+$ DLBCL [54], since our data showed correlation between the *WT-TP53* and *TP63* mRNA levels, and both WT-p53 and p63 expression were associated with increased IRF4/MUM-1 and Ki-67 expression. Fig 7 illustrates these potential causes for p63 expression and possible relationships between p63 and WT-p53/MUT-p53 function. Understanding the mechanisms regulating *TP63* may lead to therapeutic strategies. In DLBCL cell lines, FOXP1, directly represses *TP63* and cooperate with NF-κB signaling to promote lymphoma cell survival [42]. Consistently, our GEP data also suggest that molecules related to B-cell receptor signaling may be potential targets which suppresses p63 expression, as in GCB-DLBCL and *MUT-TP53*/$p63^+$ DLBCL, p63 expression was associated with downregulation of *SYK* and *ELF1* respectively (suggesting decreased B-cell receptor signaling).

In conclusion, we demonstrated the correlation of p63 expression and better survival outcomes in patients with high-risk DLBCL, ABC-DLBCL with *WT-TP53*, and biology associated with p63 expression supporting p63's tumor suppressor role in DLBCL. This study helps identify a subgroup of patients with better prognosis among patients who have ABC-DLBCL or high-risk DLBCL. Targeting p63 expression and function may be a novel therapeutic strategy for particular subgroups of DLBCL patients.

MATERIALS AND METHODS

Patients. A total of 795 patients with *de novo* DLBCL from 20 medical centers treated with R-CHOP were studied, randomly divided into a training set (n=520) and a validation set (n=275). The diagnostic criteria, selection process, therapy, and treatment response have been described previously [37]. The study was approved as being of minimal or no risk or as exempt by the

institution review boards of all participating medical centers.

Immunohistochemistry. Tissue microarrays prepared from the diagnostic formalin-fixed, paraffin-embedded (FFPE) tissue blocks of all patients studied were stained with an anti-p63 antibody (4A4, Santa Cruz Biotechnology, Santa Cruz, CA) which can detect all p63 isoforms. Expression levels of p63 were determined by estimating the percentage of p63-positive tumor cells in the tissue array cores. X-tile software and receiver operating characteristic curve analysis by GraphPad Prism 6 Software were used to determine the percentage of p63-positive cells with maximal discriminatory power for the separation of DLBCL patients into 2 different prognostic groups. Evaluation of other biomarkers by immunohistochemistry was also performed on tissue microarrays using corresponding antibodies: p53 (DO-7, Dako, Carpinteria, CA), MDM2 (IF2, Calbiochem, Billerica, MA), p21 (Dako), Bcl-2 (Clone-124, Dako, Carpinteria, CA), Ki-67 (Dako), CD30 (clone BerH2, Dako), Bcl-6 (Dako), FOXP1 (Abcam), IRF4/MUM1 (Dako), CD10 (56C6, Vantana), c-Rel (Dako), and CXCR4 (Abcam, San Francisco, CA). Details of immunohistochemistry procedures and scoring processes have been described previously [38, 44, 55-58].

TP53 and *TP63* sequencing, fluorescence *in situ* hybridization. Genomic DNA samples were extracted from FFPE tissues, and the *TP53* coding region and splice site sequence were determined for 460 patients in the training set using a p53 AmpliChip (Roche Molecular Systems, Pleasanton, CA) as described previously [37]. *TP63* coding region sequence was analyzed by Sanger sequencing method. *MYC*, *BCL2*, *BCL6*, and *REL* gene arrangements and copy number aberrations were detected by fluorescence *in situ* hybridization [56, 59, 60].

Gene expression profiling. Gene expression profiling was performed on Affymetrix GeneChips HG-U133 Plus Version 2.0 (Affymetrix, Santa Clara, CA) using total RNAs as described previously [37, 55]. The CEL files are deposited in the National Center for Biotechnology Information Gene Expression Omnibus repository (GSE#31312). The microarray data were quantified and normalized by the frozen robust multiarray analysis (RMA) algorithm. The differentially expressed genes were identified by using multiple *t*-tests.

Statistical analysis. The clinical and pathologic features at the time of presentation were compared between various DLBCL subgroups by using the chi-square test and unpaired *t* test. Correlation between expression of different genes or proteins was evaluated by Spearman rank correlation. Overall survival (OS) was calculated from the date of diagnosis to the date of last follow-up or death. Progression-free survival (PFS) was calculated from the date of diagnosis to the date of disease progression or death. OS and PFS curves of the various groups were analyzed by GraphPad Prism 6 software using the Kaplan-Meier method, and differences were compared with use of the log-rank (Cox-Mantel) test. Multivariate analysis was conducted by using the Cox proportional hazards regression model with the SPSS software version 19.0 (IBM, Armonk, NY). Any difference with a P value of < 0.05 was considered statistically significant.

Authorship

Contribution: Z.Y.X-M, S.Z., and K.H.Y designed and conducted the research and performed the statistical analysis; Z.Y.X-M, S.Z., X.L., G.C.M., X.W., Y.X., C.V., A.T., S.M.M., K.D., A.C., A.O., Y.Z., G.B., K.L.R., E.D.H., W.W.L.C., J.H.K., J.H., M.P., A.J.M.F., X.Z., M.B.M., F.B., B.M.P., M.A.P., J.N.W., L.J.M., and K.H.Y. contributed vital new reagents, resources, technology, and analytical tools; Z.Y.X-M, S.Z., C.V., A.T., S.M.M., K.D., A.C., A.O., Y.Z., G.B., K.L.R., E.D.H., W.W.L.C., J.H.K., J.H., M.P., A.J.M.F., X.Z., M.B.M., F.B., B.M.P., M.A.P., J.N.W., and K.H.Y. collected clinical and follow-up data under approval by the Institutional Review Boards and the material transfer agreement; Z.Y.X-M, S.Z., L.J.M., and K.H.Y. wrote and edited the manuscript; and all authors contributed vital strategies, participated in discussions, and provided scientific input.

Funding

This study was supported by the National Cancer Institute/National Institutes of Health (R01CA138688 and 1RC1CA146299 to K.H.Y). K.H.Y. is supported by The University of Texas MD Anderson Cancer Center Lymphoma Moonshot Program, Institutional Research and Development Fund, an Institutional Research Grant Award, an MD Anderson Cancer Center Lymphoma Specialized Programs on Research Excellence (SPORE) Research Development Program Award, an MD Anderson Cancer Center Myeloma SPORE Research Development Program Award, and partially supported by the National Cancer Institute/National Institutes of Health (P50CA136411 and P50CA142509). G.M. is supported by a grant from the Michael and Susan Dell Foundation. Z.Y.X-M is the recipient of the Shannon Timmins Leukemia Fellowship and the Harold C. and Mary L. Daily Endowment Fellowships Award at The University of Texas MD Anderson Cancer Center.

Conflict of interest statement

KHY receives research support from Roche Molecular System, Gilead Sciences Pharmaceutical, Seattle Genetics, Dai Sanyo Pharmaceutical, Adaptive Biotechnology, Incyte Pharmaceutical, and HTG Molecular Diagnostics.

REFERENCES

1. Su X, Chakravarti D and Flores ER. p63 steps into the limelight: crucial roles in the suppression of tumorigenesis and metastasis. Nat Rev Cancer. 2013; 13:136-143.

2. Yang A and McKeon F. P63 and P73: P53 mimics, menaces and more. Nat Rev Mol Cell Biol. 2000; 1:199-207.

3. Yang A, Kaghad M, Wang Y, Gillett E, Fleming MD, Dotsch V, Andrews NC, Caput D and McKeon F. p63, a p53 homolog at 3q27-29, encodes multiple products with transactivating, death-inducing, and dominant-negative activities. Molecular cell. 1998; 2:305-316.

4. Cho SJ, Jung YS and Chen X. Poly (C)-binding protein 1 regulates p63 expression through mRNA stability. PloS one. 2013; 8:e71724.

5. Pflaum J, Schlosser S and Muller M. p53 Family and Cellular Stress Responses in Cancer. Front Oncol. 2014; 4:285.

6. Levine AJ, Tomasini R, McKeon FD, Mak TW and Melino G. The p53 family: guardians of maternal reproduction. Nat Rev Mol Cell Biol. 2011; 12:259-265.

7. Flores ER, Tsai KY, Crowley D, Sengupta S, Yang A, McKeon F and Jacks T. p63 and p73 are required for p53-dependent apoptosis in response to DNA damage. Nature. 2002; 416:560-564.

8. Venkatanarayan A, Raulji P, Norton W, Chakravarti D, Coarfa C, Su X, Sandur SK, Ramirez MS, Lee J, Kingsley CV, Sananikone EF, Rajapakshe K, Naff K, et al. IAPP-driven metabolic re rogramming induces regression of p53-deficient tumours in vivo. Nature. 2015; 517:626-630.

9. Mills AA, Zheng B, Wang XJ, Vogel H, Roop DR and Bradley A. p63 is a p53 homologue required for limb and epidermal morphogenesis. Nature. 1999; 398:708-713.

10. Suh EK, Yang A, Kettenbach A, Bamberger C, Michaelis AH, Zhu Z, Elvin JA, Bronson RT, Crum CP and McKeon F. p63 protects the female germ line during meiotic arrest. Nature. 2006; 444:624-628.

11. Yang A, Schweitzer R, Sun D, Kaghad M, Walker N, Bronson RT, Tabin C, Sharpe A, Caput D, Crum C and McKeon F. p63 is essential for regenerative proliferation in limb, craniofacial and epithelial development. Nature. 1999; 398:714-718.

12. Sun R, Zhang Y, Lv Q, Liu B, Jin M, Zhang W, He Q, Deng M, Liu X, Li G, Li Y, Zhou G, Xie P, et al. Toll-like receptor 3 (TLR3) induces apoptosis via death receptors and mitochondria by up-regulating the transactivating p63 isoform alpha (TAP63alpha). J Biol Chem. 2011; 286:15918-15928.

13. Levrero M, De Laurenzi V, Costanzo A, Gong J, Wang JY and Melino G. The p53/p63/p73 family of transcription factors: overlapping and distinct functions. J Cell Sci. 2000; 113:1661-1670.

14. Dohn M, Zhang S and Chen X. p63alpha and DeltaNp63alpha can induce cell cycle arrest and apoptosis and differentially regulate p53 target genes. Oncogene. 2001; 20:3193-3205.

15. Perez-Losada J, Wu D, DelRosario R, Balmain A and Mao JH. p63 and p73 do not contribute to p53-mediated lymphoma suppressor activity in vivo. Oncogene. 2005; 24:5521-5524.

16. Chakrabarti R, Wei Y, Hwang J, Hang X, Andres Blanco M, Choudhury A, Tiede B, Romano RA, DeCoste C, Mercatali L, Ibrahim T, Amadori D, Kannan N, et al. DeltaNp63 promotes stem cell activity in mammary gland development and basal-like breast cancer by enhancing Fzd7 expression and Wnt signalling. Nat Cell Biol. 2014; 16:1004-1015,1001-1013.

17. Su X, Chakravarti D, Cho MS, Liu L, Gi YJ, Lin YL, Leung ML, El-Naggar A, Creighton CJ, Suraokar MB, Wistuba I and Flores ER. TAp63 suppresses metastasis through coordinate regulation of Dicer and miRNAs. Nature. 2010; 467:986-990.

18. Guo X, Keyes WM, Papazoglu C, Zuber J, Li W, Lowe SW, Vogel H and Mills AA. TAp63 induces senescence and suppresses tumorigenesis in vivo. Nat Cell Biol. 2009; 11:1451-1457.

19. Xu E, Zhang J, Zhang M, Jiang Y, Cho SJ and Chen X. RNA-binding protein RBM24 regulates p63 expression via mRNA stability. Mol Cancer Res. 2014; 12:359-369.

20. Truong AB, Kretz M, Ridky TW, Kimmel R and Khavari PA. p63 regulates proliferation and differentiation of developmentally mature keratinocytes. Genes Dev. 2006; 20:3185-3197.

21. Hedvat CV, Teruya-Feldstein J, Puig P, Capodieci P, Dudas M, Pica N, Qin J, Cordon-Cardo C and Di Como CJ. Expression of p63 in diffuse large B-cell lymphoma. Appl Immunohistochem Mol Morphol. 2005; 13:237-242.

22. Danilova N, Sakamoto KM and Lin S. p53 family in development. Mech Dev. 2008; 125:919-931.

23. Wolff S, Talos F, Palacios G, Beyer U, Dobbelstein M and Moll UM. The alpha/beta carboxy-terminal domains of p63 are required for skin and limb development. New insights from the Brdm2 mouse which is not a complete p63 knockout but expresses p63 gamma-like proteins. Cell Death Differ. 2009; 16:1108-1117.

24. Okada Y, Osada M, Kurata S, Sato S, Aisaki K, Kageyama Y, Kihara K, Ikawa Y and Katoh I. p53 gene family p51(p63)-encoded, secondary transactivator p51B(TAp63alpha) occurs without forming an immunoprecipitable complex with MDM2, but responds to genotoxic stress by accumulation. Exp Cell Res. 2002; 276:194-200.

25. Di Como CJ, Urist MJ, Babayan I, Drobnjak M, Hedvat CV, Teruya-Feldstein J, Pohar K, Hoos A and Cordon-Cardo C. p63 expression profiles in human normal and tumor tissues. Clin Cancer Res. 2002; 8:494-501.

26. Nylander K, Vojtesek B, Nenutil R, Lindgren B, Roos G, Zhanxiang W, Sjostrom B, Dahlqvist A and Coates PJ. Differential expression of p63 isoforms in normal tissues and neoplastic cells. J Pathol. 2002; 198:417-427.

27. Hallack Neto AE, Siqueira SA, Dulley FL, Ruiz MA, Chamone DA and Pereira J. p63 protein expression in high risk diffuse large B-cell lymphoma. J Clin Pathol. 2009; 62:77-79.

28. Alexandrova EM and Moll UM. Role of p53 family members p73 and p63 in human hematological malignancies. Leuk Lymphoma. 2012; 53:2116-2129.

29. Aubry MC, Roden A, Murphy SJ, Vasmatzis G, Johnson SH, Harris FR, Halling G, Knudson RA, Ketterling RP and Feldman AL. Chromosomal rearrangements and copy number abnormalities of TP63 correlate with p63 protein expression in lung adenocarcinoma. Mod Pathol. 2015; 28:359-366.

30. Geddert H, Kiel S, Heep HJ, Gabbert HE and Sarbia M. The role of p63 and deltaNp63 (p40) protein expression and gene

amplification in esophageal carcinogenesis. Hum Pathol. 2003; 34:850-856.

31. Ying H, Chang DL, Zheng H, McKeon F and Xiao ZX. DNA-binding and transactivation activities are essential for TAp63 protein degradation. Mol Cell Biol. 2005; 25:6154-6164.

32. Lo Muzio L, Santarelli A, Caltabiano R, Rubini C, Pieramici T, Trevisiol L, Carinci F, Leonardi R, De Lillo A, Lanzafame S, Bufo P and Piattelli A. p63 overexpression associates with poor prognosis in head and neck squamous cell carcinoma. Hum Pathol. 2005; 36:187-194.

33. Stetsenko GY, Malekirad J, Paulson KG, Iyer JG, Thibodeau RM, Nagase K, Schmidt M, Storer BE, Argenyi ZB and Nghiem P. p63 expression in Merkel cell carcinoma predicts poorer survival yet may have limited clinical utility. Am J Clin Pathol. 2013; 140:838-844.

34. Takahashi Y, Noguchi T, Takeno S, Kimura Y, Okubo M and Kawahara K. Reduced expression of p63 has prognostic implications for patients with esophageal squamous cell carcinoma. Oncol Rep. 2006; 15:323-328.

35. Alizadeh AA, Eisen MB, Davis RE, Ma C, Lossos IS, Rosenwald A, Boldrick JC, Sabet H, Tran T, Yu X, Powell JI, Yang L, Marti GE, et al. Distinct types of diffuse large B-cell lymphoma identified by gene expression profiling. Nature. 2000; 403:503-511.

36. Testoni M, Zucca E, Young KH and Bertoni F. Genetic lesions in diffuse large B-cell lymphomas. Ann Oncol. 2015. 26:1069-1080

37. Xu-Monette ZY, Wu L, Visco C, Tai YC, Tzankov A, Liu WM, Montes-Moreno S, Dybkaer K, Chiu A, Orazi A, Zu Y, Bhagat G, Richards KL, et al. Mutational profile and prognostic significance of TP53 in diffuse large B-cell lymphoma patients treated with R-CHOP: report from an International DLBCL Rituximab-CHOP Consortium Program Study. Blood. 2012; 120:3986-3996.

38. Xu-Monette ZY, Moller MB, Tzankov A, Montes-Moreno S, Hu W, Manyam GC, Kristensen L, Fan L, Visco C, Dybkaer K, Chiu A, Tam W, Zu Y, et al. MDM2 phenotypic and genotypic profiling, respective to TP53 genetic status, in diffuse large B-cell lymphoma patients treated with rituximab-CHOP immunochemotherapy: a report from the International DLBCL Rituximab-CHOP Consortium Program. Blood. 2013; 122:2630-2640.

39. Park CK and Oh YH. Expression of p63 in reactive hyperplasias and malignant lymphomas. J Korean Med Sci. 2005; 20:752-758.

40. Vasmatzis G, Johnson SH, Knudson RA, Ketterling RP, Braggio E, Fonseca R, Viswanatha DS, Law ME, Kip NS, Ozsan N, Grebe SK, Frederick LA, Eckloff BW, et al. Genome-wide analysis reveals recurrent structural abnormalities of TP63 and other p53-related genes in peripheral T-cell lymphomas. Blood. 2012; 120:2280-2289.

41. Scott DW, Mungall KL, Ben-Neriah S, Rogic S, Morin RD, Slack GW, Tan KL, Chan FC, Lim RS, Connors JM, Marra MA, Mungall AJ, Steidl C, et al. TBL1XR1/TP63: a novel recurrent gene fusion in B-cell non-Hodgkin lymphoma. Blood. 2012; 119:4949-4952.

42. van Keimpema M, Gruneberg LJ, Mokry M, van Boxtel R, Koster J, Coffer PJ, Pals ST and Spaargaren M. FOXP1 directly represses transcription of proapoptotic genes and cooperates with NF-kappaB to promote survival of human B cells. Blood. 2014; 124:3431-3440.

43. Fukushima N, Satoh T, Sueoka N, Sato A, Ide M, Hisatomi T, Kuwahara N, Tomimasu R, Tsuneyoshi N, Funai N, Sano M, Tokunaga O and Sueoka E. Clinico-pathological characteristics of p63 expression in B-cell lymphoma. Cancer Sci. 2006; 97:1050-1055.

44. Hu S, Xu-Monette ZY, Tzankov A, Green T, Wu L, Balasubramanyam A, Liu WM, Visco C, Li Y, Miranda RN, Montes-Moreno S, Dybkaer K, Chiu A, et al. MYC/BCL2 protein coexpression contributes to the inferior survival of activated B-cell subtype of diffuse large B-cell lymphoma and demonstrates high-risk gene expression signatures: a report from The International DLBCL Rituximab-CHOP Consortium Program. Blood. 2013; 121:4021-4031; quiz4250.

45. Zhang Y, Liao JM, Zeng SX and Lu H. p53 downregulates Down syndrome-associated DYRK1A through miR-1246. EMBO reports. 2011; 12:811-817.

46. Chen J, Xu-Monette ZY, Deng L, Shen Q, Manyam GC, Martinez-Lopez A, Zhang L, Montes-Moreno S, Visco C, Tzankov A, Yin L, Dybkaer K, Chiu A, et al. Dysregulated CXCR4 expression promotes lymphoma cell survival and independently predicts disease progression in germinal center B-cell-like diffuse large B-cell lymphoma. Oncotarget. 2015; 6:5597-5614. DOI: 10.18632/oncotarget.3343.

47. Li Y and Prives C. Are interactions with p63 and p73 involved in mutant p53 gain of oncogenic function? Oncogene. 2007; 26:2220-2225.

48. Dietz S, Rother K, Bamberger C, Schmale H, Mossner J andEngeland K. Differential regulation of transcription and induction of programmed cell death by human p53-family members p63 and p73. FEBS Lett. 2002; 525:93-99.

49. Gaiddon C, Lokshin M, Ahn J, Zhang T and Prives C. A subset of tumor-derived mutant forms of p53 down-regulate p63 and p73 through a direct interaction with the p53 core domain. Mol Cell Biol. 2001; 21:1874-1887.

50. Strano S, Fontemaggi G, Costanzo A, Rizzo MG, Monti O, Baccarini A, Del Sal G, Levrero M, Sacchi A, Oren M and Blandino G. Physical interaction with human tumor-derived p53 mutants inhibits p63 activities. J Biol Chem. 2002; 277:18817-18826.

51. Calabro V, Mansueto G, Parisi T, Vivo M, Calogero RA and La Mantia G. The human MDM2 oncoprotein increases the transcriptional activity and the protein level of the p53 homolog p63. J Biol Chem. 2002; 277:2674-2681.

52. Calabro V, Mansueto G, Santoro R, Gentilella A, Pollice A, Ghioni P, Guerrini L and La Mantia G. Inhibition of p63 transcriptional activity by p14ARF: functional and physical link between human ARF tumor suppressor and a member of the p53 family. Mol Cell Bio. 2004; 24:8529-8540.

53. Kadakia M, Slader C and Berberich SJ. Regulation of p63 function by Mdm2 and MdmX. DNA Cell Biol. 2001; 20:321-330.

54. Gonfloni S, Di Tella L, Caldarola S, Cannata SM, Klinger FG, Di Bartolomeo C, Mattei M, Candi E, De Felici M, Melino G and Cesareni G. Inhibition of the c-Abl-TAp63 pathway protects mouse oocytes from chemotherapy-induced death. Nature medicine. 2009; 15:1179-1185.

55. Visco C, Li Y, Xu-Monette ZY, Miranda RN, Green TM, Li Y, Tzankov A, Wen W, Liu WM, Kahl BS, d'Amore ES, Montes-Moreno S, Dybkaer K, et al. Comprehensive gene expression profiling and immunohistochemical studies support application of immunophenotypic algorithm for molecular subtype classification in diffuse large B-cell lymphoma: a report from the International DLBCL Rituximab-CHOP Consortium Program Study. Leukemia. 2012; 26:2103-2113.

56. Tzankov A, Xu-Monette ZY, Gerhard M, Visco C, Dirnhofer S, Gisin N, Dybkaer K, Orazi A, Bhagat G, Richards KL, Hsi ED, Choi

WW, van Krieken JH, et al. Rearrangements of MYC gene facilitate risk stratification in diffuse large B-cell lymphoma patients treated with rituximab-CHOP. Mod Pathol. 2014; 27:958-971.

57. Ok CY, Chen J, Xu-Monette ZY, Tzankov A, Manyam GC, Li L, Visco C, Montes-Moreno S, Dybkaer K, Chiu A, Orazi A, Zu Y, Bhagat G, et al. Clinical Implications of Phosphorylated STAT3 Expression in De Novo Diffuse Large B-cell Lymphoma. Clin Cancer Res. 2014; 20:5113-5123.

58. Hu S, Xu-Monette ZY, Balasubramanyam A, Manyam GC, Visco C, Tzankov A, Liu WM, Miranda RN, Zhang L, Montes-Moreno S, Dybkaer K, Chiu A, Orazi A, et al. CD30 expression defines a novel subgroup of diffuse large B-cell lymphoma with favorable prognosis and distinct gene expression signature: a report from the International DLBCL Rituximab-CHOP Consortium Program Study. Blood. 2013; 121:2715-2724.

59. Visco C, Tzankov A, Xu-Monette ZY, Miranda RN, Tai YC, Li Y, Liu WM, d'Amore ES, Li Y, Montes-Moreno S, Dybkaer K, Chiu A, Orazi A, et al. Patients with diffuse large B-cell lymphoma of germinal center origin with BCL2 translocations have poor outcome, irrespective of MYC status: a report from an International DLBCL rituximab-CHOP Consortium Program Study. Haematologica. 2013; 98:255-263.

60. Xu-Monette ZY, Dabaja BS, Wang X, Tu M, Manyam GC, Tzankov A, Xia Y, Li Zhang, Visco C, Dybkaer K, Yin L, Chiu A, Orazi A, et al. Clinical features, tumor biology and prognosis associated with MYC rearrangement and overexpression in diffuse large B-cell lymphoma patients treated with rituximab-CHOP. Modern Pathology. 2015; 28:1555-1573.

SUPPLEMENTAL DATA

Please browse the Full Text version of this manuscript to see Supplemental Figures and Tables.

Review

The PTEN tumor suppressor gene and its role in lymphoma pathogenesis

Xiaoxiao Wang[1,2], Huiqiang Huang[2], and Ken H. Young[1,3]

[1]Department of Hematopathology, The University of Texas M. D. Anderson Cancer Center, Houston, TX 77230, USA
[2]Department of Medical Oncology, Sun Yat-Sen University Cancer Center, Guangzhou, Guangdong, China
[3]The University of Texas Graduate School of Biomedical Science, Houston, TX 77230, USA

Key words: PTEN, tumor suppressor, PI3K, AKT, mTOR, lymphoid malignancies, diffuse large B-cell lymphoma
Key points: PTEN deficiency is related to poor clinical outcomes in patients with a variety of tumors Nuclear and cytoplasmic PTEN has distinct functions in tumor suppression
Received: 09/04/15; Accepted: 11/02/15; Published: 12/10/15 **doi:** 10.18632/aging.100855
Correspondence to: Ken H. Young, MD/PhD; **E-mail:** khyoung@mdanderson.org

Abstract: The phosphatase and tensin homolog gene *PTEN* is one of the most frequently mutated tumor suppressor genes in human cancer. Loss of PTEN function occurs in a variety of human cancers via its mutation, deletion, transcriptional silencing, or protein instability. PTEN deficiency in cancer has been associated with advanced disease, chemotherapy resistance, and poor survival. Impaired PTEN function, which antagonizes phosphoinositide 3-kinase (PI3K) signaling, causes the accumulation of phosphatidylinositol (3,4,5)-triphosphate and thereby the suppression of downstream components of the PI3K pathway, including the protein kinase B and mammalian target of rapamycin kinases. In addition to having lipid phosphorylation activity, PTEN has critical roles in the regulation of genomic instability, DNA repair, stem cell self-renewal, cellular senescence, and cell migration. Although PTEN deficiency in solid tumors has been studied extensively, rare studies have investigated PTEN alteration in lymphoid malignancies. However, genomic or epigenomic aberrations of *PTEN* and dysregulated signaling are likely critical in lymphoma pathogenesis and progression. This review provides updated summary on the role of PTEN deficiency in human cancers, specifically in lymphoid malignancies; the molecular mechanisms of PTEN regulation; and the distinct functions of nuclear PTEN. Therapeutic strategies for rescuing PTEN deficiency in human cancers are proposed.

INTRODUCTION

The phosphatase and tensin homolog gene, *PTEN*, is one of the most commonly mutated tumor suppressors in human malignancies [1-5], and complete loss of PTEN protein expression is significantly associated with advanced cancer and poor outcome [6, 7]. The importance of *PTEN* as a tumor suppressor is further supported by the fact that germline mutations of *PTEN* commonly occur in a group of autosomal dominant syndromes, including Cowden Syndrome, which are characterized by developmental disorders, neurological deficits, and an increased lifetime risk of cancer and are collectively referred to as PTEN hamartoma tumor syndromes (PHTS) [8, 9].

Biochemically, PTEN is a phosphatase that dephosphorylates phosphatidylinositol (3,4,5)-triphosphate (PIP_3), the lipid product of class I phosphoinositide 3-kinase (PI3K) [10]. To date, PTEN is the only lipid phosphatase known to counteract the PI3K pathway. Unsurprisingly, loss of PTEN has a substantial impact on multiple aspects of cancer development. Strikingly, PTEN has distinct growth-regulatory roles depending on whether it is in the cytoplasm or nucleus. In the cytoplasm, PTEN has

intrinsic lipid phosphatase activity that negatively regulates the cytoplasmic PI3K/AKT pathway, whereas in the nucleus, PTEN has AKT-independent growth activities. The continued elucidation of the roles of nuclear PTEN will help uncover the various functions of this essential tumor suppressor gene.

In this review, we describe the molecular basis of PTEN loss, discuss the regulation of PTEN expression in lymphoid malignancies, and summarize potential therapeutic targets in PTEN-deficient cancers.

STRUCTURE AND FUNCTION OF PTEN

PTEN structure

PTEN is a tumor suppressor gene located on chromosome 10q23.31 that encodes for a 403-amino acid protein that has both lipid and protein phosphatase activities. PTEN gene and protein structures are shown in Figure 1. The PTEN protein contains a sequence motif that is highly conserved in members of the protein tyrosine phosphatase family. Structurally, the PTEN protein is composed of two major functional domains (a phosphatase domain and a C2 domain) and three structural regions (a short N-terminal phosphatidylinositol [4,5]-bisphosphate [PIP_2]-binding domain, a C-terminal tail containing proline-glutamic acid-serine-threonine sequences, and a PDZ-interaction motif) [11]. The PIP_2-binding site and adjacent cytoplasmic localization signal are located at the protein's N-terminal [12, 13].

The PI3K/PTEN/AKT/mTOR pathway

PTEN's tumor-suppressing function largely relies on the protein's phosphatase activity and subsequent antagonism of the PI3K/AKT/mammalian target of rapamycin (mTOR) pathway. Following PTEN loss, excessive PIP_3 at the plasma membrane recruits and activates a subset of pleckstrin homology domain–containing proteins to the cell membrane. These proteins

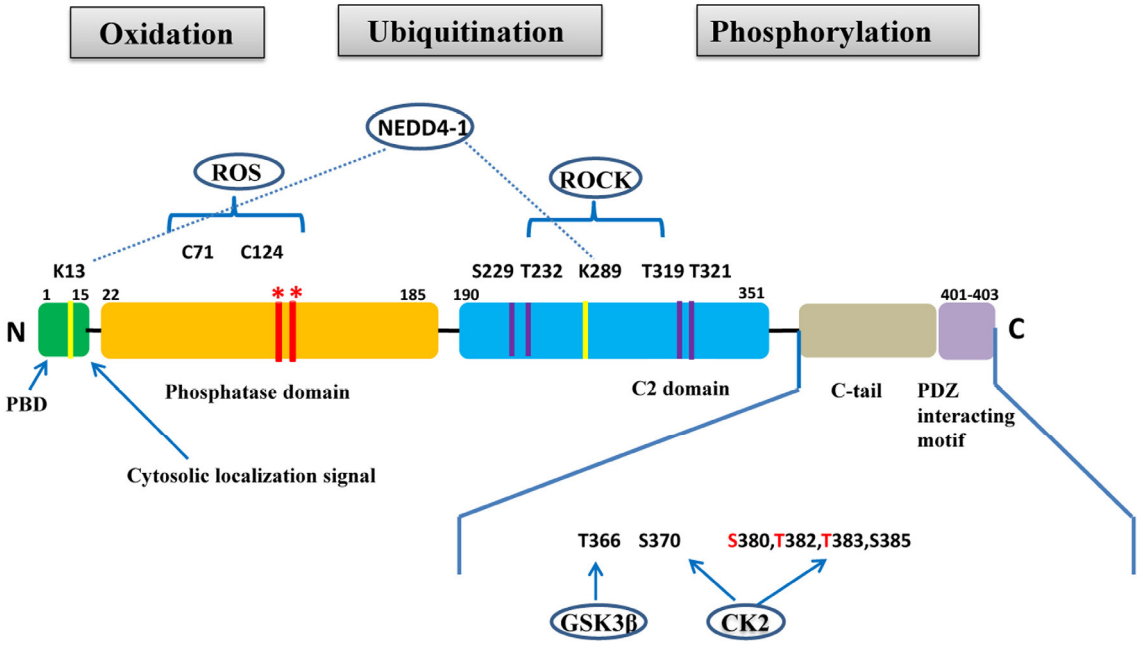

Figure 1. PTEN gene and protein structures. The PTEN protein is composed of 403 amino acids and contains an N-terminal PIP_2-binding domain (PBD), a phosphatase domain, a C2 domain, a C-terminal tail containing proline–glutamic acid–serine–threonine sequences, and a PDZ interacting motif at the end. *Mutations on the phosphatase domain that disrupt PTEN's phosphatase activity include the C124S mutation, which abrogates both the lipid and protein phosphatase activity of PTEN, and the G129E mutation, which abrogates only the lipid phosphatase activity of PTEN. The C-terminal tail residues phosphorylated by glycogen synthase kinase 3β (GSK3β) and casein kinase 2 (CK2) are shown. Mutations of S380, T382, and T383 (referred to as the STT) can destabilize PTEN and increase its phosphatase activity. The PIP_2-binding site and adjacent cytoplasmic localization signal are located at the N-terminal. The N-terminal poly-basic region appears to selectively interact with PIP_2 and contribute to the nuclear accumulation of PTEN. Ubiquitination of PTEN has also been found on K13 and K289.

include phosphoinositide-dependent kinase-1 and AKT family members [14, 15]. AKT activation also leads to the activation of the mTOR kinase complex 1 through the inhibition of the phosphorylation of tuberous sclerosis complex tumor suppressors and consequent activation of the small GTPase rat sarcoma (RAS) homologue enriched in brain. The active mTOR complex 1 phosphorylates the p70 ribosomal protein S6 kinase (S6K) and inhibits 4E-binding protein 1 to activate protein translation [16]. Accordingly, the PTEN/PI3K/AKT/mTOR pathway is emerging as a vital target for anti-cancer agents, especially in tumors with mTOR pathway activation.

AKT-independent roles of PTEN

Although AKT pathway activation can explain many of the phenotypes associated with PTEN inactivation, *PTEN* gene targeting and genetic activation of *AKT* do not have completely overlapping biological consequences. Using transcriptional profiling, Vivanco et al. identified a new PTEN-regulated pathway, the Jun-N-terminal kinase (JNK) pathway, which was constitutively activated upon PTEN knockdown [17]. In the study, PTEN null cells had higher JNK activity than PTEN positive cells did, and genetic analysis indicated that JNK functioned parallel to and independently of AKT. Thus, the blockade of PI3K signaling may shift the survival signal to the AKT-independent PTEN-regulated pathway, implicated JNK and AKT as complementary signals in PIP_3-driven tumorigenesis and suggest that JNK may be a therapeutic target in *PTEN* null tumors.

In addition to its lipid phosphatase function, PTEN also has lipid phosphatase–independent roles. PTEN has been shown to inhibit cell migration through its C2 domain, independent of PTEN's lipid phosphatase activity [18]. In breast cancer, PTEN deficiency has been shown to activate, in a manner dependent on its protein phosphatase activity, the SRC proto-oncogene, non-receptor tyrosine kinase (SRC), thereby conferring resistance to human epidermal growth factor receptor 2 inhibition [19]. Furthermore, PTEN has been shown to directly bind to tumor protein 53 (p53), regulate its stability, and increase its transcription, thereby increasing P53 protein levels [20].

PTEN REGULATION

Genetic alteration of *PTEN*

PTEN loss of function occurs in a wide spectrum of human cancers through various genetic alterations that include point mutations (missense and nonsense mutations), large chromosomal deletions (homozygous/ heterozygous deletions, frameshift deletions, in-frame deletions, and truncations), and epigenetic mechanisms (e.g., hypermethylation of the *PTEN* promoter region) [21]. Somatic mutations are the main drivers of PTEN inactivation in human cancers, and have been reviewed extensively [22].

PTEN's tumor suppressor function is usually abrogated following mutations in its phosphatase domain, which is encoded by exon 5 [23] (Figure 1). These mutations typically include a C124S mutation that abrogates both lipid and protein phosphatase activity and a G129E mutation that abrogates lipid phosphatase but not protein phosphatase activity [24]. Although the N-terminal phosphatase domain is principally responsible for PTEN's physiological activity, approximately 40% of tumorigenic *PTEN* mutations occur in the C-terminal C2 domain (corresponding to exons 6, 7, and 8) and in the tail sequence (corresponding to exon 9), which encode for tyrosine kinase phosphorylation sites. This suggests that the C-terminal sequence is critical for maintaining PTEN function and protein stability [21, 23, 25, 26]. However, many tumor-derived *PTEN* mutants retain partial or complete catalytic function, suggesting that alterative mechanisms can lead to PTEN inactivation.

Transcriptional regulation

In addition to gene mutations, complete or partial loss of PTEN protein expression may impact PTEN's tumor suppression ability. The regulation of PTEN's functions and signaling pathway is shown in Figure 2. Positive regulators of PTEN gene expression include early growth response protein 1, peroxisome proliferator-activated receptor γ (PPARγ) and P53, which have been shown to directly bind to the PTEN promoter region [27-29]. Early growth response protein 1, which regulates PTEN expression during the initial steps of apoptosis, has been shown to directly upregulate the expression of PTEN in non–small cell lung cancer. PPARγ is a ligand-activated transcription factor with anti-inflammatory and anti-tumor effects. The activation of its selective ligand, rosiglitazone, leads to the binding of PPARγ at two PTEN promoter sites, PPAR response element 1 and PPAR response element 2, thus upregulating PTEN and inhibiting PI3K activity. Negative regulators of PTEN gene expression include mitogen-activated protein kinase kinase-4, transforming growth factor beta (TGF-β), nuclear factor of kappa light polypeptide gene enhancer in B-cells (NF-κB), IGF-1, the transcriptional cofactor c-Jun proto-oncogene, and the B-cell-specific Moloney murine leukemia virus insertion site 1 (BMI1) proto-oncogene, which have been shown to suppress PTEN expression in

several cancer models [30-32]. Research found that IGF-1 could affect cell proliferation and invasion by suppressing PTEN's phosphorylation. In pancreatic cancers, TGF-β significantly suppresses PTEN protein levels concomitant with the activation of AKT through transcriptional reduction of PTEN mRNA–induced growth promotion. c-Jun negatively regulates the expression of PTEN by binding to the activator protein 1 site of the PTEN promoter, resulting in the concomitant activation of the AKT pathway. *PTEN* transcription is also directly repressed by the leukemia-associated factor ecotropic virus integration site 1 protein in the hematopoietic system [33].

Intriguingly, recent studies reported a complex crosstalk between PTEN and other pathways. For example, RAS has been found to mediate the suppression of PTEN through a TGF-β dependent mechanism in pancreatic cancer [34], and the mitogen-associated protein kinase/extracellular signal-related kinase pathway has been found to suppress PTEN transcription through c-Jun [35]. Finally, the stress kinase pathways including mitogen-activated protein kinase kinase kinase 4 and JNK promote resistance to apoptosis by suppressing PTEN transcription via direct binding of NF-κB to the PTEN promoter [36]. These findings suggest that the pathways that are negatively regulated by PTEN can in turn regulate PTEN transcription, indicating a potential feedback loop. Studies have also shown that CpG islands hypermethylated in the *PTEN* promoter lead to the silencing of *PTEN* transcription in human cancer [37].

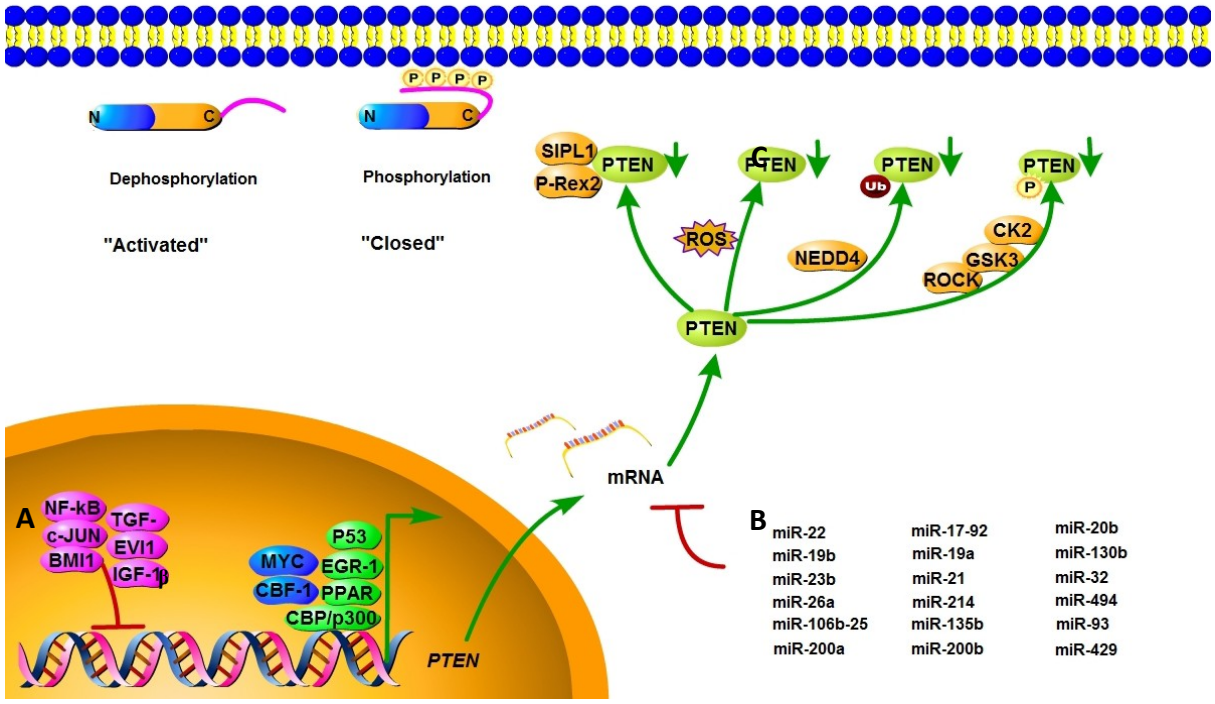

Figure 2. Mechanisms of PTEN regulation. PTEN is regulated at different levels. (**A**) PTEN mRNA transcription is activated by early growth response protein 1, P53, MYC, PPARγ, C-repeat binding factor 1, and others, and inhibited by NF-κB, proto-oncogene c-Jun, TGF-β, and BMI-1. (**B**) PTEN mRNA is also post-transcriptionally regulated by PTEN-targeting miRNAs, including miR-21, miR-17-92, and others. (**C**) Active site phosphorylation, ubiquitination, oxidation, acetylation, and protein-protein interactions can also regulate PTEN activity. The phosphorylation leads to a "closed" state of PTEN and maintains PTEN stability. Dephosphorylation of the C-terminal tail opens the PTEN phosphatase domain, thereby activating PTEN.

Table 1. MiRNAs which downregulate PTEN expression in human cancers.

miRNA	Locus	Expression status	Tumor type	Reference
MiR-21	17q23.1	Upregulated	Colorectal, bladder, and hepatocellular cancer	[112-114]
MiR-19a	13q31.3	Upregulated	Lymphoma and CLL	[87, 115]
MiR-19b	Xq26.2	Upregulated	Lymphoma	[87]
MiR-22	17p13.3	Upregulated	Prostate cancer and CLL	[116, 117]
MiR-32	9q31.3	Upregulated	Hepatocellular carcinoma	[118]
MiR-93	7q22.1	Upregulated	Hepatocellular carcinoma	[119]
MiR-494	14q32.31	Upregulated	Cervical cancer	[120]
MiR-130b	22q11.21	Upregulated	Esophageal carcinoma	[121]
MiR-135b	1q32.1	Upregulated	Colorectal cancer	[122]
MiR-214	1q24.3	Upregulated	Ovarian cancer	[123]
MiR-26a	3p22.2 (MIR26A1) 12q14.1(MIR26A2)	Upregulated	Prostate cancer	[113]
MiR-23b	9q22.32	Upregulated	Prostate cancer	[114]

Abbreviations: CLL, chronic lymphocytic leukemia.

Translational and post-translational regulation

MicroRNAs (miRNAs) are a class of endogenous, 20- to 25-nucleotide single-stranded non-coding RNAs that repress mRNA translation by base-pairing with target mRNAs [38]. Various miRNAs are known to impact PTEN expression in both normal and pathological conditions. In multiple human cancers, PTEN expressions are downregulated by miRNAs, which are shown in Table 1.

Post-translational modifications, such as active site phosphorylation, ubiquitination, oxidation, and acetylation, can also regulate PTEN activity [39]. In its inactivated state, PTEN is phosphorylated on a cluster of serine and threonine residues located on its C-terminal tail, leading to a "closed" PTEN state in which PTEN protein stability is maintained. As PTEN is being activated, dephosphorylation of its C-terminal tail opens its phosphatase domain, thereby increasing PTEN activity (Figure 2). The phosphorylation of PTEN at specific residues of the C-terminal tail (Thr366, Ser370, Ser380, Thr382, Thr383, and Ser385) is associated with increased protein stability, whereas phosphorylation at other sites may decrease protein stability. Although S370 and S385 have been identified as the major sites for PTEN phosphorylation, mutations of these residues have minimal effects on PTEN function, whereas mutations of S380, T382, and T383 can destabilize PTEN and increase its phosphatase activity, thereby enhancing PTEN's interaction with binding partners [40]. The "open" state of PTEN is more susceptible to ubiquitin-mediated proteasome degradation [13]. One recently identified E3 ligase of PTEN is neural precursor cell-expressed, developmentally down-regulated 4, E3 ubiquitin protein ligase 1 (NEDD4-1), which mediates PTEN mono- and poly-ubiquitination [41] (Figure 3). In cancer, the inhibition of NEDD4-1, whose expression has been found to be inversely correlated with PTEN levels in bladder cancer, may

upregulate PTEN levels [42]. Two major conserved sites for PTEN are K13 and K289, and ubiquitination of these sites is indispensable for the nuclear-cytoplasmic shuttling of PTEN (Figure 1).

Protein-protein interactions

PTEN contains a 3–amino acid C-terminal region that is able to bind to PDZ domain–containing proteins [43, 44]. PDZ domains are involved in the assembly of multi-protein complexes that may control the localization of PTEN and its interaction with other proteins. A number of PTEN-interacting proteins have been shown to regulate PTEN protein levels and activities. These interactions, which help recruit PTEN to the membrane, can be negatively modulated by the phosphorylation of PTEN on its C terminus [40, 45]. The phosphorylation of the C terminal end of PTEN has been attributed to the activities of casein kinase 2 and glycogen synthase kinase 3β [46, 47]. In addition, evidence suggests that the C2 domain of PTEN can be phosphorylated by RhoA-associated kinase, which may have important roles in the regulation of chemoattractant-induced PTEN localization [48] (Figure 2).

Acetylation and oxidation also contribute to PTEN activity regulation. PTEN's interaction with nuclear histone acetyltransferase–associated p300/cAMP response element-binding protein (CREB)-binding protein (CBP)–associated factor can promote PTEN acetylation, and this acetylation negatively regulates the catalytic activity of PTEN [49]. Studies have shown that the PTEN protein becomes oxidized in response to the endogenous generation of the reactive oxygen species (ROS) stimulated by growth factors and insulin, and this oxidation correlates with a ROS-dependent activation of downstream AKT phosphorylation [50, 51]. Other studies have shown that the PIP_3-dependent Rac exchange factor 2 and SHANK-associated RH domain interactor proteins bind directly to PTEN to inhibit its lipid phosphatase activity [52, 53]. High P53 expression triggers proteasome degradation of the PTEN protein [54]. In addition to antagonizing the AKT–mouse double minute 2 homolog pathway in a phosphatase-dependent manner, PTEN also can interact with P53 directly in a phosphatase-independent manner, thereby stabilizing P53 [55, 56].

PTEN IN THE NUCLEUS

Growing evidence suggests that the translocation of PTEN from the nucleus to the cytoplasm leads to malignancy. In the nucleus, PTEN has important tumor-suppressive functions, and the absence of nuclear PTEN is associated with aggressive disease in multiple cancers [57-59], implying that nuclear PTEN is a useful prognostic indicator. PTEN is predominantly localized to the nucleus in primary, differentiated, and resting cells, and nuclear PTEN is markedly reduced in rapidly cycling cancer cells [60, 61], which suggests that PTEN localization is related to cell differentiation status and cell cycle stage. High expression levels of nuclear PTEN have been associated with cell-cycle arrest at the G0/G1 phase, indicating a role of nuclear PTEN in cell growth inhibition [62]. PTEN's cytoplasmic and nuclear functions are shown in Figure 3.

PTEN enters the nucleus via its calcium-dependent interaction with the major vault protein [63], through passive diffusion [64], and by a Ran-GTPase–dependent pathway [65]. Moreover, monoubiquitination mediates PTEN's nuclear import, whereas polyubiquitination leads to PTEN's degradation in the cytoplasm [66] (Figure 3). The nuclear exportation of PTEN via a chromosome region maintenance 1–dependent mechanism during the G1-S phase transition is directly regulated by S6K, a downstream effector of the PI3K signaling pathway [67] (Figure 3). Thus, PTEN is preferentially expressed in the cytoplasm of tumor cells in which PI3K signaling is frequently activated. Nuclear PTEN has an essential role in the maintenance of chromosomal stability. First, PTEN directly interacts with centromere protein C in a phosphatase-independent manner. Second, PTEN transcriptionally regulates DNA repair by upregulating RAD51 recombinase in a phosphatase-dependent manner [68] (Figure 3). The disruption of nuclear PTEN results in centromere breakage and massive chromosomal aberrations. Nuclear PTEN may also play an important part in transcription regulation by negatively modulating the transcriptional activity of the androgen receptor, hepatocyte growth factor receptor, NF-κB, CREB, and activator protein 1. Moreover, nuclear PTEN has been shown to promote p300/CREB-binding protein–mediated p53 acetylation in the response to DNA damage [69, 70].

Most of the functions of nuclear PTEN are independent of its phosphatase activity and do not involve the PI3K/AKT pathway. Not only PTEN but also activated PI3K and functional PIP_3 have been detected in the nucleus [71], indicating that nuclear PI3K signaling mediates PTEN's antiapoptotic effect through nuclear PIP_3 and nuclear AKT. Nevertheless, only limited evidence suggests that nuclear PTEN has lipid phosphatase functions, as the nuclear pool of PIP_3 is insensitive to PTEN [72].

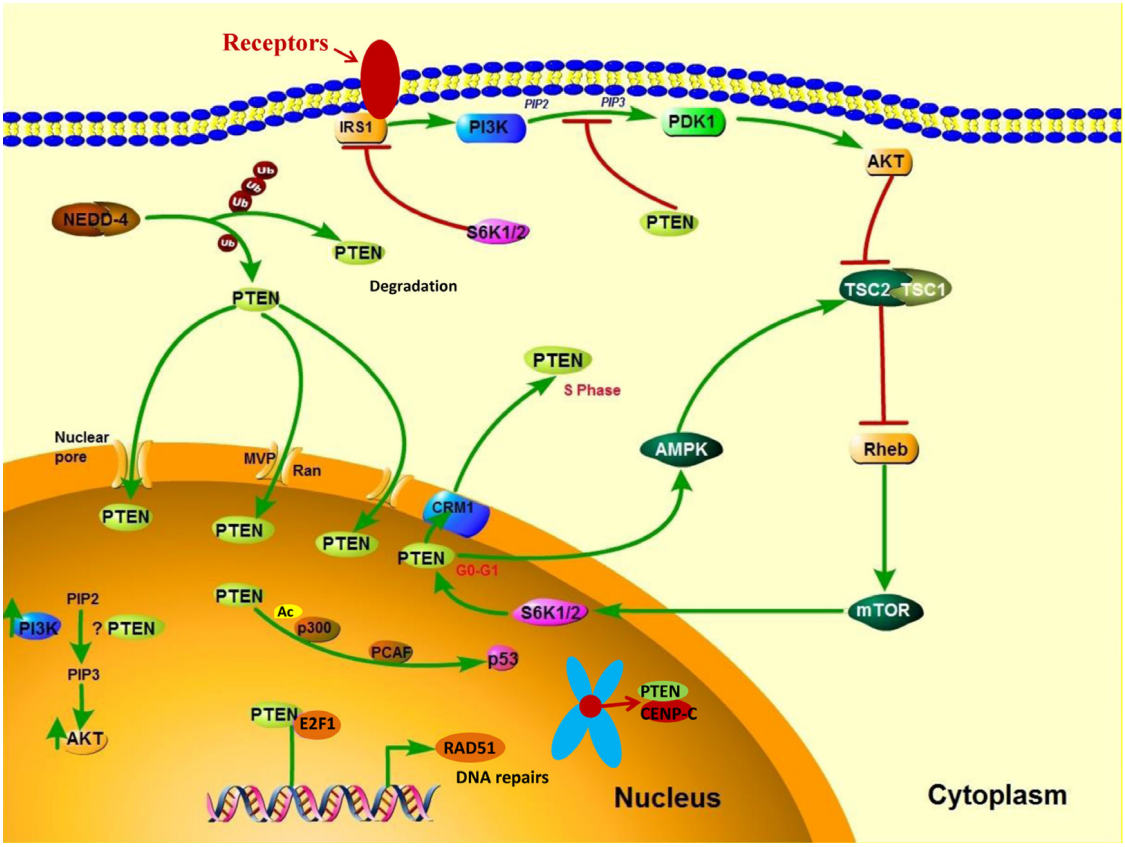

Figure 3. PTEN's cytoplasmic and nuclear functions. In the cytoplasm, PI3K is activated downstream of receptors that include receptor tyrosine kinases, G protein–coupled receptors, cytokine receptors, and integrins. PI3K activation converts PIP_2 to PIP_3, thereby leading to AKT activation, which enhances cell growth, proliferation, and survival. PTEN dephosphorylates PIP_3 and consequently suppresses the PI3K pathway. NEDD4-1 is an E3 ligase of PTEN that mediates PTEN ubiquitination. Polyubiquitination of PTEN leads to its degradation in the plasma, whereas monoubiquitination of PTEN increases its nuclear localization. PTEN can translocate into the nucleus through various mechanisms, including passive diffusion, Ran- or major vault protein–mediated import, and a monoubiquitination-driven mechanism. In the nucleus, PTEN promotes p300-mediated P53 acetylation in response to DNA damage to control cellular proliferation. Nuclear PTEN is also involved in maintaining genomic integrity by binding to centromere protein C (CENPC) and in DNA repair by upregulating RAD51 recombinase (RAD51).

PTEN DEFICIENCY IN LYMPHOMA

PTEN deficiency in T-cell acute lymphoblastic leukemia

PI3K signaling are frequently activated in T-cell acute lymphoblastic leukemia (T-ALL), which mainly due to the absent of PTEN function. Studies have shown that *PTEN* inactivation plays a prominent role in human T-ALL cell lines and primary patients [73-76]. Moreover, *PTEN* mutations have been shown induced resistance to γ-secretase inhibitors, which derepress the constitutively activated NOTCH1 signaling in T-ALL [77]. However, the *PTEN* mutations detected in these studies vary widely. Gutierrez et al. reported that T-ALL patients had a *PTEN* mutation rate of 27% and a *PTEN* deletion rate of 9%, whereas Gedman et al. reported that 27 of 43 (63%) pediatric T-ALL specimens had *PTEN* mutations. In the latter study, the high frequency of *PTEN* mutations may have been due to the fact that approximately 50% of the specimens were patients with relapsed disease. Interestingly, all mutations were identified in the C2 domain of PTEN [75, 76], not in the phosphatase domain as has been reported for other solid tumors [78].

PTEN deficiency in diffuse large B-cell lymphoma

Published reports of *PTEN* gene alterations in lymphoid malignancies are summarized in Table 2. Studies have

reported unexpectedly low frequencies of *PTEN* mutations in DLBCL patients, ranging from 3% to 22% [79-83]. Lenz et al. performed gene expression profiling in primary DLBCL and found that a recurrently altered minimal common region containing *PTEN* was lost in 11% GCB-DLBCL but not in other subtypes, suggesting

Table 2. Reported *PTEN* gene alterations in lymphoid malignancies.

Alteration type	Exon	Domain	Disease	Frequency, %	Notes	Ref
Cell lines						
Del	3-9	PHOS, C2	DLBCL	28.6 (4/14)	Del in 4 of 11 GCB-DLBCL	[85]
Mut	2-5	PHOS, C2	DLBCL	35.7 (5/14)	Mut in 4 of 11 GCB- and 1 of 3 ABC-DLBCL	
Del and Mut	2-7	PHOS, C2		22.2 (6/27)		[82]
Biopsy tissue						
Del			DLBCL	15.3 (4/26)	Heterozygous Del in 3 of 18 GCB- and 1 of 8 ABC-DLBCL	[85]
Del	1	PB	NHL	3.4 (1/29)		[81]
Mut	5, 6	PHOS, C2		6.9 (2/29)		
Del and Mut	1, 8	PHOS, C2	NHL	4.6 (3/65)		[82]
Mut	8	C2	DLBCL	5 (2/39)		[79]
Del			GCB-DLBCL	13.9 (10/72)	Homozygous Del in 2, heterozygous Del in 8	[84]
Mut	1, 2, 7	PB, PHOS, C2	NHL	10 (4/40)		[109]
Mut	7	C2	T-ALL	8 (9/111)		[74]
Del	NA		T-ALL	8.7 (4/46)	Homozygous Del in 2, heterozygous Del in 2	[76]
Mut	7	C2		27.3 (12/44)		
Del and Mut			T-ALL	62.7 (27/43)	Homozygous Del in 8	[75]

Abbreviations: Del, deletion; PHOS, phosphatase; DLBCL, diffuse large B-cell lymphoma; GCB, germinal B-cell–like; Mut, mutation; ABC, activated B-cell–like; NHL, non-Hodgkin lymphoma; T-ALL, T-cell acute lymphoblastic leukemia; AML, acute myeloid leukemia; ALL, acute lymphoblastic leukemia; PB, phosphatidylinositol (4,5)-bisphosphate–binding; NA, not applicable.

that the alteration is exclusive to GCB-DLBCL [84]. More recently, Pfeifer and Lenz found that mutations involving both the phosphatase domain and C2 domain of *PTEN* were prominent in GCB-DLBCL cell lines. Interestingly, 7 of the 11 GCB-DLBCL cell lines had complete loss of PTEN function, whereas all ABC-DLBCL cell lines expressed PTEN, suggesting that *PTEN* mutation may be related to PTEN loss in GCB-DLBCL [85] (Table 2). In the GCB-DLBCL cell lines, PTEN loss was inversely correlated with the constitutive activation of the PI3K/AKT signaling pathway, whereas GCB-DLBCL cell lines with PTEN expression rarely had PI3K/AKT activation. In contrast, all ABC-DLBCL cell lines had PI3K/AKT activation regardless of PTEN status, which suggests that the activation of PI3K/AKT in GCB-DLBCL results from PTEN deficiency. Further, gene set enrichment analysis revealed that the MYC target gene set was significantly downregulated after PTEN induction. Also, inhibition of PI3K/AKT with either PTEN re-expression or PI3K inhibition significantly downregulated MYC expression, suggesting that PTEN loss leads to the upregulation of MYC through the constitutive activation of PI3K/AKT in DLBCL [85].

Although several studies have identified discrepancies in PTEN deficiency between DLBCL subtypes, few studies have investigated PTEN localization in different subcellular compartments, not to mention the prognostic value such information would have in de novo cases. Fridberg et al. found a trend towards a stronger staining intensity of cytoplasmic and nuclear PTEN in 28 non–GCB-DLBCL patients [59], most importantly, they found that the absence of nuclear PTEN expression was correlated with worse survival. This interesting evidence should be corroborated in a larger number of primary samples in further studies.

PTEN deficiency in other lymphomas

Previous studies of mantle cell lymphoma (MCL) showed that although the disease had no detectable genetic alterations of PTEN, it did have extremely low protein expression of PTEN. To determine whether the PI3K/AKT signaling pathway is involved in the pathogenesis of MCL, Rudelius et al. investigated pAKT and PTEN expression in primary MCL specimens and cell lines. Of the 31 MCL specimens, 6 had markedly decreased PTEN expression; of the 4 MCL cell lines, 3 had complete loss of PTEN expression [86]. The authors found no phosphatidyl inositol 3-kinase catalytic subunit (*PIK3CA*) mutations in the primary specimens or cell lines, suggesting that loss of PTEN activates the PI3K/AKT pathway in MCL.

Loss of PTEN protein expression has also been reported in 32% of patients with primary cutaneous DLBCL–leg type and 27% of patients with primary cutaneous follicle center lymphomas. Remarkably, both the expression of miR-106a and that of miR-20a were significantly related to PTEN protein loss ($P<0.01$). Moreover, low PTEN mRNA levels were significantly associated with shorter disease-free survival [87].

PTEN AND SPECIFIC PI3K ISOFORMS

PI3K comprises a regulatory p85 subunit and a catalytic p110 subunit. Of particular interest, Class IA PI3Ks include three p110 isoforms (p110α, p110β, and p110δ), are primarily responsible for phosphorylating PIP_2. *PIK3CA*, the gene encoding the p110α isoform is frequently mutated in various human cancers [88]. In one study, 59% of cases with mutant *PIK3CA* had increased p-AKT levels. Therefore, the constitutive activation of PI3K is another way by which the PTEN pathway can be disturbed in cancer. In their study of 215 DLBCL patients, Abubaker et al. reported that 8% had *PIK3CA* mutations and 37% had loss of PTEN. Both *PIK3CA* mutation and loss of PTEN were correlated with poor survival. However, correlation analysis revealed that most of the *PIK3CA* mutations occurred in cases with PTEN expression ($P=0.0146$). Accordingly, 17 cases with *PIK3CA* mutations were screened for *PTEN* mutations, and none harbored both *PIK3CA* and *PTEN* mutations [89]. This suggests that *PIK3CA* mutation likely functions as an oncogene in DLBCL by contributing to PI3K pathway activation independently of PTEN deficiency.

Both p110α and p110β may generate distinct pools of PIP_3. In response to stimuli, p110α produces an acute flux of PIP_3, which is efficiently coupled to AKT phosphorylation. In contrast, p110β has been proposed to generate a basal level of PIP_3 with little effect on AKT phosphorylation [90]. Moreover, cells with AKT phosphorylation induced by PTEN loss were sensitive to a p110β-specific inhibitor but not a p110α inhibitor both in vitro and in vivo [91, 92], which suggests that the enhancement of basal PIP_3 drive oncogenesis in the absence of PTEN. Another study indicated that *PTEN*-mutant endometrioid endometrial carcinoma cells may not be sufficiently sensitive to the inhibition of p110β alone and that combined targeted agents may be required for effective treatment [93]. This finding may have been due to the fact that mutations of *PTEN* and *PIK3CA* frequently coexist in endometrioid endometrial carcinoma. In contrast, cells with wild-type PTEN seem to engage the p110α or p110δ isoforms. Accordingly, clinical trials of isoform-specific inhibitors are warranted.

Table 3. Preclinical studies of targeted therapeutics in PTEN-deficient tumors.

Inhibitor type	Drug	Study notes	Ref
Class I-PI3K			
Pan	Buparlisib (BKM120)	The drug elicited response in some PTEN-deficient tumors and induced cell death in DLBCL cell lines.	[124]
Pan	SAR245408 (XL147)	The drug significantly inhibited tumor growth in a PTEN-deficient prostate cancer model.	[109]
p110α	BYL719	The drug had antitumor activity in cell lines harboring *PIK3CA* mutations but not in PTEN-deficient solid tumors	[110]
p110β	AZD6482 (KIN-193)	The drug substantially inhibited tumor growth in PTEN-deficient cancer models.	[98]
p110β	GSK2636771	*PTEN*-mutant EEC cell lines were resistant to the drug; the drug decreased cell viability only when combined with a p110α selective inhibitor.	[93]
p110β/δ	AZD8186	The drug inhibited the growth of PTEN-deficient prostate tumors.	[102]
p110α/β	CH5132799	The drug inhibited the growth of some PTEN-deficient tumors in vitro.	[103]
p110γ/δ	IPI-145	The drug significantly inhibited the Loucy cell lines in T-ALL.	[100]
PI3K/mTOR	SF1126	The drug significantly reduced the viability of PTEN-deficient but not PTEN-positive GCB-DLBCL cells.	[104]
PI3K/HDAC	CUDC-907	The drug inhibited growth in multiple cell lines; cell lines with *PIK3CA* or *PTEN*-mutation induced loss of PTEN were markedly sensitive to the drug.	[105]
AKT	MK-2206	The drug had antitumor activity in breast cancer cell lines with *PTEN* or *PIK3CA* mutations.	[106]
mTORC1	Everolimus (RAD001)	PTEN-deficient prostate cancer had greater sensitivity to the drug; glioblastoma cell lines were resistant to the drug.	[107]
	Temsirolimus (CCI-779)	Multiple PTEN-deficient cell lines were remarkably sensitive to the drug.	[108]

Abbreviations: DLBCL, diffuse large B-cell lymphoma; EEC, endometrioid endometrial carcinoma; MCL, mantle cell lymphoma; GCB, germinal B-cell–like.

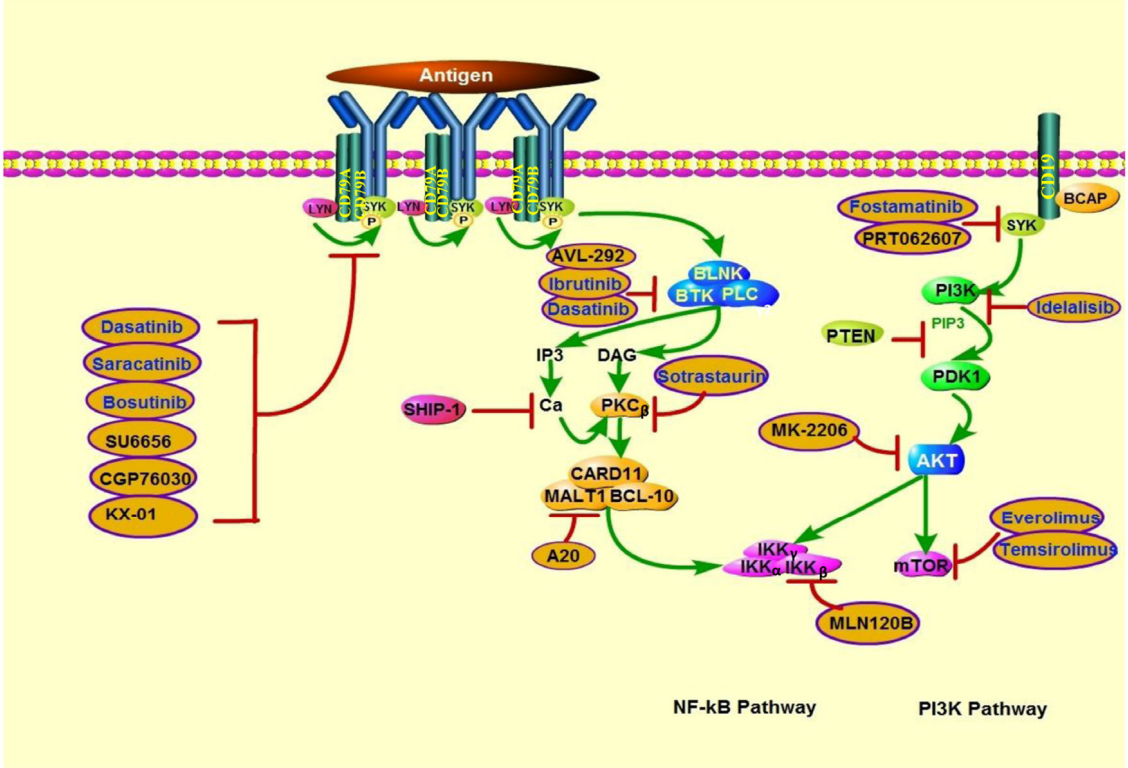

Figure 4. Actions of therapeutics targeting PTEN deficiency in lymphoid malignancies. PTEN deficiency is associated with increased sensitivity to PI3K, AKT, and mTOR inhibitors. In addition, because PI3K is involved in BCR signaling activation, BCR pathway inhibitors may also be effective in PTEN-deficient lymphoid malignancies. SRC family kinase inhibitors include dasatinib (which can also inhibit BTK), saracatinib, bosutinib, SU6656, CGP76030, and KX-01. BTK inhibitors include ibrutinib and AVL-292. Sotrastaurin is a PKCβ inhibitor; A20, a MALT1 paracaspase inhibitor; and MLN120B, an IKKβ inhibitor. SYK inhibitors include fostamatinib and PRT062607. Idelalisib is a PI3Kδ-specific inhibitor. MK-2206 is an AKT inhibitor. mTOR inhibitors include everolimus and temsirolimus.

ENGAGEMENT OF THE PI3K PATHWAY IN B-CELL RECEPTOR SIGNALING

The survival of the majority of B-cell malignancies depends on functional B-cell receptor (BCR) signaling. The successful use of a Bruton tyrosine kinase (BTK) inhibitor to target the BCR pathway in DLBCL has yielded profound discoveries regarding the genetic and biochemical basis of BCR signaling. During BCR signaling, the SRC family kinase LYN phosphorylates the transmembrane protein cluster of differentiation 19, which recruits PI3K to the BCR. The transduction of BCR signaling finally results in the activation of the NF-κB, PI3K, mitogen-associated protein kinase, and nuclear factor of activated T cells pathways, which promote the proliferation and survival of normal and malignant B cells.

BCR signaling is directly affected by frequent mutations in CD79A (immunoglobulin α) and CD79B (immunoglobulin β)-mainly CD79B-which occur in approximately 20% of patients with ABC-DLBCL [94]. Tumor cells harboring CD79B mutations have longer and stronger activation of AKT signaling. Moreover, ABC-DLBCL cell lines with mutated CD79B are more sensitive to PI3K inhibition than those with wild-type CD79B are. Thus, CD79B mutations might be responsible for preventing the negative regulation that interferes with PI3K-dependent pro-survival BCR signaling [95].

Table 4. Preclinical studies of targeted therapeutics in PTEN-deficient tumors.

Inhibitor type	Drug	Patient population	Phase	Identifier
PI3K	GSK2636771	Patients with advanced solid tumors with PTEN deficiency	1/2a	NCT01458067
	BKM120	Patients with recurrent glioblastoma with PTEN mutations or homozygous deletion of PTEN or with PTEN-negative disease	1b/2	NCT01870726
	BKM120	Patients with advanced, metastatic, or recurrent endometrial cancers with PIK3CA gene mutation, PTEN gene mutation, or null/low PTEN protein expression	2	NCT01550380
	AZD8186	Patients with advanced CRPC, sqNSCLC, TNBC, or known PTEN-deficient advanced solid malignancies	1	NCT01884285
PI3K/mTOR	BEZ235	Patients with advanced TCC; group 1 includes patients with no PI3K pathway activation, no loss of PTEN, and no activating PIK3CA mutation; group 2 includes patients with PI3K pathway activation as defined by PIK3CA mutation and/or PTEN loss	2	NCT01856101
	BEZ235	Patients with relapsed lymphoma or multiple myeloma	1	NCT01742988
AKT	MK-2206	Patients with previously treated metastatic colorectal cancer enriched for PTEN loss and PIK3CA mutation	2	NCT01802320
	MK-2206	Patients with advanced breast cancer with a PIK3CA mutation, AKT mutation, and/or PTEN loss or mutation	2	NCT01277757
	Pazopanib + everolimus	Patients with PI3KCA mutations or PTEN loss and advanced solid tumors refractory to standard therapy	1	NCT01430572
	Trastuzumab +RAD001	Patients with HER-2–overexpressing, PTEN-deficient metastatic breast cancer progressing on trastuzumab-based therapy	1/2	NCT00317720
	GDC-0068/ GDC-0980 +abiraterone	Patients previously treated prostate cancer with PTEN loss (currently in phase II)	1b/2	NCT01485861

	Rapamycin (Temsirolimus)	Patients with advanced cancer and PI3K mutation and/or PTEN loss	1/2	NCT00877773
	Ipatasertib (GDC-0068) + paclitaxel	Patients with PTEN-low metastatic TNBC	2	NCT02162719

Abbreviations: CRPC, castrate-resistant prostate cancer; sqNSCLC, squamous non-small cell lung cancer; TNBC, triple-negative breast cancer; TCC, transitional cell carcinoma; HER-2, human epidermal growth factor receptor 2.

Previous studies have demonstrated that the transgenic expression of the constitutively active form of the PI3K catalytic subunit or PTEN knockout can rescue mature B cells from conditional BCR ablation. Moreover, BCR signaling is required for PI3K pathway engagement in both GCB-DLBCL and ABC-DLBCL. Specifically, PI3K engages BCR signaling by indirectly contributing to NF-κB activity in ABC-DLBCL, whereas in GCB-DLBCL, PI3K pathway activation but not NF-κB activity is required for survival. Briefly, the "chronic" BCR signaling in ABC-DLBCL is characterized by the many pathways involved with the CARD11-mediated activation of NF-κB signaling, whereas the "tonic" BCR signaling in GCB-DLBCL is characterized by the constitutive activation of PI3K in promoting survival [96, 97].

Given these findings, the combination of PI3K pathway inhibitors with BCR pathway inhibitors may enhance the treatment response of PTEN-deficient tumors.

THERAPIES TARGETING FUNCTIONAL LOSS OF PTEN IN LYMPHOMA

PI3K/AKT/mTOR pathway inhibitors

Owing to PI3K's critical roles in human cancers, PI3K targeting is one of the most promising areas of anticancer therapy development. Since the absent of PTEN is concomitant with PI3K signaling activation, inhibitors that targeting this pathway might play a significant role in the treatment of PTEN-deficient tumors. Growing evidence indicates that multiple solid tumor cell lines and several lymphoid malignancy cell lines with PTEN-deficient are hypersensitive to PI3K inhibitors, which are summarized in Tables 3 and Figure 4.

In addition to PI3K pan-inhibition, several isoform-selective PI3K inhibitors have been shown to repress the viability of PTEN-deficient tumors. Notably, the p110β-specific PI3K inhibitor AZD6482 (KIN-193) displayed remarkable antitumor activity in PTEN-null tumors but failed to block the growth of PTEN–wild-type tumors in mouse models [98]. However, another separate study showed that endometrioid endometrial cancer with *PTEN* mutation were resistant to p110β-selective inhibition, cell lines' viability was decreased only when p110β-selective inhibition was combined with p110α-selective inhibition. Recent findings have highlighted that there is a complex interplay between the Class I PI3K isoforms, inhibition of either α or β single isoform might be compensated by reactivation of another isoform at last [99]. Furthermore, it has been proposed that the dual γ/δ inhibitor CAL-130, specifically targeting p110γ and p110δ isoforms in *PTEN* deleted T-ALL cell lines [100]. By contrast, Lonetti et al. recently indicated that PI3K pan-inhibition developed the highest cytotoxic effects when compared with both selective isoform inhibition and dual p110γ/δ inhibition, in T-ALL cell lines with or without *PTEN* deletion [101]. Nevertheless, which class of agents among isoform-specific or pan-inhibitors can achieve better efficacy is still controversial. Other target treatments including AKT, mTOR, dual PI3K/AKT and dual PI3K/mTOR inhibitors also show promising antitumor activity in cell line studies, and some of them have been testing under clinical trials [102-111] (Table 3, 4).

CONCLUSION

In summary, recent studies have identified PTEN as a tumor suppressor gene in various human cancers. It is clear that PTEN is far more than a cytosolic protein that acts as a lipid phosphatase to maintain PIP_3 levels. Therefore, we must reconsider the distinct roles PTEN have in specific subcellular compartments, identify the mechanisms underlying PTEN's shuttling between different compartments, and investigate the significance of these mechanisms in predicting disease outcome. Future studies will further elucidate the mechanistic basis of PTEN deficiency in lymphoid malignancies, thereby aiding in the clinical management of lymphoid malignancies with PTEN loss or alteration.

Funding

This study was supported by the National Cancer Institute/National Institutes of Health (R01CA138688 and 1RC1CA146299 to KHY). XW is a recipient of hematology and oncology scholarship award. KHY is supported by The University of Texas MD Anderson Cancer Center Lymphoma Moonshot Program and Institutional Research and Development Award, an MD Anderson Cancer Center Lymphoma Specialized Programs on Research Excellence (SPORE) Research Development Program Award, an MD Anderson Cancer Center Myeloma SPORE Research Development Program Award, a Gundersen Lutheran Medical Foundation Award, and partially supported by the National Cancer Institute/National Institutes of Health (P50CA136411 and P50CA142509), and by MD Anderson's Cancer Center Support Grant CA016672.

Author contributions

Conception, design, manuscript writing and final approval of manuscript**:** XW and KHY.

Conflict of interest statement

KHY receives research support from Roche Molecular System, Gilead Sciences Pharmaceutical, Seattle Genetics, Dai Sanyo Pharmaceutical, Adaptive Biotechnology, Incyte Pharmaceutical and HTG Molecular Diagnostics.

REFERENCES

1. Wang SI, Puc J, Li J, Bruce JN, Cairns P, Sidransky D and Parsons R. Somatic mutations of PTEN in glioblastoma multiforme. Cancer research. 1997;57:4183-4186.

2. Tashiro H, Blazes MS, Wu R, Cho KR, Bose S, Wang SI, Li J, Parsons R and Ellenson LH. Mutations in PTEN are frequent in endometrial carcinoma but rare in other common gynecological malignancies. Cancer research. 1997;57:3935-3940.

3. Rasheed BKA, Stenzel TT, McLendon RE, Parsons R, Friedman AH, Friedman HS, Bigner DD and Bigner SH. PTEN gene mutations are seen in high-grade but not in low-grade gliomas. Cancer research. 1997;57:4187-4190.

4. Wang SI, Parsons R and Ittmann M. Homozygous deletion of the PTEN tumor suppressor gene in a subset of prostate adenocarcinomas. Clinical Cancer Research. 1998;4:811-815.

5. Cairns P, Evron E, Okami K, Halachmi N, Esteller M, Herman JG, Bose S, Wang SI, Parsons R and Sidransky D. Point mutation and homozygous deletion of PTEN/MMAC1 in primary bladder cancers. Oncogene. 1998;16:3215-3218.

6. Nagata Y, Lan KH, Zhou X, Tan M, Esteva FJ, Sahin AA, Klos KS, Li P, Monia BP, Nguyen NT, Hortobagyi GN, Hung MC and Yu D. PTEN activation contributes to tumor inhibition by trastuzumab, and loss of PTEN predicts trastuzumab resistance in patients. Cancer cell. 2004;6:117-127.

7. Berns K, Horlings HM, Hennessy BT, Madiredjo M, Hijmans EM, Beelen K, Linn SC, Gonzalez-Angulo AM, Stemke-Hale K, Hauptmann M, Beijersbergen RL, Mills GB, van de Vijver MJ, et al. A functional genetic approach identifies the PI3K pathway as a major determinant of trastuzumab resistance in breast cancer. Cancer cell. 2007;12:395-402.

8. Trotman LC, Niki M, Dotan ZA, Koutcher JA, Di Cristofano A, Xiao A, Khoo AS, Roy-Burman P, Greenberg NM, Van Dyke T, Cordon-Cardo C and Pandolfi PP. Pten dose dictates cancer progression in the prostate. PLoS biology. 2003;1:385-396.

9. Di Cristofano A, Pesce B, Cordon-Cardo C and Pandolfi PP. Pten is essential for embryonic development and tumour suppression. Nature genetics. 1998;19:348-355.

10. Maehama T and Dixon JE. The tumor suppressor, PTEN/MMAC1, dephosphorylates the lipid second messenger, phosphatidylinositol 3,4,5-trisphosphate. The Journal of biological chemistry. 1998;273:13375-13378.

11. Lee JO, Yang H, Georgescu MM, Di Cristofano A, Maehama T, Shi Y, Dixon JE, Pandolfi P and Pavletich NP. Crystal structure of the PTEN tumor suppressor: implications for its phosphoinositide phosphatase activity and membrane association. Cell. 1999;99:323-334.

12. Denning G, Jean-Joseph B, Prince C, Durden DL and Vogt PK. A short N-terminal sequence of PTEN controls cytoplasmic localization and is required for suppression of cell growth. Oncogene. 2007;26:3930-3940.

13. Leslie NR, Batty IH, Maccario H, Davidson L and Downes CP. Understanding PTEN regulation: PIP2, polarity and protein stability. Oncogene. 2008;27:5464-5476.

14. Guertin DA and Sabatini DM. Defining the role of mTOR in cancer. Cancer cell. 2007;12:9-22.

15. Manning BD and Cantley LC. AKT/PKB signaling: Navigating downstream. Cell. 2007;129:1261-1274.

16. Ma XM and Blenis J. Molecular mechanisms of mTOR-mediated translational control. Nature reviews Molecular cell biology. 2009;10:307-318.

17. Vivanco I, Palaskas N, Tran C, Finn SP, Getz G, Kennedy NJ, Jiao J, Rose J, Xie WL, Loda M, Golub T, Mellinghoff IK, Davis RJ, et al. Identification of the JNK signaling pathway as a functional target of the tumor suppressor PTEN. Cancer cell. 2007; 11:555-569.

18. Raftopoulou M, Etienne-Manneville S, Self A, Nicholls S and Hall A. Regulation of cell migration by the C2 domain of the tumor suppressor PTEN. Science. 2004;303:1179-1181.

19. Zhang SY, Huang WC, Li P, Guo H, Poh SB, Brady SW, Xiong Y, Tseng LM, Li SH, Ding ZX, Sahin AA, Esteva FJ, Hortobagyi GN, et al. Combating trastuzumab resistance by targeting SRC, a common node downstream of multiple resistance pathways. Nature medicine. 2011;17:461-U101.

20. Tang Y and Eng C. PTEN autoregulates its expression by stabilization of p53 in a phosphatase-independent manner. Cancer research. 2006;66:736-742.

21. Waite KA and Eng C. Protean PTEN: form and function. American journal of human genetics. 2002;70:829-844.

22. Keniry M and Parsons R. The role of PTEN signaling perturbations in cancer and in targeted therapy. Oncogene. 2008;27:5477-5485.

23. Zhang S and Yu D. PI(3)king apart PTEN's role in cancer. Clinical cancer research : an official journal of the American Association for Cancer Research. 2010;16:4325-4330.

24. Liaw D, Marsh DJ, Li J, Dahia PL, Wang SI, Zheng Z, Bose S, Call KM, Tsou HC, Peacocke M, Eng C and Parsons R. Germline mutations of the PTEN gene in Cowden disease, an inherited breast and thyroid cancer syndrome. Nature genetics. 1997; 16:64-67.

25. Sansal I and Sellers WR. The biology and clinical relevance of the PTEN tumor suppressor pathway. Journal of clinical oncology : official journal of the American Society of Clinical Oncology. 2004; 22:2954-2963.

26. Chalhoub N and Baker SJ. PTEN and the PI3-kinase pathway in cancer. Annual review of pathology. 2009; 4:127-150.

27. Patel L, Pass I, Coxon P, Downes CP, Smith SA and Macphee CH. Tumor suppressor and anti-inflammatory actions of PPARgamma agonists are mediated via upregulation of PTEN. Current biology : CB. 2001; 11:764-768.

28. Virolle T, Adamson ED, Baron V, Birle D, Mercola D, Mustelin T and de Belle I. The Egr-1 transcription factor directly activates PTEN during irradiation-induced signalling. Nature cell biology. 2001; 3:1124-1128.

29. Stambolic V, MacPherson D, Sas D, Lin Y, Snow B, Jang Y, Benchimol S and Mak TW. Regulation of PTEN transcription by p53. Molecular cell. 2001; 8(2):317-325.

30. Gericke A, Munson M and Ross AH. Regulation of the PTEN phosphatase. Gene. 2006; 374:1-9.

31. Lau MT, Klausen C and Leung PC. E-cadherin inhibits tumor cell growth by suppressing PI3K/Akt signaling via beta-catenin-Egr1-mediated PTEN expression. Oncogene. 2011; 30:2753-2766.

32. Meng X, Wang Y, Zheng X, Liu C, Su B, Nie H, Zhao B, Zhao X and Yang H. shRNA-mediated knockdown of Bmi-1 inhibit lung adenocarcinoma cell migration and metastasis. Lung cancer. 2012; 77:24-30.

33. Yoshimi A, Goyama S, Watanabe-Okochi N, Yoshiki Y, Nannya Y, Nitta E, Arai S, Sato T, Shimabe M, Nakagawa M, Imai Y, Kitamura T and Kurokawa M. Evi1 represses PTEN expression and activates PI3K/AKT/mTOR via interactions with polycomb proteins. Blood. 2011; 117:3617-3628.

34. Chow JY, Quach KT, Cabrera BL, Cabral JA, Beck SE and Carethers JM. RAS/ERK modulates TGFbeta-regulated PTEN expression in human pancreatic adenocarcinoma cells. Carcinogenesis. 2007; 28(11):2321-2327.

35. Vasudevan KM, Burikhanov R, Goswami A and Rangnekar VM. Suppression of PTEN expression is essential for antiapoptosis and cellular transformation by oncogenic ras. Cancer research. 2007; 67:10343-10350.

36. Xia DR, Srinivas H, Ahn YH, Sethi G, Sheng XY, Yung WKA, Xia QH, Chiao PJ, Kim H, Brown PH, Wistuba II, Aggarwal BB and Kurie JM. Mitogen-activated protein kinase kinase-4 promotes cell survival by decreasing PTEN expression through an NF kappa B-dependent pathway. Journal of Biological Chemistry. 2007; 282:3507-3519.

37. Leslie NR and Foti M. Non-genomic loss of PTEN function in cancer: not in my genes. Trends in pharmacological sciences. 2011; 32:131-140.

38. Bartel DP. MicroRNAs: target recognition and regulatory functions. Cell. 2009; 136:215-233.

39. Tamguney T and Stokoe D. New insights into PTEN. J Cell Sci. 2007; 120):4071-4079.

40. Vazquez F, Ramaswamy S, Nakamura N and Sellers WR. Phosphorylation of the PTEN tail regulates protein stability and function. Molecular and cellular biology. 2000; 20:5010-5018.

41. Wang XJ, Trotman LC, Koppie T, Alimonti A, Chen ZB, Gao ZH, Wang JR, Erdjument-Bromage H, Tempst P, Cordon-Cardo C, Pandolfi PP and Jiang XJ. NEDD4-1 is a proto-oncogenic ubiquitin ligase for PTEN. Cell. 2007; 128:129-139.

42. Drinjakovic J, Jung H, Campbell DS, Strochlic L, Dwivedy A and Holt CE. E3 ligase Nedd4 promotes axon branching by downregulating PTEN. Neuron. 2010; 65:341-357.

43. Georgescu MM, Kirsch KH, Akagi T, Shishido T and Hanafusa H. The tumor-suppressor activity of PTEN is regulated by its carboxyl-terminal region. Proceedings of the National Academy of Sciences of the United States of America. 1999; 96:10182-10187.

44. Wu X, Hepner K, Castelino-Prabhu S, Do D, Kaye MB, Yuan XJ, Wood J, Ross C, Sawyers CL and Whang YE. Evidence for regulation of the PTEN tumor suppressor by a membrane-localized multi-PDZ domain containing scaffold protein MAGI-2. Proceedings of the National Academy of Sciences of the United States of America. 2000; 97:4233-4238.

45. Vazquez F, Grossman SR, Takahashi Y, Rokas MV, Nakamura N and Sellers WR. Phosphorylation of the PTEN tail acts as an inhibitory switch by preventing its recruitment into a protein complex. Journal of Biological Chemistry. 2001; 276:48627-48630.

46. Al-Khouri AM, Ma YL, Togo SH, Williams S and Mustelin T. Cooperative phosphorylation of the tumor suppressor phosphatase and tensin homologue (PTEN) by casein kinases and glycogen synthase kinase 3 beta. Journal of Biological Chemistry. 2005; 280:35195-35202.

47. Miller SJ, Lou DY, Seldin DC, Lane WS and Neel BG. Direct identification of PTEN phosphorylation sites. FEBS letters. 2002; 528:145-153.

48. Li Z, Dong XM, Wang ZL, Liu WZ, Deng N, Ding Y, Tang LY, Hla T, Zeng R, Li L and Wu DQ. Regulation of PTEN by Rho small GTPases. Nature cell biology. 2005; 7:399-U342.

49. Okumura K, Mendoza M, Bachoo RM, DePinho RA, Cavenee WK and Furnari FB. PCAF modulates PTEN activity. Journal of Biological Chemistry. 2006; 281:26562-26568.

50. Leslie NR, Bennett D, Lindsay YE, Stewart H, Gray A and Downes CP. Redox regulation of PI 3-kinase signalling via inactivation of PTEN. Embo J. 2003; 22:5501-5510.

51. Seo JH, Ahn Y, Lee SR, Yeol Yeo C and Chung Hur K. The major target of the endogenously generated reactive oxygen species in response to insulin stimulation is phosphatase and tensin homolog and not phosphoinositide-3 kinase (PI-3 kinase) in the PI-3 kinase/Akt pathway. Mol Biol Cell. 2005; 16:348-357.

52. Fine B, Hodakoski C, Koujak S, Su T, Saal LH, Maurer M, Hopkins B, Keniry M, Sulis ML, Mense S, Hibshoosh H and Parsons R. Activation of the PI3K Pathway in Cancer Through Inhibition of PTEN by Exchange Factor P-REX2a. Science. 2009; 325:1261-1265.

53. He L, Ingram A, Rybak AP and Tang D. Shank-interacting protein-like 1 promotes tumorigenesis via PTEN inhibition in human tumor cells. The Journal of clinical investigation. 2010; 120:2094-2108.

54. Tang Y and Eng C. p53 down-regulates phosphatase and tensin homologue deleted on chromosome 10 protein stability partially through caspase-mediated degradation in cells with proteasome dysfunction. Cancer research. 2006; 66:6139-6148.

55. Mayo LD, Dixon JE, Durden DL, Tonks NK and Donner DB. PTEN protects p53 from Mdm2 and sensitizes cancer cells to chemotherapy. The Journal of biological chemistry. 2002; 277:5484-5489.

56. Freeman DJ, Li AG, Wei G, Li HH, Kertesz N, Lesche R, Whale AD, Martinez-Diaz H, Rozengurt N, Cardiff RD, Liu X and Wu H. PTEN tumor suppressor regulates p53 protein levels and activity through phosphatase-dependent and -independent mechanisms. Cancer cell. 2003; 3:117-130.

57. Tachibana M, Shibakita M, Ohno S, Kinugasa S, Yoshimura H, Ueda S, Fujii T, Rahman MA, Dhar DK and Nagasue N. Expression and prognostic significance of PTEN product protein in patients with esophageal squamous cell carcinoma. Cancer. 2002; 94:1955-1960.

58. Zhou XP, Loukola A, Salovaara R, Nystrom-Lahti M, Peltomaki P, de la Chapelle A, Aaltonen LA and Eng C. PTEN mutational spectra, expression levels, and subcellular localization in microsatellite stable and unstable colorectal cancers. The American journal of pathology. 2002; 161:439-447.

59. Fridberg M, Servin A, Anagnostaki L, Linderoth J, Berglund M, Soderberg O, Enblad G, Rosen A, Mustelin T, Jerkeman M, Persson JL and Wingren AG. Protein expression and cellular localization in two prognostic subgroups of diffuse large B-cell lymphoma: higher expression of ZAP70 and PKC-beta II in the non-germinal center group and poor survival in patients deficient in nuclear PTEN. Leuk Lymphoma. 2007; 48:2221-2232.

60. Gimm O, Perren A, Weng LP, Marsh DJ, Yeh JJ, Ziebold U, Gil E, Hinze R, Delbridge L, Lees JA, Mutter GL, Robinson BG, Komminoth P, et al. Differential nuclear and cytoplasmic expression of PTEN in normal thyroid tissue, and benign and malignant epithelial thyroid tumors. American Journal of Pathology. 2000; 156:1693-1700.

61. Perren A, Komminoth P, Saremaslani P, Matter C, Feurer S, Lees JA, Heitz PU and Eng C. Mutation and expression analyses reveal differential subcellular compartmentalization of PTEN in endocrine pancreatic tumors compared to normal islet cells. The American journal of pathology. 2000; 157:1097-1103.

62. Ginn-Pease ME and Eng C. Increased nuclear phosphatase and tensin homologue deleted on chromosome 10 is associated with G0-G1 in MCF-7 cells. Cancer research. 2003; 63:282-286.

63. Minaguchi T, Waite KA and Eng C. Nuclear localization of PTEN is regulated by Ca2+ through a tyrosil phosphorylation-independent conformational modification in major vault protein. Cancer research. 2006; 66:11677-11682.

64. Liu FH, Wagner S, Campbell RB, Nickerson JA, Schiffer CA and Ross AH. PTEN enters the nucleus by diffusion. Journal of cellular biochemistry. 2005; 96:221-234.

65. Gil A, Andres-Pons A, Fernandez E, Valiente M, Torres J, Cervera J and Pulido R. Nuclear localization of PTEN by a ran-dependent mechanism enhances apoptosis: Involvement of an N-terminal nuclear localization domain and multiple nuclear exclusion motifs. Mol Biol Cell. 2006; 17:4002-4013.

66. Trotman LC, Wang X, Alimonti A, Chen Z, Teruya-Feldstein J, Yang H, Pavletich NP, Carver BS, Cordon-Cardo C, Erdjument-Bromage H, Tempst P, Chi SG, Kim HJ, et al. Ubiquitination regulates PTEN nuclear import and tumor suppression. Cell. 2007; 128:141-156.

67. Liu JL, Mao Z, LaFortune TA, Alonso MM, Gallick GE, Fueyo J and Yung WKA. Cell cycle-dependent nuclear export of phosphatase and tensin homologue tumor suppressor is regulated by the phosphoinositide-3-kinase signaling cascade. Cancer research. 2007; 67:11054-11063.

68. Shen WH, Balajee AS, Wang J, Wu H, Eng C, Pandolfi PP and Yin Y. Essential role for nuclear PTEN in maintaining chromosomal integrity. Cell. 2007; 128:157-170.

69. Li AG, Piluso LG, Cai X, Wei G, Sellers WR and Liu X. Mechanistic insights into maintenance of high p53 acetylation by PTEN. Molecular cell. 2006; 23:575-587.

70. Gu TT, Zhang Z, Wang JL, Guo JY, Shen WH and Yin YX. CREB Is a Novel Nuclear Target of PTEN Phosphatase. Cancer research. 2011; 71:2821-2825.

71. Tanaka K, Horiguchi K, Yoshida T, Takeda M, Fujisawa H, Takeuchi K, Umeda M, Kato S, Ihara S, Nagata S and Fukui Y. Evidence that a phosphatidylinositol 3,4,5-trisphosphate-binding protein can function in nucleus. Journal of Biological Chemistry. 1999; 274:3919-3922.

72. Lindsay Y, McCoull D, Davidson L, Leslie NR, Fairservice A, Gray A, Lucocq J and Downes CP. Localization of agonist-sensitive PtdIns(3,4,5)P3 reveals a nuclear pool that is insensitive to PTEN expression. J Cell Sci. 2006; 119:5160-5168.

73. Silva A, Yunes JA, Cardoso BA, Martins LR, Jotta PY, Abecasis M, Nowill AE, Leslie NR, Cardoso AA and Barata JT. PTEN posttranslational inactivation and hyperactivation of the PI3K/Akt pathway sustain primary T cell leukemia viability. The Journal of clinical investigation. 2008; 118:3762-3774.

74. Palomero T, Sulis ML, Cortina M, Real PJ, Barnes K, Ciofani M, Caparros E, Buteau J, Brown K, Perkins SL, Bhagat G, Agarwal AM, Basso G, et al. Mutational loss of PTEN induces resistance to NOTCH1 inhibition in T-cell leukemia. Nat Med. 2007; 13:1203-1210.

75. Larson Gedman A, Chen Q, Kugel Desmoulin S, Ge Y, LaFiura K, Haska CL, Cherian C, Devidas M, Linda SB, Taub JW and Matherly LH. The impact of NOTCH1, FBW7 and PTEN mutations on prognosis and downstream signaling in pediatric T-cell acute lymphoblastic leukemia: a report from the Children's Oncology Group. Leukemia. 2009; 23:1417-1425.

76. Gutierrez A, Sanda T, Grebliunaite R, Carracedo A, Salmena L, Ahn Y, Dahlberg S, Neuberg D, Moreau LA, Winter SS, Larson R, Zhang J, Protopopov A, et al. High frequency of PTEN, PI3K, and AKT abnormalities in T-cell acute lymphoblastic leukemia. Blood. 2009; 114:647-650.

77. Liu X, Karnell JL, Yin B, Zhang R, Zhang J, Li P, Choi Y, Maltzman JS, Pear WS, Bassing CH and Turka LA. Distinct roles for PTEN in prevention of T cell lymphoma and autoimmunity in mice. The Journal of clinical investigation. 2010; 120:2497-2507.

78. Bonneau D and Longy M. Mutations of the human PTEN gene. Human mutation. 2000; 16:109-122.

79. Gronbaek K, Zeuthen J, Guldberg P, Ralfkiaer E and Hou-Jensen K. Alterations of the MMAC1/PTEN gene in lymphoid malignancies. Blood. 1998; 91:4388-4390.

80. Dahia PL, Aguiar RC, Alberta J, Kum JB, Caron S, Sill H, Marsh DJ, Ritz J, Freedman A, Stiles C and Eng C. PTEN is inversely correlated with the cell survival factor Akt/PKB and is inactivated via multiple mechanismsin haematological malignancies. Human molecular genetics. 1999; 8:185-193.

81. Nakahara Y, Nagai H, Kinoshita T, Uchida T, Hatano S, Murate T and Saito H. Mutational analysis of the PTEN/MMAC1 gene in non-Hodgkin's lymphoma. Leukemia. 1998; 12:1277-1280.

82. Sakai A, Thieblemont C, Wellmann A, Jaffe ES and Raffeld M. PTEN gene alterations in lymphoid neoplasms. Blood. 1998; 92:3410-3415.

83. Butler MP, Wang SI, Chaganti RS, Parsons R and Dalla-Favera R. Analysis of PTEN mutations and deletions in B-cell non-Hodgkin's lymphomas. Genes, chromosomes & cancer. 1999; 24:322-327.

84. Lenz G, Wright GW, Emre NC, Kohlhammer H, Dave SS, Davis RE, Carty S, Lam LT, Shaffer AL, Xiao W, Powell J, Rosenwald A, Ott G, et al. Molecular subtypes of diffuse large B-cell lymphoma arise by distinct genetic pathways. Proceedings of the National Academy of Sciences of the United States of America. 2008; 105:13520-13525.

85. Pfeifer M and Lenz G. PI3K/AKT addiction in subsets of diffuse large B-cell lymphoma. Cell cycle. 2013; 12:3347-3348.

86. Rudelius M, Pittaluga S, Nishizuka S, Pham TH, Fend F, Jaffe ES, Quintanilla-Martinez L and Raffeld M. Constitutive activation of Akt contributes to the pathogenesis and survival of mantle cell lymphoma. Blood. 2006;108:1668-1676.

87. Battistella M, Romero M, Castro-Vega LJ, Gapihan G, Bouhidel F, Bagot M, Feugeas JP and Janin A. The High Expression of the microRNA 17-92 Cluster and its Paralogs, and the Down-Regulation of the Target Gene PTEN are Associated with Primary Cutaneous B-cell Lymphoma Progression. The Journal of investigative dermatology. 2015; 135:1659-1667.

88. Samuels Y, Wang Z, Bardelli A, Silliman N, Ptak J, Szabo S, Yan H, Gazdar A, Powell SM, Riggins GJ, Willson JK, Markowitz S, Kinzler KW, et al. High frequency of mutations of the PIK3CA gene in human cancers. Science. 2004;304:554.

89. Abubaker J, Bavi P, Al-Harbi S, Siraj A, Al-Dayel F, Uddin S and Al-Kuraya K. PIK3CA mutations are mutually exclusive with PTEN loss in diffuse large B-cell lymphoma. Leukemia. 2007; 21:2368-2370.

90. Knight ZA, Gonzalez B, Feldman ME, Zunder ER, Goldenberg DD, Williams O, Loewith R, Stokoe D, Balla A, Toth B, Balla T, Weiss WA, Williams RL, et al. A pharmacological map of the PI3-K family defines a role for p110 alpha in insulin signaling. Cell. 2006; 125:733-747.

91. Jia SD, Liu ZN, Zhang S, Liu PX, Zhang L, Lee SH, Zhang J, Signoretti S, Loda M, Roberts TM and Zhao JJ. Essential roles of PI(3)K-p110 beta in cell growth, metabolism and tumorigenesis. Nature. 2008; 454:776-U102.

92. Edgar KA, Wallin JJ, Berry M, Lee LB, Prior WW, Sampath D, Friedman LS and Belvin M. Isoform-Specific Phosphoinositide 3-Kinase Inhibitors Exert Distinct Effects in Solid Tumors. Cancer research. 2010; 70:1164-1172.

93. Weigelt B, Warne PH, Lambros MB, Reis-Filho JS and Downward J. PI3K pathway dependencies in endometrioid endometrial cancer cell lines. Clin Cancer Res. 2013; 19:3533-3544.

94. Davis RE, Ngo VN, Lenz G, Tolar P, Young RM, Romesser PB, Kohlhammer H, Lamy L, Zhao H, Yang Y, Xu W, Shaffer AL, Wright G, et al. Chronic active B-cell-receptor signalling in diffuse large B-cell lymphoma. Nature. 2010;463:88-92.

95. Kloo B, Nagel D, Pfeifer M, Grau M, Duwel M, Vincendeau M, Dorken B, Lenz P, Lenz G and Krappmann D. Critical role of PI3K signaling for NF-kappaB-dependent survival in a subset of activated B-cell-like diffuse large B-cell lymphoma cells. Proceedings of the National Academy of Sciences of the United States of America. 2011; 108:272-277.

96. Chen L, Juszczynski P, Takeyama K, Aguiar RC and Shipp MA. Protein tyrosine phosphatase receptor-type O truncated (PTPROt) regulates SYK phosphorylation, proximal B-cell-receptor signaling, and cellular proliferation. Blood. 2006; 108:3428-3433.

97. Chen LF, Monti S, Juszczynski P, Daley J, Chen W, Witzig TE, Habermann TM, Kutok JL and Shipp MA. SYK-dependent tonic B-cell receptor signaling is a rational treatment target in diffuse large B-cell lymphoma. Blood. 2008; 111:2230-2237.

98. Li B, Sun A, Jiang W, Thrasher JB and Terranova P. PI-3 kinase p110beta: a therapeutic target in advanced prostate cancers. Am J Clin Exp Urol. 2014;2:188-198.

99. Schwartz S, Wongvipat J, Trigwell CB, Hancox U, Carver BS, Rodrik-Outmezguine V, Will M, Yellen P, de Stanchina E, Baselga J, Scher HI, Barry ST, Sawyers CL, et al. Feedback Suppression of PI3K alpha Signaling in PTEN-Mutated Tumors Is Relieved by Selective Inhibition of PI3K beta. Cancer cell. 2015;27:109-122.

100. Subramaniam PS, Whye DW, Efimenko E, Chen J, Tosello V, De Keersmaecker K, Kashishian A, Thompson MA, Castillo M, Cordon-Cardo C, Dave UP, Ferrando A, Lannutti BJ, et al. Targeting Nonclassical Oncogenes for Therapy in T-ALL. Cancer cell. 2012; 21:459-472.

101. Lonetti A, Cappellini A, Sparta AM, Chiarini F, Buontempo F, Evangelisti C, Evangelisti C, Orsini E, McCubrey JA and Martelli AM. PI3K pan-inhibition impairs more efficiently proliferation and survival of T-cell acute lymphoblastic leukemia cell lines when compared to isoform-selective PI3K inhibitors. Oncotarget. 2015; 6:10399-10414. DOI: 10.18632/oncotarget.3295.

102. Hancox U, Cosulich S, Hanson L, Trigwell C, Lenaghan C, Ellston R, Dry H, Crafter C, Barlaam B, Fitzek M, Smith PD, Ogilvie D, D'Cruz C, et al. Inhibition of PI3Kbeta signaling with AZD8186 inhibits growth of PTEN-deficient breast and prostate tumors alone and in combination with docetaxel. Mol Cancer Ther. 2015; 14:48-58.

103. Tanaka H, Yoshida M, Tanimura H, Fujii T, Sakata K, Tachibana Y, Ohwada J, Ebiike H, Kuramoto S, Morita K, Yoshimura Y, Yamazaki T, Ishii N, et al. The selective class I PI3K inhibitor CH5132799 targets human cancers harboring oncogenic PIK3CA mutations. Clinical cancer research : an official journal of the American Association for Cancer Research. 2011; 17:3272-3281.

104. Garlich JR, De P, Dey N, Su JD, Peng X, Miller A, Murali R, Lu Y, Mills GB, Kundra V, Shu HK, Peng Q and Durden DL. A vascular targeted pan phosphoinositide 3-kinase inhibitor prodrug, SF1126, with antitumor and antiangiogenic activity. Cancer research. 2008; 68:206-215.

105. Qian C, Lai CJ, Bao R, Wang DG, Wang J, Xu GX, Atoyan R, Qu H, Yin L, Samson M, Zifcak B, Ma AW, DellaRocca S, et al. Cancer network disruption by a single molecule inhibitor targeting both histone deacetylase activity and phosphatidylinositol 3-kinase signaling. Clinical cancer research : an official journal of the American Association for Cancer Research. 2012; 18:4104-4113.

106. Hirai H, Sootome H, Nakatsuru Y, Miyama K, Taguchi S, Tsujioka K, Ueno Y, Hatch H, Majumder PK, Pan BS and Kotani H. MK-2206, an allosteric Akt inhibitor, enhances antitumor efficacy by standard chemotherapeutic agents or molecular targeted drugs in vitro and in vivo. Molecular cancer therapeutics. 2010; 9:1956-1967.

107. Baselga J, Campone M, Piccart M, Burris HA, 3rd, Rugo HS, Sahmoud T, Noguchi S, Gnant M, Pritchard KI, Lebrun F, Beck JT, Ito Y, Yardley D, et al. Everolimus in postmenopausal hormone-receptor-positive advanced breast cancer. The New England journal of medicine. 2012;366:520-529.

108. Elit L. CCI-779 Wyeth. Curr Opin Investig Drugs. 2002; 3:1249-1253.

109. Reynolds CP, Kang MH, Carol H, Lock R, Gorlick R, Kolb EA, Kurmasheva RT, Keir ST, Maris JM, Billups CA, Houghton PJ and

Smith MA. Initial testing (stage 1) of the phosphatidylinositol 3' kinase inhibitor, SAR245408 (XL147) by the pediatric preclinical testing program. Pediatric blood & cancer. 2013; 60:791-798.

110. Furet P, Guagnano V, Fairhurst RA, Imbach-Weese P, Bruce I, Knapp M, Fritsch C, Blasco F, Blanz J, Aichholz R, Hamon J, Fabbro D and Caravatti G. Discovery of NVP-BYL719 a potent and selective phosphatidylinositol-3 kinase alpha inhibitor selected for clinical evaluation. Bioorg Med Chem Lett. 2013; 23:3741-3748.

111. Hall CP, Reynolds CP and Kang MH. Modulation of glucocorticoid resistance in pediatric T-cell Acute Lymphoblastic Leukemia by increasing BIM expression with the PI3K/mTOR inhibitor BEZ235. Clinical cancer research: an official journal of the American Association for Cancer Research. 2015; in press.

112. Yang Y, Yang JJ, Tao H and Jin WS. MicroRNA-21 controls hTERT via PTEN in human colorectal cancer cell proliferation. Journal of physiology and biochemistry. 2015; 71:59-68.

113. Yang X, Cheng Y, Li P, Tao J, Deng X, Zhang X, Gu M, Lu Q and Yin C. A lentiviral sponge for miRNA-21 diminishes aerobic glycolysis in bladder cancer T24 cells via the PTEN/PI3K/AKT/mTOR axis. Tumour biology : the journal of the International Society for Oncodevelopmental Biology and Medicine. 2015; 36:383-391.

114. Meng F, Henson R, Wehbe-Janek H, Ghoshal K, Jacob ST and Patel T. MicroRNA-21 regulates expression of the PTEN tumor suppressor gene in human hepatocellular cancer. Gastroenterology. 2007; 133:647-658.

115. Calin GA, Liu CG, Sevignani C, Ferracin M, Felli N, Dumitru CD, Shimizu M, Cimmino A, Zupo S, Dono M, Dell'Aquila ML, Alder H, Rassenti L, et al. MicroRNA profiling reveals distinct signatures in B cell chronic lymphocytic leukemias. Proceedings of the National Academy of Sciences of the United States of America. 2004; 101:11755-11760.

116. Tian L, Fang YX, Xue JL and Chen JZ. Four microRNAs promote prostate cell proliferation with regulation of PTEN and its downstream signals in vitro. PloS one. 2013; 8:e75885.

117. Palacios F, Prieto D, Abreu C, Ruiz S, Morande P, Fernandez-Calero T, Libisch G, Landoni AI and Oppezzo P. Dissecting chronic lymphocytic leukemia microenvironment signals in patients with unmutated disease: microRNA-22 regulates phosphatase and tensin homolog/AKT/FOXO1 pathway in proliferative leukemic cells. Leukemia & lymphoma. 2015:1-6.

118. Yan SY, Chen MM, Li GM, Wang YQ and Fan JG. MiR-32 induces cell proliferation, migration, and invasion in hepatocellular carcinoma by targeting PTEN. Tumour biology: the journal of the International Society for Oncodevelopmental Biology and Medicine. 2015; 36:4747-4755.

119. Ohta K, Hoshino H, Wang J, Ono S, Iida Y, Hata K, Huang SK, Colquhoun S and Hoon DS. MicroRNA-93 activates c-Met/PI3K/Akt pathway activity in hepatocellular carcinoma by directly inhibiting PTEN and CDKN1A. Oncotarget. 2015; 6:3211-3224. DOI: 10.18632/oncotarget.3085.

120. Yang YK, Xi WY, Xi RX, Li JY, Li Q and Gao YE. MicroRNA494 promotes cervical cancer proliferation through the regulation of PTEN. Oncology reports. 2015; 33:2393-2401.

121. Yu TT, Cao RS, Li S, Fu MG, Ren LH, Chen WX, Zhu H, Zhan Q and Shi RH. MiR-130b plays an oncogenic role by repressing PTEN expression in esophageal squamous cell carcinoma cells. BMC cancer. 2015; 15:29.

122. Xiang SJ, Fang JQ, Wang SY, Deng B and Zhu L. MicroRNA-135b regulates the stability of PTEN and promotes glycolysis by targeting USP13 in human colorectal cancers. Oncology reports. 2015; 33:1342-1348.

123. Yang H, Kong W, He L, Zhao JJ, O'Donnell JD, Wang J, Wenham RM, Coppola D, Kruk PA, Nicosia SV and Cheng JQ. MicroRNA expression profiling in human ovarian cancer: miR-214 induces cell survival and cisplatin resistance by targeting PTEN. Cancer research. 2008; 68:425-433.

124. Zang C, Eucker J, Liu H, Coordes A, Lenarz M, Possinger K and Scholz CW. Inhibition of pan-class I phosphatidyl-inositol-3-kinase by NVP-BKM120 effectively blocks proliferation and induces cell death in diffuse large B-cell lymphoma. Leuk Lymphoma. 2014; 55:425-434.

Research Paper

The p53 tumor suppressor protein protects against chemotherapeutic stress and apoptosis in human medulloblastoma cells

Sarah Waye[1#], Aisha Naeem[1#], Muhammad Umer Choudhry[1#], Erika Parasido[1], Lucas Tricoli[1], Angiela Sivakumar[1], John P. Mikhaiel[1], Venkata Yenugonda[1], Olga C. Rodriguez[1], Sana D. Karam[2], Brian R. Rood[3], Maria Laura Avantaggiati[1*], and Chris Albanese[1,4,*]

[1]Lombardi Comprehensive Cancer Center and Department of Oncology, Georgetown University Medical Center, Washington, DC 20057, USA
[2]Department of Radiation Oncology, University of Colorado, Denver, CO 80208, USA
[3]Center for Cancer and Immunology Research, Children's National Medical Center, Washington, DC 20057, USA
[4]Department of Pathology, Georgetown University Medical Center, Washington, DC 20057, USA
[#]These authors contributed equally
[*]Equal Senior Author Contributions

Key words: p53, apoptosis, autophagy, medulloblastoma, Endonuclease G, BIK, p63, p73
Received: 08/30/15; Accepted: 10/02/15; Published: 10/27/15 **doi:** 10.18632/aging.100831
Correspondence to: Chris Albanese, PhD; **E-mail:** albanese@georgetown.edu

Abstract: **Medulloblastoma (MB), a primitive neuroectodermal tumor, is the most common malignant childhood brain tumor and remains incurable in about a third of patients. Currently, survivors carry a significant burden of late treatment effects. The p53 tumor suppressor protein plays a crucial role in influencing cell survival in response to cellular stress and while the p53 pathway is considered a key determinant of anti-tumor responses in many tumors, its role in cell survival in MB is much less well defined. Herein, we report that the experimental drug VMY-1-103 acts through induction of a partial DNA damage-like response as well induction of non-survival autophagy. Surprisingly, the genetic or chemical silencing of p53 significantly enhanced the cytotoxic effects of both VMY and the DNA damaging drug, doxorubicin. The inhibition of p53 in the presence of VMY revealed increased late stage apoptosis, increased DNA fragmentation and increased expression of genes involved in apoptosis, including *CAPN12* and *TRPM8, p63, p73, BIK, EndoG, CIDEB, P27^{Kip1} and P21^{cip1}*. These data provide the groundwork for additional studies on VMY as a therapeutic drug and support further investigations into the intriguing possibility that targeting p53 function may be an effective means of enhancing clinical outcomes in MB.**

INTRODUCTION

Medulloblastoma (MB) is a primitive neuroectodermal tumor that arises from granule neuron precursors in the cerebellum or from neural stem cells of the rhombic lip and is the most frequently diagnosed malignant brain tumor in children [1]. Approximately 70% of MB cases occur in children under the age of 10. While less common, MB is also seen in patients between 20 and 44 years of age, with incidences falling off significantly thereafter. A combination of surgery, radiotherapy, and chemotherapy has contributed to improved treatment outcomes, resulting in a 70-80% five-year disease-free patients with medulloblastoma remain significant and recurrence is frequently observed. As with many malignancies, disease recurrence is nearly always fatal, and late mortality remains a serious health issue in long-term MB survivors [2]. Moreover, current therapies result in significant negative impacts on neurological, cognitive and social development, especially in the youngest affected children. Significant efforts are therefore underway to develop more effective and less toxic MB treatments.

The efficacy of many anti-tumor agents relies on their ability to trigger the tumor suppressive activities of p53, which leads to the induction of cell death, frequently via cellular pathways of apoptosis, senescence or mitotic catastrophe. While the activity of the p53 tumor suppressor protein is highly complex [3], its expression is induced by a broad array of cell stressors including DNA-damaging chemotherapeutic drugs and can be an excellent target for therapeutic intervention ([4], see also [3]). Impairment of *p53* signaling by gene mutation or gene silencing/loss has been shown to contribute to the induction, progression and/or recurrence of many tumor types and can confer resistance to tumor therapy. p53 plays unique roles in neural development. For example, p53 has been directly implicated in neurogenesis as well as in neural stem cell self-renewal, neurite outgrowth and axonal regeneration (reviewed in [5]), and acetylation of p53 is required for the induction of neurite outgrowth [6]. Despite this knowledge and that related to the role of p53 in many malignancies, the function of p53 in MB remains under-explored. For example, unlike lung, pancreas and bladder cancers, only a minority of primary MB patients present with p53 mutation or loss, with reported frequencies between 7% [7] and 15% [8]. Interestingly, while the frequency of p53 mutations increases upon recurrence, the percentage of cells with nuclear p53 also increases, rising from 26% at diagnosis to 33% at relapse [8], suggesting that certain mechanisms underlying p53 function may still be intact. Importantly, the MAGIC consortium identified chromosome 17 deletions, where the *p53* locus is located, to be associated with chromothripsis (chromosomal fragmentation) in Group 3 MB [9], while reduced expression of p53 was seen in Group 4 MB [10]. Collectively, these findings highlight the complex and poorly defined role for p53 in human MB, and support the need for mechanistic studies into p53 activity as a possible therapeutic effector protein.

The *in vitro* [11-13] and *in vivo* [14] anti-tumor activities of an experimental CDK inhibitor, VMY-1-103 (VMY), have previously been described by us in both prostate and other solid tumors [11, 13, 15] and in MB [12, 14]. Our previous MB studies established that the extrinsic apoptotic pathway was induced by VMY, as was mitotic catastrophe in a subset of the cells [12]. In the present study, we sought to further define the molecular and genetic mechanisms by which VMY induces MB cell death. Herein, we show in both p53-wild type (D556) and p53-mutant (DAOY) MB cells lines that treatment with VMY resulted in the translocation of p53 into the nucleus, an induction of γH2AX, a decrease in MDM2 protein levels and activation of non-survival macro-autophagy. Interestingly, suppression of p53 function via shRNA knockdown or treatment with the p53 inhibitory compound Pifithrin-α (Pif) [16] resulted in significant increases in cell death following treatment with either VMY or doxorubicin. Gene expression analyses performed on D556 cells treated with VMY and Pif versus VMY alone revealed a significant increase in genes associated with apoptosis and necrosis, including the calcium pathway signaling genes *CAPN12 and TRPM8* suggesting alterations in intracellular calcium signaling may play a role in enhancing cell death. In addition, *p63* and its transcriptional target the pro-apoptotic gene *BIK* were induced, as were *p73* and its target, the caspase-independent intranucleosomal DNase, *Endonuclease-G* (Endo-G) [17].

Given the difficulties in effectively treating MB, especially recurrent disease, targeting p53 in combination with chemotherapy potentially represents a new treatment strategy for medulloblastoma.

RESULTS

Treatment of MB cells induces a durable cytotoxic effect

We have previously reported that VMY induces MB cell death [12, 14]. To test whether VMY's antiproliferative effects were sustained after removal of the compound, colony forming assays were performed. D556 cells were treated with VMY or its parent compound purvalanol B (PVB) for 18 hrs, at which point the media was changed and the cells were allowed to recover in the absence of the drugs until the control plate reached 80% confluency (approximately 3-5 days). VMY treatment resulted in a significant reduction in both the number of colonies (Fig 1A, B, C) as well as the number of cells per colony (Fig 1D) versus either DMSO- or PVB- treated D556 cells, which express wild type p53. The DNA damaging drug, doxorubicin (1uM), effectively killed all cells (not shown).

VMY induces a partial DNA damage-like response in DAOY and D556 MB cell lines

Our previous studies established that the induction of cell death in MB cells occurred, at least in part, through the extrinsic apoptotic pathway and mitotic disruption [12, 14]. To further investigate the mechanisms by which VMY impacts cell survival, we interrogated proteins involved in DNA damage response and stress signaling. Time course studies of VMY treatment were performed first in DAOY cells, which express mutant p53 ($p53^{C252F}$). Doxorubicin was used as a positive control for induction of a DNA damage response [18],

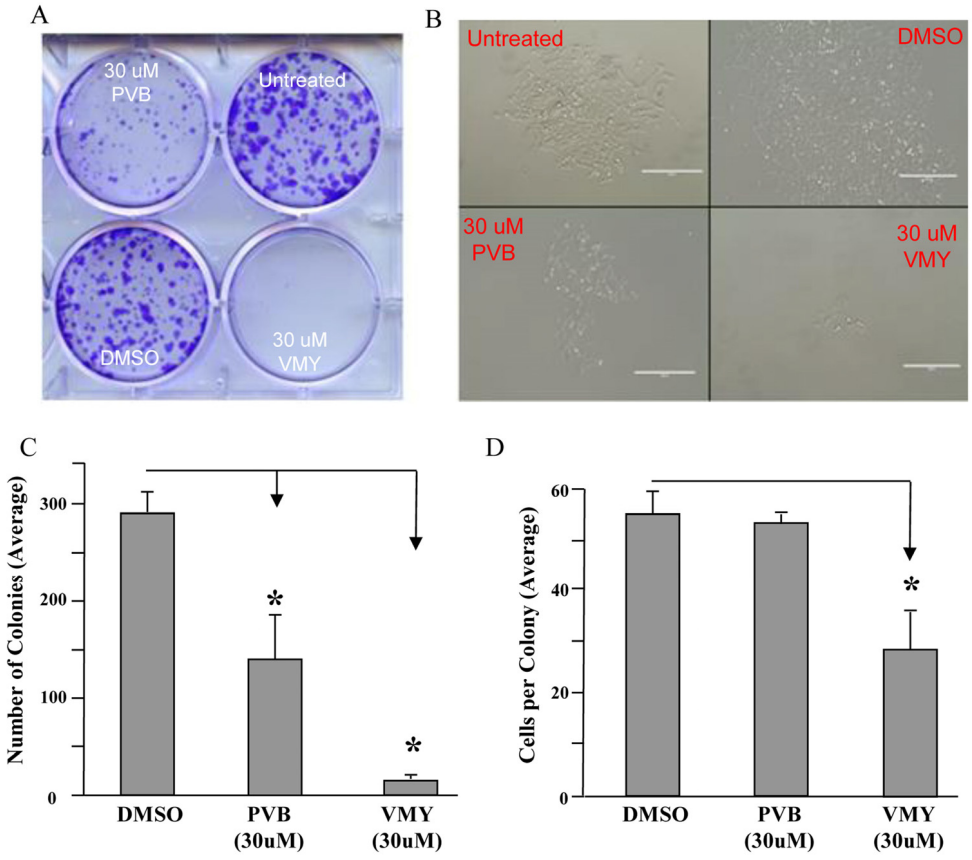

Figure 1. VMY induced cell death. The durability of effects of VMY on cell viability was determined via colony forming assays. D556 cells were treated with DMSO, PVB or VMY for 18 hrs. Fresh media was added and the cells cultured for an additional 3-5 days. (**A**) Cells stained with crystal violet. (**B**) Colonies as visualized by microscopy. (**C**) Quantification of colony number. (**D**) Quantification of cells per colony. The data are shown as average ± standard deviation. PVB; purvalanol B, *; $p<0.05$.

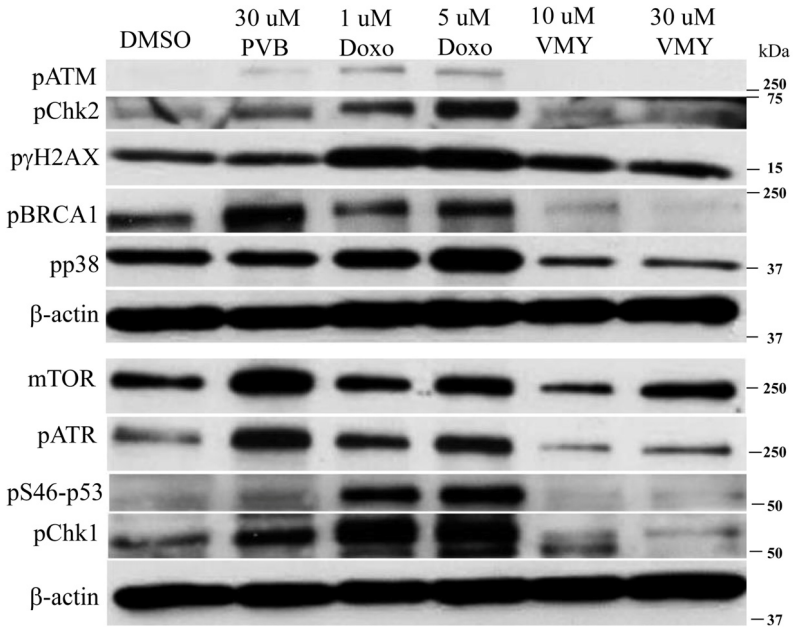

Figure 2. Effects of VMY on stress related proteins. DAOY cells were treated for 18 hrs with DMSO, PVB, VMY or doxorubicin at the concentrations listed and immunoblotting was performed for the proteins shown. β-actin was used as a loading control. PVB; purvalanol B, Doxo; doxorubicin.

and PVB was also tested. Compared to DMSO control, treatment with doxorubicin for 18 hours increased the levels of phosphorylated isoforms of ATM, Chk2, γH2AX, BRCA1 and p38 (Fig. 2) as well as ATR, pS46-p53 and Chk1 (Fig 2). A modest increase in mTOR was also noted. In contrast, the levels of all of these proteins, with the exception of p-γH2AX (Fig 2) and to a lesser extent mTOR, were reduced following treatment with VMY. Interestingly, PVB behaved in a manner similar to doxorubicin despite the fact that PVB is an inefficient inhibitor of MB cell proliferation [12]. In contrast to DAOY cells, the levels of total- and phospho- p38 remained relatively constant in D556 cells and phospho-p38 decreased slightly following 18 hrs of VMY treatment (Fig 3A), however sustained induction of γH2AX was confirmed by western blot and by immunofluorescence in both DAOY and D556 cells (Fig 3A, B).

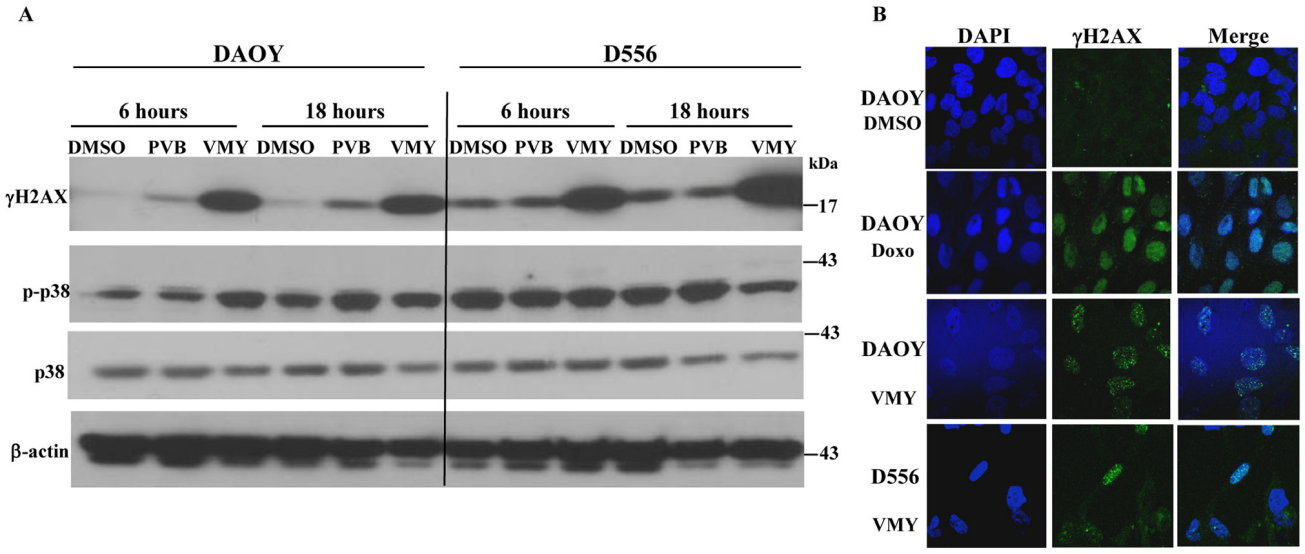

Figure 3. Effects of VMY on stress related proteins in MB cells. DAOY and D556 cells were treated with PVB or VMY. (**A**) Immunoblotting was performed for total and phosphorylated p38 and phosphorylated γ-H2AX following treatment for 6 or 18 hrs. (**B**) Immunofluorescence microscopy for γ-H2AX was performed on DAOY cells treated with 1 uM doxorubicin for 18 hrs and DAOY and D556 cells treated with 10 uM VMY for 18 hrs. DAPI was used to stain the nuclei. PVB; purvalanol B, Doxo; doxorubicin.

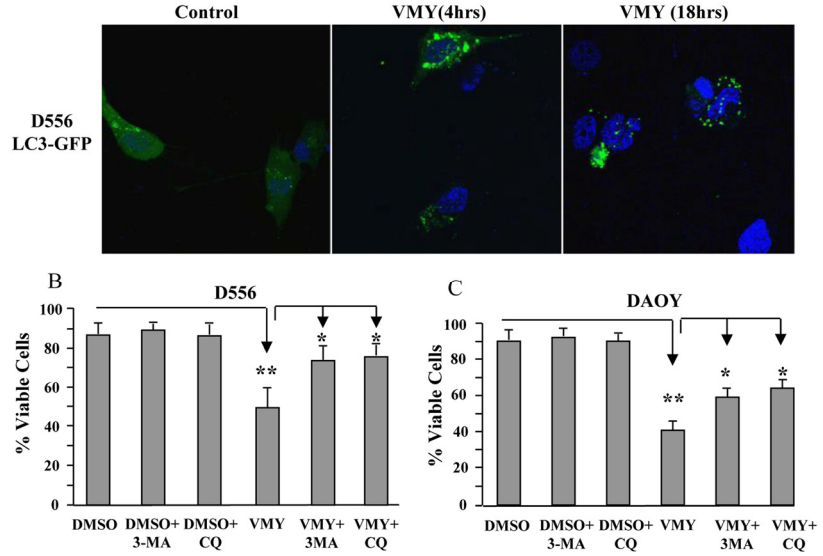

Figure 4. Induction of Autophagy by VMY reduces cell viability. (**A**) D556 cells, transfected with LC3-GFP, were treated with DMSO or VMY for 4 and 18 hrs. Autophagic LC3-GFP puncta were visualized by fluorescence microscopy. Cell nuclei were stained with DAPI. (**B**) D556 and (**C**) DAOY cells were treated with VMY for 18hrs in the presence or absence of 5 uM 3-MA (an inhibitor of early autophagy) or 50 uM chloroquine (an inhibitor of acidification of lysosomes and autophagosomes), and trypan blue viability assays were performed to establish cell viability. The data are shown as the average ± standard deviation of N=3 separate experiments. *; p<0.05, **; p<0.01, 3-MA; 3-methyladenine, CQ; chloroquine.

.

VMY induces autophagy in MB cells

VMY has the ability to block proliferation in prostate cancer cells in part through the induction of catastrophic autophagy [15]. During autophagy, LC3-I (microtubule-associated protein 1 light chain 3) becomes lipidated by the class III phosphoinositide 3-kinase, Vps34, and re-localizes from the microtubules to autophagosomal membranes (reviewed in Kang, et al. [19]). We therefore studied the pattern of subcellular localization of LC3-I in MB cells. D556 cells were transiently transfected with an LC3-GFP expression vector and subjected to fluorescence microscopy as previously described [15]. VMY treatment induced LC3-GFP re-localization and concentration into prototypical autophagic puncta (Fig 4A) with an average of 6 puncta per VMY-treated, LC3-GFP positive cell at 4 hours and 7.8 puncta per cell at 18 hrs, versus an average of 2.3 puncta per cell in control cells (Fig 4A). Our previous data established that inhibition of autophagy protected against VMY-induced cell death in prostate cancer cells [15]. We therefore investigated whether inhibitors of early (3-methyladenine, 3-MA) or late (chloroquine, CQ) autophagy influenced cell survival. Using D556 and DAOY cells, trypan blue dye exclusion assays established that neither 3-MA nor CQ influenced survival in control cells, however significant increases ($p<0.05$, N=3 separate experiments) in cell viability were seen in both cell lines when treated with VMY and the inhibitors (Fig 4B, C).

Regulation of p53 activity is similar in DAOY and D556 MB cell lines

Our earlier investigations into the mechanisms by which VMY reduced overall cell survival in solid tumors clearly established a role for wild type p53 in inducing cell death through both apoptosis and catastrophic autophagy. For example, in adenocarcinoma cell lines with wild type p53, VMY caused a rapid induction of p53 protein levels whereas p53 levels remained constant in cells harboring p53 mutations [15]. Furthermore, the loss of p53 function via deletion, mutation or genetic silencing resulted in a complete loss of VMY-induced cytotoxicity in a variety of cancers, including prostate, breast and pancreas, while re-expression of wild type p53 in PC3 cells or treatment of DU145 cells with PRIMA1 restored VMY-induced autophagy and cell death [11, 15].

We therefore next investigated the effects of VMY on p53 expression in DAOY (p53 C242F mutant [20]) and D556 cells (p53 wild type). Unlike our previous findings in adenocarcinoma cells, p53 levels were high in both cell lines and were not affected by treatment with VMY (Supplemental Fig. 1). Similar results were seen with PVB (Supplemental Fig. 1). The levels of the p53-regulatory protein MDM2 were decreased in both cell lines (Fig 5A) and immunofluorescence microscopy demonstrated that p53 shifted from diffusely cyto-plasmic with some nuclear positivity in control cells to

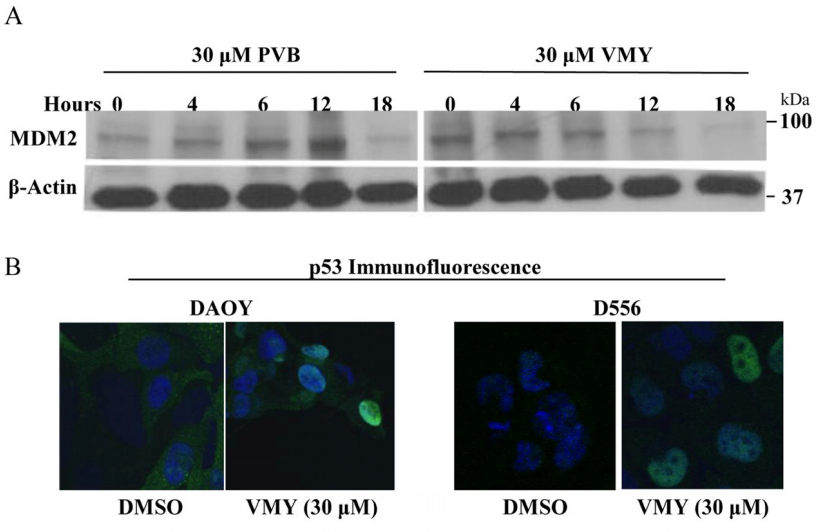

Figure 5. VMY alters the subcellular localization of p53. (**A**) Immunoblotting for MDM2 following exposure of D556 cells to PVB and VMY for the times indicated. β-actin was used as a loading control. (**B**) Immunofluorescence microscopy for p53 subcelluar localization was performed on DAOY (left panels) and D556 (right panels). DAPI was used to stain the nuclei. PVB; purvalanol B.

predominantly nuclear in both cell lines following VMY treatment (Fig 5B). As both the wild type and mutant p53 proteins localize to the nucleus following exposure to VMY, these data suggest that both proteins may retain some functional activity.

The role of p53 in inducing cell death

To determine the role of p53 in regulating MB cell survival in the presence of VMY, p53 was genetically silenced with the previously validated p53 shRNA [15] or chemically inhibited by the p53-inhibitory compound, Pifithrin-α (Pif), which we have used in previous experiments to investigate p53's role in regulating autophagy [16]. The silencing of p53 by shRNA resulted in up to a 68% decrease in p53 protein levels versus pLKO control across all treatment groups in both D556 and DAOY cells (Fig 6A). Surprisingly, both the genetic and chemical silencing of p53 led to significant increases in cell death by VMY as measured by colony forming assay (Fig 6B). Equally surprising was the observation that the loss of p53 failed to protect against cell death by doxorubicin (Fig 6B, C). Dose escalation experiments performed in D556 cells in the presence and absence of Pif established that the heightened chemosensitivity was consistent across a broad range of concentrations (Fig 6D). In addition, experiments performed in DAOY showed that cell-survival declined by 33 percent in VMY-treated cells with p53 shRNA knockdown compared to VMY-treated pLKO control cells (Sup Fig S2).

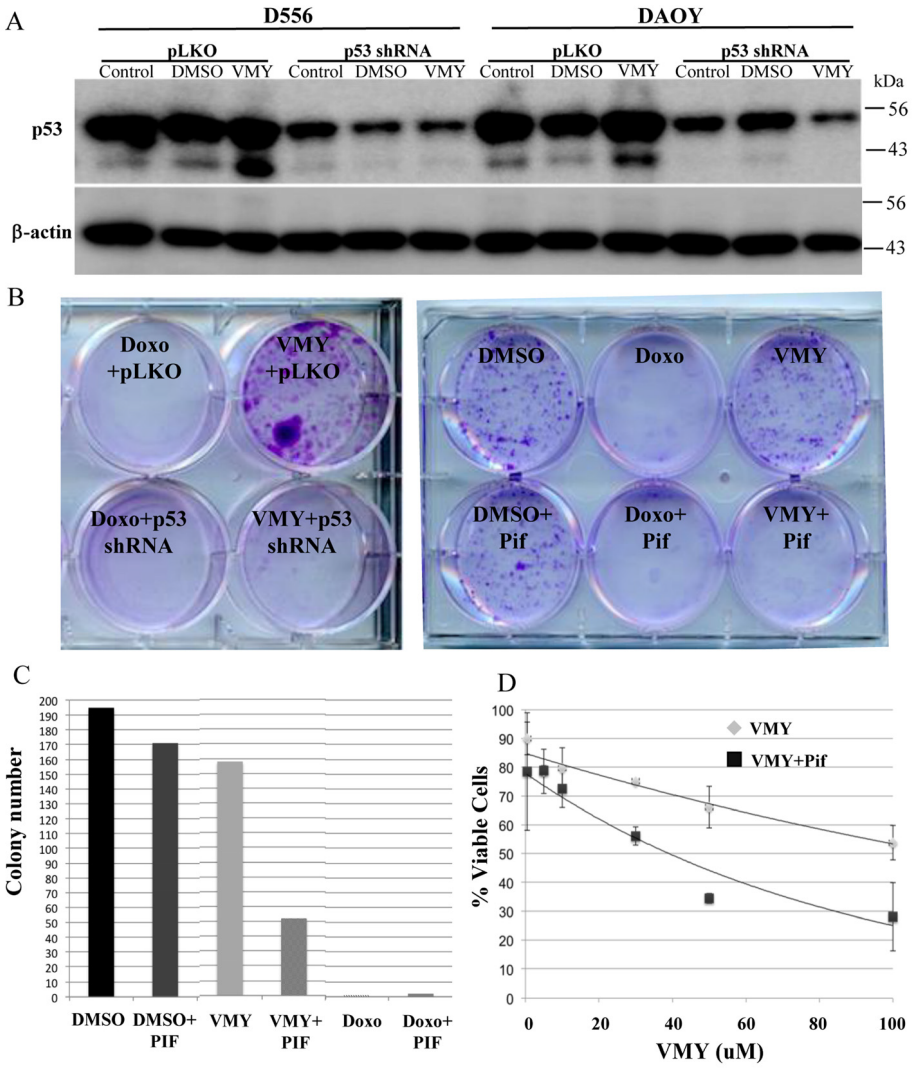

Figure 6. Effects of silencing of p53 on cell survival. (**A**) Genetic silencing of p53. D556 and DAOY cells were infected with p53siRNA or pLKO lentivirus'. The cells were left untreated or exposed for 18 hrs to DMSO or 30uM VMY as indicated, and western blots for p53 and β-actin were run. (**B**) The effects of p53shRNA knockdown (left) and Pifithrin (Pif, right) on cell viability were determined via colony forming assays. D556 cells were treated with DMSO, doxorubicin or VMY for 18 hrs. Fresh media was added and the cells cultured for an addition 3-5 days, followed by staining with crystal violet. (**C**) Quantification of the number of colonies in (**B**). (**D**) Dose response curves of D556 cells treated with VMY at the concentrations shown in the presence and absence of Pifithrin. The data are shown as average ± standard deviation of N=3 separate experiments.

Table 1. Top 25 genes altered in the presence of Pifithrin α plus VMY vs. VMY alone.

Pif + VMY *vs.* VMY			
Up-regulated	**Fold**	**Down-regulated**	**Fold**
EndoG	8.77809E+30	FIGF	-6.10476E+11
CIDEB	1.9687E+12	ANGPT4	-6.017072518
PRSS54	1299.03	GSK3A	-5.35
BIK	19.44	INCA1	-5.18
MAP3K9	18.19	TNFSF14	-4.01
ERBB3	15.17	GDF15	-4.01
BRAT1	7.48	HGF	-3.89
CISH	6.73	BIRC3	-3.41
FADD	6.73	LIF	-2.85
TP63	6.63	NTF3	-2.77
CBX6	6.23	DRD2	-2.75
SRC	5.98	SNCG	-2.67
CBX7	5.98	MAGEA9	-2.67
HDAC4	5.24	ZNF385D	-2.67
RASSF4	4.49	CRIP3	-2.67
TRPM8	4.49	TNFSF15	-2.45
ERBB2	4.06	NAP1L6	-2.45
AKT1	3.84	TENC1	-2.33
UNC5B	3.83	NRCAM	-2.23
TNFRSF10D	3.74	DNAJB7	-2.21
NLRP12-14	3.74	MAGEB2	-2.19
TP73	3.74	PPAPDC2	-2.14
ARHGEF18	3.55	PRSS12	-2.14
TNFRSF25	3.49	CFLAR	-2.07
FASTK	3.48	GADD45A	-2.07

Loss of p53 in the presence of VMY alters calcium, p63 and p73 signaling pathways

In order to more completely define the mechanism underlying the paradoxical effect of p53 silencing, RNAseq next generation sequencing was performed on D556 cells treated with VMY in the presence or absence of Pif. RNA sequence analysis revealed an increase in expression of *calpain 12* in the VMY/Pif treated cells vs. VMY/DMSO control cells (Table 1). In addition, elevated expression of the transient receptor potential channel subfamily (*TRPM8*) gene was seen (Table 1), collectively suggesting that intracellular calcium signaling pathways were affected by p53 silencing. Dysregulation of the calcium signaling pathway downstream of stressors such as excitotoxicity can lead to necrotic cell death in neurons (reviewed in [21, 22]), with one of the hallmarks of necrosis being Endo G induction and intranucleosomal DNA cleavage [22]. As both the pro-apoptosis regulatory genes p63 and p73 were induced by p53 silencing, as were possible downstream targets including Endo-G [23], the pro-apoptotic BH3-protein, BIK (Bcl-2-interacting killer) and CIDEB (cell death-inducing DFFA-like effector B), we assessed levels of late stage apoptosis and necrosis by flow cytometry, by gating for annexin V-positive/propidium iodide (PI)-positive cells. D556 cells were infected with either pLKO or p53shRNA as described above and treated for 18-hours with DMSO, 30uM VMY or 1uM doxorubicin, after which they were analyzed by flow cytometry as previously described [15]. While the annexin$^-$/PI$^+$ fraction of cells was unaffected, the silencing of p53 increased the proportion of annexin V$^+$/PI$^+$ cells following exposure to VMY or doxorubicin

A

	Relative Change (%)			
	Annexin V$^-$/PI$^+$		Annexin V$^+$/PI$^+$	
	PLKO	p53shRNA	PLKO	p53shRNA
DMSO	1	< 1.0	1	7
VMY	1	2.5	1	14
Doxo	1	< 1.0	1	11

B

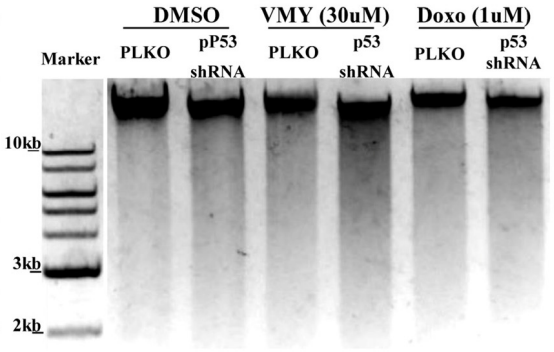

Figure 7. Effects of p53 knockdown on apoptosis and DNA fragmentation in D556 cells. (**A**) The proportion of cells undergoing apoptotic cell death as a result of p53 shRNA knockdown in D556 cells treated for 18 hrs with DMSO, VMY (30uM) or doxorubicin (1uM) as assessed using annexin V and propidium iodide (PI) staining and measured by flow cytometry. Data are shown as percent change in staining versus pLKO-control infected cells. (**B**) D556 cells were infected with pLKO or p53shRNA and treated with DMSO, VMY or doxorubicin for 18hrs. DNA fragmentation of nuclear DNA was assessed by ethidium bromide-agarose gel electrophoresis.

(Fig 7A). Finally, similar effects were seen using agarose gel electrophoresis assays where 18-hour treatment with VMY or doxorubicin plus p53shRNA resulted in enhanced DNA degradation, indicative of necrosis and apoptosis (Fig 7B).

Taken together, these experiments show that p53 protects against drug-induced cell death in medulloblastoma cells and its genetic- or chemical-suppression results in a significant increase in cell sensitivity to VMY and doxorubicin, an experimental and a clinical drug, respectively.

DISCUSSION

Necrosis, apoptosis and autophagy are activated under a variety of cell stress conditions (see references [24, 25] among others), however, little is known about how these complex and partially overlapping mechanisms are induced in medulloblastoma cells. In addition, to date, there have been few publications exploring the effects in medulloblastoma cells of the synthetic modulation of p53 activity during exposure to chemotherapeutic drugs.

We have recently shown in prostate cancer cell lines as well as in primary prostate cancer cells established using our conditional cell reprogramming approach [26, 27], that the induction of p53 by VMY was a prerequisite for inducing both autophagy and apoptosis, and that silencing p53 effectively blocked cell death [15]. Additionally, our earlier studies on VMY's effects on MB established that this experimental drug induced apoptosis and mitotic catastrophe *in vitro* [12]. Furthermore, while our *in vivo* studies showed that 20 mg/kg of VMY administered three times per week for more than four weeks was well tolerated and was effective at treating a mouse model of SHH-driven medulloblastoma [14], a detailed investigation into the mechanism of VMY-induced cell death, and the role that p53 may play had not been explored. We now show that in MB cells, VMY induces the relocalization of p53 into the nucleus, an accumulation of γH2AX, a decrease in MDM2 protein levels and activation of non-survival macro-autophagy. Since the protein levels of key stress-related proteins were reduced by VMY, the possibility existed that components of the CAP-dependent protein translation pathway may be inhibited by VMY. MNK1 is a target of p38 and MAPK and acts to increase CAP-dependent translation through the phosphorylation of the elongation factor eIF4E [28]. 4E-BP1 is a negative regulator of translation and phosphorylation of 4E-BP1 by mTOR inhibits its repressor function. Thus, if VMY negatively regulated CAP-dependent translation, the phosphorylation levels of 4E-BP1 and pMNK1 would be expected to reduce, however VMY increased the levels of these proteins in both D556 and DAOY cells (S.W and C.A, unpublished data). Interestingly, rather than protecting against chemotherapeutic cell killing, the suppression of p53 through shRNA knoc kdown or chemical inhibition by Pifithrin-α resulted in a significant increase in cell death by either VMY or doxorubicin, suggesting that p53 acts as a chemoprotective protein in these primitive neuroectoderm-derived cancer cells.

Regarding its function in the neuroectoderm, p53 performs roles different to those found in other tissues. In the past decade a role for p53 has emerged in neuronal differentiation, axon guidance, neurite outgrowth and axonal regeneration [29, 30]. Analysis of p53-dependent transcriptional activation in normal development *in vivo* by using a lacZ reporter gene under the control of a p53-responsive promoter showed that p53 activity was maximal during neuronal differentiation and clustered in areas that showed little correlation with the apoptosis normally ongoing in the developing nervous system [31, 32]. Furthermore, other studies have shown that approximately one quarter of p53-null mice developed exencephaly due to cellular overgrowth, rather than decreased apoptosis [33, 34].

The dependence of neurite outgrowth and elongation on p53 has also been shown in the developing cerebellum. Gaub et al., 2010 showed that acetylated p53 is required for neurite outgrowth in cerebellar granule cell progenitors. Conversely, the loss of the function acetyl p53 mutant (K-R) inhibits physiological neurite outgrowth in those cells [35]. In cultured rat cerebellar granule cells, Maruoka et al., 2011, showed a p53-mediated neuroprotective effect against glutathione depletion-induced oxidative stress [36].

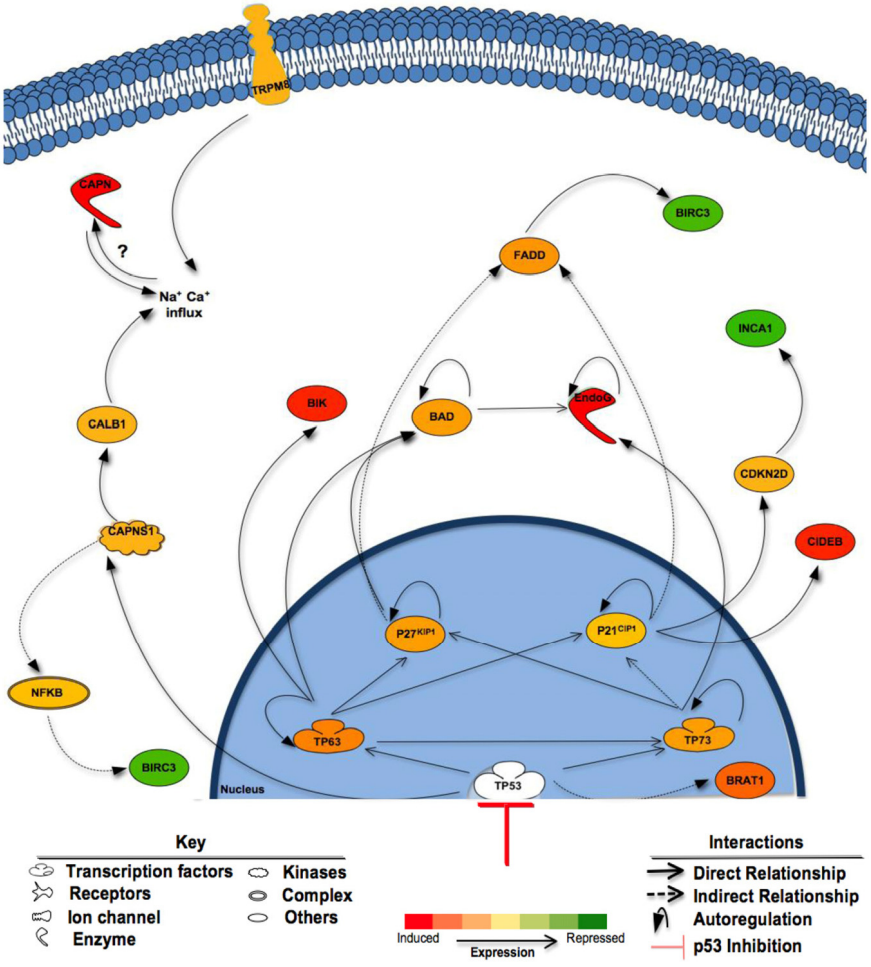

Figure 8. **Proposed mechanisms of enhanced cell death following inhibition of p53**. Shown are the effects of p53 suppression on components of cell death pathways in Pif + VMY *vs.* VMY treated D556 cells. p53 inhibition by Pifithrin resulted in the induction of *p63* and *p73* genes and subsequent enhanced cell death via apoptosis. Induction of the *p63* and *p73* genes leads to the activation of $p21^{CIP1}$ and $p27^{KIP1}$ both of which can indirectly trigger FADD, reducing the expression of BIRC3 (cIAP2). Induction of p73 led to large increases in EndoG and CIDEB expression leading to DNA fragmentation while increased levels of p63 induced apoptosis though BIRC3 and BIK, the latter of which along with TRPM8 can influence intracellular calcium levels. BAD; BCL2-Associated Agonist Of Cell Death, BIK; BCL2-Interacting Killer (Apoptosis-Inducing), BIRC3; baculoviral IAP repeat containing 3 (cIAP2), BRAT1; BRCA1-Associated ATM Activator 1, CAPN; Calpain, CALB1; Calbindin 1, CDKN2D; Cyclin-Dependent Kinase Inhibitor 2D ($p19^{Ink4D}$), CIDEB; Cell Death-Inducing DFFA-Like Effector B, EndoG; Endonuclease G, FADD; Fas-Associated Via Death Domain, INCA1; Inhibitor Of CDK, Cyclin A1 Interacting Protein 1, NF-KappaB; Nuclear Factor Of Kappa Light Polypeptide Gene Enhancer In B-Cells, TRPM8, Transient receptor potential cation channel subfamily M member 8.

Further validation of the role for p53 in neurite outgrowth and neuronal differentiation and maturation comes from studies establishing p53 as a downstream target of neurotrophic receptors. Loss of function experiments of p53 via either gene silencing or dominant negative p53 proteins lacking transactivation capacity have been shown to block NGF-dependent neurite outgrowth and differentiation in PC-12 cells [6, 37]. Another neurotrophic factor, BDNF, has also been shown to stimulate p53 phosphorylation and transcriptional activation in primary cortical neurons [30]. Activation of signaling molecules downstream of NGF or BDNF that are known to induce p53 post-translational modifications and enhance its transcriptional activity has been reported, including ERK1 and ERK2, p38MAPK, JNK1-2 (c-Jun N-terminal kinases 1-2), cytoskeleton remodeling genes, such as GAP-43, the actin-binding protein Coronin 1b and the RAS family member Rab13 [6, 38].

Unresolved however is an actual role for p53 in the biology of human MB. Frequencies of *p53* mutations are low in primary MB but increase significantly in recurrences, and mutant p53 proteins and Myc may collaborate to drive aggressive disease [8]. Additionally, modifications of p53 function are required in *Myc*- [39, 40] but not *Smoothened*- based mouse models to drive MB. The genetic silencing of *p53* in mice with conditional deletion of the *BRCA2-interacting protein* (*BCCIP*) gene also resulted in MB [41]; however the resulting tumor formation was predicated upon the loss of the BCCIP knockdown cassette, which restored BCCIP expression in the neuroectoderm, supporting a role for p53 in neuronal genomic stability. Interestingly, p53 expression levels are lower in group 4 MB, due to the iso-dicentric (17)(p11.2) recombination events frequently seen in this group [10]. However, neither the levels of p53 expression nor its subcellular localization were reported following chemotherapy. It should be noted that etoposide induced p53 activity in D283, MEDI and D458 MB cell lines *in vitro* [42] and the p53 target miR-34a was able to reduce the viability in the p53-impared MB cell line, MEB-Med8a [43], however the effects of silencing of p53 *per se* were not reported. Furthermore, docosahexaenoic acid and etoposide were found to reduce the levels of MDM2 in both p53-mutant DAOY cells as well as in p53-wildtype D283 cells [44] and we also observe decreases in MDM2 with VMY, along with rapid translocation of p53 into the nucleus. Collectively these published studies and our new data suggest that components of the p53 pathway remain intact in a variety of p53-mutant and p53-wild type MB cells.

It was therefore surprising that rather than causing chemotherapeutic resistance, the suppression of p53 function by either shRNA knockdown or Pif sensitized DAOY and D556 cells to both VMY and doxorubicin. Mechanistically, the induction of the *p63* and *p73* and their targeted genes by VMY in the Pif-treated cells was one of the most prominent features (Table 1 and Figure 8). These p53 family-member genes, and their various splice variants, play both similar and distinct roles in development as well as in cancer (reviewed in [45]) and can interact with each other with a high degree of complexity. There is abundant evidence that modulation of p53 function can influence the activity of p63 and p73 (reviewed in [46]) and conversely that p63 and p73 can influence p53 activity in adult neural precursor cells [47]. While the mechanism(s) by which the genetic knockdown or chemical suppression of p53 regulates *p63* and *p73* expression in MB cells has yet to be elucidated, our data suggest that the induction of *p63* and *p73* following p53 suppression fundamentally alters the pro-apoptotic machinery in MB cells (Fig 8). It is also unknown whether the increased sensitivity seen in the cell lines tested extends to a broader array of clinical samples or to the chemo-radiation interventions currently used for treating MB. However as both DAOY and D556 cells show similar sensitivities to p53 functional blockade, the possibility exists that at least a subset of the p53 mutations found in MB patients may not adversely impact p53-targeting regimens. Additional experiments assessing whether the p53 mutant proteins identified in recurrent MB exhibit similar responses to combined p53 suppression and exposure to VMY, doxorubicin or other drugs are clearly warranted.

MATERIALS AND METHODS

Cell lines and cell culture. The human medulloblastoma (MB) cell lines D556 and DAOY were maintained in complete DMEM containing 10% FBS, L-glutamine, and 100 U/ml Penicillin-Streptomycin as previously described [12]. DNA STR fingerprint analyses were performed on both cell lines as a quality control measure. The DAOY data matched the ATCC database for this line, while early and late passage D556 cultures were compared with no significant changes observed and no matches with the available STR database (not shown).

Cell viability and growth. Cell viability was determined using trypan blue dye exclusion and viable and total cell counting using a hemocytometer as previously described [11, 12, 15].

Colony forming assays. A total of 1000 cells were plated in 6 well plates. Cells were allowed to adhere for 24 hrs before treatment, at which point they were

treated with VMY or Doxorubicin for 18 hrs. The media was changed after 18hrs and the plates were incubated in the absence of drug for 3-5 days to reach 80% confluency in the negative control wells. Cells were washed with PBS, fixed with 10% neutral buffered formalin solution for 15-30 minutes and stained with 0.5% (w/v) crystal violet for 30-60 minutes. The crystal violet was aspirated, cells were washed with PBS and dried for one hour before counting.

Flow cytometry. The prostate cells were fixed and stained with 20ug/ml propidium iodide (PI) and 5 U RNase A, and the DNA content and subG1 DNA fragmentation was measured using a FACStar Plus system (Becton-Dickson, Franklin Lakes, NJ) as previously described [11, 12]. Cellular apoptosis was also assessed by APC-Annexin V antibody (Biolegend, San Diego, CA) staining immediately after treatment with VMY and analyzed using FACStar Plus dual laser FACSort system (Becton-Dickson, Franklin Lakes, NJ) as previously described by us [11, 12, 48, 49].

Immunoblotting. Protein extracts were prepared and separated on 4-20% Tris-glycine gels and electro-blotted onto PVDF membranes as previously described [11, 12, 50]. Protein levels were assessed using antibodies against p53 (Millipore, Bellerica, MA #05-224), p-ATM (Cell Signaling, Danvers, MA #5883P), p-Chk2 (Cell Signaling, Danvers, MA #2661P), p-Chk1 (Cell Signaling, Danvers, MA #2348P), p38 (Cell Signaling, Danvers, MA #8690), histone γ-H2AX (Cell Signaling, Danvers, MA #7631), p-histone γH2AX (Cell Signaling, Danvers, MA #9718P), p-BRCA1 (Ser1524) (Cell Signaling, Danvers, MA #9009P), p-P38 MAPK (Cell Signaling, Danvers, MA #9216S), mTOR (Cell Signaling, Danvers, MA #2983), p-ATR (Cell Signaling, Danvers, MA #2853P), p-p53 (Cell Signaling, Danvers, MA #9286P), p-MNK1 (cell signaling, #2111S), p-4E-BP1 (Cell Signaling, Danvers, MA #2855S), MDM2 (Santa Cruz Biotechnology, #sc-965), β-actin (Cell Signaling, Danvers, MA #4967). Densitometry was performed using ImageJ analysis software (NIH, Bethesda, MD) as previously described [11, 12, 50].

Immunofluorescent imaging. Cells were seeded on glass coverslips and treated with DMSO or VMY for 4 or 18 hrs. Cells were washed with PBS and fixed in 10% formalin for 10 min. The coverslips were washed three times with PBS, the cells were permeabilized with 0.1% Triton X-100 and washed three times with PBS. The samples were blocked with 1% BSA for 20 minutes and washed an additional three times in PBS. The cells were exposed to anti-p53 (1:150, Millipore #05-224) or anti-γH2AX (1:150, Cell Signaling #7631) antibodies for 1 hr at room temperature. The slides were washed with PBS an additional three times and stained with the secondary antibody Alexa Fluor goat 488 anti-mouse (1:150, Life Technologies, A-10667) for 30 min at room temperature. Slides were then counter-stained with DAPI for 5 min. The coverslips were mounted onto glass slides with Tris-buffered fluoro-gel (Electron Microscopy Sciences). Confocal microscopy was performed on a Zeiss (Thornwood, NY) LSM510 Meta microscope using a 40x lens.

LC3-GFP. LC3 translocation was detected using the green fluorescent protein (GFP)-fused LC3 construct that was generously donated by Dr Robert Clarke [51]. Briefly, cells were seeded in 6 well plates containing glass coverslips and allowed to attach overnight. The LC3-GFP expression plasmid (14ug) was transfected using Lipofectamine LTX reagent (Life Technologies, Carlsbad, CA #15338-100) as previously described by us [15]. 24 hours after transfection, the cells were treated with VMY or vehicle. After 18 hours, the coverslips with attached cells were stained with DAPI and rinsed 3 times with PBS and the coverslips mounted. Imaging was performed by confocal microscopy as previously described [12, 15].

Autophagy inhibitors. For autophagy inhibition, 3-methyladenine (3-MA) (Sigma-Aldrich, St Louis, MO #M921) was used at 5mM and chloroquine diphosphate (CQ) (Sigma-Aldrich, St Louis, MO #C6628) was used at 50 μM as previously described [15]. Cells were exposed to these inhibitors for 20 minutes prior to treatment with either DMSO or VMY [15].

p53 expression and shRNA knockdown. For lentivirus knockdown experiments, the p53shRNA and pLKO vectors were purchased commercially (Vector Biolabs, Philadelphia, PA, #1854) and used as described by the manufacturer as previously described [15]. Briefly, 293T cells (ATCC, Manassas, VA) were cotransfected with shRNA constructs along with the pHR′8.2ΔR and pCMV-VSV-G helper constructs. After 24 hours, the media was changed and the virus-containing media was harvested after an additional 24 hours of incubation. The MB cells were seeded at 30% confluency and viral infections were performed for 72 hours prior to treatment with VMY or DMSO. Efficiency of the knockdown was monitored by p53 immunoblotting and quantification by ImageJ as previously described [15, 52, 53].

Chemical inhibition of p53. For chemical inhibition of p53, 30uM Pifithrin-α (Sigma-Aldrich, St Louis, MO #P4359) was added one hour prior to treatment with VMY, doxorubicin or DMSO.

DNA fragmentation. D556 cells were infected with pLKO or p53shRNA virus's for 72 hrs prior to treatment with VMY or DMSO. Doxorubicin was used as a positive control. The genomic DNA was isolated after 18 hr treatment with VMY or doxorubicin using the DNeasy blood and tissue kit (Qiagen, MD #69506). 500ng of DNA was run on 1% agarose gel containing ethidium bromide with the electrophoresis carried out at 100V for one hour.

RNAseq and pathway analyses. Total RNA was extracted from D556 cells treated with Pif and VMY as described above using an RNeasy Plus Mini Kit (Qiagen, MD, #74134) and submitted to Otogenetics Corporation (Norcross, GA USA) for RNA-Seq assays. Sequencing was performed on the Illumina HiSeq 2500 (20 million reads, Rapid run, Illumina, CA USA) with chemistry v1.0 and using the 2×106bp paired-end read mode and original chemistry from Illumina according to the manufacturer's instructions. The initial data analysis was started directly on the HiSeq 2500 System during the run. The HiSeq Control Software 2.0.5 in combination with RTA 1.17.20.0 (real time analysis) performed the initial image analysis and base calling. Quality control (QC) was performed using FastQC software. All the samples passed the "Basic Statistics", "Per Base Sequence Quality", "Per Sequence Quality Scores", "Per Base N Content", and "Sequence Length Distribution". No specific filtering was done for the samples. The final FASTQ files comprising the sequence information which was used for all subsequent bioinformatics analyses. Sequences were de-multiplexed according to the 6bp index code with 1 mismatch allowed. After QC, Tophat2 was used for the alignment, and BAM files were obtained. Partek Genomics Suite (6.6 version 6.12.0713 software (Partek Inc.) was utilized to calculate RPKM as normalization, and fold changes were calculated based on the RPKM results. The pathways analysis was performed through the use of QIAGEN's Ingenuity® Pathway Analysis (Qiagen, Redwood City, CA).

ACKNOWLEDGEMENTS

Cell cycle analyses were performed in the Lombardi Comprehensive Cancer Center's Flow Cytometry Shared Resource, microscopy was performed in the Lombardi Comprehensive Cancer Center's Microscopy and Imaging Shared Resource, the DNA fingerprint analyses were done through the Lombardi Comprehensive Cancer Center's Tissue Culture Shared Resource and the RNAseq was performed through the Lombardi Comprehensive Cancer Center's Genomics and Epigenomics Shared Resource.

Funding

Funding was provided by; ABCC (Albanese), R01CA193698 (Avantaggiati) and NIH P30 CA51008-18 (Weiner). This work was also supported by the Paul Calabresi Career Development Award for Clinical Oncology (K12, Karam) an American Cancer Society Institutional Grant (Karam) and a Howard Hughes Medical Institute University Grant (Waye). We thank Milton Brown for supplying VMY-1-103.

Conflict of interest statement

Georgetown University has submitted a patent application on VMY-1-103 where V.Y. is an inventor.

REFERENCES

1. Samkari A, White JC and Packer RJ. Medulloblastoma: toward biologically based management. Semin Pediatr Neurol. 2015; 22:6-13.

2. Ning MS, Perkins SM, Dewees T and Shinohara ET. Evidence of high mortality in long term survivors of childhood medulloblastoma. J Neurooncol. 2015;122:321-327.

3. Soussi T and Wiman KG. TP53: an oncogene in disguise. Cell Death Differ. 2015;22:1239-1249.

4. Muller PA and Vousden KH. Mutant p53 in cancer: new functions and therapeutic opportunities. Cancer Cell. 2014; 25:304-317.

5. Quadrato G and Di Giovanni S. Gatekeeper between quiescence and differentiation: p53 in axonal outgrowth and neurogenesis. Int Rev Neurobiol. 2012;105:71-89.

6. Di Giovanni S, Knights CD, Rao M, Yakovlev A, Beers J, Catania J, Avantaggiati ML and Faden AI. The tumor suppressor protein p53 is required for neurite outgrowth and axon regeneration. Embo J. 2006; 25:4084-4096.

7. Pfaff E, Remke M, Sturm D, Benner A, Witt H, Milde T, von Bueren AO, Wittmann A, Schottler A, Jorch N, Graf N, Kulozik AE, Witt O, Scheurlen W, von Deimling A, Rutkowski S, et al. TP53 mutation is frequently associated with CTNNB1 mutation or MYCN amplification and is compatible with long-term survival in medulloblastoma. J Clin Oncol. 2010; 28:5188-5196.

8. Hill RM, Kuijper S, Lindsey JC, Petrie K, Schwalbe EC, Barker K, Boult JK, Williamson D, Ahmad Z, Hallsworth A, Ryan SL, Poon E, Robinson SP, Ruddle R, Raynaud FI, Howell L, et al. Combined MYC and P53 defects emerge at medulloblastoma relapse and define rapidly progressive, therapeutically targetable disease. Cancer Cell. 2015; 27:72-84.

9. Rausch T, Jones DT, Zapatka M, Stutz AM, Zichner T, Weischenfeldt J, Jager N, Remke M, Shih D, Northcott PA, Pfaff E, Tica J, Wang Q, Massimi L, Witt H, Bender S, et al. Genome sequencing of pediatric medulloblastoma links catastrophic DNA rearrangements with TP53 mutations. Cell. 2012;148:59-71.

10. Bien-Willner GA and Mitra RD. Mutation and expression analysis in medulloblastoma yields prognostic variants and a putative mechanism of disease for i17q tumors. Acta Neuropathol Commun. 2014; 2:74.

11. Ringer L, Yenugonda VM, Ghosh A, Divito K, Trabosh V, Patel Y, Brophy A, Grindrod S, Lisanti MP, Rosenthal D, Brown ML, Avantaggiati ML, Rodriguez O and Albanese C. VMY-1-103, a dansylated analog of purvalanol B, induces caspase-3-dependent apoptosis in LNCaP prostate cancer cells. Cancer Biol Ther. 2010; 10:320-325.

12. Ringer L, Sirajuddin P, Heckler M, Ghosh A, Suprynowicz F, Yenugonda VM, Brown ML, Toretsky JA, Uren A, Lee Y, MacDonald TJ, Rodriguez O, Glazer RI, Schlegel R and Albanese C. VMY-1-103 is a novel CDK inhibitor that disrupts chromosome organization and delays metaphase progression in medulloblastoma cells. Cancer Biol Ther. 2011; 12:818-826.

13. Smahi A, Courtois G, Vabres P, Yamaoka S, Solange H, Munnich A, Israël A, Heiss NS, Klauck SKP and Wiemann Sea. Genomic rearrangment in NEMO impairs NF-kB activation and is a cause of incontinentia pigmenti (IP). Nature. 2000; 405:466-472.

14. Sirajuddin P, Das S, Ringer L, Rodriguez O, Sivakumar A, Lee Y, Uren A, Fricke S, Rood B, Ozcan A, Wang SS, Karam S, Yenugonda VM, Salinas P, Petricoin EF, 3rd, Lisanti MP, et al. Quantifying the CDK inhibitor VMY-1-103's activity and tissue levels in an in vivo tumor model by LC-MS/MS and by MRI. Cell Cycle. 2012; 11:3801-3809.

15. Ringer L, Sirajuddin P, Tricoli L, Waye S, Parasido E, Lee RJ, Feldman A, Wu C-L, Dritschilo A, Lynch J, Schlegel R, Rodriguez O, Pestell RG, Avantaggiati ML and Albanese C. The Induction of the p53 Tumor Suppressor Protein Bridges the Apoptotic and Autophagic Signaling Pathways to Regulate Cell Death in Prostate Cancer Cells. Oncotarget. 2014; 5:10678-10691.

16. Garufi A, Pucci D, D'Orazi V, Cirone M, Bossi G, Avantaggiati ML and D'Orazi G. Degradation of mutant p53H175 protein by Zn(II) through autophagy. Cell Death Dis. 2014; 5:e1271.

17. Li LY, Luo X and Wang X. Endonuclease G is an apoptotic DNase when released from mitochondria. Nature. 2001; 412:95-99.

18. Petruccelli LA, Pettersson F, Del Rincon SV, Guilbert C, Licht JD and Miller WH, Jr. Expression of leukemia-associated fusion proteins increases sensitivity to histone deacetylase inhibitor-induced DNA damage and apoptosis. Mol Cancer Ther. 2013; 12:1591-1604.

19. Kang R, Zeh HJ, Lotze MT and Tang D. The Beclin 1 network regulates autophagy and apoptosis. Cell Death Differ. 2011; 18:571-580.

20. Raffel C, Thomas GA, Tishler DM, Lassoff S and Allen JC. Absence of p53 mutations in childhood central nervous system primitive neuroectodermal tumors. Neurosurgery. 1993; 33:301-305; discussion 305-306.

21. Hara MR and Snyder SH. Cell signaling and neuronal death. Annu Rev Pharmacol Toxicol. 2007; 47:117-141.

22. Fujikawa DG. The role of excitotoxic programmed necrosis in acute brain injury. Comput Struct Biotechnol J. 2015; 13:212-221.

23. Kitagawa K and Niikura Y. Caspase-independent mitotic death (CIMD). Cell Cycle. 2008; 7:1001-1005.

24. Galluzzi L, Vitale I, Abrams JM, Alnemri ES, Baehrecke EH, Blagosklonny MV, Dawson TM, Dawson VL, El-Deiry WS, Fulda S, Gottlieb E, Green DR, Hengartner MO, Kepp O, Knight RA, Kumar S, et al. Molecular definitions of cell death subroutines: recommendations of the Nomenclature Committee on Cell Death 2012. Cell Death Differ. 2012; 19:107-120.

25. Klionsky DJ, Abdalla FC, Abeliovich H, Abraham RT, Acevedo-Arozena A, Adeli K, Agholme L, Agnello M, Agostinis P, Aguirre-Ghiso JA, Ahn HJ, Ait-Mohamed O, Ait-Si-Ali S, Akematsu T, Akira S, Al-Younes HM, et al. Guidelines for the use and interpretation of assays for monitoring autophagy. Autophagy. 2012; 8:445-544.

26. Liu X, Ory V, Chapman S, Yuan H, Albanese C, Kallakury B, Timofeeva O, Nealon C, Dalic A, Simic V, Haddad B, Rhim J, Dritschilo A, Riegel A, McBride A and Schlegel R. ROCK inhibitor and feeder cells induce the conditional reprogramming of epithelial cells. American Journal of Pathology. 2012; 180:590-607.

27. Palechor-Ceron N, Suprynowicz FA, Upadhyay G, Dakic A, Minas T, Simic V, Johnson M, Albanese C, Schlegel R and Liu X. Radiation Induces Diffusible Feeder Cell Factor(s) That Cooperate with ROCK Inhibitor to Conditionally Reprogram and Immortalize Epithelial Cells. Am J Pathol. 2013; 183:1862-1870.

28. Bhat M, Robichaud N, Hulea L, Sonenberg N, Pelletier J and Topisirovic I. Targeting the translation machinery in cancer. Nat Rev Drug Discov. 2015; 14:261-278.

29. Arakawa H. p53, apoptosis and axon-guidance molecules. Cell Death Differ. 2005; 12:1057-1065.

30. Tedeschi A and Di Giovanni S. The non-apoptotic role of p53 in neuronal biology: enlightening the dark side of the moon. EMBO Rep. 2009; 10:576-583.

31. Komarova EA, Chernov MV, Franks R, Wang K, Armin G, Zelnick CR, Chin DM, Bacus SS, Stark GR and Gudkov AV. Transgenic mice with p53-responsive lacZ: p53 activity varies dramatically during normal development and determines radiation and drug sensitivity in vivo. Embo J. 1997; 16:1391-1400.

32. Gottlieb E, Haffner R, King A, Asher G, Gruss P, Lonai P and Oren M. Transgenic mouse model for studying the transcriptional activity of the p53 protein: age- and tissue-dependent changes in radiation-induced activation during embryogenesis. Embo J. 1997; 16:1381-1390.

33. Sah VP, Attardi LD, Mulligan GJ, Williams BO, Bronson RT and Jacks T. A subset of p53-deficient embryos exhibit exencephaly. Nat Genet. 1995; 10:175-180.

34. Armstrong JF, Kaufman MH, Harrison DJ and Clarke AR. High-frequency developmental abnormalities in p53-deficient mice. Curr Biol. 1995; 5:931-936.

35. Gaub P, Tedeschi A, Puttagunta R, Nguyen T, Schmandke A and Di Giovanni S. HDAC inhibition promotes neuronal outgrowth and counteracts growth cone collapse through CBP/p300 and P/CAF-dependent p53 acetylation. Cell Death Differ. 2010; 17(9):1392-1408.

36. Maruoka H, Sasaya H, Sugihara K, Shimoke K and Ikeuchi T. Low-molecular-weight compounds having neurotrophic activity in cultured PC12 cells and neurons. J Biochem. 2011; 150:473-475.

37. Knights CD, Catania J, Di Giovanni S, Muratoglu S, Perez R, Swartzbeck A, Quong AA, Zhang X, Beerman T, Pestell RG and Avantaggiati ML. Distinct p53 acetylation cassettes differentially influence gene-expression patterns and cell fate. J Cell Biol. 2006; 173:533-544.

38. Tedeschi A, Nguyen T, Puttagunta R, Gaub P and Di Giovanni S. A p53-CBP/p300 transcription module is required for GAP-43 expression, axon outgrowth, and regeneration. Cell Death Differ. 2009; 16:543-554.

39. Kawauchi D, Robinson G, Uziel T, Gibson P, Rehg J, Gao C, Finkelstein D, Qu C, Pounds S, Ellison DW, Gilbertson RJ and Roussel MF. A mouse model of the most aggressive subgroup of human medulloblastoma. Cancer Cell. 2012; 21:168-180.

40. Pei Y, Moore CE, Wang J, Tewari AK, Eroshkin A, Cho YJ, Witt H, Korshunov A, Read TA, Sun JL, Schmitt EM, Miller CR, Buckley AF, McLendon RE, Westbrook TF, Northcott PA, et al. An animal model of MYC-driven medulloblastoma. Cancer Cell. 2012; 21:155-167.

41. Huang YY, Dai L, Gaines D, Droz-Rosario R, Lu H, Liu J and Shen Z. BCCIP suppresses tumor initiation but is required for tumor progression. Cancer Res. 2013; 73:7122-7133.

42. Meley D, Spiller DG, White MR, McDowell H, Pizer B and See V. p53-mediated delayed NF-kappaB activity enhances etoposide-induced cell death in medulloblastoma. Cell Death Dis. 2010; 1:e41.

43. Fan YN, Meley D, Pizer B and See V. Mir-34a mimics are potential therapeutic agents for p53-mutated and chemo-resistant brain tumour cells. PLoS One. 2014;9:e108514.

44. Wang F, Bhat K, Doucette M, Zhou S, Gu Y, Law B, Liu X, Wong ET, Kang JX, Hsieh TC, Qian SY and Wu E. Docosahexaenoic acid (DHA) sensitizes brain tumor cells to etoposide-induced apoptosis. Curr Mol Med. 2011; 11:503-511.

45. Moll UM and Slade N. p63 and p73: roles in development and tumor formation. Mol Cancer Res. 2004;2:371-386.

46. Pflaum J, Schlosser S and Muller M. p53 Family and Cellular Stress Responses in Cancer. Front Oncol. 2014;4:285.

47. Fatt MP, Cancino GI, Miller FD and Kaplan DR. p63 and p73 coordinate p53 function to determine the balance between survival, cell death, and senescence in adult neural precursor cells. Cell Death Differ. 2014; 21:1546-1559.

48. Albanese C, D'Amico M, Reutens AT, Fu M, Watanabe G, Lee RJ, Kitsis RN, Henglein B, Avantaggiati M, Somasundaram K, Thimmapaya B and Pestell RG. Activation of the *cyclin D1* gene by the E1A-associated protein p300 through AP-1 inhibits cellular apoptosis. J Biol Chem. 1999;274:34186-34195.

49. Albanese C, Wu K, D'Amico M, Jarrett C, Joyce D, Hughes J, Hulit J, Sakamaki T, Fu M, Ben-Ze'ev A, Bromberg JF, Lamberti C, Verma U, Gaynor RB, Byers SW and Pestell RG. IKKalpha Regulates Mitogenic Signaling through Transcriptional Induction of Cyclin D1 via Tcf. Mol Biol Cell. 2003; 14:585-599.

50. Rodriguez OC, Choudhury S, Kolukula V, Vietsch EE, Catania J, Preet A, Reynoso K, Bargonetti J, Wellstein A, Albanese C and Avantaggiati ML. Dietary downregulation of mutant p53 levels via glucose restriction: mechanisms and implications for tumor therapy. Cell Cycle. 2013; 11:4436-4446.

51. Schwartz-Roberts JL, Shajahan AN, Cook KL, Warri A, Abu-Asab M and Clarke R. GX15-070 (obatoclax) induces apoptosis and inhibits cathepsin D- and L-mediated autophagosomal lysis in antiestrogen-resistant breast cancer cells. Mol Cancer Ther. 2013; 12:448-459.

52. Perez RE, Knights CD, Sahu G, Catania J, Kolukula VK, Stoler D, Graessmann A, Ogryzko V, Pishvaian M, Albanese C and Avantaggiati ML. Restoration of DNA-binding and growth-suppressive activity of mutant forms of p53 via a PCAF-mediated acetylation pathway. J Cell Physiol. 2010; 225:394-405.

53. Catalina-Rodriguez O, Kolukula VK, Tomita Y, Preet A, Palmieri F, Wellstein A, Byers S, Giaccia AJ, Glasgow E, Albanese C and Avantaggiati ML. The mitochondrial citrate transporter, CIC, is essential for mitochondrial homeostasis. Oncotarget. 2012; 3:1220-1235.

Research Paper

MDL-1, a growth- and tumor-suppressor, slows aging and prevents germline hyperplasia and hypertrophy in *C. elegans*

Michèle Riesen[1], Inna Feyst[1], Nattaphong Rattanavirotkul[1], Marina Ezcurra[1], Jennifer M.A. Tullet[1], Irene Papatheodorou[2], Matthias Ziehm[2], Catherine Au[1], Ann F. Gilliat[1], Josephine Hellberg[1], Janet M. Thornton[2], and David Gems[1]

[1]Institute of Healthy Ageing, and Research Department of Genetics, Evolution and Environment, University College London, London, United Kingdom
[2]European Molecular Biology Laboratory, European Bioinformatics Institute, Wellcome Trust Genome Campus, Hinxton, Cambridge, United Kingdom

Key words: aging, C. elegans, FoxO, germline, hyperplasia, hypertrophy, Mad transcription factor
Received: 12/22/13; Accepted: 2/14/14; Published: 2/16/14 **doi:** 10.18632/aging.100638
Correspondence to: David Gems, PhD; **E-mail:** david.gems@ucl.ac.uk

Abstract: In *C. elegans*, increased lifespan in *daf-2* insulin/IGF-1 receptor mutants is accompanied by up-regulation of the MDL-1 Mad basic helix-loop-helix leucine zipper transcription factor. Here we describe the role of *mdl-1* in *C. elegans* germline proliferation and aging. The deletion allele *mdl-1(tm311)* shortened lifespan, and did so significantly more so in long-lived *daf-2* mutants implying that *mdl-1(+)* contributes to effects of *daf-2* on lifespan. *mdl-1* mutant hermaphrodites also lay increased numbers of unfertilized oocytes. During aging, unfertilized oocytes in the uterus develop into tumors, whose development was accelerated by *mdl-1(tm311)*. Opposite phenotypes were seen in *daf-2* mutants, i.e. *mdl-1* and *daf-2* mutant germlines are hyperplastic and hypoplastic, respectively. Thus, MDL-1, like its mammalian orthologs, is an inhibitor of cell proliferation and growth that slows progression of an age-related pathology in *C. elegans* (uterine tumors). In addition, intestine-limited rescue of *mdl-1* increased lifespan but not to wild type levels. Thus, *mdl-1* likely acts both in the intestine and the germline to influence age-related mortality.

INTRODUCTION

In most animals, advancing age is accompanied by the deteriorative process of aging (senescence). Aging is the main cause of severe illness and death in humans, but the proximate biological mechanisms that cause it have proved difficult to identify. One approach to understand aging is to study simple model organisms [1], such as the nematode *Caenorhabditis elegans* which is particularly suitable for this purpose given e.g. its sequenced genome and very short lifespan (2-3 weeks). The identification from the 1980s onwards of many *C. elegans* mutants with altered aging rate [1] led to optimism that discovery of gene products of aging control genes would reveal the mechanisms of aging in this organism. Yet although many signaling pathways and processes affecting aging rate have been identified, the nature of aging itself has remained obscure. For example, mutation of the *daf-2* insulin/IGF-1 receptor gene can more than double adult lifespan [2]. This increase requires the presence of the DAF-16 FoxO transcription factor [2-4], suggesting that transcriptional targets of DAF-16 encode proximal biochemical determinants of aging. But these target genes have proved to be very numerous [5, 6], 2,274 by one estimate [7], complicating the search for DAF-16 target genes that control aging. Understanding DAF-16/FoxO action is important, particularly because the role of insulin/IGF-1 signaling and FoxO in the control of aging shows evolutionary conservation, e.g. in the fruitfly Drosophila [8], and perhaps even in humans,

where age changes in allele frequency e.g. of the IGF-1 receptor and FoxO3A genes have been detected [1].

One approach to understand DAF-16 action is to map the gene regulatory network in which it acts. Previously we used a genome-wide approach to identify genes to which DAF-16 both binds and causes a change in gene expression [9]. This identified a mere 65 high confidence DAF-16 direct targets, which were enriched for genes encoding proteins involved in signaling and gene regulation, and transcription factors. Among the latter class was *mdl-1* (Mad-like 1), which encodes a basic helix-loop-helix (bHLH) TF homologous to mammalian Mad transcription factors [10] (Figure 1A). In mammals, Mad TFs act as heterodimers with Max bHLH TFs. Mad competes with Myc bHLH TFs to dimerize with Max, and bind to target genes containing E-box sequences (5'-CANNTG-3') [11]. Myc/Max dimers mainly activate gene expression, and are a major activator of cell proliferation of growth. By contrast, Mad/Max dimers mainly inhibit gene expression, antagonizing Myc/Max, and suppressing cell division and growth [11]. Inhibition of gene expression by Mad/Max is facilitated by recruitment of the Sin3 histone deacetylase (HDAC) corepressor complex. Myc TFs are potent oncogenes, while Mad TFs show some properties of tumor suppressors [11].

Our attention was drawn to *mdl-1* for several reasons. First, many genes that promote growth also promote aging [12]. Thus, growth suppressors activated by DAF-16 are candidates for downstream effectors slowing aging, and MDL-1, as a Mad TF, is a potential growth suppressor and, in fact, can suppress activated cMyc/Ras-induced cell transformation in mammalian cells [10]. Second, four mammalian Mad TFs, *mad1, mxi1, mad3* and *mad4*, are up-regulated by FoxO3a in a human colorectal adenocarcinoma cell line [13]. Thus, regulatory interactions between FoxO and Mad show at least some evolutionarily conservation between nematodes and mammals. Consistent with this, in *C. elegans mdl-1* is an activator of intestinal expression of *ftn-1* (H ferritin, an iron storage protein) [14], while in mammals, Myc can repress H ferritin expression, which contributes to cell proliferation [15].

C. elegans possesses several Max-like (*mxl*) genes, including *mxl-1* which can form heterodimers with MDL-1 but, surprisingly, lacks Myc [10, 16, 17]. Previous RNAi screens have not detected major effects of expression knockdown of *mdl-1* or *mxl-1* (Wormbase.org). However, *mdl-1* exerts some influence upon the germline, as follows. Loss of *daf-2* inhibits lethal, *gld-1*-induced distal germline tumors via decreased cell division and increased DAF-16/p53-dependent apoptosis [18], and *mdl-1* is a mediator of this inhibition [19]. Moreover, RNAi of *mdl-1* can reduce *daf-2* mutant longevity, but has little effect on lifespan in *daf-2*(+) worms [6].

In this study, we explore the possible role of *mdl-1* as a downstream effector of DAF-16 in the control of aging. In particular, we detail the phenotypic effects of mutation of *mdl-1*. We report that *mdl-1* acts as a repressor of germline hyperplasia and hypertrophy which otherwise contributes to age-related pathology in the germline.

RESULTS

mdl-1(tm311) increases production of unfertilized oocytes

To investigate *mdl-1* gene function, we studied the *mdl-1(tm311)* mutant allele, which contains a 471 bp base pair deletion that removes exon 2 of the gene (Figure 1A). This results in a frame shift after 51/281 amino acid residues and loss of the entire bHLH domain, implying that this is a null allele. The mutation was first backcrossed 6x into the *Caenorhabditis* Genetics Center wild type male stock to remove possible second site mutations, and ensure a wild type background [20].
Previous work on *mdl-1* and the function of Mad TFs in mammals led to several expectations about the possible effects of *mdl-1(0)*. First, since it is a DAF-16-activated gene, it might suppress *daf-2* mutant traits, e.g. constitutive dauer larva formation (Daf-c), stress resistance and increased longevity (Age). Second, since Mad TFs inhibit cell division and growth, *mdl-1(0)* might increase either somatic growth or germline proliferation.

We first examined effects of *mdl-1(0)* on somatic development and growth in wild type and *daf-2* mutant backgrounds. *mdl-1(0)* had no detectable effect on larval or adult growth (Figure 1B), but caused a slight reduction in constitutive dauer formation in *daf-2(m577)* mutants (Figure 1C). Next we probed the effects of *mdl-1* on the germline, first by looking at levels of fertility. The number of progeny produced by self-fertilized hermaphrodites was not affected by *mdl-1(0)*, either in terms of overall brood size or reproductive schedule (Figure 1D,E). As self sperm becomes depleted, N2 hermaphrodites start laying unfertilized oocytes [21]. Notably, *mdl-1(0)* caused a marked increase in the number of unfertilized oocytes laid, from 121 ± 15 to 219 ± 30, an 81% increase (Figure 1D). *mdl-1*(RNAi) applied to RNAi-sensitive *rrf-3(pk1426)* mutants also increased unfertilized oocyte number (data not shown).

In *daf-2(m577)* mutants, progeny number was also not different to N2, but the number of unfertilized oocytes laid was significantly reduced (Figure 1D,E), consistent with previous findings [22]. For convenience, to describe this mutant phenotype we introduce the term Uno (abnormal in unfertilized oocyte production), and Uno-o, to describe mutants that are unfertilized oocyte over-producers (e.g. *mdl-1*), and Uno-d, to describe mutants that are unfertilized oocyte deficient (e.g. *daf-2*).

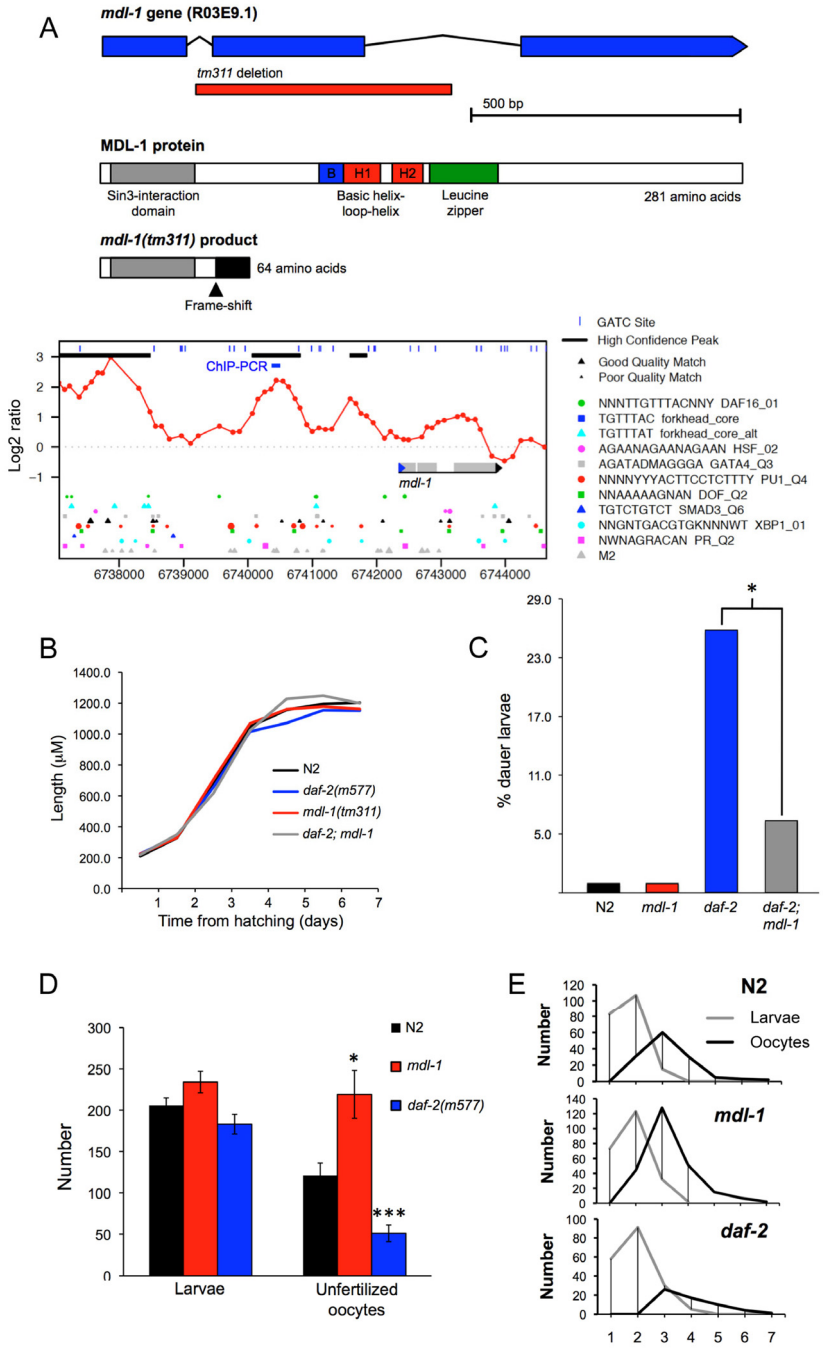

Figure 1. Phenotypic analysis of *mdl-1(tm311)* mutant. (A) *mdl-1* gene and protein description, including *tm311* deletion and effects on protein, DAF-16 binding sites (chromatin profile [DamID] data and DBEs) and site of ChIP analysis. For chromatin profile, y axis represents log2 ratio of DAF-16 binding relative to control, and peaks correspond to potential DAF-16 binding sites [9]. **(B –F)**. Phenotypic effects of *mdl-1(0)*. **(B)** Little effect on larval and adult growth. Samples sizes ranged from 23-39. **(C)** *mdl-1(0)* slightly reduces *daf-2(m577)* Daf-c, measured at 22.9°C. * $0.01 < p < 0.05$ (Student's *t* test). 4 trials conducted, in which *mdl-1(0)* reduced dauer formation in 3. **(D, E)** Effect of *mdl-1* and *daf-2* on fertility. Number of broods scored: N2, 19; *daf-2*, 20; *mdl-1*, 17. **(D)** Mean total progeny and unfertilized oocytes. * $0.01 < p < 0.05$, *** $p < 0.001$ (Student's *t* test). **(E)** Mean daily progeny and unfertilized oocyte numbers.

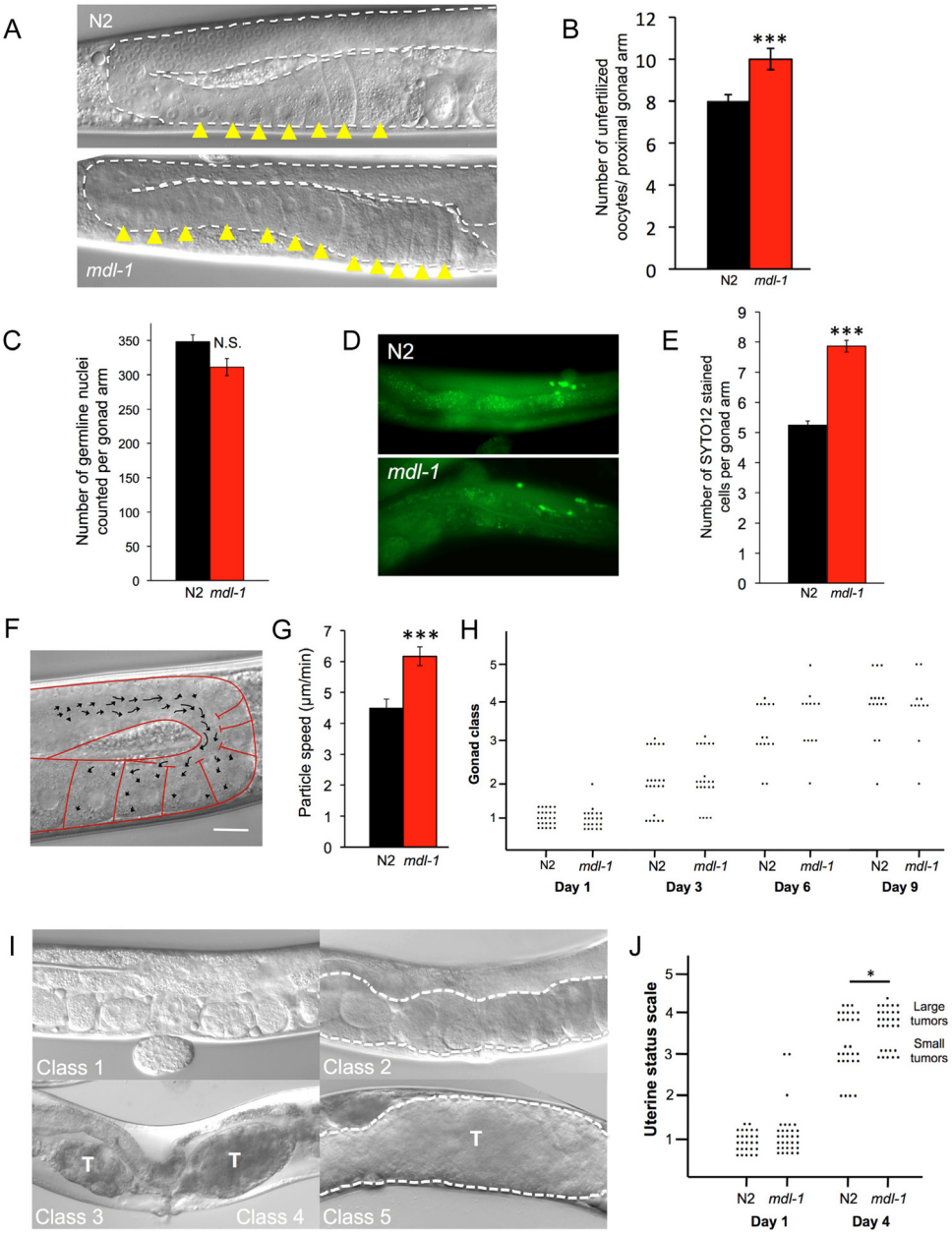

Figure 2. *mdl-1* causes hyperplasia and hypertrophy. (A, B) *mdl-1(0)* causes oocyte stacking in 1 day old worms. **(A)** Nomarski images. **(B)** Quantitation of stacking. Sample sizes: N2, 23; *mdl-1*, 17. *** $p < 0.001$ (Student's *t* test). **(C)** No effect of *mdl-1* on number of germline nuclei. $p > 0.05$ (Student's *t* test). **(D, E)** *mdl-1* increases levels of germline apoptosis. **(D)** Epifluorescence images of SYTO12 stained cells in young adult hermaphrodite germline. **(E)** Quantitated data. Number of gonads scored: N2, 153; *mdl-1*, 132. *** $p < 0.001$ (Student's *t* test). **(F, G)** *mdl-1* increases cytoplasmic streaming in the proximal gonad. **(F)** Single image obtained from a time-lapse recording. Arrows represent DIC-particle tracks. DIC-particles were tracked over a period of 1 minute. Scale bar: 20 µm. **(G)** Cytoplasmic streaming rate (mean particle speed ± standard error). 30 particle speed measurements performed for each genotype. Number of worms examined: N2, 4; *mdl-1*, 3. *** $p < 0.001$ (Student's *t* test). **(H)** Absence of effect of *mdl-1(0)* on gonad disintegration (25°C). $p > 0.05$ for all comparisons of N2 *vs.* *mdl-1* of the same age (Wilcoxon Mann test). **(I)** Uterine status scale for quantitation of uterine tumor formation rate (5 classes). Class 1, normal uterus containing eggs (day 1 adult). Class 2, slightly abnormal uterine contents, but no tumor visible. Class 3, small tumor. Class 4, medium sized tumor. Class 5, large tumor, filling body cavity and squashing the intestine. Dotted line, outline of uterus. T, tumor. **(J)** *mdl-1(0)* increases uterine tumor formation (25°C), data summed from 3 trials. * $0.01 < p < 0.05$ (Wilcoxon Mann test).

mdl-1(tm311) causes germline hyperplasia and hypertrophy

The *mdl-1* Uno-o phenotype suggests increased cell production in the germline distal to the spermatheca. To test this we compared proximal gonad contents in wild type and *mdl-1* animals on day 1 of adulthood. This revealed increased oocyte density, or stacking [23, 24], in *mdl-1* (Figure 2A,B), implying increased oocyte synthesis. This in turn suggests increased germ cell proliferation in the distal gonad. To probe this, we examined germ cell number by staining nuclei with the fluorescent DNA-binding dye 4',6-diamidino-2-phenylindole (DAPI), but no effect of *mdl-1* was detected (Figure 2C). However, an increase in the overall rate of germline cell turnover in *mdl-1* mutants could leave cell number unaffected.

If the distal proliferative zone is the source of germ cell nuclei, then the major sink is germline apoptosis. At least 50% [25] and as many as 97% [26] of germ cells undergo p53-independent, "physiological" apoptosis, their cytoplasm supplying expanding oocytes near the gonad bend. Using the SYTO 12 dye to detect apoptotic cell corpses, we found that *mdl-1* mutants showed a significant increase in apoptotic cell number in the germline in 3 out of 4 trials (Figure 2D, E).

The transfer of cytoplasm released by germ cells to nascent oocytes occurs by a process of cytoplasmic streaming (Figure 2F) [27]. We examined the effect of *mdl-1(0)* on the rate of cytoplasmic streaming in the mid-late pachytene region of the distal gonad, on day 1 of adulthood. Cytoplasmic streaming rate in *mdl-1* worms was significantly greater than in wild type (Figure 2G). Taken together, these results suggest that an increase in production of germ cells is matched by an increase in apoptosis, resulting in little change in overall germ cell number in the distal arm. Overall, this suggests that the increase in oocyte production is driven by a hyperplastic state in the distal gonad.

Next we studied the effect of *mdl-1* on pathologies of aging in the germline. The aging hermaphrodite gonad undergoes dramatic pathological changes. The distal gonad shrivels and eventually disintegrates [28, 29], while in the uterus large, amorphous masses (tumors) with very high DNA content develop [24, 29-31]. These tumors form from unfertilized oocytes which undergo multiple rounds of endoreduplication, and can grow to fill the entire body cavity in the mid-body. Continued germline apoptosis in late life contributes to gonad disintegration, and increased apoptosis rate is sufficient to increase gonad disintegration rate (Y. de la Guardia and D. Gems, unpublished). However, despite their increased apoptosis rate (Figure 2D,E) gonad disintegration rate was not detectably altered in *mdl-1* mutants (Figure 2H).

Casual observation of *mdl-1* hermaphrodites under Nomarski microscopy suggested an increase in uterine tumors in these mutants. To verify this, we used a semi-quantitative approach [28] with a uterine status scale. According to the appearance of the uterus, worms were scored from 1 (healthy, no tumors) to 5 (large tumors) (Figure 2I) (see Materials and Methods). Using this scale to compare N2 and *mdl-1* mutants confirmed that uterine tumors grow significantly faster in *mdl-1* worms (Figure 2J).

mdl-1 does not mediate effects of daf-2 on germline proliferative status

We next investigated whether MDL-1, like DAF-16, is an effector of *daf-2* mutant phenotypes. We first verified that DAF-16 acts directly on *mdl-1* to increase its expression, as predicted by mRNA and chromatin profiling studies [9]. Quantitative RT-PCR confirmed that *mdl-1* mRNA levels are higher in *daf-2* than in *daf-16; daf-2* strains (Figure 3A). Chromatin immuno-precipitation and PCR (ChIP-PCR) confirmed that DAF-16 binds to the *mdl-1* promoter (Figure 3B). This implies that *mdl-1* expression is activated by DAF-16 binding to its promoter.

mdl-1 mutants are Uno-o while *daf-2* mutants are Uno-d (Figure 1D,E) [22], and DAF-16 activates *mdl-1* expression (Figure 3A,B) [9]. This could imply that increased *mdl-1* activity in *daf-2* mutants reduces oocyte production. To test this we asked whether *mdl-1(tm311)* would suppress *daf-2* Uno-d, but it did not. Instead, *daf-2(m577); mdl-1* worms were Uno-d (Figure 3C), i.e. *daf-2* is epistatic to *mdl-1*. *daf-2(m577)* also suppressed *mdl-1* effects on oocyte stacking and uterine tumor formation (data not shown). These results negate our hypothesis that *daf-2* Uno-d is caused by *mdl-1* over-activity. A different model was suggested by additional epistasis data as follows. In a *daf-2*(+) background, *daf-16* suppressed *mdl-1* Uno-o, consistent with the observation that *daf-16* over-expression in a *daf-2*(+) background can cause germline hyperplasia [32]. Thus, DAF-16 promotes oocyte production in a *daf-2*(+) background but inhibits it in a *daf-2(m577)* background (Figure 3D). Moreover, mutation of *daf-16* in a *daf-2; mdl-1* mutant did not restore MDL-1 Uno-o (Figure 3C). This suggests that MDL-1 suppresses the effect of DAF-16 on oocyte production in *daf-2*(+) worms, but plays no role in *daf-2* mutants (Figure 3D).

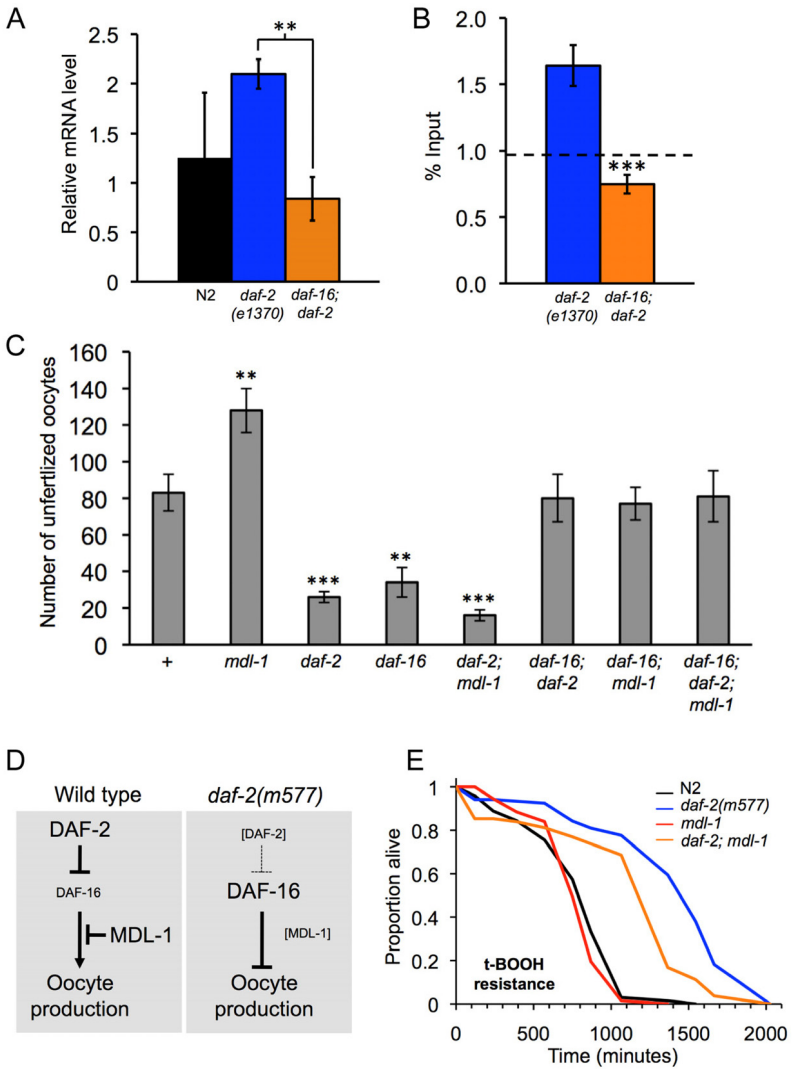

Figure 3. Distinct epistatic relationships between *daf-2* and *mdl-1* in hyperplasia and hypertrophy. (A, B). *mdl-1* is a direct transcriptional target of DAF-16. **(A)**. *mdl-1* mRNA levels are increased in *daf-2* relative to *daf-2; daf-16* (Q-PCR data). ** $0.001 < p < 0.01$. **(B)** DAF-16 binds to the *mdl-1* promoter (ChIP-PCR data). One experiment is shown which contained 3 immuno-precipitation replicates from the same chromatin preparation (error bars show the standard deviation between them). The dotted line shows the average inputs from 3 genes/genomic regions that do not show enrichment for DAF-16 binding in *daf-2 vs daf-16; daf-2* in this particular trial, i.e. it reflects background DAF-16 binding levels. Significant DAF-16 binding was detected one of two additional trials. The position of the DAF-16 binding site detected is shown in Figure 1A. **(C)** *mdl-1*, *daf-2* and *daf-16* epistasis analysis with respect to unfertilized oocytes production (Uno). Total unfertilized oocyte production per worm was measured at 25°C. Means of 12 broods assessed; error bars, standard error. ** $0.001 < p < 0.01$; *** $p < 0.001$ (Student's *t* test). **(D)** Model for interactions between DAF-2, DAF-16 and MDL-1, deduced from interactions between mutations. DAF-16 promotes oocyte production in *daf-2*(+) worms, but inhibits it in *daf-2(m577)* worms. MDL-1 acts via DAF-16 to inhibit oocyte formation in *daf-2*(+) worms, but does not influence oocyte production in *daf-2(m577)* worms. **(E)** Resistance to 7.5 mM *tert*-butylhydroperoxide (*t*-BOOH). Sample sizes (censored values): N2, 67 (7); *daf-2(m577)*, 61 (8); *mdl-1,* 67 (8); *daf-2; mdl-1,* 70 (12). Probability of being the same: N2 *vs. mdl-1*, $p = 0.24$; *daf-2 vs. daf-2; mdl-1*, $p < 0.001$ (log rank test).

daf-2 mutants exhibit various forms of stress resistance, including oxidative stress resistance (Oxr) [33]. We tested whether MDL-1 contributes to *daf-2* Oxr, specifically to *tert*-butylhydroperoxide (*t*-BOOH). In a wild-type background, *mdl-1(0)* did not affect Oxr, while *daf-2(m577)* markedly increased Oxr (Figure 3E). Notably, in a *daf-2(m577)* background, *mdl-1(0)* significantly decreased Oxr. This implies that MDL-1 contributes to *daf-2* Oxr.

MDL-1 contributes to *daf-2* mutant longevity by reducing baseline hazard

Next, we examined the effect of *mdl-1* on aging. First we compared effects of *mdl-1*(RNAi) on lifespan in *rrf-3* and *rrf-3; daf-2(e1368)* strains (25˚C), and detected a reduction in lifespan only in the latter strain (data not shown), consistent with previous observations [6]. We then assessed the effect of *mdl-1(tm311)* on lifespan in wild-type or *daf-2(m577)* mutant backgrounds. *mdl-1* decreased lifespan in both wild-type and *daf-2* backgrounds, but the decrease was proportionally greater in the latter (Figure 4A, Table S1). This corresponded to a significantly greater *mdl-1*-induced increase in mortality in a *daf-2* background (4.5-fold vs 1.8-fold; significant interaction term, $p < 10^{-15}$, Cox proportional hazard analysis), suggesting that *mdl-1* activity contributes to the *daf-2* longevity increase.

To further characterize the effect of *mdl-1* on aging, we examined its effect on the pattern of age-specific mortality in wild-type and *daf-2(m577)* backgrounds.

Aging animal populations typically show exponential increases in mortality rate, and in *C. elegans* this occurs in two stages, with an initial faster exponential increase and a subsequent slower exponential increase [34, 35]. We fitted mortality data to a logistic model, which contains 3 components: a baseline hazard (initial mortality rate, parameter *a*), a mortality increase rate (parameter *b*) and a late-life mortality deceleration (parameter *s*).

In this analysis we wanted to probe whether *mdl-1(tm311)* shortens lifespan by accelerating aging or whether it could act by a life-shortening effect unrelated to aging. An effect of *mdl-1* on parameters *b* and *s* would imply an effect on aging, whereas an effect on parameter *a* could imply a non-aging related deleterious effect. In fact, *mdl-1* increased baseline hazard (*a*) without affecting the mortality increase rate (*b*) (Figure 4B-D). By contrast, relative to wild type, *daf-2(m577)* markedly decreased parameters *b* and *s*, while also slightly increasing parameter *a*. Reducing insulin/IGF-1 signaling has long been known to slow the age-related mortality rate increase [36]. In a *daf-2* background, *mdl-1(0)* again increased baseline hazard, and had no significant effect on parameters *b* and *s* ($p > 0.05$) (Figure 4C,D). In summary, this analysis confirms that *daf-2* increases lifespan by slowing demographic aging, while *mdl-1* shortens lifespan mainly by increasing baseline hazard. That *mdl-1* shortens lifespan more in a *daf-2* background could imply that MDL-1 contributes to *daf-2* longevity by reducing baseline hazard (see Discussion).

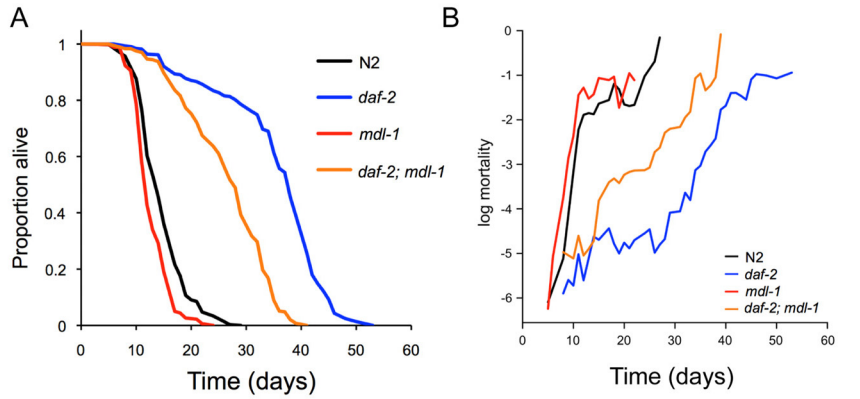

C

	a	*b*	*s*
N2	0.00051	0.500	1.679
daf-2(m577)	0.00069	0.133	0.032
mdl-1(tm311)	0.00094	0.500	1.023
daf-2; mdl-1	0.00155	0.152	$2.5*10^{-07}$

D

	a	*b*	*s*
N2 - *daf-2*	$7.8*10^{-03}$	$2.2*10^{-46}$	$2.0*10^{-26}$
N2 - *mdl-1*	$8.2*10^{-07}$	0.984	$9.6*10^{-06}$
daf-2 - *daf-2; mdl-1*	$4.0*10^{-03}$	0.065	0.582
mdl-1 - *daf-2; mdl-1*	$5.1*10^{-06}$	$2.7*10^{-46}$	$1.2*10^{-12}$

Figure 4. Effects of *mdl-1* on aging. **(A)** Effects of *mdl-1(tm311)* on lifespan (for statistics, see Table S1, combined data). **(B)** Effect of *mdl-1* on age-specific mortality profiles. **(C, D)** Mortality analysis using logistic model. **(C)** Estimated values of logistic model parameters. **(D)** Probability, *p*, of parameters in compared genotypes being the same, holding other parameters constant.

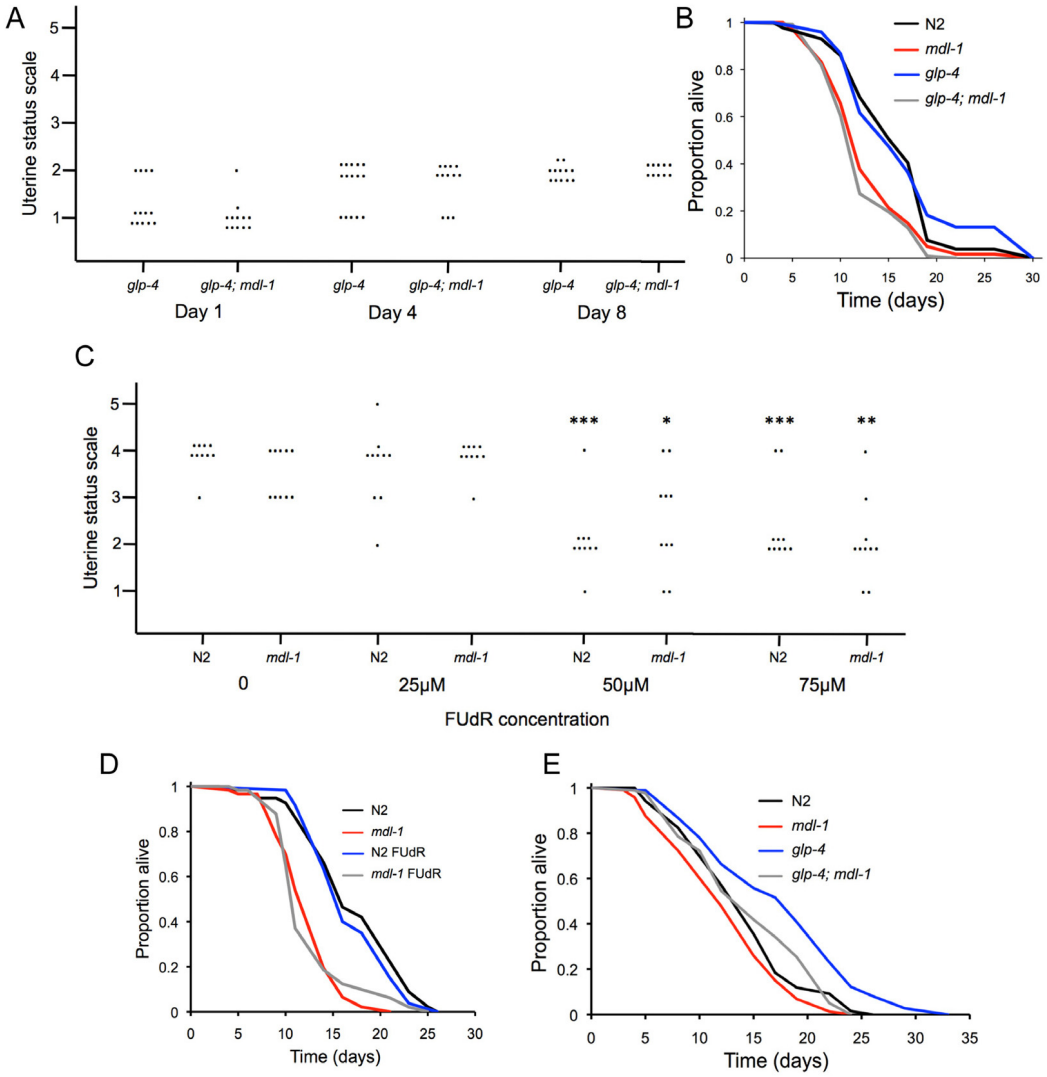

Figure 5. **No effect of uterine tumors on lifespan. (A)** Uterine tumors are not seen in *glp-4(bn2)* mutants (raised at 15°C to L4 then shifted to 25°C). Uterine classes 2-5 indicate presence of tumors. Each dot corresponds to a uterine status measurement. **(B)** *glp-4* does not suppress *mdl-1* effects on lifespan (for statistics, see Table S2, trial 1). **(C)** FUdR suppresses formation of uterine tumors at 50μM or greater. Stars represent a significant difference to worms of the same genotype in the absence of FUdR. No significant difference in tumor levels between N2 and *mdl-1* were detected at this age at any FUdR concentration. * $0.01 < p < 0.05$; ** $0.001 < p < 0.01$; *** $p < 0.001$ (Wilcoxon Mann test). **(D)** 50 M FUdR does not suppress *mdl-1* shortevity or increase N2 lifespan (for statistics, see Table S2, trial 1). **(E)** Effect of *mdl-1* on *glp-4* longevity (for statistics, see Table S2, trial 2).

Uterine tumors do not limit lifespan

mdl-1(0) accelerates formation of uterine tumors, which frequently grow very large, filling the body cavity in the mid-body region and squashing the intestine [31]. One possibility is that uterine tumors can contribute to mortality and that increased tumor formation in *mdl-1(0)* mutants causes a shortened lifespan. To test this, we examined the effect of *mdl-1* on lifespan in the absence of uterine tumors. *glp-4(bn2)* mutants have a temperature-sensitive germline proliferation defect; if raised at 15˚C to L4 and then switched to 25˚C, oocyte production is blocked but longevity is not increased [7]. We first confirmed that *glp-4* blocks formation of uterine tumors (Figure 5A). We then compared lifespan in *glp-4*, *mdl-1* and *glp-4; mdl-1* worms. *glp-4* worms were normal-lived, but both *mdl-1* strains were similarly short lived (Figure 5B; Table S2).

We also blocked uterine tumor formation using the inhibitor of DNA replication 5-fluoro-deoxyuridine (FUdR), which is also commonly used to treat colorectal cancer. Application of FUdR at low concentrations (e.g. 10-25μM) from L4 stage is a convenient means to block progeny production, and has little effect on lifespan [37]. 50μM FUdR, but not lower FUdR concentrations, was sufficient to block formation of uterine tumors (Figure 5C). We then compared effects of 50μM FUdR on lifespan in wild type and *mdl-1* worms, and saw no effect on lifespan in either case (Figure 5D; Table S2). These results show that accelerated formation of uterine tumors do not cause the shorter lifespan of *mdl-1* worms. They also demonstrate that uterine tumors do not limit lifespan in wild type worms under standard culture conditions. This contrasts with the case of *daf-16* over-expression, where life shortening is suppressed by blocking germline hyperplasia either with *glp-1* or FUdR [32].

A number of interventions that remove the hermaphrodite germline cause increased lifespan, including raising *glp-4(bn2)* mutants at 25˚C, and this effect is *daf-16* dependent [38, 39]. Notably, *mdl-1(0)* also reduced the longevity of *glp-4* mutants raised at 25˚C (Figure 5E, Table S2). *mdl-1* shortened lifespan more in a *glp-4* background than in a wild-type background (Table S2). This suggests that *mdl-1(+)* contributes to *glp-4* longevity as well as *daf-2* longevity.

Evidence that *mdl-1* can act in the intestine to promote longevity

The intestine plays an important role in *daf-2* mutant longevity [40], and is a site of *mdl-1* expression [10]. One possibility is that *mdl-1* affects intestinal protein synthesis. Mutation of *daf-2* causes a global reduction in protein synthesis, which may contribute to longevity [41, 42]. In aging hermaphrodites, yolk proteins (vitellogenins) become very abundant indeed [43, 44], and this accumulation is suppressed *daf-2*, apparently by inhibition of protein translation in the intestine [45] where yolk is synthesized [46]. Thus, vitellogenin accumulation rate gives some indication of intestinal protein synthesis rate. However, *mdl-1(0)* did not alter vitellogenin accumulation, either in wild type or *daf-2* mutant backgrounds (Figure 6A,B). One possibility is that *mdl-1* mutants do synthesize more vitellogenin, but due to increased laying of unfertilized oocytes, this does not result in increased vitellogenin accumulation. To check this we compared sterile *glp-4* and *glp-4; mdl-1* worms (shifted at L4 to 25˚C), but again no effect of *mdl-1* was seen (Figure 6A,B).

Next, we asked whether intestine-limited rescue of *mdl-1* using the *ges-1* promoter [47] would rescue *mdl-1* shortevity. A transgene array from which *mdl-1* was expressed using its own promoter was able to restore wild-type lifespan to *mdl-1(tm311)* mutants (Figure 6C; Table S3). Notably, *pges-1::mdl-1* too increased lifespan in *mdl-1* mutants, though the effect was smaller such that lifespan was not restored to wild type. This suggests short lifespan in *mdl-1* mutants is caused by loss of *mdl-1* from several sites, including the intestine. Possibly, a second site of action of *mdl-1* on lifespan is the germline, given its impact on that tissue.

The extent of loss of Myc among nematodes

One puzzle relating to *mdl-1* function is the absence of Myc in *C. elegans*. In mammals, the Mad/Max/Myc system works in concert with the Tor pathways to control growth [48]. *C. elegans* also lacks key components of the Tor pathway, including the Tsc1/Tsc2 complex [49], and 4E-BP [50] (Figure 7A). To try to understand the significance of the absence of Myc in the broader context of nematode gene loss, we tested for the presence of Myc, Tsc1, Tsc2 and 4E-BP throughout the Nematoda. It was previously noted that Myc orthologs are absent not only from *C. elegans* and *C. briggsae*, but also the filarial parasite *Brugia malayi* (nematode order Spirurida), and even the bilharzia parasite *Schistosoma mansoni* (phylum Platyhelminth) [51]. Searching the genomes of 13 nematode species, including representatives of the major nematode orders, no Myc orthologs were detected (Figure 7B). Myc was also absent from all 5 platyhelminth species examined. This implies that Myc evolved in the common ancestor of arthropods and chordates after divergence from the common ancestor of nematodes and platyhelminths, as previously suggested [51]. Thus, the Myc-less Mad-Max circuit in *C. elegans* appears to represent a more ancient regulatory system.

By contrast, both Tsc1/Tsc2 and 4E-BP were found in several nematode groups but were absent from many others, in a pattern indicating that each gene has been lost several times during nematode evolution. For Tsc1 and Tsc2, gene loss was correlated, i.e. both genes were either present or absent. There was no correlation between loss of Tsc/Tsc2 and 4E-BP: nematode species exist with Tsc1/Tsc2 but lacking 4E-BP and vice versa. The distribution of Tsc1/Tsc2 is surprising in that most nematode and all platyhelminth groups lack this complex, apart from spirurid nematodes, and two rhabditid species. Sequence comparisons of Tsc1 and Tsc2 protein sequences from nematodes and other animal groups is consistent with multiple instances of gene loss (rather than horizontal gene transfer) (Figure 7C).

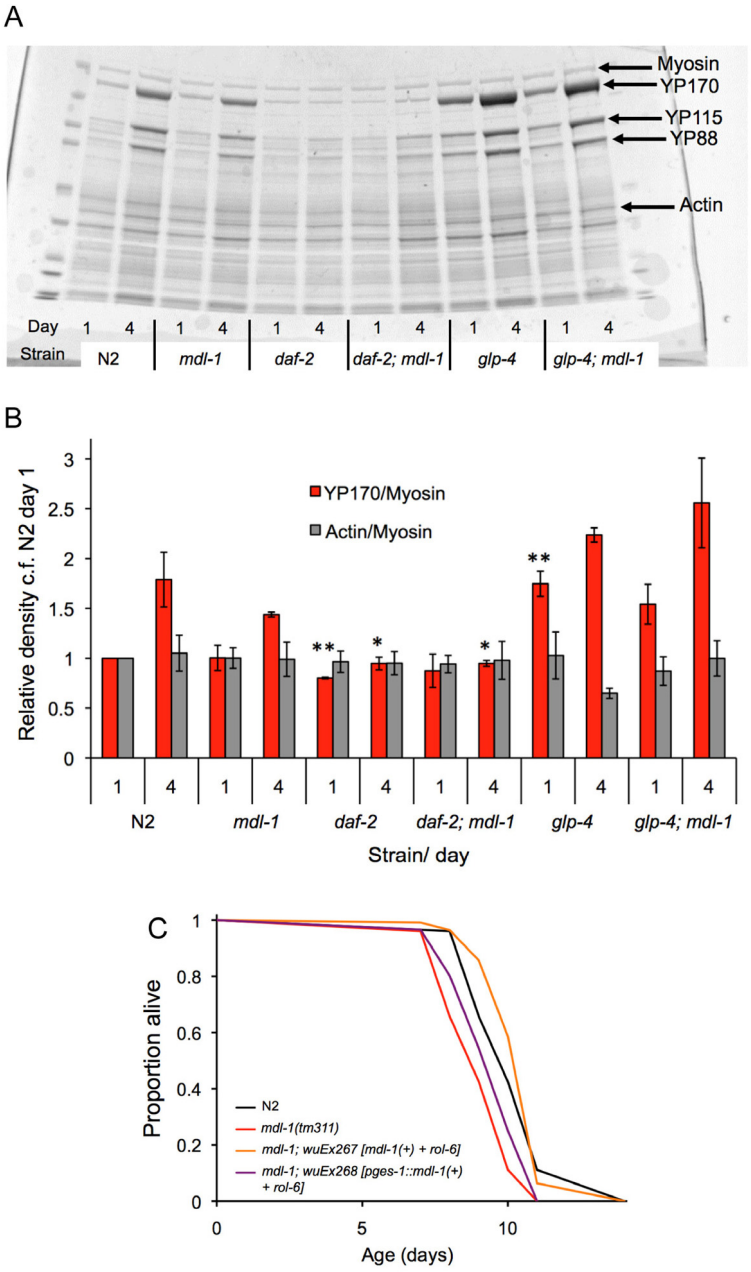

Figure 6. Tests for action of *mdl-1* in the intestine. (A,B) Effect of *mdl-1* on yolk accumulation. **(A)** Example of Coomassie stained gel with *C. elegans* protein extracts. **(B)** Bar graph data is derived from densitometric measurement of protein on gels (means of 3 biological replicates; error bars, standard error). It shows levels of the major yolk protein YP170 normalized to myosin levels (which are not expected to change), and again to levels in N2 on day 1. Actin/myosin ratio gives an indication of the reliability of myosin as a standard. * $0.01 < p < 0.05$; ** $0.001 < p < 0.01$, compared to N2 of the same age. **(C)** Effects on lifespan of *pges-1::mdl-1(+)* rescue of *mdl-1(0)* (for statistics, see Table S3, trial 2).

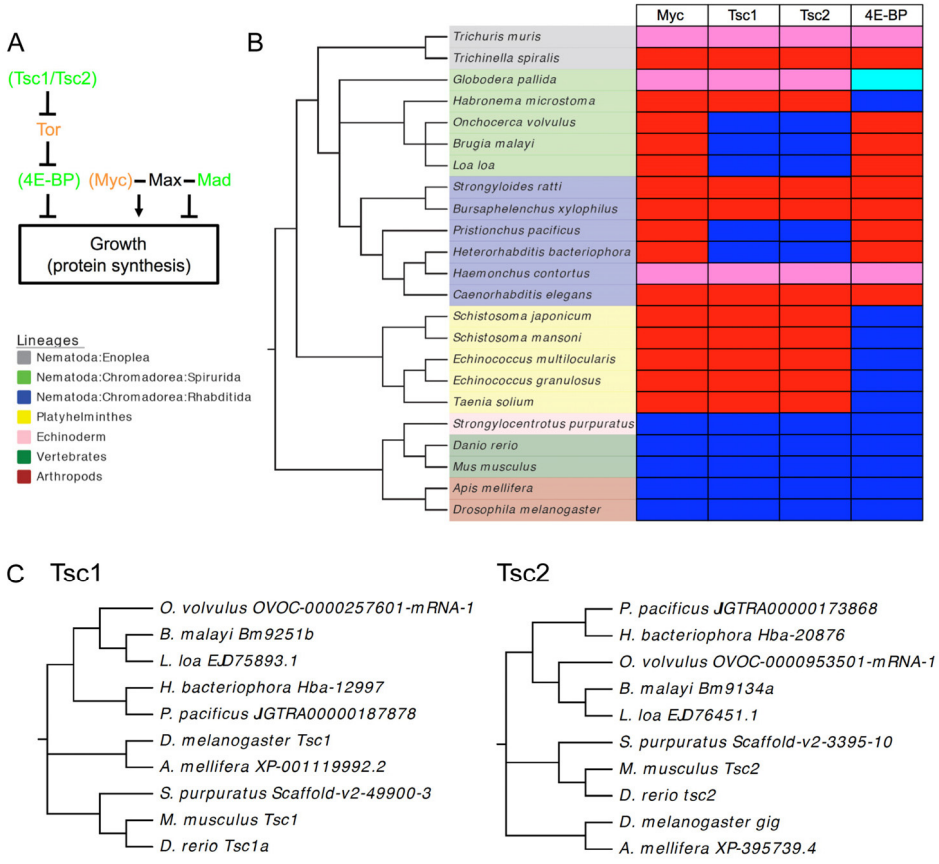

Figure 7. Extent of loss of Myc, Tsc1/Tsc2 and 4E-BP among the Nematoda. (A) Outline of missing elements of Tor and Myc/Max/Mad pathways in *C. elegans*. Green, tumor-suppressor/anti-aging; orange, oncogene/pro-aging. In brackets, proteins missing from *C. elegans*. **(B)** Presence and absence of Myc, Tsc1, Tsc2 and 4E-BP among nematodes and platyhelminths. Red, absent; dark blue, present; pink, not found; pale blue, putative but somewhat divergent 4E-BP. Not found: a caveat to this analysis may be the incompleteness of the genomic sequences of some of these species with draft assemblies being available for *G. pallida* and *H. contortus* and only contigs available for *T. muris*. **(C)** Phylodendrograms of Tsc1 and Tsc2 sequences for nematodes and other animal groups. Note that species and sequence phylogenies correspond.

DISCUSSION

In this study we have shown that MDL-1 acts as an inhibitor of germline proliferation, and of oocyte hypertrophy, thereby inhibiting a salient aging-related pathology (uterine tumors). These properties of *mdl-1* mutants recapitulate effects of Mad TFs in mammals, e.g. mice lacking the Mad TF Mxi1 show hyperplasia in a number of tissues (e.g. prostatic epithelium), and are tumor prone [52]. We also confirm that MDL-1 inhibits aging, consistent with the observed association between tumor suppressors and inhibition of aging [53, 54].

Does *mdl-1* act downstream of *daf-16*?

Our initial hypothesis was that activation of *mdl-1* expression by DAF-16 contributes to *daf-2* longevity. The results of analysis of *mdl-1* expression (Figure 3A,B) and the effects on lifespan of *mdl-1(tm311)* (Figure 4A) are consistent with this hypothesis. We also noted that *mdl-1* and *daf-2* have opposing effects on the germline: *mdl-1(0)* causes Uno-o, increased oocyte stacking and increased uterine tumors (this study), while mutation of *daf-2* has opposite effects [22, 29]. This suggested that the effects of *daf-2* on the germline

might be mediated by *mdl-1*. However, epistasis analysis shows that this is not the case for oocyte production (Figure 3C). Instead *mdl-1* appears to have no effect on the germline in *daf-2* mutants, but to inhibit promotion of germline proliferation by DAF-16 in *daf-2*(+) worms (Figure 3D).

Does *mdl-1* affect aging?

The life-shortening effect of *mdl-1(0)* is mainly the result of increased base-line hazard (Figure 4B-D). This could imply that *mdl-1(0)* does not affect aging but, rather, shortens lifespan by causing a pathology that is distinct from aging. In similar fashion, a comparison of mortality in two groups of people during the 1940s, either in Australia or interned by the Japanese, showed increased base-line hazard but not increased demographic aging in the latter [55]. It is interesting to consider whether this necessarily means that the effect of *mdl-1* on lifespan does not involve an effect on aging. The impact of *mdl-1(0)* on lifespan is greater in a *daf-2* background, suggesting that MDL-1 does contribute to *daf-2* longevity, i.e. that *mdl-1* does affect aging. Arguably, the critical point here is that something that affects demographic aging necessarily affects biological aging, while something that affects base-line hazard may or may not affect biological aging. In other words, the biological process of aging is not always the same thing as demographic aging.

One working definition of biological aging is the set of endogenously generated pathologies that increase in later life [56]. In principle, interventions that reduce one or more age-related pathology (i.e. part or all of aging) could increase lifespan by reducing base-line hazard, demographic aging, or both. One possibility is that the wider the spectrum of age-related pathologies that an intervention suppresses, the more likely will a reduction in demographic aging be seen. In conclusion, *mdl-1(0)* may or may not affect aging. Its greater effect on *daf-2* could imply that it does; however, an alternative possibility is that *mdl-1(0)* causes a pathology that is distinct from those seen during aging, and that *daf-2(-)* slightly increases the severity of this pathology, or increases its effect on mortality.

Where and how does *mdl-1* act to impact lifespan?

The phenotype of *mdl-1(tm311)* mutants demonstrates that MDL-1 acts as a repressor of growth and proliferation in the germline. This is consistent with the role of Mad TFs as repressors of growth and proliferation in mammals [11]. A long-standing hypothesis about aging is that it is caused by molecular damage, but more recently it has been suggested that aging is caused by the run on of developmental and reproductive processes in late life, leading e.g. to pathological hyperplasia, hypertrophy and atrophy [57-59]. The action of MDL-1 as a DAF-16-activated suppressor of growth is broadly consistent with this model.

The *mdl-1* mutant phenotype also suggests that this gene may affect lifespan through its effects on the germline. One possibility is that over-production of oocytes or increased formation of uterine tumors *per se* cause a decrease in lifespan. However, our findings argue against this: suppression of these effects in *mdl-1* mutants using *glp-4* or FUdR does not suppress the life-shortening effects of *mdl-1(0)* (Figure 5B,D). A second possibility is that *mdl-1(0)* affects signaling from the germline; removal of the germline can extend lifespan, and this effect is *daf-16* dependent [39]. Consistent with this possibility, *mdl-1(0)* shortens lifespan somewhat more in long-lived germlineless *glp-4* mutants than in otherwise wild-type worms (Figure 5E).

Another possible site of *mdl-1* action on lifespan is the intestine, which plays a significant role in the control of aging [40], and where *mdl-1* is expressed [10]. Notably, intestine-limited rescue of *mdl-1(+)* in otherwise *mdl-1(0)* worms was sufficient to modestly increase lifespan. However, how *mdl-1* acts in the intestine remains unclear. Mutation of *daf-2* increases intestinal expression of *ftn-1*, which encodes the iron storage protein ferritin. This increase is wholly *daf-16* dependent and partially *mdl-1* dependent [14]. Free iron is required for growth (e.g. ferroprotein synthesis) but also generates oxidative stress. Thus, increased activity of MDL-1 in *daf-2* mutants might retard intestinal aging as part of a program of suppression of protein biosynthesis. However, we did not detect an effect of *mdl-1* on accumulation of the most abundant protein class in *C. elegans* hermaphrodites, the vitellogenins (Figure 6A,B), which are synthesized in the intestine [46]. However, it remains possible that other aspects of protein synthesis are reduced by *mdl-1*.

Alternatively, mutation of *mdl-1* might increase levels of free iron in the intestine, perhaps accelerating aging by increasing oxidative damage, as suggested by the free radical theory. Consistent with this, *mdl-1(0)* partially suppress *daf-2* Oxr (Figure 3E), suggesting that MDL-1 promotes Oxr in *daf-2* mutants. However, *mdl-1(0)* alone did not affect Oxr; moreover, free iron levels appear to have little effect on aging under standard culture conditions [60]. More broadly, a range of studies suggest that oxidative damage is not a central determinant of aging, particularly in *C. elegans* [61, 62]. Together, these findings suggest that the intestine is one of several sites of action of *mdl-1* on lifespan.

The significance of uterine tumors in *C. elegans*

The oocyte-derived growths in the *C. elegans* uterus have been noted in previous studies and referred to as *'tumor-like' growths* [30], *masses* [24] and *oocyte clusters* [29]. Dictionary definitions of the word *tumor* vary, but in the common understanding of *tumor*, as in "a growth — a mass of tissue — that has no function" [63], these entities are tumors, hence our use of the term in this study. Arguably, *C. elegans* uterine tumors are both different and similar to mammalian cancer. It seems likely that *C. elegans* uterine tumors result from aging-associated overgrowth rather than mutations in oncogenes or tumor suppressor genes. But much of mammalian cancer, like worm uterine tumors, is part of the aging process. While it is clear that aging and cancer are associated, the relationship between the two remains unclear. One possibility is that aging results in changes in tissue microenvironment, e.g. due to senescent cell accumulation, that create more permissive conditions for cancer growth [64]. Aging-related tumors can occur even in the absence of transforming mutation, as in benign prostatic hyperplasia (BPH). We postulate that *C. elegans* uterine tumors, like BPH, exemplify the non-mutationally driven component of aging-associated cancer.

The regulatory network within which *mdl-1* might function

In mammals, Mad TFs act antagonistically to Myc TFs, which promote the cell cycle, growth and apoptosis, and reduce H ferritin expression [11, 15]. Consistent with this, MDL-1 inhibits germline growth and apoptosis (this study), and activates *ftn-1* expression [14]. Moreover, in mammals over-expression of Myc can induce endomitosis and cause increased ploidy [65], often seen in tumors, and also in senescent cells [66, 67], while MDL-1 antagonizes growth of uterine tumors formed from endomitotic oocytes (this study). Thus, MDL-1 in *C. elegans* behaves as one would expect of an antagonist of Myc – which is perhaps surprising given that *C. elegans* does not possess Myc. Indeed, Myc appears to be absent from the entire Nematode phylum (this study) [51].

In mammals, the Tor pathway and Myc TFs work in concert to control protein synthesis. Myc TFs activate expression of translational machinery genes, including eIF4E, eIF4A and eIF4G, which are components of the eIF4F complex that promotes translational initiation [48]. *C. elegans* lacks many genes that are present in other animal phyla [68], which can limit its usefulness as a model organism. Besides Myc, this also affects the worm Tor pathway, which lacks several key proteins, notably Tsc1/Tsc2 and 4E-BP. Thus, *C. elegans* possesses what appears to be a different version of the IIS/Tor/Mad network of higher animals. To fully understand the worm network requires understanding these differences.

Several interpretations have been made of the absence of Myc in *C. elegans*. First, that it reflects the relatively restricted *C. elegans* cell proliferation program [10]. Second, that in *C. elegans* the Myc role is played by a different bHLH TF, for example MML-1 (Myc and Mondo-like 1) [16]. However, arguing against this interpretation, MML-1 resembles Mondo rather than Myc, it dimerizes with MXL-2 while MDL-1 dimerizes with MXL-1, and deletion of *mxl-2* has only minor phenotypic effects (abnormal migration of ray 1 precursor cells in the male tail), and does not affect e.g. growth or lifespan [16].

Another possibility is that the Myc-less Mad-Max circuit ensures rapid growth, i.e. the nematode machinery for protein translation is, in the absence of DAF-16 and MDL-1, constitutively active. Consistent with this, Tsc1/Tsc2 and 4E-BP, which both antagonize growth, are absent from *C. elegans*, and most other nematodes (Figure 7B). Notably, in *Drosophila*, inhibition of growth resulting from reduced Tor kinase activity (e.g. by over-expression of Tsc1 and Tsc2) can be rescued by overexpression of dMyc [69]. An intriguing detail is the presence of Tsc1/Tsc2 in several spirurid nematodes (Figure 7B, Table S4); notably this group includes the longest lived nematode species known, e.g. the maximum lifespan of adult *Loa loa* is at least 20 years [70]. Another possibility is that the growth inhibitory functions of Tsc1/Tsc2 and 4E-BP have been taken over by DAF-16/FoxO, which is a major regulator of protein synthesis in *C. elegans* [41, 42, 45]. Thus, perhaps DAF-16 suppresses growth in soma and germline, while MDL-1 suppresses growth in the germline alone.

Conclusions

These results confirm that the Mad TF MDL-1 contributes to the *daf-2* longevity phenotype, and reveal a major role in inhibition of germline growth and reduction of uterine tumor development. They also suggest a role for intestinal MDL-1 in longevity assurance. The action of *mdl-1* as a DAF-16 activated gene that inhibits growth is broadly consistent with the possibility that the effects of insulin/IGF-1 signaling and DAF-16 on aging are a function of their effects on growth.

EXPERIMENTAL PROCEDURES

C. *elegans* culture and strains. Worms were cultured as previously described [71], at 20˚C unless otherwise stated. Nematode strains used include N2 (wild type),

DR1567 *daf-2(m577)III*, SS104 *glp-4(bn2)I*, GA1200 *mdl-1(tm311)X* (6X out-crossed), GA91 *daf-16(mgDf50)I; daf-2(m577),* GA1204 *daf-2(m577); mdl-1(tm311),* GA1208 *daf-16(mgDf50); daf-2(m577); mdl-1(tm311)*, GA1226 *daf-16(mgDf50); mdl-1(tm311)*, GA1230 *glp-4(bn2); mdl-1(tm311)*, GA1604 *mdl-1(tm311); wuEx267[mdl-1 + rol-6(su1006)]*, GA1605 *mdl-1(tm311); wuEx268[pges-1::mdl-1 + rol-6(su1006)]*. Primers to identify *mdl-1(tm311)* were atggaacagcaactcaaccttgg and ttaaacttggaggttgattggcaag, and heterozygotes aatgatgtgatctcgggctcg. Primers to genotype *daf-16(mgDf50)* were as described [72].

Strain construction. Multiple mutant strains were generated using standard genetic and molecular methodologies. Strains carrying mutations on the X chromosome (e.g. *mdl-1(tm311)*) were crossed with N2 males to generate hemizygous mutant males which were mated with L4 hermaphrodites of the strain carrying the second mutation of interest. F1 offspring were picked, and allowed to self-fertilise and 80 F2 were picked, allowed to lay eggs overnight, lysed and stored at -20˚C. Genomic deletions were identified using PCR. In the presence of the temperature sensitive *daf-2(m577)* allele, F1 animals were shifted to 25˚C to select for dauer formation in the F2, dauers were picked and left to recover at 15˚C to lay eggs, the F2 were lysed and tested for deletions. The *daf-16(mgDf50); daf-2(m577); mdl-1(tm311)* triple mutant was constructed by mating *daf-16; daf-2* males with *daf-2; mdl-1* hermaphrodites. The F2 generation was cloned, lysed and offspring raised at 25˚C. *daf-16(mgDf50)* homozygotes in the F3 were initially identified as non-dauer formers, and *mdl-1(tm311)* homozygotes identified by PCR.

mdl-1 transgenic lines were created by microinjection using PCR products and PCR fusion [73]. Primers used to make GA1604 were aaattgcacatgcagagacg and gaaagatacggaaggtgtgc. Primers used to make GA1605 were ttgtctattggtatggctgc; ggttgagttgctgttccattacaaggaa tatccgcatctg; gcgctaccaataaggctaag; aatggaacagcaactc aacc; gaaagatacggaaggtgtgc; and tttacaacacgatccacacg.

Staining protocols. To quantify germ cell number, nuclei were stained using DNA-binding dye 4',6-diamidino-2-phenylindole (DAPI). Animals were fixed in methanol, washed with M9 buffer and incubated in the dark in a 500ng/µl DAPI solution for 30 min. Thereafter they were washed again in M9 buffer. To quantify the number of apoptotic cells in living animals, nematodes were stained with SYTO 12 Green Fluorescent Nucleic Acid Stain (Molecular Probes). The animals were incubated in the dark in a 33µM SYTO 12 solution for 4 hr, and then placed on an OP50 lawn for 1 hr.

Quantitative RT-PCR and chromatin immuno-precipitation PCR (ChIP-PCR). RT-PCR and ChIP-PCR were performed largely as previously described [9, 74]. Primers for RT-PCR amplification from *mdl-1* mRNA were cccgtttgcgtgtcattgt and atggattgtgagagtgttgagaat. Primers for ChIP-PCR of an *mdl-1* promoter region (Figure 1A) were ccccctcgttttctccatgt and gccgctcgctccaatg.

Microscopy. Freshly prepared agar pads were created by dropping 35µl of 2% agarose onto a glass slide. Worms were anaesthesised using 5µl 0.2% levamisole. Nomarski microscopy was performed on a Zeiss Axioskop2 plus microscope with a Hamamatsu ORCA-ER digital camera C4742-95. Images were acquired using Volocity 5.5 software, with 10x eyepieces and a 40x objective lens. For body size measurements, worms were synchronized and hatched overnight in M9 buffer. The next day, ~30 worms per strain were imaged, and the remainder cultured on OP50 and thereafter imaged consecutively for 6 days. Volocity 5.5 was used to quantify the length of the worm from head to tail and the width across the pharyngeal-intestinal valve region.

Uterine tumor scoring system. Uterine status was scored from 1 to 5, where scores of 3-5 indicates the presence of a tumor. Class 1 denotes a normal, youthful uterus containing fertilized eggs and/or unfertilized oocytes of normal appearance. Class 2 denotes a uterus whose contents appear somewhat abnormal, but without a clear increase in size. Class 3 denotes a uterus containing a small tumor. Class 4 denotes a uterus containing a medium sized tumor, that does not fill the body cavity in the mid-body region. Class 5 denotes a uterus where the tumor is large, and fill the entire body cavity in the mid-body region, and even causes distension of the body wall. For the scoring, the tumor images was randomised, and the scoring was performed blinded by 3 different scorers. The non-parametric Wilcoxon test was used to compare tumor classes between worm strains and within the same strain on day 1 and day 4. The analysis was performed using the statistical programme JMP 9 (SAS Institute Inc.)

Fertility measurements. Brood sizes were assayed as previously described [22]. Briefly, 10-12 L4 hermaphrodites, raised at 20˚C were cloned on individual plates, shifted to 25˚C and transferred daily for 7 days. Plates were incubated at 20˚C for 24 hr to allow offspring to hatch and then larvae, unfertilized oocytes and dead eggs were scored.

Yolk level measurements. For each test sample, 50 hermaphrodites at day 1 and 4 of adulthood were transferred into an Eppendorf tube filled with 1 ml M9

buffer. Worms were spun at 800 rpm for 2 min and supernatant removed, leaving 25 µl. Then 25 µl of 2x Laemmli buffer (Sigma) was added, and samples incubated at 70˚C for 15 min, vortexed every other minute and then shifted to 95˚C for 5 min. Lysates were centrifuged at 13,000 rpm at 4˚C for 15 min. 20 µl of each sample was loaded onto a Criterion XT Tris-Acetate gel. The gel was run at 200V in SDS-PAGE chamber with 1x 3-(N-morpholino) propanesulfonic acid (MOPS) buffer for 45 min. The gel was fixed in methanol, acetic acid and ultrapure water in ratio of 50:10:40 for 30 min. The fixing solution was then discarded and replaced with Coomassie fixation solution (50:3:40:10 methanol: Coomassie stock solution: ultrapure water: acetic acid). 12.0 g of Brilliant Blue R-250, 300 ml methanol and 60ml acetic acid were used to prepare Coomassie stock solution. The gel was incubated overnight in destaining solution (45:10:45 methanol: acetic acid: ultrapure water). Protein bands on the gel were visualised by a Image Quant GE Healthcare scanner system connected to a computer, and analysed by ImageQuant software with which densitometry was performed. Each experiment was done in triplicate.

Lifespan measurements**.** These were conducted as previously described [22]. Briefly, 5 plates per condition were seeded with OP50 2 days before the start of the experiment. 10 µM FUdR was topically applied before beginning the trial. Animals were raised at 20˚C, or for assays including *glp-4(bn2)* mutants, animals were raised at 15˚C and switched to 25˚C at L4 stage. All animals were transferred to fresh plates on day 5 and 10. Deaths were scored and losses due to causes other than death were censored. Lifespan data were deposited in SurvCurv [75] <IDs filled in proof>.

Dauer formation measurement. Dauer formation was assessed at 22.9˚C as previously described [22]. Briefly, 12 L4s were picked and raised to adulthood at 20˚C for 2 days. These gravid adults were then placed on 35mm plates to lay eggs for 6 hrs at the test temperature, after which the adults were removed and the larvae were allowed to develop at the test temperature. Dauers and normal larvae were scored 72 hr after the midpoint of the egg lay and the percentage dauer formation was calculated by dividing the number of dauer larvae by the total number of offspring.

Oxidative stress resistance. 1 day old adults were tested for resistance to 7.5 mM *tert*-butylhydroperoxide (*t*-BOOH) as previously described [33]. Briefly, L4 animals were picked from mixed stage plates raised at 20˚C, then shifted to 25˚C overnight. NGM agar was supplemented with 7.5 mM *t*-BOOH and the plates were left to dry overnight. The next day, each plate was supplemented with a blob of densely grown OP50, and 15 young adults were added per plate. The trial was conducted at 25˚C and animals were scored every 2 to 3 hr until the last animal had perished.

Bioinformatics. Myc, Tsc1, Tsc2 and 4E-BP orthologs were sought by local alignment searches of the 4 protein sequences to the gene models in *Mus musculus* using BLASTP searches. Since not all genomes were available in WormBase, orthologs for the parasitic helminths (*B. xylophilus*, *E. granulosus, E. multilocularis, T. solium, H. microstoma*, *S. mansoni* and *S. japonicum*) were derived from GeneDB. Orthologs for *G. pallida, H. contortus, O. volvulus, S. ratti and T. muris* were sought using the data available on the Sanger Institute Resources. Orthologs to *T. muris* were sought by local alignment searches of the 4 genes to contigs, using a "protein versus translated DNA" a TBLASTN search. Finally, orthologs of *P. pacificus* were sought among the gene predictions available from www.pristionchus.org. Multiple sequence alignments of the Tsc1/2 protein sequences were done using MUSCLE [76]. All trees were constructed and visualised as previously described [74].

Statistical analysis. Lifespans were analysed using the Cox Proportional Hazard method with the Efron approximation for ties of the survival package in R. The logistic mortality models were fitted to the lifespan data and parameter difference tested using the Survomatic R package. The body sizes were analysed using a linear regression model taking into account the trial as random factor in R. The Wilcoxon Mann test was used for tumors and the brood sizes were compared using a standard Student's t Test.

ACKNOWLEDGEMENTS

We wish to thank Mikhail Nikiforov for useful discussion, and Filipe Cabreiro for comments on the manuscript. Some nematode strains used in this work were provided by the Caenorhabditis Genetics Center, which is funded by the National Institutes of Health National Center for Research Resources and the National Bioresource Project of Japan. This work was supported by the Wellcome Trust (Strategic Award), EMBL and the European Union (IDEAL).

Conflicts of Interest Statement

The authors of this manuscript have no conflict of interest to declare.

REFERENCES

1. Kenyon C. The genetics of ageing. Nature. 2010;464:504-512.

2. Kenyon C, Chang J, Gensch E, Rudener A and Tabtiang R. A *C. elegans* mutant that lives twice as long as wild type. Nature. 1993; 366:461-464.

3. Lin K, Dorman JB, Rodan A and Kenyon C. *daf-16*: An HNF-3/forkhead family member that can function to double the life-span of *Caenorhabditis elegans*. Science. 1997; 278:1319-1322.

4. Ogg S, Paradis S, Gottlieb S, Patterson GI, Lee L, Tissenbaum HA and Ruvkun G. The Fork head transcription factor DAF-16 transduces insulin-like metabolic and longevity signals in *C. elegans*. Nature. 1997; 389:994-999.

5. McElwee J, Bubb K and Thomas J. Transcriptional outputs of the Caenorhabditis elegans forkhead protein DAF-16. Aging Cell. 2003; 2:111-121.

6. Murphy CT, McCarroll SA, Bargmann CI, Fraser A, Kamath RS, Ahringer J, Li H and Kenyon CJ. Genes that act downstream of DAF-16 to influence the lifespan of *C. elegans*. Nature. 2003; 424:277-284.

7. McElwee JJ, Schuster E, Blanc E, Thomas JH and Gems D. Shared transcriptional signature in *C. elegans* dauer larvae and long-lived *daf-2* mutants implicates detoxification system in longevity assurance. J Biol Chem. 2004; 279:44533-44543.

8. Partridge L, Alic N, Bjedov I and Piper MD. Ageing in Drosophila: the role of the insulin/Igf and TOR signalling network. Exp Gerontol. 2011; 46:376-381.

9. Schuster E, McElwee JJ, Tullet JMA, Doonan R, Matthijssens F, Reece-Hoyes JS, Hope IA, Vanfleteren JR, Thornton J and Gems D. DamID in *C. elegans* reveals longevity-associated targets of DAF-16/FoxO. Mol Syst Biol. 2010; 6:399.

10. Yuan J, Tirabassi RS, Bush AB and Cole MD. The C. elegans MDL-1 and MXL-1 proteins can functionally substitute for vertebrate MAD and MAX. Oncogene. 1998; 17:1109-1118.

11. Grandori C, Cowley SM, James LP and Eisenman RN. The Myc/Max/Mad network and the transcriptional control of cell behavior. Ann Rev Cell Dev. 2000; 16:653-699.

12. Gems D and Partridge L. Genetics of longevity in model organisms: Debates and paradigm shifts. Annual Review of Physiology. 2013; 75:621-644.

13. Delpuech O, Griffiths B, East P, Essafi A, Lam EW, Burgering B, Downward J and Schulze A. Induction of Mxi1-SR alpha by FOXO3a contributes to repression of Myc-dependent gene expression. Mol Cell Biol. 2007; 27:4917-4930.

14. Ackerman D and Gems D. Insulin/IGF-1 and hypoxia signaling act in concert to regulate iron homeostasis in C. elegans. PLoS Genet. 2012; 8:e1002498.

15. Le N and Richardson D. The role of iron in cell cycle progression and the proliferation of neoplastic cells. Biochim Biophys Acta. 2002; 1603:31–46.

16. Pickett CL, Breen KT and Ayer DE. A C. elegans Myc-like networks cooperates with semaphorin and Wnt signaling pathways to control cell migration. Dev Biol. 2007; 310:226-239.

17. Grove CA, De Masi F, Barrasa MI, Newburger DE, Alkema MJ, Bulyk ML and Walhout AJ. A multiparameter network reveals extensive divergence between C. elegans bHLH transcription factors. Cell. 2009; 138:314-327.

18. Pinkston JM, Garigan D, Hansen M and Kenyon C. Mutations that increase the life span of C. elegans inhibit tumor growth. Science. 2006; 313:971-975.

19. Pinkston-Gosse J and Kenyon C. DAF-16/FOXO targets genes that regulate tumor growth in Caenorhabditis elegans. Nat Genet. 2007; 39:1403-1409.

20. Gems D and Riddle DL. Defining wild-type life span in *Caenorhabditis elegans*. J Gerontol A Biol Sci Med Sci. 2000; 55:B215-B219.

21. Ward S and Carrel JS. Fertilization and sperm competition in the nematode *Caenorhabditis elegans*. Dev Biol. 1979; 73:304-321.

22. Gems D, Sutton AJ, Sundermeyer ML, Larson PL, Albert PS, King KV, Edgley M and Riddle DL. Two pleiotropic classes of *daf-2* mutation affect larval arrest, adult behavior, reproduction and longevity in *Caenorhabditis elegans*. Genetics. 1998; 150:129-155.

23. Jud M, Razelun J, Bickel J, Czerwinski M and Schisa JA. Conservation of large foci formation in arrested oocytes of Caenorhabditis nematodes. Dev Genes Evol. 2007; 217:221-226.

24. Hughes SE, Huang C and Kornfeld K. Identification of mutations that delay somatic or reproductive aging of Caenorhabditis elegans. Genetics. 2011; 189:341-356.

25. Gumienny TL, Lambie E, Hartwieg E, Horvitz HR and Hengartner MO. Genetic control of programmed cell death in the Caenorhabditis elegans hermaphrodite germline. Development. 1999; 126:1011-1022.

26. Jaramillo-Lambert A, Ellefson M, Villeneuve AM and Engebrecht J. Differential timing of S phases, X chromosome replication, and meiotic prophase in the C. elegans germ line. Dev Biol. 2007; 308:206-221.

27. Wolke U, Jezuit EA and Priess JR. Actin-dependent cytoplasmic streaming in C. elegans oogenesis. Development. 2007; 134:2227-2236.

28. Garigan D, Hsu A, Fraser A, Kamath R, Ahringer J and Kenyon C. Genetic analysis of tissue aging in *Caenorhabditis elegans*: a role for heat-shock factor and bacterial proliferation. Genetics. 2002; 161:1101-1112.

29. Luo S, Kleemann GA, Ashraf JM, Shaw WM and Murphy CT. TGF-beta and insulin signaling regulate reproductive aging via oocyte and germline quality maintenance. Cell. 2010; 143:299-312.

30. Golden T, Beckman K, Lee A, Dudek N, Hubbard A, Samper E and Melov S. Dramatic age-related changes in nuclear and genome copy number in the nematode Caenorhabditis elegans. Aging Cell. 2007; 6:179-188.

31. McGee MD, Day N, Graham J and Melov S. cep-1/p53-dependent dysplastic pathology of the aging C. elegans gonad. Aging. 2012; 4:256-269.

32. Qi W, Huang X, Neumann-Haefelin E, Schulze E and Baumeister R. Cell-nonautonomous signaling of FOXO/DAF-16 to the stem cells of Caenorhabditis elegans. PLoS Genet. 2012; 8:e1002836.

33. Tullet JM, Hertweck M, An JH, Baker J, Hwang JY, Liu S, Oliveira RP, Baumeister R and Blackwell TK. Direct inhibition of the longevity-promoting factor SKN-1 by insulin-like signaling in C. elegans. Cell. 2008; 132:1025-1038.

34. Johnson T, Wu D, Tedesco P, Dames S and Vaupel J. Age-specific demographic profiles of longevity mutants in *Caenorhabditis elegans* show segmental effects. J Gerontol A Biol Sci Med Sci. 2001; 56:B331-B339.

35. Vanfleteren JR, De Vreese A and Braeckman BP. Two-parameter logistic and Weibull equations provide better fits to survival data from isogenic populations of *Caenorhabditis*

elegans in axenic culture than does the Gompertz model. J Gerontol A Biol Sci Med Sci. 1998; 53:B393-B403.

36. Johnson TE. The increased lifespan of *age-1* mutants of *Caenorhabditis elegans* results from a lowering of the Gompertz rate of aging. Science. 1990;249:908-912.

37. Gandhi S, Santelli J, Mitchell DG, Stiles JW and Raosanadi D. A simple method for maintaining large, aging populations of *Caenorhabditis elegans*. Mech Ageing Dev. 1980; 12:137-150.

38. Arantes-Oliveira N, Apfeld J, Dillin A and Kenyon C. Regulation of life-span by germ-line stem cells in *Caenorhabditis elegans*. Science. 2002;295:502-505.

39. Hsin H and Kenyon C. Signals from the reproductive system regulate the lifespan of *C. elegans*. Nature. 1999; 399:362-366.

40. Libina N, Berman J and Kenyon C. Tissue-specific activities of *C. elegans* DAF-16 in the regulation of lifespan. Cell. 2003; 115:489-502.

41. Depuydt G, Xie F, Petyuk VA, Shanmugam N, Smolders A, Dhondt I, Brewer HM, Camp DG, Smith RD and Braeckman BP. Reduced insulin/IGF-1 signaling and dietary restriction inhibit translation but preserve muscle mass in Caenorhabditis elegans. Mol Cell Proteomics. 2013.

42. Stout GJ, Stigter EC, Essers PB, Mulder KW, Kolkman A, Snijders DS, van den Broek NJ, Betist MC, Korswagen HC, Macinnes AW and Brenkman AB. Insulin/IGF-1-mediated longevity is marked by reduced protein metabolism. Mol Syst Biol. 2013; 9:679.

43. McGee MD, Weber D, Day N, Vitelli C, Crippen D, Herndon LA, Hall DH and Melov S. Loss of intestinal nuclei and intestinal integrity in aging C. elegans. Aging Cell. 2011; 10:699-710.

44. Herndon L, Schmeissner P, Dudaronek J, Brown P, Listner K, Sakano Y, Paupard M, Hall D and Driscoll M. Stochastic and genetic factors influence tissue-specific decline in ageing *C. elegans*. Nature. 2002; 419:808-814.

45. Depina A, Iser W, Park S, Maudsley S, Wilson M and Wolkow C. Regulation of Caenorhabditis elegans vitellogenesis by DAF-2/IIS through separable transcriptional and posttranscriptional mechanisms. BMC Physiol. 2011; 11:11.

46. Kimble J, Sharrock, WJ. Tissue-specific synthesis of yolk proteins in *Caenorhabditis elegans*. Dev Biol. 1983; 96:189-196.

47. Aamodt EJ, Chung MA and McGhee JD. Spatial control of gut-specific gene expression during Caenorhabditis elegans development. Science. 1991;252:579-582.

48. Lin C-J, Malina A and Pelletier J. c-Myc and eIF4F consistute a feedforward loop that regulates cell growth: implications for anticancer therapy. Cancer Res. 2009;69:7491-7494.

49. Kapahi P, Chen D, Rogers AN, Katewa SD, Li PW, Thomas EL and Kockel L. With TOR, less is more: a key role for the conserved nutrient-sensing TOR pathway in aging. Cell Metab. 2010; 11:453-465.

50. Syntichaki P, Troulinaki K and Tavernarakis N. eIF4E function in somatic cells modulates ageing in Caenorhabditis elegans. Nature. 2007; 445:922-926.

51. McFerrin LG and Atchley W. Evolution of the Max and Mlx networks in animals. Genome Biol Evol. 2011; 3:915–937.

52. Schreiber-Agus N, Meng Y, Hoang T, Hou H, Jr., Chen K, Greenberg R, Cordon-Cardo C, Lee HW and DePinho RA. Role of Mxi1 in ageing organ systems and the regulation of normal and neoplastic growth. Nature. 1998;393:483-487.

53. Blagosklonny MV. Cell cycle arrest is not yet senescence, which is not just cell cycle arrest: terminology for TOR-driven aging. Aging. 2012; 4:159-165.

54. Budovsky A, Tacutu R, Yanai H, Abramovich A, Wolfson M and Fraifeld V. Common gene signature of cancer and longevity. Mech Ageing Dev. 2009;130:33-39.

55. Finch CE, Pike MC and Witten M. Slow mortality rate accelerations during aging in some animals approximate that of humans. Science. 1990;249:902-905.

56. Gems D. What is an anti-aging treatment? Exp Gerontol. 2014 (In press).

57. Blagosklonny MV. Aging and immortality: quasi-programmed senescence and its pharmacologic inhibition. Cell Cycle. 2006; 5:2087-2102.

58. Blagosklonny MV. Paradoxes of aging. Cell Cycle. 2007; 6:2997-3003.

59. Gems D and de la Guardia Y. Alternative perspectives on aging in C. elegans: reactive oxygen species or hyperfunction? Antioxid Redox Signal. 2013;19:321-329.

60. Valentini S, Cabreiro F, Ackerman D, Alam MM, Kunze MBA, Kay CWM and Gems D. Manipulation of *in vivo* iron levels can alter resistance to oxidative stress without affecting ageing in the nematode *C. elegans*. Mech Ageing Dev. 2012;133:282-290.

61. Van Raamsdonk JM and Hekimi S. Reactive oxygen species and aging in Caenorhabditis elegans: causal or casual relationship? Antioxid Redox Signal. 2010; 13:1911-1953.

62. Gems D and Doonan R. Antioxidant defense and aging in C. elegans: is the oxidative damage theory of aging wrong? Cell Cycle. 2009;8:1681-1687.

63. Vocabulary.com. (2013).tumor.

64. Campisi J. Senescent cells, tumor suppression, and organismal aging: good citizens, bad neighbors. Cell. 2005; 120:513-522.

65. Yin XY, Grove L, Datta NS, Long MW and Prochownik EV. C-myc overexpression and p53 loss cooperate to promote genomic instability. Oncogene. 1999;18:1177-1184.

66. Smogorzewska A and de Lange T. Different telomere damage signaling pathways in human and mouse cells. EMBO J. 2002; 21:4338-4348.

67. Wagner M, Hampel B, Bernhard D, Hala M, Zwerschke W and Jansen-Durr P. Replicative senescence of human endothelial cells in vitro involves G1 arrest, polyploidization and senescence-associated apoptosis. Exp Gerontol. 2001;36:1327-1347.

68. Coghlan A. (2005). Nematode genome evolution. In: Community TCeR, ed. WormBook.

69. Gallant P. Myc/Max/Mad in invertebrates: the evolution of the Max network. Curr Top Microbiol Immunol 2006; 302:235-253.

70. Gems D. Longevity and ageing in parasitic and free-living nematodes. Biogerontology. 2000; 1:289-307.

71. Brenner S. The genetics of *Caenorhabditis elegans*. Genetics. 1974; 77:71-94.

72. Love D, Ghosh S, Mondoux M, Fukushige T, Wang P, Wilson M, Iser W, Wolkow C, Krause M and Hanover J. Dynamic O-GlcNAc cycling at promoters of Caenorhabditis elegans genes regulating longevity, stress, and immunity. Proc Natl Acad Sci U S A. 2010; 107:7413-7418.

73. Hobert O. PCR fusion-based approach to create reporter gene constructs for expression analysis in transgenic C. elegans. Biotechniques. 2002; 32(4):728-730.

74. Tullet JMA, Araiz C, Sanders MJ, Au C, Benedetto A, Papatheodorou I, Clark E, Schmeisser K, Jones D, Schuster EF, Thornton JM and Gems D. DAF-16/FoxO directly regulates an atypical AMP-activated protein kinase gamma isoform to

mediate the effects of insulin/IGF-1 signaling on aging in C. elegans. PLoS Genet. 2013; In press.

75. Ziehm M and Thornton JM. Unlocking the potential of survival data for model organisms through a new database and online analysis platform: SurvCurv. Aging Cell. 2013; 12:910-916.

76. Edgar RC. MUSCLE: a multiple sequence alignment method with reduced time and space complexity. BMC Bioinformatics. 2004; 5:113.

SUPPLEMENTAL TABLES

Table S1. Effect of *mdl-1* on life span in *C. elegans.* The trials were performed at 25°C without FUdR. Genotype: N2 wildtype, GA1200 *mdl-1(tm311),* DR1567 *daf-2 (m577),* GA1204 *daf-2(m577); mdl-1(tm311)*. *p*, log rank test. [n] biological replicates number. [C], combined data from 4 trials.

Genotype	Deaths/ censored	Mean life span (days)	% *vs.* wild type	*p vs.* wild type	% *vs. daf-2*	*p vs. daf-2*
Wild type	**[C] 513/18**	**14.7**				
	[1] 120/5	15.2				
	[2] 121/5	14.1				
	[3] 133/7	15.3				
	[4] 139/1	14.3				
mdl-1(tm311)	**[C] 500/17**	**12.8**	**-13.1**	**<.0001**		
	[1] 119/4	14.4	-5.4	0.0288		
	[2] 115/4	12.0	-15.1	<.0001		
	[3] 125/8	12.9	-16.0	<.0001		
	[4] 141/1	12.1	-15.5	<.0001		
daf-2 (m577)	**[C] 412/57**	**35.2**	**+139.2**	**<.0001**		
	[1] 87/26	31.0	+104.4	<.0001		
	[2] 86/3	34.0	+141.1	<.0001		
	[3] 121/8	35.1	+129.2	<.0001		
	[4] 118/20	39.2	+174.1	<.0001		
daf-2(m577); mdl-1(tm311)	**[C] 438/78**	**26.6**	**+80.9**	**<.0001**	**-24.5**	**<.0001**
	[1] 75/59	21.2	+39.4	<.0001	-31.7	<.0001
	[2] 113/1	28.0	+98.5	<.0001	-17.6	<.0001
	[3] 132/4	27.0	+76.4	<.0001	-22.9	<.0001
	[4] 118/14	28.3	+97.9	<.0001	-27.9	<.0001

Table S2. *glp-4(bn2)* and FUdR do not suppress *mdl-1* shortevity. Genotypes: N2 wildtype, GA1200 *mdl-1(tm311),* SS104 *glp-4(bn2)*, GA1230 *glp-4*; *mdl-1*. p, log rank test. [n] biological replicates number. *glp-4* trial, worms raised at 15°C to L4, then shifted to 25°C.

Genotype	Deaths/ censored	Mean life span (days)	% *vs.* wild type	*p vs.* wild type	% *vs. glp-4*	*p vs. glp-4*
***glp-4* Trials** (worms raised at 15˚C, shifted at L4 stage to 25˚C)						
Wild type	[1] 77/11	15.5				
	[2] 69/11	13.2				
mdl-1(tm311)	[1] 61/11	12.9	-17.0	0.0002		
	[2] 48/11	11.3	-14.5	0.0023		
glp-4(bn2)	[1] 86/14	15.7	+1.59	0.46		
	[2] 64/9	14.3	+8.4	0.43		
glp-4; mdl-1	[1] 120/4	12.3	-4.4	<0.0001	-21.6	<0.0001
	[2] 75/6	9.1	-19.2	<0.0001	-36.3	<0.0001
***glp-4* Trials** (worms raised and maintained at 25˚C)						
Wild type	[1] 87/7	12.2				
	[2] 78/12	14.2				
mdl-1(tm311)	[1] 78/19	11.4	-6.6	0.20		
	[2] 76/22	12.7	-10.7	0.05		
glp-4(bn2)	[1] 94/9	14.0	+14.8	0.0035		
	[2] 77/16	17.6	+24.0	0.0002		
glp-4; mdl-1	[1] 83/17	12.3	+0.8	0.21	-12.0	0.024
	[2] 70/17	15.0	-15.2	0.36	-14.7	0.0051
FUdR Trials			**% *vs.* wild type (no FUdR)**	***p vs.* wild type (no FUdR)**	**% *vs.* no FUdR**	***p vs.* no FUdR**
Wild type	[1] 46/14	17.5				
	[2] 41/19	16.8				
mdl-1(tm311)	[1] 49/11	12.4	-41.1	<0.0001		
	[2] 49/11	13.3	-26.3	0.0027		
Wild type (50μM FUdR)	[1] 55/5	17.3	-1.2	0.55	-1.2	0.55
	[2] 57/3	14.6	-15.1	0.022	-15.1	0.022
mdl-1(tm311) (50μM FUdR)	[1] 54/6	12.7	-37.8	<0.0001	+2.4	0.80
	[2] 49/11	11.6	-44.8	<0.0001	-14.7	0.032

Table S1. Effect of *mdl-1* on life span in *C. elegans.*

Strain	Deaths/ censored	Mean life span (days)	% *vs.* wild type	*p vs.* wild type	% *vs. mdl-1*	*p vs. mdl-1*
Wild type	**[C] 198/0**	**11.30**				
	[1] 99/0	11.83				
	[2] 99/0	10.97				
mdl-1(tm311)	**[C] 198/1**	**9.36**	**-17.97**	**<0.0001**		
	[1] 99/0	9.57	-19.10	<0.0001		
	[2] 99/1	9.15	-15.20	<0.0001		
mdl-1; wuEx267 [mdl-1 rol-6]	**[C] 191/0**	**10.91**	**-3.45**	**0.0060**	**+19.55**	**<0.0001**
	[1] 80/0	11.36	-3.97	0.04	+18.70	<0.0001
	[2] 111/0	10.59	-1.85	0.22	+15.74	<0.0001
mdl-1; wuEx268 [pges-1::mdl-1 rol-6].	**[C] 210/0**	**9.97**	**-11.77**	**<0.0001**	**+9.51**	**<0.0001**
	[1] 94/0	10.47	-11.50	<0.0001	+9.40	<0.0001
	[2] 116/0	9.56	-11.40	<0.0001	+4.48	0.0059

Research Paper

Immortalization of MEF is characterized by the deregulation of specific miRNAs with potential tumor suppressor activity

Milena Rizzo[1], Monica Evangelista[1], Marcella Simili[1] , Laura Mariani[1], Letizia Pitto[1], Giuseppe Rainaldi[1,2]

[1]Laboratory of Gene and Molecular Therapy, Institute of Clinical Physiology, CNR, Pisa, Italy
[2] Istituto Toscano Tumori, Firenze, Italy

Running title: MEF immortalization and microRNAs
Key words: mouse embryo fibroblasts, immortalization, microRNAs, genome instability

Received: 5/11/11; Accepted: 6/27/11; Published: 7/11/11 **doi:** 10.18632/aging.100353
Correspondence to Giuseppe Rainaldi at, g.rainaldi@ifc.cnr.it

Abstract: The life span (Hayflick limit) of primary mouse embryo fibroblasts (MEF) in culture is variable but it is still unclear if the escape of the Hayflick limit is also variable. To address this point MEF were expanded every fifteen days (6T15) instead of every three days (6T3) until they became immortal. With this protocol MEF lifespan was extended and immortalization accordingly delayed. By testing a panel of genes (p19ARF, p16, p21) and miRNAs (miR-20a, miR-21, miR-28, miR-290) related to primary MEF senescence, a switch of p21 from up to down regulation, the down regulation of specific miRNAs as well as a massive shift from diploidy to hyperdiploidy were observed in coincidence with the resumption of cell proliferation. Collectively, these data indicate that the inactivation of genes and miRNAs, important in controlling cell proliferation, might be determinant for the escape from the Hayflick limit. In support of this hypothesis was the finding that some of the down regulated miRNAs transfected in immortalized MEF inhibited cell proliferation thus displaying a tumor suppressor-like activity.

INTRODUCTION

The Hayflick limit of primary mouse embryo fibroblasts (MEF) is variable since the growth conditions can either reduce or extend it [1-3]. We have reported that primary MEF expanded every three days (6T3 protocol) underwent four population cell doubling and thereafter cell proliferation was fully abolished and SA-β-gal$^+$ cells induced [4]. However it is known that MEF senescence can be induced prematurely, before the end of the physiological lifespan, by cellular stresses such as the over expression [5] or down regulation [6] of single oncogenes and DNA damaging drugs [7-9]. Recently, it has been reported that miRNAs are involved in senescence of MEF as well as of human diploid fibroblasts [10, 11].

An unsolved question is which cells are able to escape the *in vitro* lifespan limit. So far, the molecular characterization of immortalized MEF cell lines has shown that functional silencing of either the *INK4a/ARF* locus [12] or p53 [13] appears necessary to bypass senescence. A recurrent concept is that mutational events occurring in culture have a key role. If mutations confer a proliferative advantage, mutated cells can bypass the *in vitro* lifespan limit and rapidly replace the existing population [14, 15]. According to this view, the time spent in culture should affect immortalization. We modified the 6T3 expansion protocol of primary MEF [4] by lengthening the interval between passages (15 days versus 3 days) and reiterating it until MEF became immortal. Here we report that: i) the life span was extended up to 8 population cell doubling and immortalization was consequentially delayed; ii) p21 down regulation marks the switch from primary to immortalized MEF; iii) deregulation of genes and miRNAs which control

cell proliferation pathways correlate with the immortalization process; iv) down regulated miRNAs can behave as tumor suppressors.

RESULTS

1. The pro senescence axis p53/p21 is disrupted in immortalized MEF.

To investigate the relative importance of the time in culture versus the number of population cell doubling in the MEF immortalization process we modified the split time. MEF p0 (passage 0) were thawed, and expanded to obtain MEF p1. Thereafter MEF p1 were collected, diluted at the appropriate concentration ($6x10^5$) and grown for 15 days with a medium change every three days (6T15 protocol), before the next trypsinization and expansion. The 6T15 protocol was reiterated 10 times for a total of 150 days in culture. During the first three passages a reduced number of population cell doubling was observed; afterwards a population of proliferating MEF emerged, which rapidly increased (p5) and replaced the preexisting cell population (p10) (Fig. 1A). At the molecular level we found that both p19ARF and p16 were progressively up regulated during passages (with respect to the spontaneous level of MEF p0) (Fig. 1B). Vice versa the expression of p21 was biphasic: while it was up regulated till p3 it decreased thereafter with a clear switch toward under expression at p6 (Fig. 1B,C). As p21 is under the direct control of p53, a disruption of the p53/p21 axis can be hypothesized at the basis of immortalization.

2. Genome stability and miRNA signatures are modified in immortalized MEF.

The down regulation of p21 strongly suggests a loss of p53 activity. In accordance with the hypothesis, FACS analysis showed that while the DNA content distribution curve per cell of MEF p1 and MEF p5 were very similar and typical of diploid cells (Fig. 2A) a massive shift toward cells with higher DNA contents was observed in MEF p6 (Fig. 2B). Hyperdiploid cells, which emerged from diploid primary MEF, are indicative that genomic stability, controlled by p53 [16-18], is lost. It is of note that a stable hyperdiploid cell population is selected within four passages (p6-p10) (Fig. 2C). To strengthen the hypothesis of a functional loss of p53, in parallel we determined the expression profiles of p53 and of miR-34a directly controlled by p53. We found that p53 mRNA (Fig. 2D) and protein levels did not significantly change up to p6 (Fig. 2E); conversely miR-34a appears to increase till p4, starts to decrease at p5 to become markedly down regulated at p6 (Fig. 2D) reinforcing the idea that p53 becomes non-functional.

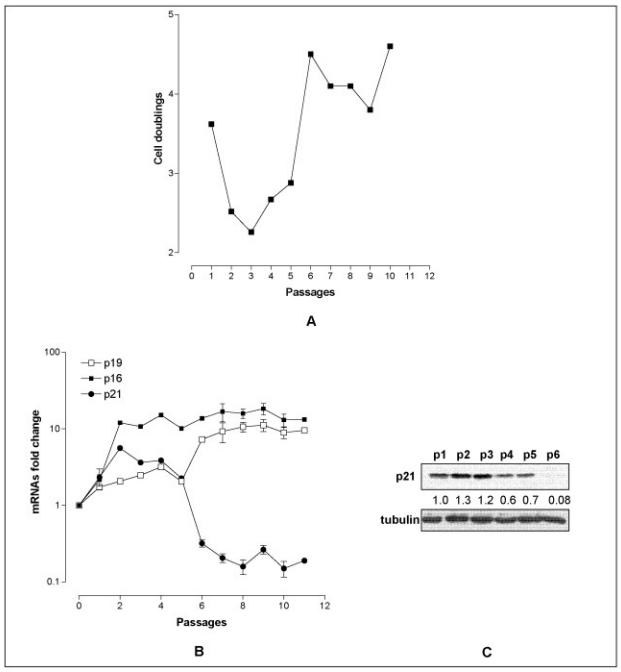

Figure 1. Characterization of MEF under 6T15 propagation regimen. (A) Proliferation curve of MEF expressed as cell doublings per passage. (B) Quantification of *p19ARF*, *p16* and *p21* transcripts per passage (each point represent one passage) normalized to that of MEF at passage 0. (C) p21 protein level at the various passages. The value reported under each lane represents the average of two independent experiments.

3. The senescence related miRNAs are down regulated in immortalized MEF.

As the p53/p21 axis of primary MEF was disrupted in immortalized MEF, we investigated whether the time course of the signatures of miRNAs related to either premature (miR-20a [19]) or replicative (miR-21, miR-28 [20], miR-290 [4]) primary MEF senescence were also modified. The analysis showed that while miR-20a and miR-290 were down regulated till p6 (Fig 3A) miR-21 and miR-28 were up regulated. It is worth noting that the up regulation of miR-21 and miR-28 is in agreement with findings in MEF replicative senescence, while miR-290 down regulation is the opposite of previous observations because we have shown that miR-290 steadily increased when either spontaneous or nocodazole-induced MEF G1 blocked tetraploid cells were present [4]. For that, we examined the cell cycle of p1-p5 MEF. We found that under 6T15 protocol no significant accumulation of G2/M cells was observed (Fig. 3B) suggesting that the failed accumulation of G2/M cells was responsible for the lack of miR-290 up

regulation. The miRNA signatures changed markedly after p6: while miR-20a and miR-290 remain down regulated, although to a lesser extent, miR-21 and miR-28 switched from up to down regulation (Fig. 3A). These data suggest that the deregulation of these two senescence related miRNAs, besides miR-34a, is involved in MEF immortalization.

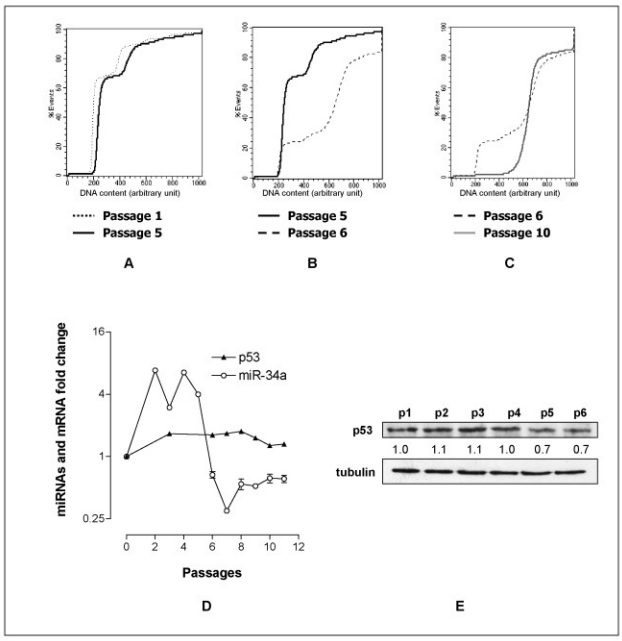

Figure 2. MEF immortalization is characterized by a p53-dependent events. DNA content profile per cell at p1/p5 (A), p5/p6 (B) and p6/p10 (C). (D) Fold change of miR-34a and p53 transcripts at various passages normalized to that of MEF at passage 0. (E) p53 protein level at the various passages. The value reported under each lane represents the average of two independent experiments.

4. The transfection of the down regulated miRNAs reduces the proliferation of immortalized MEF.

To investigate if the deregulated miRNAs play an active role in the immortalization, immortalized MEF (p10) were transfected with miR-21, miR-28 and miR-34. In addition we tested miR-20a and miR-290 whose expression was not affected by the immortalization. The proliferation data showed that miR-20a and miR-290 did not affect cell proliferation as expected, the down regulated miR-28 and miR-34 significantly reduced the proliferation of immortalized MEF with similar efficiency, while miR-21 did not inhibit cell proliferation (Fig. 3C). These data indicate that the re-expression of miR-34a and miR-28 (and consequently of their controlled pathways) was sufficient to reduce the proliferative rate of immortalized MEF and suggest that miR-28, like the tumor suppressor miR-34a, could have a tumor suppressor activity.

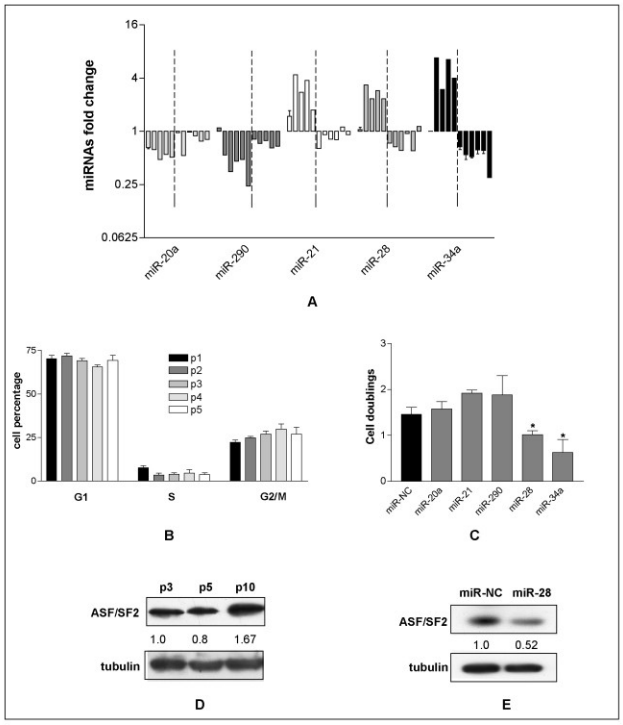

Figure 3. The re-expression of miRNAs down regulated in immortalized MEF reduces cell proliferation. (A) Quantification of miR-20a, miR-21, miR-28, miR-290 and miR-34a per passage normalized to that of MEF at passage 0. Dashed lines indicate the transition from passage 5 to 6. (B) Cell cycle phase distribution (%) of MEF from p1 to p5. (C) Population cell doubling of immortalized MEF after transfection of miR-NC, miR-20a, miR-21, miR-28, miR-290 and miR-34a. Each bar represents the mean ± SD of three biological replicates (*=p<0.05). (D) Expression of ASF/SF2 protein in primary (p3 and p5) and immortalized (p10) MEF. The value reported under each lane represents the average of two independent experiments. (E) Expression of ASF/SF2 after the transfection of immortalized MEF with either miR-NC or miR-28 . The value reported under each lane represents the average of two independent experiments.

5. MiR-28 behaves as tumor suppressor miRNA.

It is well known that miR-34a has a widespread tumor suppressor activity [21, 22]. We show that it behaved as such in immortalized MEF as its re-expression inhibits cell proliferation, probably by partially restoring the p53 pathway. Interestingly miR-28, as far as we know, is not directly linked to the p53 controlled pathways. We have previously reported that in primary MEF miR-28 targets the proto-oncogenic splicing factor ASF/SF2 and that in turn miR-28 over-expression induces both apoptosis and senescence of primary MEF via ASF/SF2 down

regulation [20]. This prompted us to verify the expression of ASF/SF2 in primary and immortalized MEF. As expected the expression of ASF/SF2 was higher in immortalized than in primary MEF (Fig. 3D) suggesting a possible post transcriptional control of miR-28 on ASF/SF2 expression. To confirm the hypothesis, we transfected immortalized MEF (p10) with miR-28 and found 50% reduction of ASF/SF2 expression (Fig. 3E), suggesting that miR-28 control cell proliferation by targeting ASF/SF2. These results strengthen the idea that miR-28 has a tumor suppressor-like activity and might be suitable to be tested in tumor cell lines defective in miR-28 content.

DISCUSSION

The *in vitro* life span defines the number of population cell doubling which primary cells can undergo in culture. We have reported that MEF under the 6T3 expansion regimen were able to undergo four population cell doubling before achieving senescence . In this work we reported that by modifying the propagation regimen and growth conditions (6T15 protocol) MEF slowed down without reaching a complete cell proliferation block and restarted proliferation after about eight population cell doubling (passage 3). These results suggest that activation of p53 with the consequent induction of p21 in this case may favor proliferation arrest rather than senescence as previously described [23]. Interestingly the *in vitro* life span of MEF was extended both in terms of population cell doubling and in terms of days in culture, in keeping with the hypothesis that p53 activation, by inducing quiescence rather than senescence may increase the cell life span [24]. The immortalization process is delayed accordingly, suggesting that it does not strictly depend on the number of cell doubling or the time that the cells spend in culture (45 culture days in this case).

The spontaneous immortalization of primary MEF has been attributed to either the inactivation of p53 or the loss of the *INK4a/ARF* locus (p19ARF, p16) [25], two loci strictly related to cell proliferation. In this work we found that both loci were transcribed and translated during passages whereas p21 shifted from up to down regulation after p5. As p21 expression is mostly p53 dependent we argued that despite p53 continued to be expressed, it may not be functional any more. In support of this conclusion are the down regulation of the p53 dependent miR-34a and the loss of genomic stability revealed by the massive appearance of hyperdiploid cells [16-18]

A recurrent concept is that immortalization is due to mutations induced by DNA damage occurring during the population expansion [14]. The loss of p53 activity found in immortalized MEF could be due to either point mutation or loss of one allele which appears to be sufficient to alter cell growth [15]. In any case the sharp increase of cell proliferation suggests that the immortalization process is caused by the concomitant alteration of multiple pathways. We found that the expression of miR-20a, miR-21, miR-28 and miR-290, all involved in MEF senescence, were deregulated in coincidence with p21 down regulation and increase of cell proliferation. As a high number of genes are potentially targeted by one miRNA [26], we argued that the deregulation of these miRNAs could be in part responsible for the absence of cell proliferation control characteristic of immortal cells. In particular we demonstrate that by replacing miR-28 and miR-34a, under expressed in immortalized MEF, cell proliferation was reduced suggesting that both miRNAs are implicated in immortalization. Evidence in support of an anti proliferative role of miR-28 is already available. We have shown in primary MEF that miR-28 targets the proto-oncogene ASF/SF2, a splicing factor involved in the alternative splicing of many transcripts [27, 28] and its over expression induces apoptosis and senescence by down regulating ASF/SF2 [20]. Our results demonstrate that also in immortalized MEF miR-28 targets ASF/SF2 suggesting that its tumor suppressor activity is due to ASF/SF2 inhibition, although other targets cannot be excluded.

The fact that the replacement of miR-28 in immortalized MEF reduced cell proliferation to the same extent as miR-34a further strengthens the hypothesis that miR-28 represents a novel TS miRNA. MiR-34a is a well known TS miRNA able to inhibit cell proliferation of a wide range of tumor cells [21, 29-31] as well as of human fibroblasts which extend their replicative capacity when treated with miR-34a antisense [32]. Conversely miR-290 and miR-20a involved in culture and stress induced senescence of primary MEF were not able to inhibit proliferation of immortal MEF in keeping with the idea that miRNAs behave differently in different cellular context [33]. In conclusion the delayed immortalization obtained with this protocol implies that point mutations; due to DNA damage accumulated during population expansion [14], are not the only molecular events at the basis of immortalization. The most notable feature which marks the immortalization process is the drastic p21 down regulation possibly due to p53 functional inactivation. Associated to the sudden down regulation of p21 was the induction of hyperploidy, suggesting that genomic instability and/or epigenetic changes are also responsible for the immortalization process. Interestingly, the switch of p21 expression was

accompanied by the change of the signature of miRNAs related to MEF senescence, including the p53-dependent miR-34 and miR-28 [20]. In particular, the down regulated miR-28, behaved as a TS miRNA, when transfected in immortalized MEF, analogously to the well known TS miR-34a, indicating that the comparison of the miRNA signature of primary versus immortalized cells could allow the identification of novel miRNAs with potential tumor suppressor-like activity.

MATERIALS AND METHODS

Reagents. miRNeasy mini kit, QuantiTect Reverse Trascription Kit, miScript Reverse Transcription Kit, miScript SYBR Green PCR Kit (QIAGEN, Milano, Italy); Dulbecco's Modified Eagle Medium-High Glucose (D-MEM-HG), foetal bovine serum (FBS) (Invitrogen, CA, USA); LightCycler 480 Probes Master, Universal ProbeLibrary LNA Probes; LightCycler 480 SYBR Green I Master (Roche Diagnostic, Mannheim, Germany); X-Gal (5-bromo-4-chloro-3-indolylb-D-galactoside); propidium iodide, anti-α-tubulin (Sigma-Aldrich Corporation, Missouri, USA); anti-p21 (Santa Cruz Biotechnology, Inc.); ECL, Hybond-C extra membranes (Amersham); anti-p53 (Cell Signaling Technology). The anti-ASF/SF2 was a gift of Dr. Adrian Krainer. MiR-20a, miR-21, miR-28, miR-34, miR-290 and miR-NC (negative control) (GenePharma Shanghai, China)

Cells and culture conditions. MEF were isolated from 13.5d mouse embryos, expanded and then replated every three days (6T3 protocol). For 6T15 protocol MEF p1 were collected, diluted at the appropriate concentration ($6x10^5$) and grown for 15 days with a medium change every three days, before the next trypsinization and expansion. MEF were grown in Dulbecco's Modified Eagle Medium-high glucose (DMEM-HG)-10% FBS at 37°C in a humidified atmosphere containing 6% CO_2.

Cell proliferation. Cell proliferation was measured as number of population cell doubling per passage (CD= $\ln(N_f/N_i)/\ln 2$) where N_f is the final number of collected cells (day 3) and N_i the initial number of seeded cells (day 0).

MiRNAs transfection. Immortalized MEF (p10) were seeded at cell density of $1.0x10^5$ per 30 mm diameter dish. After 24 hours cells were transfected with either miRNAs under test or a double-stranded oligonucleotide, named miR-NC. Briefly, 15 µl Optimem and 25 µl transfection buffer plus 80 nM miRNA were mixed with a solution of Gene Silencer (5 µl) plus Optimem (25 µl). After 15 minutes incubation, Optimem was added up to 800 µl. After 6 hours the medium was replaced with complete DMEM.

Quantification of miRNAs and genes with Q-Real-time PCR. Total RNA was extracted from $1x10^6$ cells using the miRNeasy mini kit (Qiagen) following the manufacturer's recommendations. To quantify p19ARF, p16 and p21 transcripts, 1µg of total RNA was reverse transcribed using QuantiTect Reverse Trascription Kit (Qiagen). Real-time PCR (qRT-PCR) was carried out with LightCycler 480 (Roche) using LightCycler 480 SYBER Green I Master (Roche). Mature miR-20a, miR-21, miR-28, miR-34a and miR-290 were quantified using the miScript System: 1µg of total RNA was retrotranscribed with miScript Reverse Transcription Kit (Qiagen) and qRT-PCR was carried out using miScript SYBR Green PCR Kit (Qiagen). All reactions were performed in triplicate. Relative quantification of gene expression was calculated with the fit point method. Transcript values were normalized with those obtained from the amplification of the internal controls (GAPDH for transcripts and U6 for miRNAs). The following oligonucleotides were used: p19ARF, forward (F) (5'-CATGGGTCGCAGGTTCTTG-3') and reverse (R) (5'-GCTCGCTGTCCTGG GTCTC-3'); p16, F (5'-CGACGGGCATAGCTTCAG-3') and R (5'-GCTCTGCTCTTGGGATTGG-3'); p21, F (5'-TCCACAGCGATATCCAGACA-3') and R (5'-GGACATCACCAGGATTGGAC-3'); p53, F (5'-ATGCCCATGCTACAGAGGAG-3') and R (5'-AGACTGGCCCTTCTTGGTCT-3'); GAPDH, F (5'-GCCTTCCGTGTTCCTACCC-3'), R (5'-TGCCTGCTTCACCACCTTC-3'); miR-20a, F (5'-TAAAGTGCTTATAGTGCAGGTAG-3'); miR-21, F (5'-TAGCTTATCAGACTGATGTTGA-3'), miR-28, F (5'-AAGGAGCTCACAGTCTATTGAG-3'); miR-34a, F (5'-TGGCAGTGT CTTAGCTGGTTGT-3'); miR-290, F (5'-gctaatcttctctgtatcgttccaa-3'); U6, F (5'-CGCAAGGATGACACGCAAATTC-3').

Western Blot analysis. Equivalent amounts of proteins were resolved on 10% SDS-PAGE gels and transferred to Hybond-C extra membranes by electro blotting. The resulting blots were blocked with 5% nonfat dry milk solution. Anti-α-tubulin (1:1000), anti-p53 (1:500), anti-p21 (1:1000), anti-ASF/SF2 (1:2000) were used. Incubation was performed overnight at 4°C and bands were revealed after incubation with the recommended secondary antibody coupled to peroxidase using ECL. Scanned images were quantified using scion Image software and normalized to α-tubulin.

Cell cycle. Samples of $5x10^5$ of cells under test were fixed with 95% ethanol, stained with 50 µg/ml propidium iodide (PI), incubated over night at 4°C and

cell cycle analyzed using a FACScalibur cytofluorimeter. The Kolmogorov-Smirnov Statistic was used to represent the DNA content profile of MEF at the various passages.

Statistical analysis. Data were analyzed using GraphPad Prism (GraphPad Sofware, Inc., San Diego, CA). Comparisons were evaluated by unpaired *t*-test. A value of $p<0.05$ (*) was considered statistically significant.

ACKNOWLEDGEMENTS

This work was supported by Associazione Italiana per la Ricerca sul Cancro, AIRC [project no. 4753] and by Istituto Superiore di Sanità, ISS [project no. 527/A/3A/4].

REFERENCES

1. Parrinello S, Samper E, Krtolica A, Goldstein J, Melov S, Campisi J. Oxygen sensitivity severely limits the replicative lifespan of murine fibroblasts. Nat Cell Biol. 2003; 5:741-7.

2. Campisi J. Senescent cells, tumor suppression, and organismal aging: good citizens, bad neighbors. Cell. 2005; 120:513-22.

3. vom Brocke J, Schmeiser HH, Reinbold M, Hollstein M. MEF immortalization to investigate the ins and outs of mutagenesis. Carcinogenesis. 2006; 27:2141-7.

4. Pitto L, Rizzo M, Simili M, Colligiani D, Evangelista M, Mercatanti A, Mariani L, Cremisi F, Rainaldi G. miR-290 acts as a physiological effector of senescence in mouse embryo fibroblasts. Physiol Genomics. 2009; 39:210-8.

5. Serrano M, Lin AW, McCurrach ME, Beach D, Lowe SW. Oncogenic ras provokes premature cell senescence associated with accumulation of p53 and p16INK4a. Cell. 1997; 88:593-602.

6. Maeda T, Hobbs RM, Merghoub T, Guernah I, Zelent A, Cordon-Cardo C, Teruya-Feldstein J, Pandolfi PP. Role of the proto-oncogene Pokemon in cellular transformation and ARF repression. Nature. 2005; 433:278-85.

7. Di Micco R, Fumagalli M, Cicalese A, Piccinin S, Gasparini P, Luise C, Schurra C, Garre M, Nuciforo PG, Bensimon A, Maestro R, Pelicci PG, d'Adda di Fagagna F. Oncogene-induced senescence is a DNA damage response triggered by DNA hyper-replication. Nature. 2006; 444:638-42.

8. Yogev O, Anzi S, Inoue K, Shaulian E. Induction of transcriptionally active Jun proteins regulates drug-induced senescence. J Biol Chem. 2006; 281:34475-83.

9. Chen JH, Hales CN, Ozanne SE. DNA damage, cellular senescence and organismal ageing: causal or correlative? Nucleic Acids Res. 2007; 35:7417-28.

10. Bhaumik D, Scott GK, Schokrpur S, Patil CK, Orjalo AV, Rodier F, Lithgow GJ, Campisi J. MicroRNAs miR-146a/b negatively modulate the senescence-associated inflammatory mediators IL-6 and IL-8. Aging (Albany NY). 2009; 1:402-11.

11. Marasa BS, Srikantan S, Martindale JL, Kim MM, Lee EK, Gorospe M, Abdelmohsen K. MicroRNA profiling in human diploid fibroblasts uncovers miR-519 role in replicative senescence. Aging (Albany NY). 2010; 2:333-43.

12. Quelle DE, Zindy F, Ashmun RA, Sherr CJ. Alternative reading frames of the INK4a tumor suppressor gene encode two unrelated proteins capable of inducing cell cycle arrest. Cell. 1995; 83:993-1000.

13. Carnero A, Hudson JD, Hannon GJ, Beach DH. Loss-of-function genetics in mammalian cells: the p53 tumor suppressor model. Nucleic Acids Res. 2000; 28:2234-41.

14. Busuttil RA, Rubio M, Dolle ME, Campisi J, Vijg J. Oxygen accelerates the accumulation of mutations during the senescence and immortalization of murine cells in culture. Aging Cell. 2003; 2:287-94.

15. Odell A, Askham J, Whibley C, Hollstein M. How to become immortal: let MEFs count the ways. Aging (Albany NY). 2010; 2:160-5.

16. Borel F, Lohez OD, Lacroix FB, Margolis RL. Multiple centrosomes arise from tetraploidy checkpoint failure and mitotic centrosome clusters in p53 and RB pocket protein-compromised cells. Proc Natl Acad Sci U S A. 2002; 99:9819-24.

17. Vitale I, Galluzzi L, Senovilla L, Criollo A, Jemaa M, Castedo M, Kroemer G. Illicit survival of cancer cells during polyploidization and depolyploidization. Cell Death Differ. 2010.

18. Vitale I, Senovilla L, Jemaa M, Michaud M, Galluzzi L, Kepp O, Nanty L, Criollo A, Rello-Varona S, Manic G, Metivier D, Vivet S, Tajeddine N, Joza N, Valent A, Castedo M, Kroemer G. Multipolar mitosis of tetraploid cells: inhibition by p53 and dependency on Mos. EMBO J. 2010; 29:1272-84.

19. Poliseno L, Pitto L, Simili M, Mariani L, Riccardi L, Ciucci A, Rizzo M, Evangelista M, Mercatanti A, Pandolfi PP, Rainaldi G. The proto-oncogene LRF is under post-transcriptional control of MiR-20a: implications for senescence. PLoS One. 2008; 3:e2542.

20. Verduci L, Simili M, Rizzo M, Mercatanti A, Evangelista M, Mariani L, Rainaldi G, Pitto L. MicroRNA (miRNA)-mediated interaction between leukemia/lymphoma-related factor (LRF) and alternative splicing factor/splicing factor 2 (ASF/SF2) affects mouse embryonic fibroblast senescence and apoptosis. J Biol Chem. 2010; 285:39551-63.

21. Yamakuchi M, Lowenstein CJ. MiR-34, SIRT1 and p53: the feedback loop. Cell Cycle. 2009; 8:712-5.

22. Tazawa H, Tsuchiya N, Izumiya M, Nakagama H. Tumor-suppressive miR-34a induces senescence-like growth arrest through modulation of the E2F pathway in human colon cancer cells. Proc Natl Acad Sci U S A. 2007; 104:15472-7.

23. Demidenko ZN, Korotchkina LG, Gudkov AV, Blagosklonny MV. Paradoxical suppression of cellular senescence by p53. Proc Natl Acad Sci U S A. 2010; 107:9660-4.

24. Vigneron A, Vousden KH. p53, ROS and senescence in the control of aging. Aging (Albany NY). 2010; 2:471-4.

25. Kim H, You S, Farris J, Kong BW, Christman SA, Foster LK, Foster DN. Expression profiles of p53-, p16(INK4a)-, and telomere-regulating genes in replicative senescent primary human, mouse, and chicken fibroblast cells. Exp Cell Res. 2002; 272:199-208.

26. Lall S, Grun D, Krek A, Chen K, Wang YL, Dewey CN, Sood P, Colombo T, Bray N, Macmenamin P, Kao HL, Gunsalus KC, Pachter L, Piano F, Rajewsky N. A genome-wide map of conserved microRNA targets in C. elegans. Curr Biol. 2006; 16:460-71.

27. Krainer AR, Conway GC, Kozak D. The essential pre-mRNA splicing factor SF2 influences 5' splice site selection by activating proximal sites. Cell. 1990; 62:35-42.

28. Krainer AR, Conway GC, Kozak D. Purification and characterization of pre-mRNA splicing factor SF2 from HeLa cells. Genes Dev. 1990; 4:1158-71.

29. Ji Q, Hao X, Zhang M, Tang W, Yang M, Li L, Xiang D, Desano JT, Bommer GT, Fan D, Fearon ER, Lawrence TS, Xu L. MicroRNA miR-34 inhibits human pancreatic cancer tumor-initiating cells. PLoS One. 2009; 4:e6816.

30. Liu C, Kelnar K, Liu B, Chen X, Calhoun-Davis T, Li H, Patrawala L, Yan H, Jeter C, Honorio S, Wiggins JF, Bader AG, Fagin R, Brown D, Tang DG. The microRNA miR-34a inhibits prostate cancer stem cells and metastasis by directly repressing CD44. Nat Med. 2011; 17:211-5.

31. Hermeking H. The miR-34 family in cancer and apoptosis. Cell Death Differ. 2010; 17:193-9.

32. Fujita K, Mondal AM, Horikawa I, Nguyen GH, Kumamoto K, Sohn JJ, Bowman ED, Mathe EA, Schetter AJ, Pine SR, Ji H, Vojtesek B, Bourdon JC, Lane DP, Harris CC. p53 isoforms Delta133p53 and p53beta are endogenous regulators of replicative cellular senescence. Nat Cell Biol. 2009; 11:1135-42.

33. Rizzo M, Mariani L, Pitto L, Rainaldi G, Simili M. miR-20a and miR-290, multi-faceted players with a role in tumourigenesis and senescence. J Cell Mol Med. 2010; 14:2633-40.

Review

Insights from model organisms on the functions of the tumor suppressor protein LKB1: Zebrafish chips in

Yme U. van der Velden and Anna-Pavlina G. Haramis

Department of Molecular Genetics, Netherlands Cancer Institute, Amsterdam, The Netherlands

Key words: LKB1, energy metabolism, cell polarity, animal models
Received: 4/12/11; Accepted: 4/25/11; Published: 4/26/11 **doi:** 10.18632/aging.100319
Corresponding author: Anna-Pavlina Haramis; **E-mail:** a.haramis@nki.nl

Abstract: The tumor suppressor LKB1 has emerged as a critical regulator of cell polarity and energy-metabolism. Studies in diverse model organisms continue to unravel the pathways downstream of LKB1; the emerging picture is that the outcomes of LKB1 signaling are mediated by a plethora of tissue-specific and context-dependent effectors.

INTRODUCTION

In 1998, the gene responsible for the rare dominantly inherited disorder Peutz-Jeghers syndrome[1], characterized by gastrointestinal hamartomatous polyposis and an increased predisposition to cancer [2], was identified as *LKB1*, which encodes a serine/threonine protein kinase. In addition to the familial syndrome, somatic mutations in *LKB1* were later found in over 30% of lung adenocarcinomas [3] and as the first identified recurrent mutation in endometrial cancer[4]. However clues as to its function were first discovered only in 2003, when it was identified as the long sought-after kinase that activates the alpha subunit of AMP-activated protein kinase (AMPK) [5],[6], linking LKB1 signaling to energy–metabolism control. Since then, LKB1 has been found to phosphorylate 12 other AMPK-related kinases including the microtubule-affinity-regulating kinase (MARK1-4), brain specific kinase (BRSK1-2), nuclear AMPK-related kinase (NUAK1-2), salt-inducible kinase (SIK1-3) and SNF-related kinase (SNRK) [7,8]. These results suggest that LKB1 is an upstream "master regulator" of energy homeostasis, cell polarity, DNA damage and cell cycle control [9].

Genetic analyses of LKB1 deficiency in higher eukaryotes have provided a framework to further dissect the functions of LKB1. However, the biology of LKB1 signaling appears to be highly complex, as loss of LKB1 function in invertebrates and vertebrates have generated divergent results in different tissues and contexts. In this research perspective, we review the current understanding of LKB1 function in cellular polarity and energy metabolism derived from loss-of-function studies performed in different model organisms. For a more comprehensive overview of LKB1, we refer the reader to these recent excellent reviews [10,11,12,13,14,15]. In the last section we will discuss how the recently generated Lkb1-deficient zebrafish can provide a new tool to gain important insight into the function of this tumor suppressor protein.

LKB1 function during early development: polarization of the oocyte

Ten years before the human *LKB1* gene was cloned, the *C. elegans* homolog, abnormal embryonic PARtitioning of cytoplasm family member 4 (par-4), was retrieved from a maternal-effect-lethal screen for genes required for proper segregation of cytoplasmic factors in the first cell cycles of embryogenesis [16]. *par-4* mutant embryos had defects in several aspects of cell polarity and asymmetric cell division, which resulted in the formation of an amorphous mass of cells without distinct morphogenesis [17].

This function for LKB1 in polarization during early embryogenesis was subsequently found to be

conserved, at least In *Drosophila melanogaster*. The *Drosophila* egg is a highly polarized structure well before fertilization and the origin of this polarization might even be traced back to the first cell division of the cytoblast in the fly ovary [18]. Differentiation of germline cells into oocytes coincides with asymmetric localization of proteins and mRNAs that set up the anterior-posterior (A-P) and dorsal-ventral (D-V) axes within the oocyte [18]. *lkb1* mutant germline clones showed disrupted localization of various mRNAs resulting in defective oocyte polarity [19]. LKB1-deficiency in follicle cells also led to polarization defects including disorganization of the epithelial monolayer [19]. These polarity defects were not fully penetrant and it was suggested that LKB1 is essential for the establishment of epithelial polarity in the follicle, but not for its maintenance [20]. However, under conditions of glucose starvation, polarity defects were observed in all examined follicle cells, indicating that LKB1 is critical also for the maintenance of epithelial polarity in follicle cells upon energetic stress. As LKB1 is known to regulate energy homeostasis, as outlined in more detail below, this suggests that diverse LKB1 functions are connected under certain physiological conditions. Similar results were obtained for *ampka* mutant follicle cells [20]. Indeed, many aspects of the polarity defects in LKB1-deficient follicle cells were rescued by introduction of a phosphomimetic *ampka* mutant demonstrating the involvement of the LKB1-AMPK axis in polarization during early development [21].

Together, this illustrates the high conservation of LKB1 function in the earliest polarization processes in both worms and flies. Although it remains to be determined whether this function is also conserved in vertebrates, interestingly LKB1 is asymmetrically localized to the animal pole in the mouse oocyte [22].

LKB1 and cell polarization in later stages of development

LKB1 also has a conserved role in polarization during later stages of development. For example, loss of LKB1 signaling leads to impaired neuronal polarity in both invertebrates and vertebrates. In *C. elegans*, temperature-sensitive *par-4* mutants showed neuronal polarity defects in ventral cord neurons. This function was thought to be regulated by PAR-4-dependent phosphorylation of PAR-1, which is the homolog of human MAP/microtubule affinity-regulating kinases, MARK [23]. In *Drosophila*, depletion of LKB1 in neuroblasts caused polyploidism in larval brains, but via a Par1-independent mechanism [24]. Instead, defects in mitotic spindle formation and mislocalization of the Baz/PAR-6/aPKC complex, a protein complex involved in cellular polarity, likely contributed to the reported phenotype [24]. In mice, conditional *lkb1* deletion in telencephalic progenitors led to impaired polarization of cortical neurons through impaired activation of the AMPK-related kinases SAD-A/B. Thus, LKB1 is required for polarization also in the vertebrate brain, although the molecular mechanisms involved are to a certain extent organism-specific [25].

In addition to neuronal polarization, LKB1 has been implicated in the polarization of epithelial structures, such as photoreceptors in the *Drosophila* eye. The *Drosophila* retina is derived from the eye imaginal disc, which is an epithelial structure. Eye-specific inactivation of LKB1 led to severe loss of polarity in photoreceptors at pupal stages [26]. Importantly, AMPK was not the primary LKB1 target in *Drosophila* eye development, but rather other AMPK-related kinases including SIK, NUAK and PAR-1 [26]. In vertebrates, activation of LKB1 induced complete polarization of single intestinal epithelial cells in culture [27]. Furthermore, AMPK activation is required for tight-junction formation and polarization in the Madin-Darby Canine Kidney (MDCK) epithelial *cell* line, although this may not be exclusively dependent on LKB1 [28], [29]. LKB1 null mice do not survive beyond E10.5 and show several defects including mesenchymal cell death as well as neural tube and vascular abnormalities associated with increased VEGF signaling [30]. Somewhat unexpectedly, inactivation of *Lkb1* in several mouse tissues did not lead to gross epithelial polarity defects, with the notable exception of the pancreas [31,32].

Thus, it appears that LKB1 regulates polarization during development throughout the animal kingdom in a tissue- and context-dependent manner, and via phosphorylation of distinct substrates.

LKB1: a master regulator of energy homeostasis

Probably the best-studied function of LKB1 to date, at least in vertebrates, is the regulation of energy homeostasis, particularly through AMPK activation and the target of rapamycin (TOR) pathway [33,34]. Upon energetic stress induced by a variety of stimuli such as food-deprivation, exercise, osmotic stress and hypoxia, AMPK is phosphorylated and activated by LKB1. AMPK then phosphorylates tuberous sclerosis complex 2 (TSC2), which leads to inhibition of TOR complex 1 (TORC1) activity [34]. TORC1 activity is associated with cell growth and viability since TORC1 stimulates anabolic processes such as protein synthesis while inhibiting catabolic processes like the degradation of

cellular components by autophagy [35]. Thus, upon LKB1-dependent activation of AMPK, TORC1 signaling is inhibited, which promotes energy conservation under conditions of energetic stress.

Given the embryonic lethal phenotype of the knockout mouse, the role of LKB1 in energy homeostasis at the whole organism level in animals has only been studied in *C. elegans* and, more recently, in *D. rerio*. These studies, which are described in detail below, have revealed a far more complex role for LKB1 in energy homeostasis beyond only the regulation of TOR signaling via AMPK. Indeed, in addition to TSC2, AMPK has a multitude of direct substrates, many of which are also involved in metabolism control [11,14]. In *C. elegans*, larvae developmentally arrest and enter the so-called "dauer" phase under unfavorable environmental conditions. Dauer larvae do not feed, become stress-resistant, are extremely long-lived and "non-aging" [36]. In order to ensure long-term survival, fat is stored in the hypodermis, which is an organ akin to the skin of higher organisms [37]. Dauer larvae with compromised LKB1/AMPK signaling rapidly depleted hypodermic fat storages and die prematurely due to vital organ failure [38]. This inappropriate fat depletion was found to be due to increased activity of adipose triglyceride lipase (ATGL-1), a direct target of AMPK. Similar to this result in *C. elegans*, we recently reported that *lkb1* mutant zebrafish are also unable to cope with energetic stress [39]. Although Lkb1 deficiency in *D. rerio* did not lead to overt developmental defects, *lkb1* mutants did fail to downregulate metabolism once the yolk, which provides energy in the first days of development, was consumed. These *lkb1* mutants exhibited hallmarks of a starvation response at the cellular and biochemical level, displayed profoundly decreased ATP levels and became energy-depleted much sooner that food-deprived wild type animals. Thus, in both worms and zebrafish, LKB1 is essential for control of whole-body energy homeostasis and adaptation of metabolism to changes in energy availability, which is essential for long-term viability of the organism.

Zebrafish *lkb1* mutants die two days after yolk absorption in stark contrast to wild-type larvae that can survive food deprivation for more than six days. Interestingly, two days of food deprivation did not lead to detectable AMPK phosphorylation in wild-type larvae, suggesting that deregulated AMPK signaling may not be the sole cause for impaired energy metabolism control in *lkb1* larvae. Furthermore, TOR signaling was not severely deregulated in *lkb1* mutants. Thus, we proposed that the AMPK-TORC1 axis might not be the critical or only effector of Lkb1-mediated maintenance of whole-organism energy homeostasis, at least in this setting. Interestingly, recent work on the effect of *Lkb1* inactivation in mouse hematopoietic stem cells showed that, while LKB1 was critically required to regulate energy metabolism and maintain cell survival, the effects were again largely independent of AMPK and TORC1 signaling [40,41,42]. Together, these findings illustrate that *in vivo* LKB1 controls metabolism though several pathways in addition to TORC1 signaling and showcase the complexity of LKB1 biology.

A zebrafish perspective on LKB1

As zebrafish *lkb1* mutants survive embryonic development, unlike mice, they provide the first embryonic viable vertebrate model of homozygous *lkb1* deletion. This, combined with the many advantages of using zebrafish as a model organism, some of which are described below, should rapidly advance our understanding of LKB1 function.

One of the advantages of zebrafish is that the oocyte is externally fertilized, allowing early developmental processes, from fertilization onwards, to be easily analyzed. In addition, germline replacement methods [43] mean that an animal lacking both maternal and zygotic LKB1 can be generated. Maternal-zygotic zebrafish *lkb1* mutants will provide a system to address whether and how Lkb1 functions in the first cleavage stages in vertebrates.

Another attractive feature of the zebrafish is their small size and transparency during development. In combination with the availability of numerous transgenic lines expressing tissue-specific fluorescently-labelled reporters, this allows real-time, *in vivo* visualization of various processes such as cell migration and organogenesis. Thus, questions pertaining to the biology of tissue physiology in a setting of Lkb1-deficiency can be addressed.

Although addressing whether neuronal polarity was impaired was beyond the scope of our previous study, it is still possible that Lkb1 is required for polarization or asymmetric cell division in neuronal tissues in zebrafish, given this function is conserved in *C. elegans* and *Drosophila*. Should that be the case, the ease of performing forward genetic screens in zebrafish could help to dissect the pathway of neuronal polarization in vertebrates by identification of new proteins involved in this process.

Interestingly, we did not observe polarity defects in either the gut or the eye of zebrafish *lkb1* mutants, in

contrast to studies in human cell lines and *Drosophila* respectively, again highlighting the cell-type specificity and context-dependency of LKB1 function.

Since Lkb1 deficiency leads to impaired metabolic control upon energetic stress, it will be interesting to determine whether *lkb1* mutants are hypersensitive to other types of stress, such as osmotic stress and DNA damage. Our preliminary results showed that *lkb1* mutants are hypersensitive to mechanical stress, but only when they are under energetic stress, again illustrating that the metabolic functions of Lkb1 are tightly linked with other Lkb1-dependent processes.

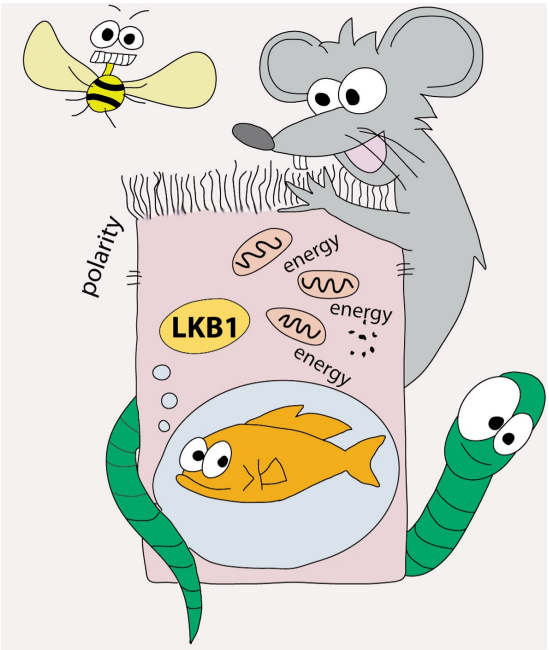

Figure 1. Studies of LKB1-deficiency in flies, worms, mice and zebrafish have revealed that the tumor suppressor LKB1 has conserved and divergent roles in the regulation of cell polarization and energy metabolism processes.

Finally, since zebrafish *lkb1* mutants are embryonic viable they provide an excellent platform to conduct chemical genetic screens to identify molecular pathways that are regulated and/or cooperate with Lkb1 and lead to deregulation of metabolism. These types of screens could also identify compounds that can modulate metabolism and may prove to be useful for inhibiting growth of LKB1-deficient tumors.

CONCLUSION

LKB1 is a tumor suppressor gene and is mutated in a wide variety of human cancers. Thus, deciphering its function could have direct clinical implications. Given the complexity of LKB1 function, which is illustrated by the diversity of its mutant phenotypes in a variety of model organisms and contexts, *lkb1* mutant zebrafish offer a powerful new tool for unraveling the numerous mechanisms and pathways regulated by LKB1. It also provides the unique opportunity to study LKB1 function at the whole organism level in vertebrates.

ACKNOWLEDGEMENTS

The work on LKB1 in the authors' laboratory was funded by a Netherlands Organization for Scientific Research Vidi Grant 91756322 to APGH.

CONFLICT OF INTERESTS STATEMENT

The authors of this manuscript have no conflict of interests to declare.

REFERENCES

1. Jeghers H, Mc KV, Katz KH. Generalized intestinal polyposis and melanin spots of the oral mucosa, lips and digits; a syndrome of diagnostic significance. N. Engl. J. Med. 1949; 241:993, illust; passim.

2. Hemminki A, Markie D, Tomlinson I, Avizienyte E, Roth S, Loukola A, Bignell G, Warren W, Aminoff M, Hoglund P, Jarvinen H, Kristo P, Pelin K, Ridanpaa M, Salovaara R, Toro T, Bodmer W, Olschwang S, Olsen AS, Stratton MR, de la Chapelle A, Aaltonen LA. A serine/threonine kinase gene defective in Peutz-Jeghers syndrome. Nature. 1998; 391:184-187.

3. Sanchez-Cespedes M, Parrella P, Esteller M, Nomoto S, Trink B, Engles JM, Westra WH, Herman JG, Sidransky D. Inactivation of LKB1/STK11 is a common event in adenocarcinomas of the lung. Cancer Res. 2002; 62:3659-3662.

4. Contreras CM, Gurumurthy S, Haynie JM, Shirley LJ, Akbay EA, Wingo SN, Schorge JO, Broaddus RR, Wong KK, Bardeesy N, Castrillon DH. Loss of Lkb1 provokes highly invasive endometrial adenocarcinomas. Cancer Res. 2008; 68:759-766.

5. Hawley SA, Boudeau J, Reid JL, Mustard KJ, Udd L, Makela TP, Alessi DR, Hardie DG. Complexes between the LKB1 tumor suppressor, STRAD alpha/beta and MO25 alpha/beta are upstream kinases in the AMP-activated protein kinase cascade. J. Biol. 2003; 2:28.1-28.16.

6. Woods A, Johnstone SR, Dickerson K, Leiper FC, Fryer LG, Neumann D, Schlattner U, Wallimann T, Carlson M, Carling D. LKB1 is the upstream kinase in the AMP-activated protein kinase cascade. Curr. Biol. 2003; 13:2004-2008.

7. Lizcano JM, Goransson O, Toth R, Deak M, Morrice NA, Boudeau J, Hawley SA, Udd L, Makela TP, Hardie DG, Alessi DR. LKB1 is a master kinase that activates 13 kinases of the AMPK subfamily, including MARK/PAR-1. Embo J. 2004; 23:833-843.

8. Jaleel M, McBride A, Lizcano JM, Deak M, Toth R, Morrice NA, Alessi DR. Identification of the sucrose non-fermenting related kinase SNRK, as a novel LKB1 substrate. FEBS Lett. 2005; 579:1417-1423.

9. Hezel AF, Bardeesy N. LKB1; linking cell structure and tumor suppression. Oncogene. 2008; 27:6908-6919.

10. Alessi DR, Sakamoto K, Bayascas JR. LKB1-dependent signaling pathways. Annu. Rev. Biochem. 2006; 75:137-163.

11. Shackelford DB, Shaw RJ. The LKB1-AMPK pathway: metabolism and growth control in tumour suppression. Nat. Rev. Cancer. 2009; 9:563-575.

12. Jansen M, Ten Klooster JP, Offerhaus GJ, Clevers H. LKB1 and AMPK family signaling: the intimate link between cell polarity and energy metabolism. Physiol. Rev. 2009; 89:777-798.

13. Shelly M, Poo MM. Role of LKB1 - SAD/MARK pathway in neuronal polarization. Dev. Neurobiol. 2011.

14. van Veelen W, Korsse SE, van de Laar L, Peppelenbosch MP. The long and winding road to rational treatment of cancer associated with LKB1/AMPK/TSC/mTORC1 signaling. Oncogene. 2011.

15. Mirouse V, Billaud M. The LKB1/AMPK polarity pathway. FEBS Lett. 2010.

16. Kemphues KJ, Priess JR, Morton DG, Cheng NS. Identification of genes required for cytoplasmic localization in early C. elegans embryos. Cell. 1988; 52:311-320.

17. Morton DG, Roos JM, Kemphues KJ. par-4, a gene required for cytoplasmic localization and determination of specific cell types in Caenorhabditis elegans embryogenesis. Genetics. 1992; 130:771-790.

18. Huynh JR, St Johnston D. The origin of asymmetry: early polarisation of the Drosophila germline cyst and oocyte. Curr. Biol. 2004; 14:R438-449.

19. Martin SG, St Johnston D. A role for Drosophila LKB1 in anterior-posterior axis formation and epithelial polarity. Nature. 2003; 421:379-384.

20. Mirouse V, Swick LL, Kazgan N, St Johnston D, Brenman JE. LKB1 and AMPK maintain epithelial cell polarity under energetic stress. J. Cell Biol. 2007; 177:387-392.

21. Lee JH, Koh H, Kim M, Kim Y, Lee SY, Karess RE, Lee SH, Shong M, Kim JM, Kim J, Chung J. Energy-dependent regulation of cell structure by AMP-activated protein kinase. Nature. 2007; 447:1017-1020.

22. Szczepanska K, Maleszewski M. LKB1/PAR4 protein is asymmetrically localized in mouse oocytes and associates with meiotic spindle. Gene Expr. Patterns. 2005; 6:86-93.

23. Kim JS, Hung W, Narbonne P, Roy R, Zhen M. C. elegans STRADalpha and SAD cooperatively regulate neuronal polarity and synaptic organization. Development. 2010; 137:93-102.

24. Bonaccorsi S, Mottier V, Giansanti MG, Bolkan BJ, Williams B, Goldberg ML, Gatti M. The Drosophila Lkb1 kinase is required for spindle formation and asymmetric neuroblast division. Development. 2007; 134:2183-2193.

25. Barnes AP, Lilley BN, Pan YA, Plummer LJ, Powell AW, Raines AN, Sanes JR, Polleux F. LKB1 and SAD kinases define a pathway required for the polarization of cortical neurons. Cell. 2007; 129:549-563.

26. Amin N, Khan A, St Johnston D, Tomlinson I, Martin S, Brenman J, McNeill H. LKB1 regulates polarity remodeling and adherens junction formation in the Drosophila eye. Proc. Natl. Acad. Sci U.S.A. 2009; 106:8941-8946.

27. Baas AF, Kuipers J, van der Wel NN, Batlle E, Koerten HK, Peters PJ, Clevers HC. Complete polarization of single intestinal epithelial cells upon activation of LKB1 by STRAD. Cell. 2004; 116:457-466.

28. Zhang L, Li J, Young LH, Caplan MJ. AMP-activated protein kinase regulates the assembly of epithelial tight junctions. Proc. Natl. Acad. Sci U.S.A. 2006; 103:17272-17277.

29. Zheng B, Cantley LC. Regulation of epithelial tight junction assembly and disassembly by AMP-activated protein kinase. Proc. Natl. Acad. Sci U.S.A. 2007; 104:819-822.

30. Ylikorkala A, Rossi DJ, Korsisaari N, Luukko K, Alitalo K, Henkemeyer M, Makela TP. Vascular abnormalities and deregulation of VEGF in Lkb1-deficient mice. Science. 2001; 293:1323-1326.

31. Hezel AF, Gurumurthy S, Granot Z, Swisa A, Chu GC, Bailey G, Dor Y, Bardeesy N, Depinho RA. Pancreatic LKB1 deletion leads to acinar polarity defects and cystic neoplasms. Mol. Cell. Biol. 2008; 28:2414-2425.

32. Granot Z, Swisa A, Magenheim J, Stolovich-Rain M, Fujimoto W, Manduchi E, Miki T, Lennerz JK, Stoeckert CJ, Jr., Meyuhas O, Seino S, Permutt MA, Piwnica-Worms H, Bardeesy N, Dor Y. LKB1 regulates pancreatic beta cell size, polarity, and function. Cell Metab. 2009; 10:296-308.

33. Shaw RJ. LKB1 and AMP-activated protein kinase control of mTOR signalling and growth. Acta Physiol. (Oxf). 2009; 196:65-80.

34. Shaw RJ, Bardeesy N, Manning BD, Lopez L, Kosmatka M, DePinho RA, Cantley LC. The LKB1 tumor suppressor negatively regulates mTOR signaling. Cancer Cell. 2004; 6:91-99.

35. Wullschleger S, Loewith R, Hall MN. TOR signaling in growth and metabolism. Cell. 2006; 124:471-484.

36. Klass M, Hirsh D. Non-ageing developmental variant of Caenorhabditis elegans. Nature. 1976; 260:523-525.

37. Burnell AM, Houthoofd K, O'Hanlon K, Vanfleteren JR. Alternate metabolism during the dauer stage of the nematode Caenorhabditis elegans. Exp. Gerontol. 2005; 40:850-856.

38. Narbonne P, Roy R. Caenorhabditis elegans dauers need LKB1/AMPK to ration lipid reserves and ensure long-term survival. Nature. 2009; 457:210-214.

39. van der Velden YU, Wang L, Zevenhoven J, van Rooijen E, van Lohuizen M, Giles RH, Clevers H, Haramis AP. The serine-threonine kinase LKB1 is essential for survival under energetic stress in zebrafish. Proc. Natl. Acad. Sci U.S.A. 2011; 108:4358-4363.

40. Gan B, Hu J, Jiang S, Liu Y, Sahin E, Zhuang L, Fletcher-Sananikone E, Colla S, Wang YA, Chin L, Depinho RA. Lkb1 regulates quiescence and metabolic homeostasis of haematopoietic stem cells. Nature. 468:701-704.

41. Gurumurthy S, Xie SZ, Alagesan B, Kim J, Yusuf RZ, Saez B, Tzatsos A, Ozsolak F, Milos P, Ferrari F, Park PJ, Shirihai OS, Scadden DT, Bardeesy N. The Lkb1 metabolic sensor maintains haematopoietic stem cell survival. Nature. 468:659-663.

42. Nakada D, Saunders TL, Morrison SJ. Lkb1 regulates cell cycle and energy metabolism in haematopoietic stem cells. Nature. 468:653-658.

43. Ciruna B, Weidinger G, Knaut H, Thisse B, Thisse C, Raz E, Schier AF. Production of maternal-zygotic mutant zebrafish by germ-line replacement. Proc. Natl. Acad. Sci U.S.A. 2002; 99:14919-14924.

Commentary

MKK4 as oncogene or tumor supressor: In cancer and senescence, the story's getting old

Steven C. Cunningham[1], Eike Gallmeier[2], and Scott E. Kern[3]

[1]Department of Surgery, St. Agnes Hospital, Baltimore, MD 21229, USA
[2]Medizinische Klinik II, Klinikum der Universität München, Campus Großhadern, München, Germany
[3]Department of Oncology, Johns Hopkins University, Baltimore, MD 21231, USA

E-mail: to Steven Cunningham at scunning@stagnes.org **doi:** 10.18632/aging.100233

The MKK4 gene is selected against by inactivating mutations in a large number of different tumor types, eg, tumors of the pancreas, bile ducts, breast, colon, lungs, testes [1-3] at a remarkably consistent rate of approximately 5-10% of tumors, identifying and defining it, therefore, as a tumor-suppressor (or genome-maintenance) gene [4].

Yet, experimental evidence exists that supports a pro-oncogenic role for MKK4 [5, 6]. Finegan and Tournier [6], for example, recently used an inducible murine model of MKK4 homozygous deletion to evaluate the role of MKK4 in skin tumorigenesis. They found that skin-specific MKK4-null mice were resistant to carcinogen-induced tumorigenesis. While the paper is well written and the model well designed, the fundamental premise may well be flawed, especially concerning MKK4's role in tumorigenesis, perhaps misleading the line of experimentation. There should be no question that MKK4 is tumor-suppressive, not oncogenic. MKK4 is widely selected against by tumors (its low rate of homozygous loss may be accounted for by a higher rate of heterozygous loss that could rationalize frequent 17p loss in diverse human cancers[7]) and unsurprisingly patients whose tumors have loss of MKK4 show statistically significant decrease in survival in the best controlled studies, using calibrated immunohistochemistry in large numbers of patients [8], consistent with a tumor-suppressive role.

Similarly consistent with a growth-suppressive role of MKK4 are observations made regarding the relationship between MKK4 and senescence. One of the ways MKK4 may suppress tumors is by inhibiting cell proliferation during replicative senescence, a widely recognized mechanism of tumor suppression. Marasa et al. [9] recently observed that MKK4 abundance increases in senescent fibroblasts. Overexpression of MKK4 decreased proliferation and promoted a senescent phenotype in young WI-38 human diploid fibroblasts and conversely, when MKK4 levels were lowered by several microRNAs targeting the MKK4 mRNA, the senescent phenotype was ameliorated and cells proliferated more rapidly [9]. In keeping with these observations, human tissue from older individuals was observed to express higher levels of MKK4 than corresponding tissue from young donors [9].

In the discussion of their inducible murine model of MKK4 homozygous deletion, Finegan and Tournier [6] rightly point out that there is conflicting literature regarding MKK4's role in tumorigenesis. The reason for the conflicting literature is largely because MKK4 is difficult to study experimentally. Their model would not be the first homozygous deletion model to model a population or a phenomenon that was not anticipated. For example, our own studies using homozygous MKK4-null cells engineered from the human pancreas cancer cell line PL-5 [10] showed that MKK4 deletion had a detrimental phenotype in a model of liver metastasis. Indeed experimental human data have shown that when tumors experiment with MKK4-null states, they are successful in developing a growth advantage allowing them to emerge through the clonal selection process in only 10% of cancers having 17p loss. We inferred from this observation that most tumor cells do not find the MKK4-null to be advantageous and that those PL-5 knock-out cells modeled this majority of cells. One may conclude from such a line of experimentation that the cell type-specific detrimental

phenotype that was modeled offered an important counterweight to the selective advantage achieved by cells experimenting with genetic null states during tumorigenesis, the resultant balance determining the low but remarkably consistent rate of observed biallelic MKK4 mutations [7, 10].

Because changes effected to this gene may have advantageous or deleterious effects on cells depending on the model, cancer investigators must rely on real tumors and not artificial models to guide experimental design and interpretation such that valuable research time, energy, and funding are not spent studying a phenomenon, viz, a "pro-oncogenic" function of MKK4, that common cancer sense should tell us does not likely exist. To put it colloquially, it does not matter how scientists vote regarding a pro-oncogenic or tumor-suppressive role of MKK4, because the tumors have already conducted that election in favor of the latter: MKK4 must be a tumor suppressor, as concluded from observations on wide varieties of examined tumors, which uniformly present evidence of having selected for its loss at a consistent rate. There is no convincing evidence from observations of tumor biology that MKK4 has any pro-oncogenic role. Scientists may argue for such a role, but the tumors have had their say, age-old dictators that they are.

REFERENCES

1. Teng DH, Perry WL, 3rd, Hogan JK, Baumgard M, Bell R, Berry S, Davis T, Frank D, Frye C, Hattier T, Hu R, Jammulapati S, Janecki T, Leavitt A, Mitchell JT, Pero R, Sexton D, Schroeder M, Su PH, Swedlund B, Kyriakis JM, Avruch J, Bartel P, Wong AK, and Tavtigian SV. Human mitogen-activated protein kinase kinase 4 as a candidate tumor suppressor. Cancer Res. 1997; 57: 4177-4182.

2. Su GH, Hilgers W, Shekher MC, Tang DJ, Yeo CJ, Hruban RH and Kern SE. Alterations in pancreatic, biliary, and breast carcinomas support MKK4 as a genetically targeted tumor suppressor gene. Cancer Res. 1998; 58: 2339-2342.

3. Parsons DW, Wang TL, Samuels Y, Bardelli A, Cummins JM, DeLong L, Silliman N, Ptak J, Szabo S, Willson JK, Markowitz S, Kinzler KW, Vogelstein B, Lengauer C, and Velculescu VE. Colorectal cancer: mutations in a signalling pathway. Nature. 2005; 436: 792.

4. Fearon ER Tumor-Suppressor Genes. In: B. Vogelstein and K. W. Kinzler (eds.), The Genetic Basis of Human Cancer, 2nd edition, pp. 197-206. New York: McGraw-Hill, 2002.

5. Wang L, Pan Y and Dai JL. Evidence of MKK4 pro-oncogenic activity in breast and pancreatic tumors. Oncogene. 2004; 23: 5978-5985.

6. Finegan KG and Tournier C. The mitogen-activated protein kinase kinase 4 has a pro-oncogenic role in skin cancer. Cancer Res. 70: 5797-5806.

7. Cunningham SC, Gallmeier E, Hucl T, Dezentje DA, Abdelmohsen K, Gorospe M and Kern SE. Theoretical proposal: allele dosage of MAP2K4/MKK4 could rationalize frequent 17p loss in diverse human cancers. Cell Cycle. 2006; 5: 1090-1093.

8. Cunningham SC, Kamangar F, Kim MP, Hammoud S, Haque R, Iacobuzio-Donahue C, Ashfaq R, Kern SE, Maitra A, Heitmiller RE, Choti MA, Lillemoe KD, Cameron JL, Yeo CJ, Montgomery E, and Schulick RD. Mkk4 Status Predicts Survival after Resection of Gastric Adenocarcinoma. Arch Surg. 2006; 141: 1095-1099.

9. Marasa BS, Srikantan S, Masuda K, Abdelmohsen K, Kuwano Y, Yang X, Martindale JL, Rinker-Schaeffer CW and Gorospe M. Increased MKK4 abundance with replicative senescence is linked to the joint reduction of multiple microRNAs. Sci Signal. 2009; 2: ra69.

10. Cunningham SC, Gallmeier E, Hucl T, Dezentje DA, Calhoun ES, Falco G, Abdelmohsen K, Gorospe M and Kern SE. Targeted deletion of MKK4 in cancer cells: a detrimental phenotype manifests as decreased experimental metastasis and suggests a counterweight to the evolution of tumor-suppressor loss. Cancer Res. 2006; 66: 5560-5564.

Editorial

Tumor suppressors revival in CLL

Giovanna Carrà, Riccardo Taulli, Alessandro Morotti

Since the 2001 FDA approval of the BCR-ABL tyrosine kinase inhibitor, Imatinib, as the standard of treatment for Chronic Myeloid Leukemia (CML), these last 16 years have clearly showed the raise and the fall of strategies to target oncogenes in cancer. Beside the successful story of Imatinib in CML, no other drugs able to target oncogenes at the bench have shown such impressive results at the bedside. While various compounds have indeed clearly prompted themselves as effective drugs with promising clinical results, still the cure for cancer, meaning complete eradication, remains a mirage with these inhibitors.

Conversely, murine models have proven that the re-establishment of tumor suppressors in cancer remains the unique strong strategy to obtain cancer eradication: in a very simple, yet dramatically effective manner, the re-expression of p53 in various cancer models have indeed been associated with cancer exhaustion [1].

For many years, the strategies to target tumor suppressors have been neglected from drugs cocktails. The idea that tumor suppressors are involved in tumorigenesis through genetic impairments of both alleles and the lack of strategies to restore these genes in cancer cells have wiped out all the promises in targeting these genes. Yet, the mechanisms of tumor suppressors impairment in cancer have changed: it is now clear that even wild-type tumor suppressors can play an essential role in tumorigenesis, when functionally inhibited [2]. Mechanisms that promote tumor suppressors de-localization, degradation and/or inactivation inevitably result in tumor suppressors inhibition. The identification of tumors that depend on functionally inactive tumor suppressors is of extraordinary importance because these tumors can potentially benefit from therapies designed to restore the function of the inactive tumor suppressors.

Very recently, we have demonstrated that the de-ubiquitinase USP7, also known as HAUSP, is aberrantly expressed and active in Chronic Lymphocytic Leukemia (CLL) [3]. Besides being one of the hundreds of differentially expressed genes in a cancer, USP7 has the privilege of controlling the expression, localization and function of three major tumor suppressors: PTEN [4-5], p53 [6] and FOXO [7].

In this work, we demonstrated that CLL is characterized by an increased USP7 expression, through miRNA de-regulation, and by aberrant USP7 regulation through Casein Kinase II. Consequently, USP7 was shown to promote PTEN delocalization from the nucleus with consequence loss of part of its tumor suppressive functions. Conversely, USP7 inhibitor restores PTEN nuclear pool with re-establishment of its tumor suppressive functions. In this work, we focused on the ability of USP7 to modulate PTEN in a p53 null scenario, which remains the most challenging battlefield for CLL therapy. However, it should be noted that USP7 is also well known to module p53 protein levels, as well [6]. USP7 promotes mdm2 de-ubiquitination, which in turn modulates p53 protein degradation. High levels of USP7 activation can indeed affect the mdm2/p53 network with potentially intriguing consequences on p53 protein levels and functional regulation. Similarly, USP7 was shown to module the mono-ubiquitination of FOXOs, very known tumor suppressors able to control cellular proliferation [7]. USP7 favors FOXOs nuclear exclusion and inactivation. While we did not investigate FOXO cellular compartmentalization and p53 protein levels in CLL, it could be speculated that high levels of USP7 may also affects FOXO localization and p53 protein levels in CLL.

Our published observation that USP7-PTEN is a targetable network in CLL [3], and the above speculations that USP7 may also affect p53 and FOXOs in the CLL context, attribute to USP7 a potential pivotal role in the functional regulation of three major tumor suppressors in CLL. Therefore, USP7 inhibitors may represent strong apoptotic inducers in CLL through: *i*) the reactivation of wild-type PTEN and, potentially, p53 and FOXO; *ii*) by-passing the resistance mediated by mutations/deletions of one of these tumor suppressors through the reactivation of the others, as we observed in the presence of p53 mutations [3].

In summary, our data clearly indicate that the characterization of molecular circuits involved in the control of oncosuppressor stability, localization and activity is critical to develop novel therapeutic strategies aimed at re-activating oncosuppressor functions. Thus, it is now advisable that USP7 inhibitors will be included among the drugs to be further investigated for their ability to positively modulate oncosuppressor regulatory networks in cancer.

REFERENCES

1. Ventura A, et al. Nature. 2007; 445:661–65. doi:10.1038/nature05541
2. Berger AH, et al. Nature. 2011; 476:163-69. doi:10.1038/nature10275
3. Carrà G, et al. Oncotarget. 2017; 8:35508-22. doi:10.18632/oncotarget.16348
4. Song MS, et al. Nature. 2008; 455:813-17. doi:10.1038/nature07290
5. Morotti A, et al. Leukemia. 2014; 28:1326-33. doi:10.1038/leu.2013.370
6. Cummins JM, et al. Nature. 2004; 428:1-486. doi:10.1038/nature02501
7. Van der Horst A, et al. Nature Cell Biol. 2006; 8:1064-73. doi 10.1038/ncb1469.

Alessandro Morotti: Department of Clinical and Biological Sciences, University of Turin, 10043 Turin, Italy

Correspondence: *Alessandro Morotti*
Email: *alessandro.morotti@unito.it*

Keywords: *Chronic Lymphocytic Leukemia, tumor suppressors, USP7, PTEN, p53, FOXO*

Received: June 14, 2017
Published: June 26, 2017

Research Paper

SOCS1 regulates senescence and ferroptosis by modulating the expression of p53 target genes

Emmanuelle Saint-Germain[1], Lian Mignacca[1], Mathieu Vernier[2], Diwakar Bobbala[3], Subburaj Ilangumaran[3] and Gerardo Ferbeyre[1]

[1]Département de Biochimie et Médecine Moléculaire; Université de Montréal, Montréal, Québec, H3C 3J7; Canada.
[2]Department of Biochemistry, Medicine & Oncology, Faculty of Medicine, McGill University, Goodman Cancer Research Centre, Montreal, Quebec, H3A 1A3, Canada
[3]Immunology Division, Department of Pediatrics, Faculty of Medicine, University of Sherbrooke, Sherbrooke, Quebec, J1K 2R1, Canada

Correspondence to: Gerardo Ferbeyre; **email:** g.ferbeyre@UMontreal.CA
Keywords: suppressor of cytokine signaling, tumor suppressor, ferroptosis, senescence, KAP1
Received: June 30, 2017 **Accepted:** October 15, 2017 **Published:** October 28, 2017

ABSTRACT

The mechanism by which p53 suppresses tumorigenesis remains poorly understood. In the context of aberrant activation of the JAK/STAT5 pathway, SOCS1 is required for p53 activation and the regulation of cellular senescence. In order to identify p53 target genes acting during the senescence response to oncogenic STAT5A, we characterized the transcriptome of STAT5A-expressing cells after SOCS1 inhibition. We identified a set of SOCS1-dependent p53 target genes that include several secreted proteins and genes regulating oxidative metabolism and ferroptosis. Exogenous SOCS1 was sufficient to regulate the expression of p53 target genes and sensitized cells to ferroptosis. This effect correlated with the ability of SOCS1 to reduce the expression of the cystine transporter SLC7A11 and the levels of glutathione. SOCS1 and SOCS1-dependent p53 target genes were induced during the senescence response to oncogenic STAT5A, RasV12 or the tumor suppressor PML. However, while SOCS1 sensitized cells to ferroptosis neither RasV12 nor STAT5A mimicked the effect. Intriguingly, PML turned cells highly resistant to ferroptosis. The results indicate different susceptibilities to ferroptosis in senescent cells depending on the trigger and suggest the possibility of killing senescent cells by inhibiting pathways that mediate ferroptosis resistance.

INTRODUCTION

p53 is by far the most commonly mutated gene in human cancers with mutations present in 36% of all patients [1]. p53 acts mainly as a transcription factor suggesting that p53-target genes should have important functions in cancer biology. Combining chromatin immunoprecipitation and gene expression data of different cellular models revealed a number of p53 target genes that range between 122 to 3697 genes with little overlap between studies but including both genes that are activated or repressed by p53 [2,3,4,5]. A meta-analysis of different p53 and cell cycle regulatory networks revealed that p53 acts mainly as an activator through proximal promoter binding while gene repression is mostly indirect and dependent on the DREAM or RB/E2F complexes [5]. Identifying the key p53 targets that mediate tumor suppression and the cellular processes they regulate is a pressing goal for cancer research.

The tumor suppressor activity of p53 in mice does not correlate with the expression of p53 targets controlled by an acute DNA damage response [6]. For example, mice deficient for p21, Puma and Noxa, which are p53 target genes mediating cell cycle arrest and apoptosis, do not display the tumor prone phenotype typical of p53 null mice [7]. Genes controlling cell signalling, the cytoskeleton, DNA repair and ferroptosis were then identified as new candidates to mediate the tumor suppressor functions of p53 [4,6]. Genome wide analysis of p53 binding under conditions of acute or chronic stimulation revealed distinct p53 binding sites and regulated genes suggesting that upon chronic stimulation p53 DNA binding properties are regulated differently than in acute conditions [8]. The present state of knowledge indicates that context largely determines the transcriptional response to p53 activation. Hence, the identification of p53 targets in conditions where p53 regulates tumor suppression will help to identify important pathways and mechanisms to halt tumorigenesis.

Activation of p53 is often mediated by the DNA damage response that triggers a series of post-translational modifications on p53 preventing its degradation by E3 ubiquitin ligases such as MDM2 [9,10]. A similar mechanism is activated by the nucleolar protein p19ARF [11], the tumor suppressor PML [12] and several ribosomal proteins linking p53 activation to nucleolar stresses [13]. During cellular senescence induced by aberrant STAT5A stimulation both DNA damage and SOCS1 expression are required for p53 activation [14,15]. The specific role of SOCS1 in the senescence response to activated STAT5A and the p53 target genes modulated in this context remain for the most part unknown.

In order to identify and characterize p53 target genes whose regulation depends on SOCS1 we compared the transcriptome of cells that enter senescence in response to constitutive STAT5A-signaling with the transcriptome of cells that failed to do so due to inactivation of SOCS1. We define a set of SOCS1-dependent p53 target genes, some of which are downregulated in many human cancers. Interestingly, this set of genes included the ferroptosis regulators SLC7A11 and SAT1 as well as p53 target genes previously linked to the cellular response to oxidized phospholipids. Consistent with the gene expression analysis, overexpression of SOCS1 sensitized cells to ferroptosis. In contrast, induction of senescence by RasV12, STAT5A or PML did not sensitize cells to ferroptosis indicating different susceptibilities to ferroptosis depending on the senescence trigger. We also provide new insights into the mechanism of modulation of p53 by SOCS1 by showing that SOCS1 can stabilize p53 independently of its effects on serine 15-phosphorylation and that SOCS1 can form a complex with the p53 repressor KAP1.

RESULTS

SOCS1 inhibition affects a selective group of p53 target genes

To investigate how SOCS1 modulates the p53 pathway we used a model of oncogene-induced senescence where p53 activation is dependent on SOCS1 [14,15]. In this model, a constitutively active allele of STAT5A (cS5A) is introduced into human fibroblasts IMR90-E7. These cells express the papillomavirus protein E7 to inactivate the retinoblastoma tumor suppressor, allowing us to focus on the p53 pathway contribution to cellular senescence. Expression of cS5A in these cells induced a cell cycle arrest and reduced the expression of proliferation markers (MCM6 and phospho-histone H3) that was rescued by expression of a small hairpin RNA against SOCS1 (Figure 1A-C). Consistent with the reported role of SOCS1 in p53 phosphorylation at serine 15, cS5A failed to induce this modification in cells expressing the shRNA against SOCS1 (Figure 1D). We then compared the transcriptome of IMR90-E7 cells expressing cS5A and co-expressing an shRNA against SOCS1 or a non-targeted shRNA using RNA purified from cells 7 days after introduction of cS5A. The microarray data was deposited in NCBI's Gene Expression Omnibus (GEO) GSE98216. Genes whose expression changed +/- 1.5 fold were used for pathway analysis with the online bioinformatics platform DAVID. The most significant pathways regulated by SOCS1 in cells expressing cS5A are indicated in Figure 1E and S1. They include genes coding for secreted proteins (Figure S1A-C) and a few genes in the p53-signaling pathway (Figure 1E and Table 1). The bypass of senescence induced by cS5A and the inhibition of p53 activity was also confirmed by a second shRNA against SOCS1 (shS1b), (Figure S2). Therefore, although these results confirm the requirement for SOCS1 in p53 phosphorylation and the senescence response to aberrant STAT5A activation, the pattern of p53 target genes identified does not include the classic p53 target genes associated to the DNA damage response.

To further investigate whether SOCS1 modulates the p53 pathway, we performed Gene set enrichment analysis (GSEA) of the microarray data. We found that SOCS1-disabled cells have high levels of genes in the set TANG_SENESCENCE_TP53_TARGETS_DN that contain, genes upregulated by a dominant negative p53 in normal human fibroblasts (Figure 1F). This gene set mostly includes cell cycle regulated genes, which are

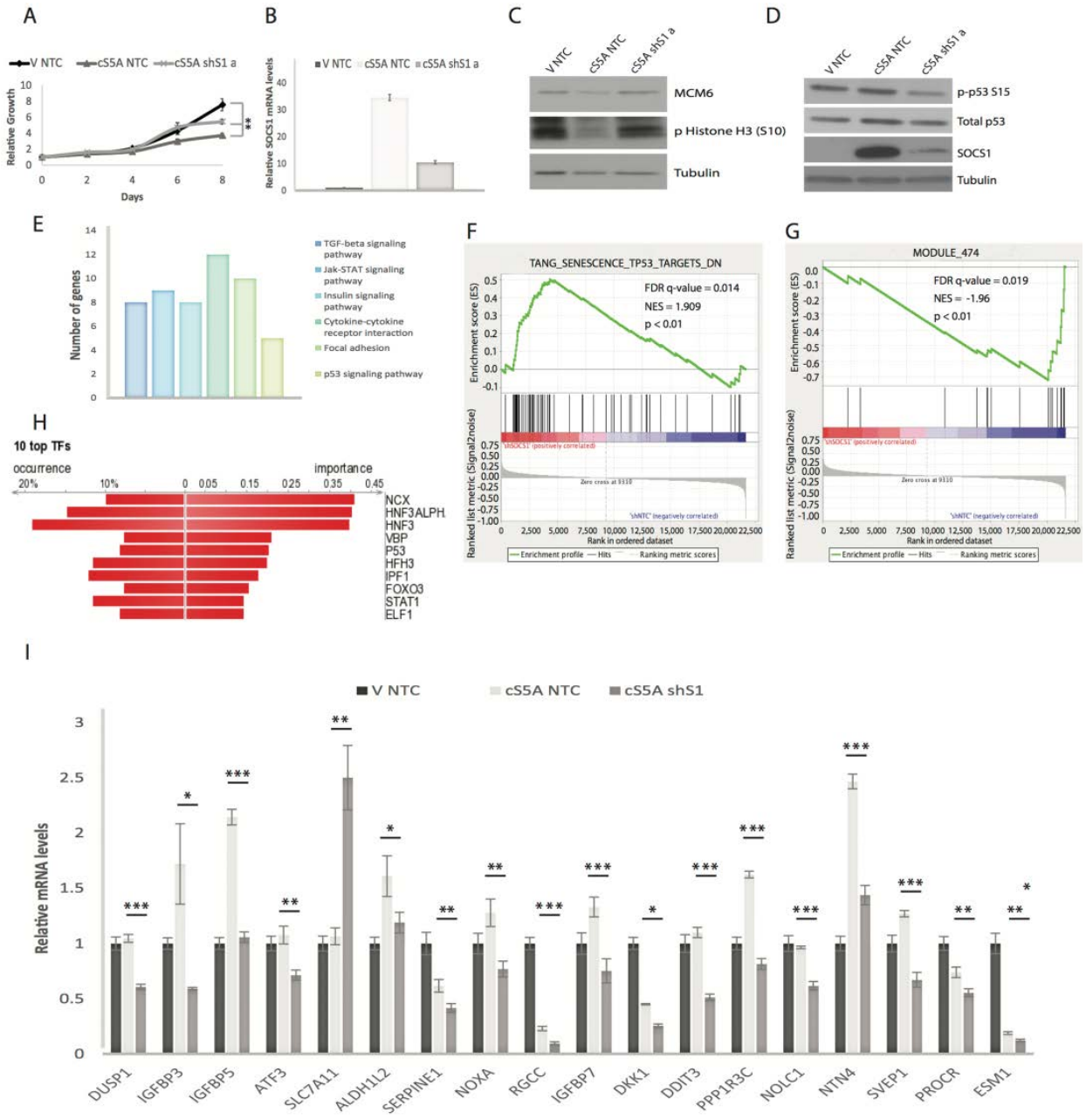

Figure 1. Microarray analysis identifies SOCS1-dependent p53 target genes. (**A**) Growth curves. Normal human fibroblasts (IMR90) expressing viral oncoprotein E7 were retrovirally infected with either an empty vector (V) or with constitutively activated STAT5A (cS5A) and with either a control shRNA (shNTC) or a shRNA against SOCS1 (shS1 a). Cells were counted and plated for the growth assay. (**B**) SOCS1 mRNA levels were measured by qPCR using cells collected 7 days post infection, as in (A). (**C**) Western blots of IMR90 cells at day 7 post infection, as described in (A) for MCM6, phosphorylated Histone H3 (S10) and Tubulin. (**D**) Western blots of IMR90 cells described in (A) for p53, phosphorylated p53 at serine 15 (p-p53 S15) and SOCS1 levels. (**E**) DAVID analysis (Kegg pathway) of Affymetrix microarray experiment performed on triplicates of IMR90 cells expressing E7 and either constitutively active STAT5A (cS5A) combined with a control shRNA (NTC) versus cells expressing cS5A combined with an shRNA against SCOS1 (shS1), collected 7 days after infection. (**F**) Gene Set Enrichment Analysis (GSEA) of differentially regulated genes between the conditions in (D). (**G**) GSEA of differentially regulated genes. (**H**) DiRE analysis of genes differentially regulated between cS5A NTC and cS5A shS1 conditions of the Affymetrix microarray analysis. (**I**) QPCR validation in IMR90 cells expressing the same constructs as mentioned in (A), for the p53 target genes identified by the microarray analysis. All experiments were performed three times, error bars indicate SD of triplicates (growth curves) or standard errors of triplicates (QPCR), *= p<0.05, using the Student's t test. **=p<0.01, ***=p<0.005.

Table 1. List of SOCS1-dependent p53 target genes identified by microarray analysis.

Reported p53 target genes	Fold Change	PMID
DDIT3	-1.79	16917513
GADD45B	-1.74	23948959
IGFBP3	-1.85	20182617
PMAIP1	-1.65	19641509
SERPINE1	-1.52	17882266
LOXL1	-1.81	16888633
DKK1	-2.37	16888633
GDF15	-1.65	16888633
DDB2	-1.47	16888633
SLC7A11	1.58	25799988
ALDH1L2	-1.42	25799988
ABHD4	-1.43	25799988
BCAT1	-1.44	25799988
LRP1	-1.53	25799988
DUSP1	-1.52	25799988
PROCR	-1.52	25799988
RGCC	-2.49	17146433
IGFBP7	-1.72	21095038
SAT1	-1.56	27698118

Of note, the microarray data indicates many more known p53 target genes regulated by SOCS1 than found by DAVID. Relevant references for those genes are indicated by their PMID.

known to be regulated by RB. However, the RB pathway was disabled in the IMR90-E7 cell line used in our experiments. These results thus imply a SOCS1-p53-dependent pathway that regulates cell cycle genes independently of the RB tumor suppressor. SOCS1-disabled cells also have a downregulation of the gene set MODULE_474 (http://robotics.stanford.edu/~erans/cancer/) containing several genes upregulated in senescent cells such as IGFBP2, 3, 5, 6 and 7, NOV and SOCS3 (Figure 1G). Further proof that SOCS1 controls the expression of p53 target genes was obtained using the platform DiRE that analyses the promoters of gene sets for signatures of transcription factors. P53 was one of the top transcription factors associated to transcriptome changes induced by an shRNA against SOCS1 (Figure 1H). In addition, this algorithm identified 12 new candidates for p53-target genes (Table 2). Many of these genes are poorly expressed in human cancers suggesting that they could be novel tumor suppressors (Table 3). The microarray data was validated using qPCR for either known p53-target genes or the new candidates suggested by the DiRE platform (Figure 1I). We also used data in TCGA from hepatocellular carcinoma, a tumor type where promoter DNA methylation often silences SOCS1 expression [16]. We found a significant correlation between the expression of SOCS1 and the SOCS1-dependent p53 target genes defined in human fibroblasts (Figure 2). For several genes (SLC7A11, SAT1, SERPINE1, IGFBP7, GADD45 and ATF3) these correlations decreased in samples from p53 mutant tumors (Figure S3). Taken together, our results show that SOCS1 controls a unique set of p53 target genes.

To investigate the biological importance of SOCS1-dependent p53 target genes we analysed their overlap with gene sets mediating specific p53-dependent responses. First, genes regulated by SOCS1 matched gene sets that regulate the response to chemotherapy (Figure S4A), which is largely influenced by the p53 pathway [17]. Second, SOCS1-disabled cells expressed high levels of genes upregulated by a dominant negative BRCA1 allele (Figure S4B), which also disrupts the p53 pathway [18]. Third, SOCS1-disabled cells have a decrease in the expression of genes that blocked angiogenesis in endothelial cells (Figure S4C). These genes include IGFBP3 [19] and COL4A2 which encodes the potent antiangiogenic factor canstatin [20]. It is well known that p53 inhibits angiogenesis [21,22], and our gene expression data suggest that SOCS1 modulates this p53 function as well. Finally, SOCS1-regulated genes also overlapped with a set of genes induced by oxidized phospholipids (Figure S4D), which has been recently linked to iron-dependent cell death or ferroptosis [23]. P53 sensitizes cells to ferroptosis by repressing the cystine transporter SLC7A11 [4] and inducing the polyamine metabolic enzyme SAT1 [24]. The regulation of those two genes in cS5A expressing cells was SOCS1-dependent (Table 1) suggesting a role for SOCS1 in ferroptosis.

The inhibition of SOCS1 expression in IMR90-E7 bypasses cS5A-induced senescence, raising the possibility that the defects in p53 target gene expression we described above are the consequence of senescence inhibition and are not directly linked to SOCS1. In IMR90 cells, where the retinoblastoma pathway remains intact, inactivation of SOCS1 does not bypass cS5A-induced senescence [14]. This is due to the known fact that the RB pathway is sufficient to regulate senescence in the absence of p53 [25,26]. We thus took advantage of this fact to investigate whether expression of p53 target genes still required SOCS1 in these cells.

Table 2. List of potential SOCS1 dependent p53 target genes identified by DiRE analysis.

DiRE Analysis	Fold change	Function
ABCA8	-1.56	Transmembrane lipid transporter
ATF3	-1.69	Transcription factor, response to stress (16888633)
CITED4	-1.63	Transcriptional co-activator
CYGB	-1.51	Regulation of oxidative stress
DEPDC1B	1.62	Cell adhesion, mitosis regulation
ESM1	-1.53	Secreted factor, role in inflammation and cancer
KIAA1467	1.56	Uncharacterized protein
NOLC1	-1.87	Ribosome biosynthesis (21642980)
NTN4	-1.61	Role in metastasis (25590240)
PCDH10	-1.57	Cell adhesion and motility
PPP1R3C	-1.83	Regulation of glycogen metabolism
SRPX2	-1.83	Role in angiogenesis and migration
SVEP1	-1.67	Cell attachment
TMEM159	-1.73	Uncharacterized protein
ZNF2	-1.53	May be involved in transcriptional regulation

For previously linked p53 target genes, PMID is indicated in parenthesis as reference.

Table 3. Cancer vs. Normal expression of SOCS1-dependent p53 target genes identified by DiRE.

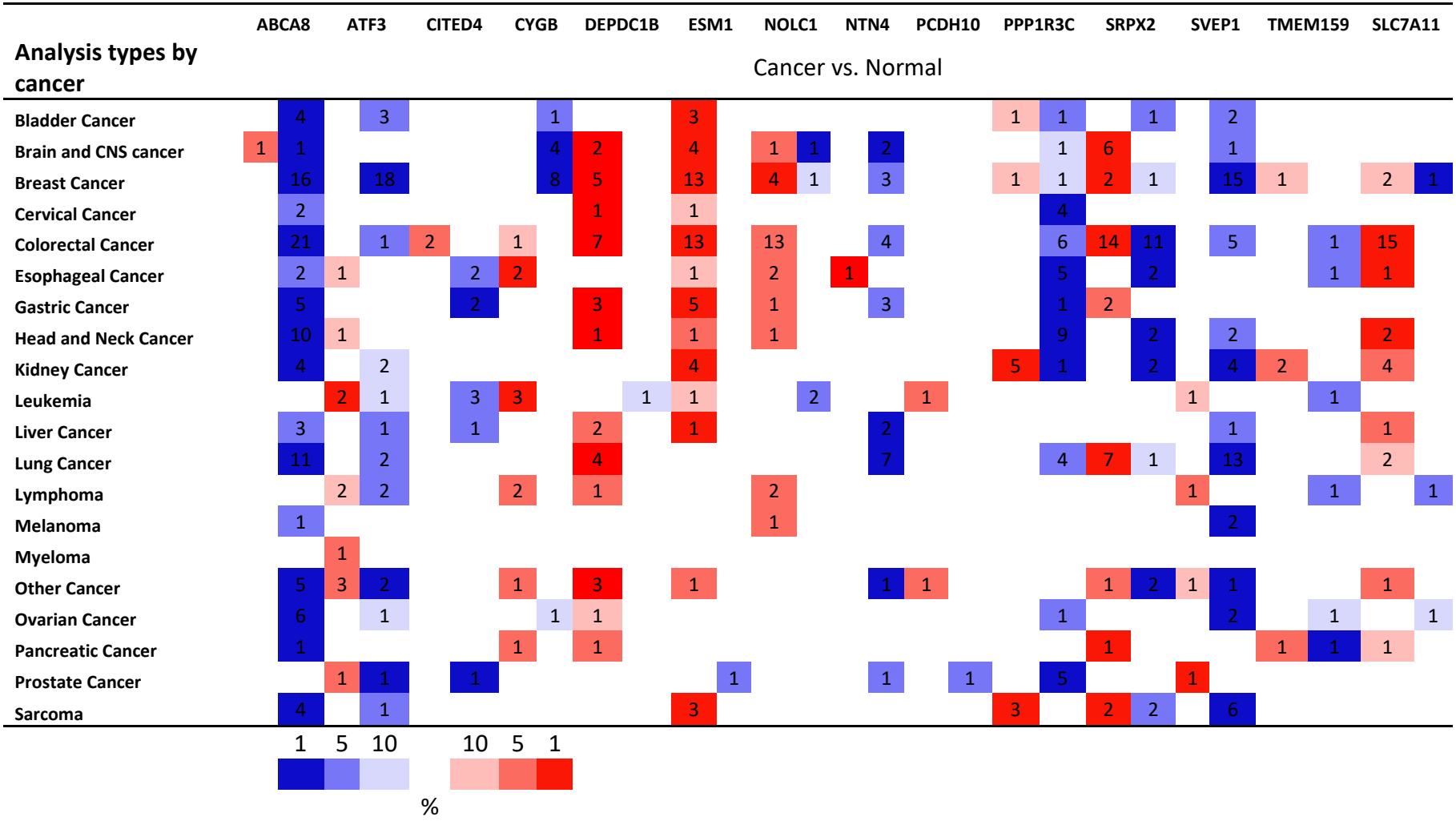

Red squares signal the number of studies showing upregulation and blue squares the number of studies showing downregulation. Cell color is determined by the best gene rank percentile for the analyses within the cell.

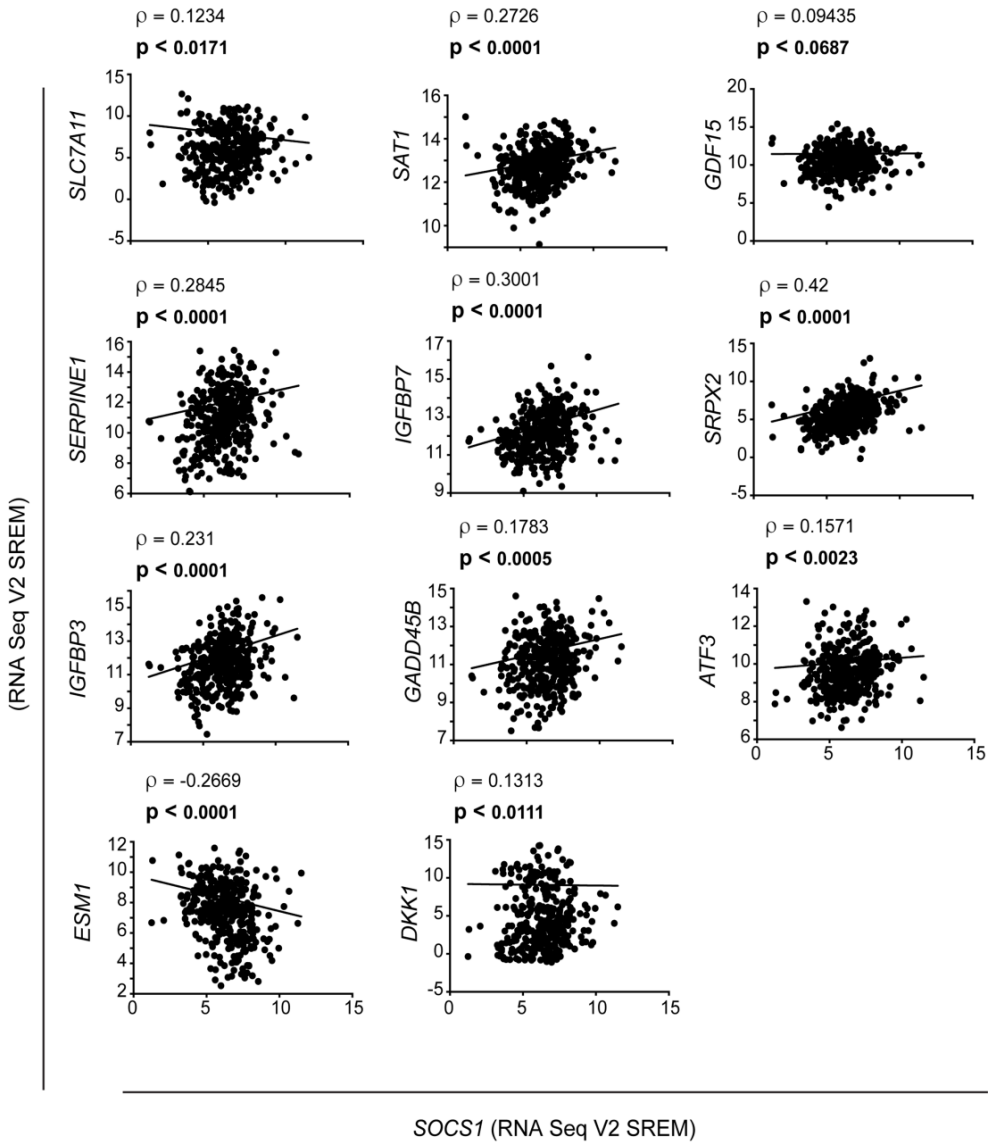

Figure 2. Correlation between SOCS1 and p53-target gene expression in hepatocellular carcinoma samples. The TCGA dataset human HCC specimens was analysed to determine the correlation between the expression of *SOCS1* (*x*-axis) and the indicated p53 target genes (*y*-axis), as indicated by the slope. The Spearman correlation (ρ) and the *p* values are given at the top of each plot.

For most of the genes measured, disabling SOCS1 also inhibited the expression of p53 targets as well (Figure 3A-B) although cells remained senescent (Figure 3C-E). We conclude that the defects in p53 target gene expression we have seen after disabling SOCS1 are not the result of cell cycle re-entry after bypass of senescence and suggest a direct effect of SOCS1 on p53.

SOCS1 is sufficient to activate p53 and regulate the expression of its target genes

Previous research established a function for SOCS1 as an adaptor protein facilitating the phosphorylation of p53 at serine 15 by the DNA damage response activated kinases ATM and ATR [14]. In culture, cells are exposed to high concentrations of oxygen and growth factors, increasing the probability of DNA damage by either replication stress or reactive oxygen species. We reasoned that enforcing SOCS1 expression might cooperate with these factors and engage the p53 pathway. Indeed, expressing SOCS1, in U2OS cells (Figure 4A-B) or IMR90 cells (Figure 4C-E) increased the expression of most of the genes that were positively regulated by p53 in cS5A-induced senescence and decreased the expression of SLC7A11, a gene that is repressed by p53. As reported before, SOCS1 was sufficient to trigger senescence in close to 50% of the

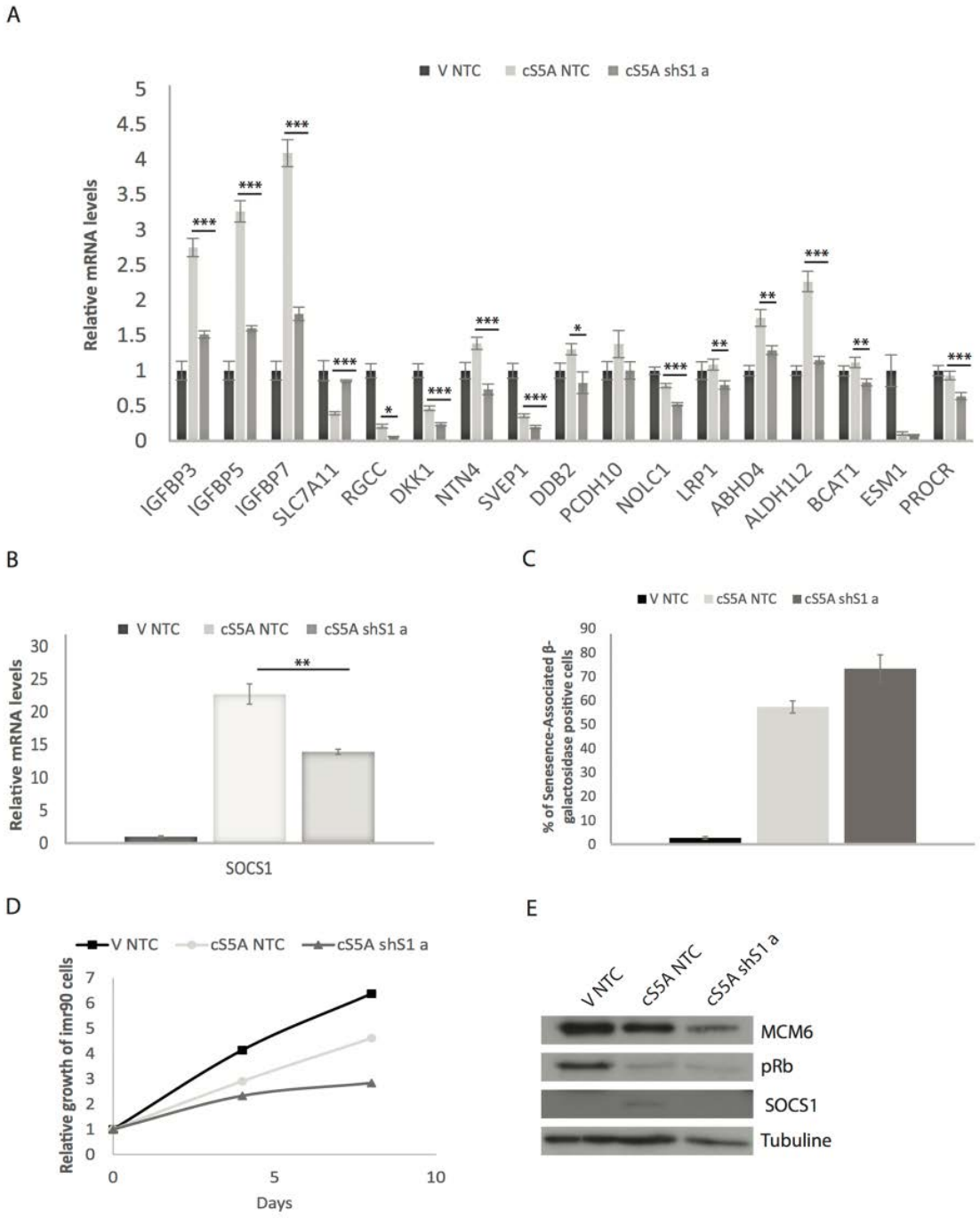

Figure 3. The regulation of p53 target genes by SOCS1 is not dependent on a disabled RB pathway. (**A**) QPCR validation of the p53 target genes identified by microarray analysis but in normal IMR90 fibroblasts expressing either an empty vector (V) or a constitutively activated STAT5A (cS5A) and with either a control shRNA (shNTC) or an shRNA against SOCS1 (shS1). Cells were collected 7 days after infection. (**B**) SOCS1 knockdown efficiency measured by qPCR in the conditions described in (A). (**C**) Status of the cells was assessed at the day of RNA collection (day 7 post infection) with a Senescence-Associated β-Galactosidase staining. Positively stained and unstained cells were counted under a light microscope in order to obtain the percentage of senescent cells. (**D**) Growth curves. Normal human fibroblasts (IMR90) were retrovirally infected with either an empty vector (V) or with constitutively activated STAT5A (cS5A) and with either a control shRNA (shNTC) or a shRNA against SOCS1 (shS1 a). Cells were counted and plated for the growth assay. (**E**) Western blots of senescence markers (MCM6, pRb and SOCS1) of cells as in (A). Tubulin was used as a loading control. All experiments were performed three times, error bars indicate the standard errors of triplicates, * = p<0.05, using the Student's t test, **=p<0.01, ***=p<0.005

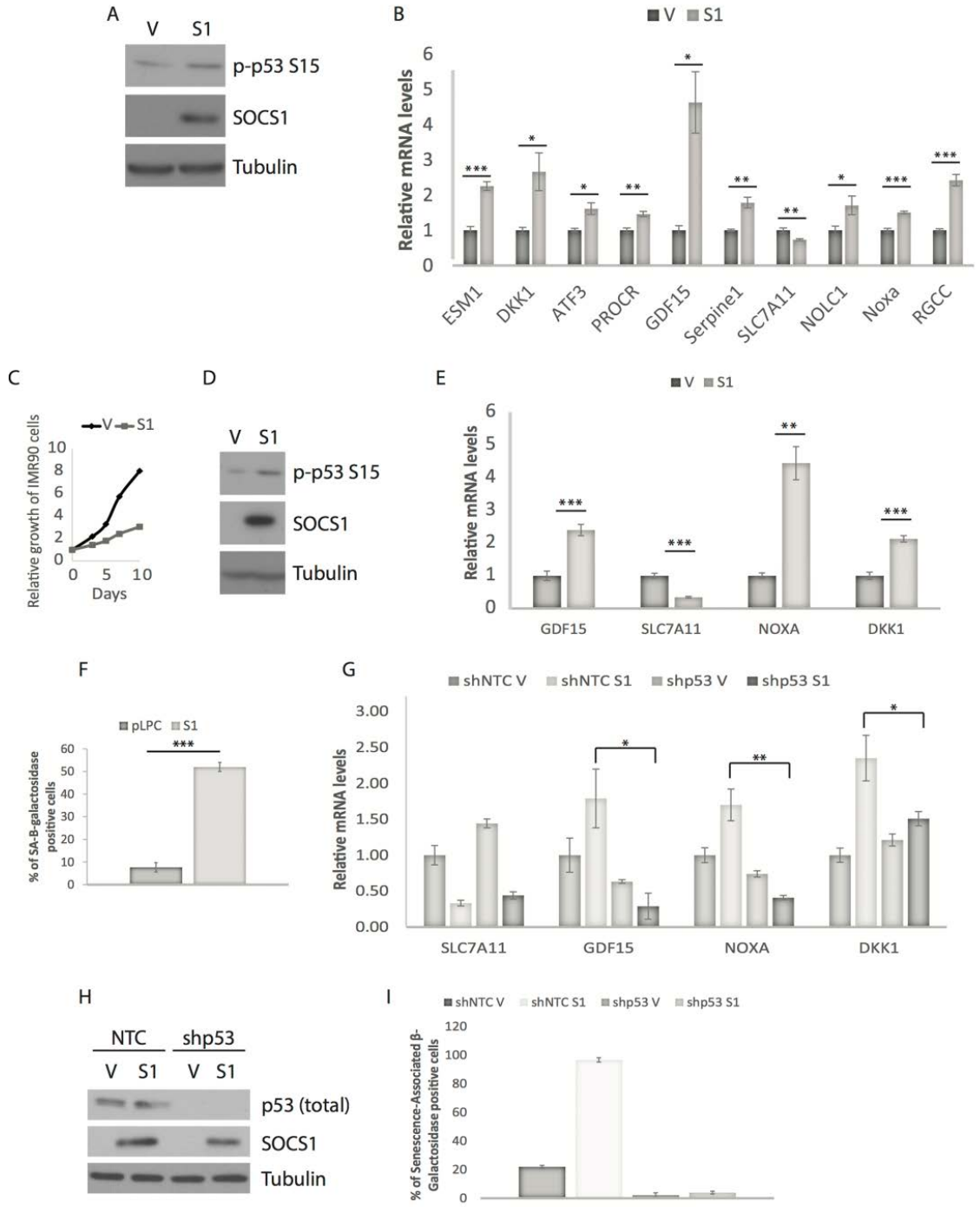

Figure 4. SOCS1 overexpression is sufficient to regulate the expression of SOCS1-dependent p53 target genes. (**A**) Western blots of SOCS1 and phospho-p53 (p-p53 S15) in U2OS cells expressing either empty vector (V) or SOCS1 (S1). (**B**) QPCR for p53 target genes in cells as in (A). Cells were collected at day 5 or 7 post-infection. (**C**) Growth curves of IMR90 cells expressing either empty vector (V) or SOCS1 (S1). (**D**) Western blots of SOCS1 and phospho-p53 (p-p53 S15) in IMR90 cells expressing either empty vector (V) or SOCS1 (S1). (**E**) QPCR for p53 target genes in cells as in (C). Cells were collected at day-7 post infection. (**F**) Senescence associated β-galactosidase of IMR90 cells expressing either empty vector (V) or SOCS1 (S1). Cells were fixed and stained at day 12 post- infection. (**G**) QPCR of IMR90 cells expressing either a control shRNA (shNTC) or a shRNA against p53 (shp53) combined with SOCS1 (S1) or empty vector (V) to confirm that the genes in (E) are targets of p53. (**H**) Western blots for the indicated proteins in IMR90 cells expressing a control shRNA (NTC) or an shRNA against p53 (shp53) and also infected with a SOCS1 expressing vector (S1) or a vector control (V). (**I**) Senescence-Associated β-Galactosidase staining. Positively stained and unstained cells were counted under a light microscope in order to obtain the percentage of senescent cells. All experiments were performed three times, error bars indicate the standard errors of triplicates, * = p<0.05, using the Student's t test, **=p<0.01, ***=p<0.005.

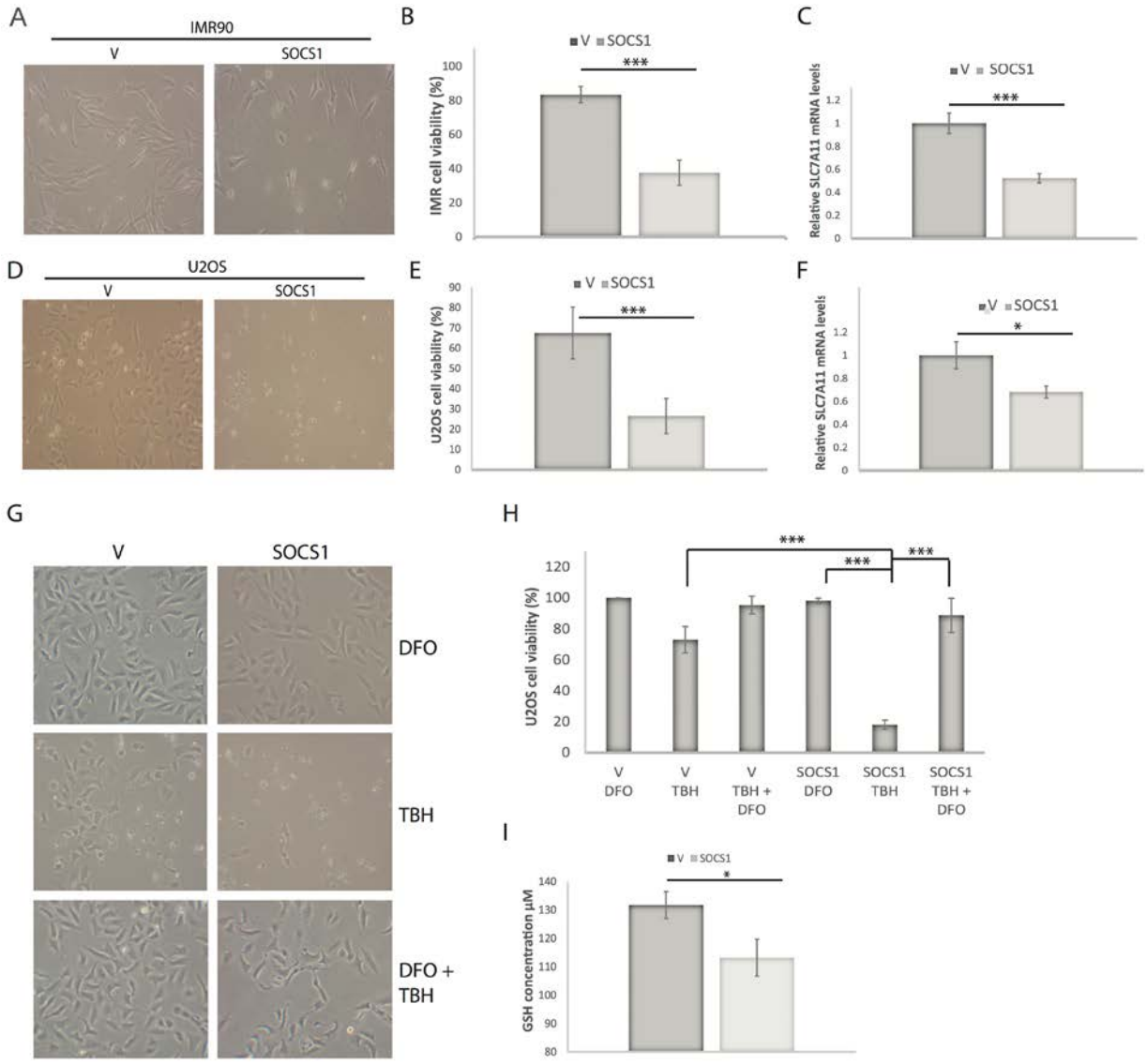

Figure 5. SOCS1 sensitizes cells to ferroptosis. (**A**) Representative photos of IMR90 cells expressing an empty vector (V) or SOCS1 (S1) and treated 24 hours after plating with 88 µM tert-butyl-hydroperoxide (TBH). Cells were assayed for cell death 16 hours after treatment. (**B**) Quantification of cell viability portrayed in (A) by Trypan blue staining. (**C**) SLC7A11 mRNA levels measured by qPCR of IMR90 cells described in (A). (**D**) Representative photos of U2OS cancer cells expressing either V or S1 by retroviral infection and treated 24 hours after plating with 350 µM TBH for 16 hours. (**E**) Quantification of cell viability of U2OS cells as portrayed in (D) by Trypan blue staining. (**F**) Relative SLC7A11 mRNA expression measured by qPCR in U2OS cells expressing either V or S1 as described in (D). (**G**) Representative photos of U2OS cancer cells expressing either V or S1 by retroviral infection and treated 24 hours after plating with either 350 µM TBH alone, 100 µM Deferoxamine mesylate (DFO) alone or the combination of both drugs. (**H**) Quantification of cell viability portrayed in (G) by Trypan blue cell counts. (**I**) GSH quantification in U2OS cells expressing either V or S1. All experiments were performed three times, error bars indicate the standard deviation of triplicates, * = p<0.05, using the Student's t test, **=p<0.01, ***=p<0.005.

cells overexpressing the protein (Figure 4F). The increase in expression of p53 target genes by SOCS1 was, for the most part, dependent on p53 since knockdown of p53 (Figure 4G-H) abolished their stimulation and prevented senescence (Figure 4I). However, the decrease in SLC7A11 was not blocked after knockdown of p53 suggesting that SOCS1 regulates the expression of this gene by additional mechanisms. Of note, not all p53 target genes that required SOCS1 in cS5A-induced senescence were induced by SOCS1 expression alone. The following genes (IGFBP3, GFBP5, DUSP1, ALDH1L12, IGFBP7, DDIT3, PPP1R3C, NOLC1, NTN4 and SVEP1) were not significantly induced by SOCS1 in

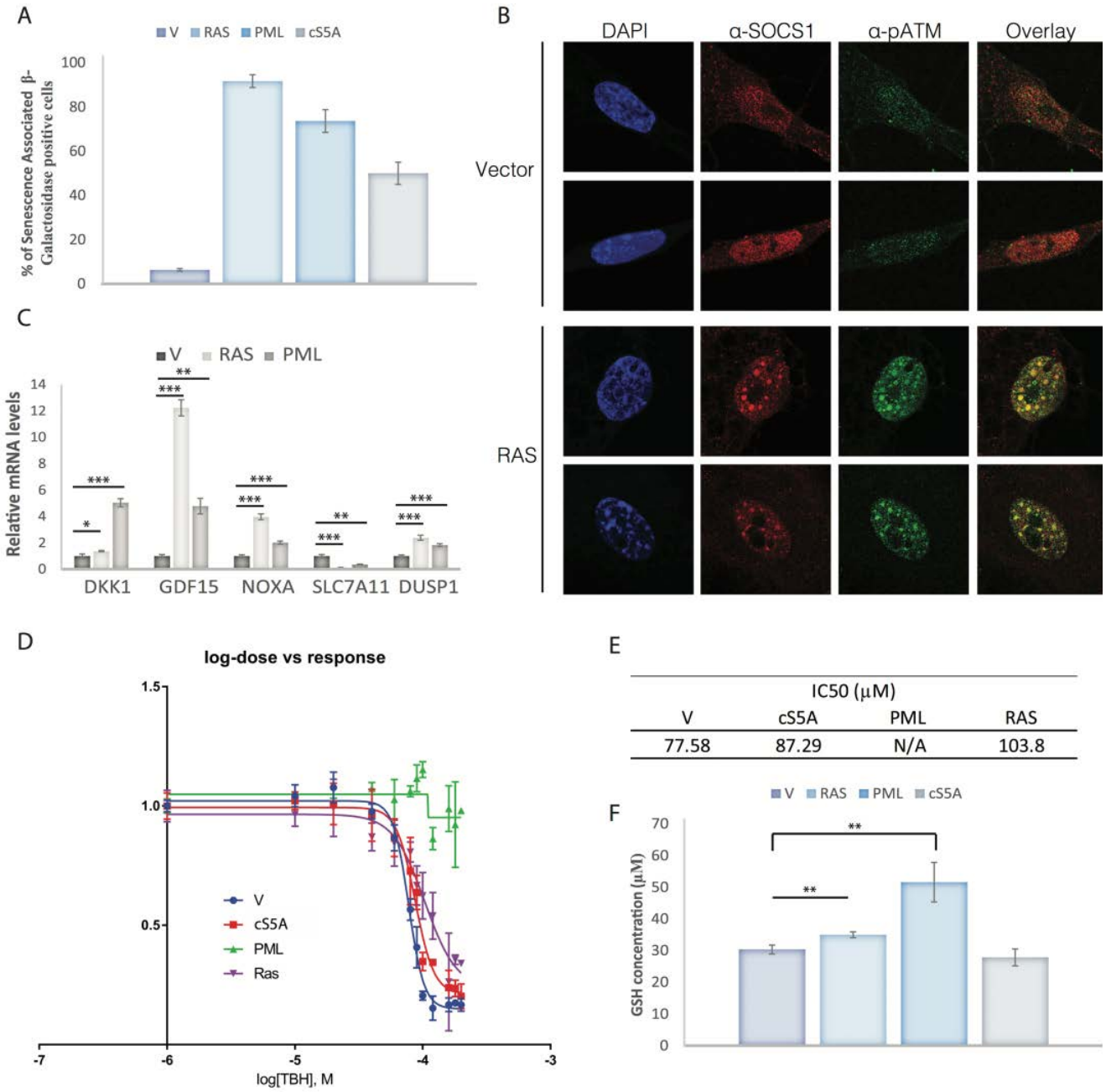

Figure 6. Ferroptosis sensitivity in senescent cells depends on the trigger. (**A**) Senescence was assessed by staining cells for the Senescence-Associated β-Galactosidase in IMR90 cells expressing either a control vector (V), the RASV12 oncogene (RAS), PML or STAT5A (cS5A). (**B**) Immunofluorescence of SOCS1 (anti-SOCS1) and phosphorylated ATM at S1981 (anti-ATM) in IMR90 cells rendered senescent by overexpressing the RASV12 oncogene compared to IMR90 expressing a control vector (Vector). (**C**) QPCR for mRNA levels of SOCS1-dependent p53 target genes in IMR90 cells expressing a control vector (V) or rendered senescent by overexpression of RASV12 (RAS) or PML (PML). (**D**) IC50 curves of IMR90 cells overexpressing a control vector (V), the RASV12 oncogene (RAS), PML or STAT5A (cS5A). Cells were treated 24 hours after plating with 12 different doses (0, 10, 20, 40, 60, 80, 100, 120, 160, 180 and 200 µM) of tert-butyl-hydroperoxide (TBH). Cells were fixed and stained with Crystal Violet to assess cell death 16 hours after treatment. The dye was then solubilized with acetic acid 10% and measured with a spectrophotometer. (**E**) The value of IC50 of each condition graphed in D is presented. No IC50 could be calculated for PML as it was resistant at the doses used. (**F**) GSH quantification in IMR90 cells rendered senescent by overexpression of RASV12, PML IV or STAT5A, compared with empty vector control (V). All experiments were performed three times, error bars indicate the standard deviation of triplicates, * = p<0.05, using the Student's t test, **=p<0.01, ***=p<0.005.

either U2OS or IMR90 cells. In addition, RGCC, ESM1, ATF3 and PROCR were induced in U2OS but not in IMR90 cells. These results indicate that SOCS1 partially reproduces oncogenic STAT5A signaling to p53 but additional STAT5A functions also contribute to p53 activation.

SOCS1 sensitizes cells to ferroptosis

The mechanisms by which p53 prevents tumor progression include apoptosis, senescence and ferroptosis [27,28]. The latter is an iron-dependent cell death mechanism that involves reactive oxygen species and lipid oxidation and that does not depend on caspases or Bcl2 family members Bak and Bax [28]. The SOCS1-dependent p53 target genes SLC7A11 [4] and SAT1 [24] play key roles in ferroptosis suggesting that SOCS1 could be a novel regulator of this process. As anticipated, expression of SOCS1 in U2OS or IMR90 cells sensitized them to the ferroptosis inducer tert-butyl-hydroperoxide (TBH). This effect of SOCS1 correlated with its ability to reduce the expression of the cystine transporter SLC7A11 (Figure 5A-F) and was efficiently blocked by treatment with deferoxamine, an iron chelator known to inhibit ferroptosis (Figure 5G-H and Figure S4). Ferroptosis depends on the actions of oxidized lipids, which are detoxified by the glutathione (GSH)-dependent enzyme GPX4 [29]. Cystine is used in the cells to generate cysteine, a metabolite required for the synthesis of glutathione (GSH). As expected, expression of SOCS1 reduced the levels of GSH (Figure 5I) explaining in part its ability to sensitize cells to ferroptosis.

The SOCS1-p53 axis is active in oncogene-induced senescence (OIS) but additional factors control ferroptosis in these cells

OIS is triggered by activated oncogenes and involves replication stress, mitochondrial dysfunction, reactive oxygen species and the DNA damage response [30,31,32]. We anticipated that SOCS1 is generally upregulated during OIS and not only in the specific case of cS5A-induced senescence. This is because senescent cells secrete a variety of inflammatory mediators that activate JAK-STAT signaling [33], the major regulator of SOCS1 expression [14,34]. We thus induced senescence in IMR90 normal human fibroblasts with constitutively active RAS (RASV12), cS5A or the tumor suppressor PML, that acts downstream of RAS and cS5A to induce senescence (Figure 6A). As published before for cells expressing cS5A [14], we found SOCS1 localizing with phospho-ATM [35] in DNA damage foci in senescent cells, which are known to contain phosphorylated p53 at serine 15 [36] (Figure 6B). Also, induction of senescence by RASV12 or PML led to induction of SOCS1-dependent p53 target genes and the downregulation of the p53-repressible gene SLC7A11 (Figure 6C). Hence, despite the differences in the mechanisms triggering senescence by RasV12, STAT5A, SOCS1 or PML, they regulate a common set of p53 target genes.

Next, we performed ferroptosis assays in cells expressing RASV12, STAT5A or PMLIV using the ferroptosis inducer TBH and the ferroptosis inhibitor deferoxamine. For this assay we plated the same amount of cells for each condition and found that neither RasV12 nor STAT5A sensitized cells to ferroptosis, despite both having an increase in endogenous SOCS1 expression and a reduction in SLC7A11. Intriguingly, PML expression turned cells highly resistant to ferroptosis providing a mechanistic insight into a ferroptosis resistance pathway in senescent cells (Figure 6D-E). Glutathione levels correlated with ferroptosis resistance in senescent cells (Figure 6F) suggesting compensatory mechanisms of GSH biosynthesis as a possible mechanism for resistance to ferroptosis. Targeting anti-ferroptosis pathways activated in senescent cells might selectively kill them in the same way as targeting anti-apoptotic proteins.

SOCS1 activates p53 via both phosphorylation and stabilization

The pattern of p53 target genes regulated by SOCS1, including ferroptosis regulators, is unique and anticipates unique mechanisms of p53 activation by SOCS1. So far, SOCS1 has been linked to the regulation of serine 15 phosphorylation of p53 [14,15], a modification that is also efficiently induced during an acute DNA damage response, which does not necessarily evolve into a permanent senescent cell cycle arrest [37,38]. Therefore, the ability of SOCS1 to induce senescence must involve additional mechanisms capable of changing the quality of the p53 response.

To investigate how SOCS1 modulates p53 activity, we first induced endogenous p53 using the DNA damaging drug doxorubicin and measured both p53 phosphorylation and total p53 levels. SOCS1 expression increased p53 levels during the course of a doxorubicin treatment without changing the levels of serine 15-phosphorylation of p53, which are highly induced by the drug (Figure 7A and B). In other words, in the context of oncogenic stress that involves relatively modest rates of DNA damage, SOCS1 stimulates serine 15 phosphorylation of p53 by promoting p53-ATM interactions as described before [14]. In cells treated with doxorubicin, high levels of DNA damage maximally stimulate serine 15 phosphorylation of p53

in a SOCS1-independent manner but SOCS1 can still stabilize p53 in this condition.

In order to find additional mechanisms of p53 activation by SOCS1, we looked at the SOCS1 interactome [15]. Interestingly, KAP1, a repressor of p53 [39], immunoprecipitated with SOCS1 [15]. To confirm this finding we expressed wild type SOCS1 in U2OS cells and immunoprecipitated endogenous KAP1 using a specific antibody. We found SOCS1 in KAP1 immunoprecipitates but not in immunoprecipitates obtained with a control antibody (Figure 7C). The reciprocal co-IP analysis confirmed that endogenous KAP1 interacted with SOCS1 (Figure 7D). Next, we used a GST-pull-down assays with two fragments of KAP1 and an *in vitro* translated and ^{35}S labelled SOCS1. We found that the Bromo/PHD domain of KAP1 directly interacted with SOCS1 (Figure 7E-G). We thus propose that SOCS1 activates the senescence functions of p53 via two mechanisms (Figure 7H): 1) facilitating serine 15 phosphorylation of p53 and 2) p53 stabilization by interfering with KAP1. Together, these mechanisms can contribute to convert an acute p53 response into a chronic response characterized by the expression of a unique pattern of p53 target genes.

DISCUSSION

The tumor suppressor activity of the transcription factor p53 does not correlate with the expression of target genes induced by acute DNA damage [6]. The discovery and characterization of p53 targets in conditions of chronic stimulation of the p53 pathway should give critical insights into the mechanisms of tumor suppression by p53. Oncogene-induced senescence is a tumor suppressor mechanism where a lasting p53 response mediates a stable cell cycle arrest and the clearance of senescent cells, which prevents tumor progression [40]. The suppressor of cytokine signaling SOCS1 was previously shown to be required for p53 activation and senescence in response to constitutive JAK-STAT5 signaling [14,15,41,42]. However, the p53 target genes requiring SOCS1 remained poorly characterized. Here, we used RNA interference and transcriptome analysis to identify the set of SOCS1-dependent p53 target genes. Although SOCS1 was required for the expression of several previously identified p53 targets, most of the classic targets associated with acute DNA damage response such as p21 and MDM2 were not affected by SOCS1 inhibition (Table 1). In addition, bioinformatics analysis using the platform DiRE, uncovered several genes that required SOCS1 expression and contained p53-binding sites in their promoter regions (Table 2). This unbiased transcriptome analysis confirms that SOCS1 regulates the p53 pathway and reveals a unique and interesting biology for the SOCS1-p53 axis.

The identification of SOCS1-dependent p53 targets links p53 to several interesting tumor suppression pathways. For example, DDIT-3 (also known as C/EBP Zeta) is a dominant negative inhibitor of C/EBP family of transcription factors [43]. This family is important for the expression of inflammatory cytokines in senescent cells that contribute to the SASP [44,45]. SOCS1 may regulate the SASP via p53 and DDIT-3 (Table 2). In addition, several SOCS1-dependent p53 targets are secreted proteins suggesting that the SOCS1-p53 pathway changes the quality of the SASP. They include the bona fide p53 targets IGFBP3, IGFBP7, SERPINE1/PAI1, DKK1 and GDF15 (Table 1) and the new candidate p53 targets ESM1 and SRPX2 (Table 2). Another interesting target is GADD45B that mediates activation of the p38MAPK pathway, which is required for OIS [46]. Perhaps the most intriguing connection found by our analysis involves the ferroptosis pathway. This form of cell death was linked to p53-dependent tumor suppression and involves the SOCS1-dependent p53 targets SLC7A11 [4] and SAT1 [24]. In addition, ferroptosis is mediated by oxidized lipids [23] and the overall gene expression pattern of SOCS1-expressing cells overlaps with genes regulated by oxidized lipids (Figure S3D). The SOCS1-dependent p53 targets DDIT3, PMAIP1, ATF3 and ESM1 are part of the gene set induced by oxidized phospholipids and therefore bona fide new candidates to regulate ferroptosis downstream the SOCS1-p53 axis.

SOCS1 does not only play a role in the senescence response to constitutively active JAK-STAT5 signaling. In cells expressing oncogenic RAS, SOCS1 is recruited to DNA damage foci, colocalizing with phospho-ATM. The extent to which SOCS1 modifies gene expression in RAS-induced senescence remains to be fully characterized. However, DKK1, GDF15, Noxa, Dusp1 and SLC7A11 were modulated in Ras- or PML-expressing cells in the same way as in cells expressing STAT5A or SOCS1. In contrast to SOCS1-cells, RAS- or STAT5A-senescent cells were not more sensitive to ferroptosis induced by TBH, suggesting that other pathways activated in these cells control ferroptosis. Intriguingly, PML expressing cells were highly resistant to ferroptosis providing a mechanistic insight into ferroptosis resistance pathways. In addition to influencing p53 target gene expression, SOCS1 could play a general role in senescence by stabilizing the interactions of p53 with protein complexes at DNA damage foci. This would allow the maintenance of a pool of pre-active p53 that can be slowly released during the senescence cell cycle arrest contributing to

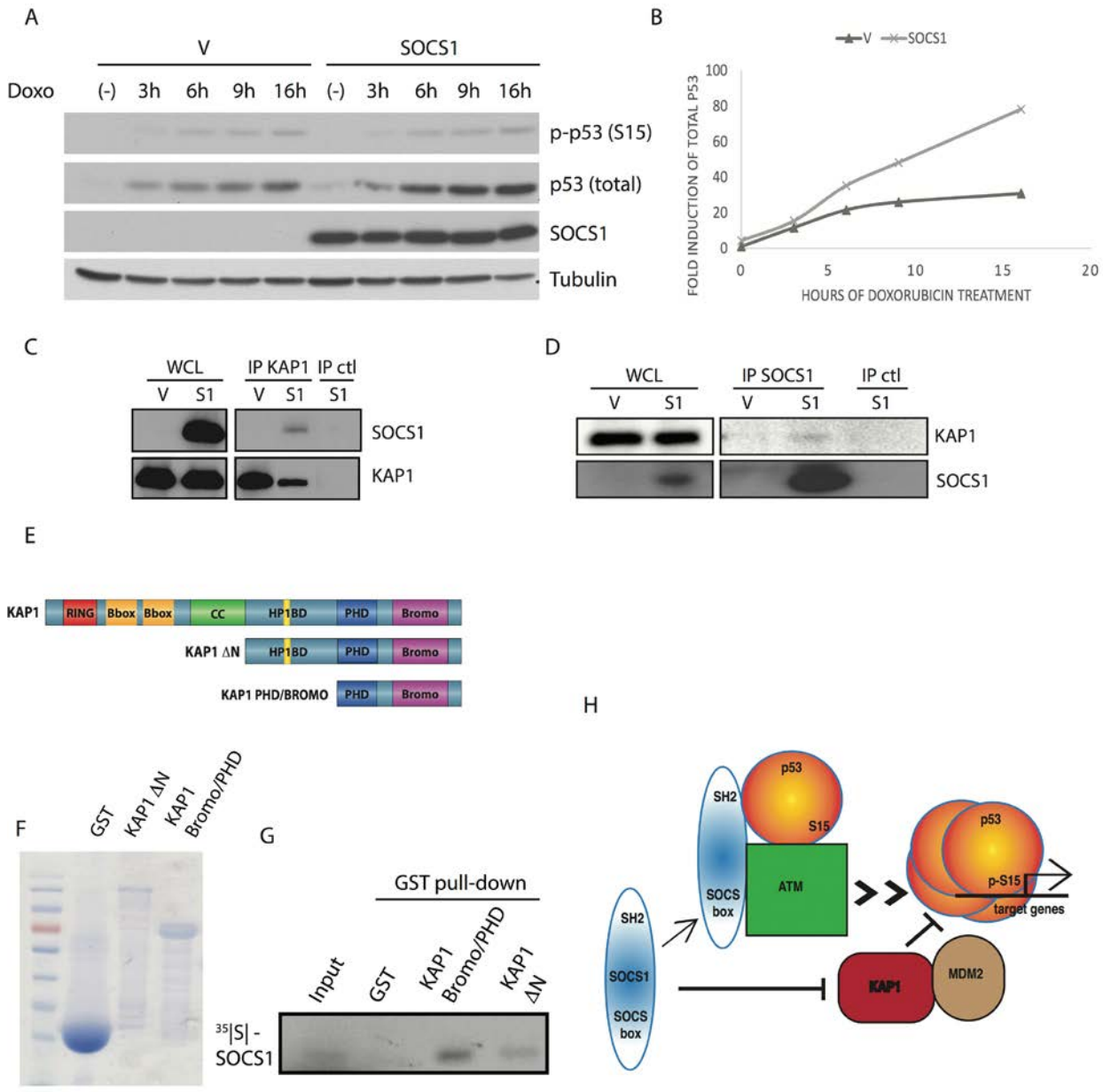

Figure 7. SOCS1 favors p53 accumulation in response to Doxorubicin. (**A**) Western blots of SOCS1, phosphorylated p53 at serine 15 [p-p53 (S15)] total p53 and tubulin in IMR90 cells expressing either empty vector (V) or SOCS1 and treated with doxorubicin (Doxo: 300 ng/mL) for 3, 6, 9, 16 hours or untreated (-). (**B**) Graphic representation of Western blots as in (A). Bands were quantified using image analysis software and normalized to tubulin, then plotted in a graph to show the kinetics of p53 stabilization. (**C**) Co-Immunoprecipitation of KAP1 with SOCS1. U2OS cell lysates of either empty vector cells (V) or SOCS1 overexpressing cells (S1) were immunoprecipitated with an antibody against KAP1 or a control antibody (IP ctl). Western blots against both KAP1 and SOCS1 were performed to confirm the presence of SOCS1 in complex with KAP1. Whole cell lysates (WCL) are used to control the expression of SOCS1 and KAP1 levels. (**D**) Co-immunoprecipitation as described in C. Cell lysates were immunoprecipitated with an antibody against SOCS1 or with a control antibody (IP ctl). Whole cell lysates (WCL) show the expression level of SOCS1 and KAP1. (**E**) Maps of the different KAP1 constructs used in experiments are depicted: KAP1 full length (KAP1), KAP1 with a deletion of its N-terminal RBCC domains (KAP1 ΔN) or KAP1 C-terminus including PHD and Bromo domains (KAP1 PHD/BROMO). (**F**) The constructs depicted in E. were expressed by IPTG induction in BL21 bacterial cells. Expression levels of the various constructs were assessed by migration of an SDS-PAGE gel and Coomassie staining. (**G**) GST pull down was performed on KAP1 constructs which were incubated with radiolabeled SOCS1. Autoradiography revealed the absence or presence of SOCS1 in each pull down. GST was used as a negative control. (**H**) Model for p53 activation by SOCS1 via two pathways.

generate a lasting chronic p53 response. Another function for maintaining p53 in DNA damage foci could be to suppress homologous recombination in cells arrested in G1 [47,48], an event that could lead to chromosome aberrations and potentially tumor development.

In summary, we report here that SOCS1 impacts the pattern of secreted products in cells with active p53 and is required for the expression of a selective set of p53 target genes including those involved in ferroptosis. SOCS1 can use several mechanisms to activate p53, including promotion of serine-15 phosphorylation by ATM/ATR kinases and inhibition of the p53 repressor KAP1. Further investigation of the SOCS1-p53 pathway will help to better understand p53 tumor suppression activity and provide insights for novel cancer therapies.

MATERIALS AND METHODS

Cell lines, reagents, growth analysis and senescence

U2OS were purchased from the American Type Culture Collection, (Manassas, VA) and normal human diploid fibroblasts IMR90 were purchased from the Coriell Institute (Camden, New Jersey, USA). IMR90 were cultured in DMEM supplemented with 10% fetal bovine serum (FBS; Wisent, Montréal, QC, Canada) and 1% penicillin G/streptomycin sulphate. U2OS were supplemented with 5% FBS (Wisent) and 5% Newborn Calf serum (Wisent), with 1% penicillin G/streptomycin sulphate and with 2mM L-glutamine. Tert-butyl Hydroperoxide was purchased from Sigma (cat #458139) and used at 350 µM in U2OS cells and 88 µM in IMR90 cells. Doxorubicin was purchased from Sigma. Growth curves and the senescence associated β-galactosidase were performed as previously described [49].

Plasmid constructions and viral gene transfer

Ca-STAT5A was previously described in [50]. pLPC-SOCS1 was previously described in [14]. pLPC PML IV and pBabe RASV12 were previously described in [49]. GST-KAP1 constructs were a kind gift of Dr. Xavier Mascle. Lentiviral shRNAs against SOCS1 were purchased from Sigma-Aldrich in the pLKO vector. ShSOCS1a (shS1) (TRCN0000356245, Sigma) has the following sequence: CCGGCTGGTTGTTGTAGCAGCTTAACTCGAGTT AAGCTGCTACAACAACCAGTTTTTG and shSOCS1b (TRCN0000057065, Sigma) has the following sequence: CCGGCTTCCGCACATTCCGTTCGCACTCGAGTG CGAACGGAATGTGCGGAAGTTTTTG. shNTC has the following sequence: CCGGCAACAAGATGAAGAGCACCAACTCGAG TTGGTGCTCTTCATCTTGTTGTTTTT. pLXSN E7 was a kind gift from Dr. D. Galloway. Retroviral gene transduction was performed as previously described [49]. Lentiviral gene transduction was performed by co-transfecting 6 µg of the lentiviral vector with the packaging vectors in 293T cells as follows: 3 µg of the VSV-G envelope protein expression plasmid pMD2, 1.5 µg of the regulator of virion expression (REV) expression plasmid pRSV and 1.5 µg of gag/pol elements expression plasmid pMDLg/pRRE. 24 hours post transfection, media were changed and the supernatants (viral soup) were collected 48 hours post transfection, filtered through 0.45 µm filters (Sarstedt) and added to target cells together with DMEM and 4 µg/mL polybrene. Viruses were removed after 8 hours and replaced by fresh medium. Selection was started 24 hours post-infection. For triple infections in IMR90 cells, G418 (300 µg/mL, 6 days) and puromycin (1.5 µg/mL, 3 days) were used first. After puromycin selection was over, hygromycin (80 µg/mL) was added for 4 days. Cells were selected for a total of 7 days before RNA collection. For U2OS and IMR90 single infections, puromycin was used at 3 µg/mL for 3 days.

Ferroptosis cell death assays

U2OS and IMR90 cells were seeded 24 hours prior to treatments in 10 cm plates (Corning) at 60% confluence. Cells were then treated with 350 µM (U2OS) or 88 µM (IMR90) TBH (Sigma #458139) for 16 hours. Cell death was assessed by imaging the cells under a white-light microscope and by counting live and dead cells using Trypan-Blue (BioRad) and a cell counter. Supernatants were collected and added to trypsinized cells before counting. All assays were performed at least three times. For IC50 assays, 20 000 IMR90 cells of each condition were plated per well of a 48 well plate. Cells were plated 24 hours prior to TBH treatment. Cells were then treated with either: 0, 10, 20, 40, 60, 80, 90, 100, 120, 160, 180 or 200 µM of TBH for 16 hours. Cells were then fixed with 1% gluteraldehyde in PBS and stained with Crystal Violet (Sigma #C0775). The dye was then resuspended in 10% acetic acid and dosed with a spectrophotometer. GraphPad Prism was used to generate IC50 curves and determine IC50 values.

Western blotting

Protein analysis was performed by lysing cells in Cell Lysis Buffer (20 mM Tris-HCl pH 7.5, 150 mM NaCl, 1 mM EDTA, 1 mM EGTA, 1% Triton X-100, 2.5 mM sodium pyrophosphate, 1 mM β-glycerolphosphate and a cocktail of protease inhibitors (Roche). Quantification

of protein content was performed with the Bradford method. Extracts were prepared with Laemmli buffer (1X final). For endogenous SOCS1 detection, 150 µg of total extract was loaded on a 12% SDS-PAGE gel and transferred on an Immobilon P membrane (Millipore). For SOCS1 overexpression and other protein detection, 50 µg of total cells extract was loaded on a 12% SDS polyacrylamide gel. Western blots were performed as described previously [14]. The following primary antibodies were used: anti-SOCS1, clone 4H1 MBL (cat #K0175-6) used at 1:1000 dilution overnight at 4 °C. Anti-phospho-p53 (Serine15), NEB (cat #9284) used at 1:1000 dilution overnight at 4 °C. Total p53 (DO1 clone), Santa Cruz biotechnology (cat# sc-126) used at 1:1000 overnight at 4 °C. Anti-MCM6, Bethyl (#A300-194A) used at 1:1000 overnight at 4°C. Anti-phosphorylated-Rb (Serine 795), Cell Signaling (#9301) used at 1:1000 overnight at 4°C. Anti-phosphorylated Histone H3 (Serine 10), Millipore (#6570) used at 1:1000 overnight at 4°C. Alpha Tubulin antibody clone B-5-1-2, Sigma (cat # T6074) used at 1:20,000 1 hour at Room Temperature and served as loading control. Signals were revealed by using secondary antibodies coupled to peroxidase (BioRad laboratories) and ECL (GE Healthcare, cat# RPN2106) or Clarity ECL (BioRad #cat 1705061).

Co-immunoprecipitation

U2OS cells were collected in Cell Lysis Buffer (20 mM Tris-HCl pH 7.5, 150 mM NaCl, 1 mM EDTA, 1 mM EGTA, 1% Triton X-100, 2.5 mM sodium pyrophosphate, 1 mM β-glycerolphosphate and a cocktail of protease inhibitors (Roche)) and protein concentration measured using the Bradford method. 2 mg of cell extract from each condition was used for IP and 50 ug was loaded as input (Whole Cell Lysate). Immunoprecipitation of either KAP1 (Bethyl #A300-274A) or SOCS1 (SantaCruz #sc-7005R) were performed at an antibody dilution of 1:200 overnight at 4°C. Protein A Sepharose 4B fast flow beads (Sigma #P9424) were used to immunoprecipitate antibody-protein complexes for 1 hour at 4°C. Beads were then washed four times with Cell Lysis Buffer and complexes were eluted by adding Laemmli 2X buffer directly to the beads. Samples were heated for 5 minutes at 100°C prior to loading on an SDS-PAGE gel for western blotting.

GST-pull-down

BL21 *E. coli* strain harboring each of the KAP1-GST-fusion vectors were grown at 37°C to an OD of 0.6 in 400 ml YTA 2X medium (16g/l tryptone, 10g/l yeast extract, 5g/l NaCl) and induced with 0.4 mM IPTG for 4 hr at 30°C. Cell pellets were resuspended in STE buffer (10 mM Tris-HCl pH 8.0, 1 mM EDTA, 100 mM NaCl) supplemented with DTT (5mM) and a Protease Inhibitor Cocktail (Roche). Cells were lysed by adding 1mg/mL lysozyme and incubating 45 minutes on ice prior to sonicating with a microtip five times for 10 s. Extracts were centrifuged (13 000 rpm 10 minutes) and supernatants were incubated for 2 hr at 4°C with glutathione Sepharose-4B (Amersham) and washed four times with NETN buffer (10 mM Tris-HCl pH 8.0, 1 mM EDTA, 100 mM NaCl, 0.5% NP-40). Beads were resuspended in PBS after the last wash.

Briefly, ^{35}[S] Flag-SOCS1 was produced by *in vitro* transcription/translation (Promega #L1170) and incubated with GST, GST-KAP1, GST KAP1 PHD/BROMO or GST-KAP1 ΔN purified proteins bound to glutathione Sepharose-4B for 2 hr at 4°C. Equal amounts of GST fusion proteins were used as judged from SDS gel electrophoresis and Coomassie blue staining. Beads were washed 5 times with NETN buffer. Precipitates were eluted in 20 µl of SDS Sample Buffer and 10 µl of Bromophenol Blue and boiled for 5 min. Eluates (30 µl) were separated on SDS-PAGE, dried and exposed for autoradiography.

GSH quantification

Cells were collected in Cell Lysis Buffer (20 mM Tris-HCl pH 7.5, 150 mM NaCl, 1 mM EDTA, 1 mM EGTA, 1% Triton X-100, 2.5 mM sodium pyrophosphate, 1 mM β-glycerolphosphate and a cocktail of protease inhibitors (Roche)). GSH was then quantified with the QuantiChrom Glutathione (GSH) Assay Kit (BioAssay Systems, DIGT-250) following manufacturer's instructions. Quantification was normalized to total protein concentration of each sample.

Real-Time Quantitative PCR (qPCR)

Total RNA was isolated using Trizol (Invitrogen). Reverse transcription was performed using 5X All-In-One RT MasterMix (Abmgood) on 2 µg of total RNA in 20 µL final volume according to the kit's instructions. Reverse transcription products were diluted 10-fold in RNAse free water before proceeding to qPCR. QPCR was performed using primers and probe sets from Roche Universal Probe Library (https://lifescience.roche.com/en_ca/brands/universal-probe-library.html?_ga=1.38905443.192324701.1470126343#overview). 96-well plate formats with SYBR-green technology was used as described previously [26]. Relative target-gene quantification was obtained by using the ΔΔCT method in a light Cycler 480 (Roche). The mRNA expressions were measured relative to the

Table 4.

Gene symbol	Forward primer	Reverse primer
DUSP1	caacgaggccattgacttcataga	atggtggctgaccgggaaat
IGFBP3	tctcccaggctacaccaccaa	ggcatatttgagctccacattaacct
IGFBP5	ccgcgagcaagtcaagatcg	taggtctcctcggccatctca
ATF3	tgaggtttgccatccagaacaa	tttcatcttcttcaggggctacc
SLC7A11	ctccatgaacggtggtgtgttt	ccctctcgagacgcaacataga
ALDH1L2	tctggctttggaaaagacttagg	cctgatgatggtgttgctctaat
Serpine1	cggtcaagcaagtggacttttc	ggctccttttcccaagcaagtt
NOXA	gaagaaggcgcgcaagaacg	tgagtagcacactcgacttcca
RGCC	cgccacttccactacgaggag	cactgaagctgaagctgttcct
IGFBP7	cctgtcctcatctggaacaaggt	tctgaatggccaggttgtcc
DKK1	atgatcatagcaccttggatggg	gcacaacacaatcctgaggcaca
DDIT3	catacatcaccacacctgaaagca	gctggtctgatgcctgtttttgt
PPP1R3C	agcgggtgctggcttttagg	tggatctaaaacctggatcattctg
NOLC1	gcggcagtggtagtttccaaat	tgaagctttatcttcttggcctga
NTN4	cgtgcacaataagagcgaacca	tgttccttacattcgcatttacctg
SVEP1	tctgttggtttgcccatacctg	ttatggagcccacaaaagactc
PROCR	aacattgctgccgatactgctg	tctggagcatatgaagtctttgga
ESM1	catggatggcatgaagtgtg	ccagatgccatgtcatgctcttt
IGFBP4	gcaacttccaccccaagcag	cggtccacacaccagcactt
IGFBP6	aggaatccaggcacctctacca	agtccagatgtctacggcatgg
SOCS1	ggtccccctggttgttgta	taggaggtgcgagttcaggt
GDF15	agtccggatactcacgccagaa	gcccgagagatacgcaggtg
GADD45B	tgcattgtctcctggtcacgaa	cccggctttcttcgcagtag

mRNAs of two housekeeping genes: HMBS and TBP. All forward and reverse primers are listed in Table 4.

Microarray analysis

RNA was collected from IMR90 cells expressing oncoprotein E7, seven days after co-infection with pWZL ca-STAT5A (5A) and pLKO shNTC or pWZL 5A and pLKO shSOCS1 a. Total RNA samples were isolated with the RNeasy mini kit (Qiagen) and sent to the Genome Quebec facility at McGill University for cRNA amplification and subsequent hybridization on GeneChIP Human Gene 2.0 ST Array Affymetrix DNA Chip. Data were analyzed using Affymetrix Expression Console Software and Transcriptome Analysis Console (www.affymetrix.com). Each condition was analysed in biological triplicates and the cut-off applied for analysis was an ANOVA p-value <0.05 for genes that have a fold change ≥±1.5. Data are available at https://www.ncbi.nlm.nih.gov/geo/query/acc.cgi?acc=GSE98216 Further analysis were conducted with DiRE (https://dire.dcode.org/), Gene-Set Enrichment Analysis (GSEA) (http://software.broadinstitute.org/gsea/index.jsp) and DAVID database (https://david.ncifcrf.gov/). Genes identified by DiRE were further analysed with Oncomine (https://www.oncomine.org/resource/login.html).

Gene expression analysis in hepatocellular carcinoma (HCC) specimens

The correlation between *SOCS1* gene expression and that of p53 target genes related to ferroptosis was analysed using The Cancer Genome Atlas (TCGA) [51] provisional dataset containing 373 hepatocellular carcinoma (HCC) specimens, which was accessed via the cBioportal (http://www.cbioportal.org) [52]. The transcript levels were expressed as RNASeq Ve RESM (RNA-Seq by Expectation Maximization) [53]. The

downloaded data were plotted using the GraphPad Prism software to determine the Spearman correlation (ρ) and statistical significance (*p*).

ACKNOWLEDGEMENTS

We thank all members of the Ferbeyre laboratory for their useful comments.

CONFLICTS OF INTEREST

The authors have no conflict of interests to declare.

FUNDING

This work was funded by a grant from the Canadian Institute of Health and Research (CIHR-MOP229774) to GF.

REFERENCES

1. Lawrence MS, Stojanov P, Mermel CH, Robinson JT, Garraway LA, Golub TR, Meyerson M, Gabriel SB, Lander ES, Getz G. Discovery and saturation analysis of cancer genes across 21 tumour types. Nature. 2014; 505:495–501. https://doi.org/10.1038/nature12912

2. Wei CL, Wu Q, Vega VB, Chiu KP, Ng P, Zhang T, Shahab A, Yong HC, Fu Y, Weng Z, Liu J, Zhao XD, Chew JL, et al. A global map of p53 transcription-factor binding sites in the human genome. Cell. 2006; 124:207–19. https://doi.org/10.1016/j.cell.2005.10.043

3. Li M, He Y, Dubois W, Wu X, Shi J, Huang J. Distinct regulatory mechanisms and functions for p53-activated and p53-repressed DNA damage response genes in embryonic stem cells. Mol Cell. 2012; 46:30–42. https://doi.org/10.1016/j.molcel.2012.01.020

4. Jiang L, Kon N, Li T, Wang SJ, Su T, Hibshoosh H, Baer R, Gu W. Ferroptosis as a p53-mediated activity during tumour suppression. Nature. 2015; 520:57–62. https://doi.org/10.1038/nature14344

5. Fischer M, Grossmann P, Padi M, DeCaprio JA. Integration of TP53, DREAM, MMB-FOXM1 and RB-E2F target gene analyses identifies cell cycle gene regulatory networks. Nucleic Acids Res. 2016; 44:6070–86. https://doi.org/10.1093/nar/gkw523

6. Brady CA, Jiang D, Mello SS, Johnson TM, Jarvis LA, Kozak MM, Kenzelmann Broz D, Basak S, Park EJ, McLaughlin ME, Karnezis AN, Attardi LD. Distinct p53 transcriptional programs dictate acute DNA-damage responses and tumor suppression. Cell. 2011; 145:571–83. https://doi.org/10.1016/j.cell.2011.03.035

7. Valente LJ, Grabow S, Vandenberg CJ, Strasser A, Janic A. Combined loss of PUMA and p21 accelerates c-MYC-driven lymphoma development considerably less than loss of one allele of p53. Oncogene. 2016; 35:3866–71. https://doi.org/10.1038/onc.2015.457

8. Kirschner K, Samarajiwa SA, Cairns JM, Menon S, Pérez-Mancera PA, Tomimatsu K, Bermejo-Rodriguez C, Ito Y, Chandra T, Narita M, Lyons SK, Lynch AG, Kimura H, et al. Phenotype specific analyses reveal distinct regulatory mechanism for chronically activated p53. PLoS Genet. 2015; 11:e1005053. https://doi.org/10.1371/journal.pgen.1005053

9. Banin S, Moyal L, Shieh S, Taya Y, Anderson CW, Chessa L, Smorodinsky NI, Prives C, Reiss Y, Shiloh Y, Ziv Y. Enhanced phosphorylation of p53 by ATM in response to DNA damage. Science. 1998; 281:1674–77. https://doi.org/10.1126/science.281.5383.1674

10. Sakaguchi K, Herrera JE, Saito S, Miki T, Bustin M, Vassilev A, Anderson CW, Appella E. DNA damage activates p53 through a phosphorylation-acetylation cascade. Genes Dev. 1998; 12:2831–41. https://doi.org/10.1101/gad.12.18.2831

11. Pomerantz J, Schreiber-Agus N, Liégeois NJ, Silverman A, Alland L, Chin L, Potes J, Chen K, Orlow I, Lee HW, Cordon-Cardo C, DePinho RA. The Ink4a tumor suppressor gene product, p19Arf, interacts with MDM2 and neutralizes MDM2's inhibition of p53. Cell. 1998; 92:713–23. https://doi.org/10.1016/S0092-8674(00)81400-2

12. Bernardi R, Scaglioni PP, Bergmann S, Horn HF, Vousden KH, Pandolfi PP. PML regulates p53 stability by sequestering Mdm2 to the nucleolus. Nat Cell Biol. 2004; 6:665–72. https://doi.org/10.1038/ncb1147

13. Donati G, Peddigari S, Mercer CA, Thomas G. 5S ribosomal RNA is an essential component of a nascent ribosomal precursor complex that regulates the Hdm2-p53 checkpoint. Cell Reports. 2013; 4:87–98. https://doi.org/10.1016/j.celrep.2013.05.045

14. Calabrese V, Mallette FA, Deschênes-Simard X, Ramanathan S, Gagnon J, Moores A, Ilangumaran S, Ferbeyre G. SOCS1 links cytokine signaling to p53 and senescence. Mol Cell. 2009; 36:754–67. https://doi.org/10.1016/j.molcel.2009.09.044

15. Mallette FA, Calabrese V, Ilangumaran S, Ferbeyre G. SOCS1, a novel interaction partner of p53 controlling oncogene-induced senescence. Aging (Albany NY). 2010; 2:445–52. https://doi.org/10.18632/aging.100163

16. Yoshikawa H, Matsubara K, Qian GS, Jackson P, Groopman JD, Manning JE, Harris CC, Herman JG. SOCS-1, a negative regulator of the JAK/STAT pathway, is silenced by methylation in human hepatocellular carcinoma and shows growth-suppression activity. Nat Genet. 2001; 28:29–35. https://doi.org/10.1038/ng0501-29

17. Khoo KH, Verma CS, Lane DP. Drugging the p53 pathway: understanding the route to clinical efficacy. Nat Rev Drug Discov. 2014; 13:217–36. https://doi.org/10.1038/nrd4288

18. Fabbro M, Savage K, Hobson K, Deans AJ, Powell SN, McArthur GA, Khanna KK. BRCA1-BARD1 complexes are required for p53Ser-15 phosphorylation and a G1/S arrest following ionizing radiation-induced DNA damage. J Biol Chem. 2004; 279:31251–58. https://doi.org/10.1074/jbc.M405372200

19. Liu B, Lee KW, Anzo M, Zhang B, Zi X, Tao Y, Shiry L, Pollak M, Lin S, Cohen P. Insulin-like growth factor-binding protein-3 inhibition of prostate cancer growth involves suppression of angiogenesis. Oncogene. 2007; 26:1811–19. https://doi.org/10.1038/sj.onc.1209977

20. Magnon C, Galaup A, Mullan B, Rouffiac V, Bouquet C, Bidart JM, Griscelli F, Opolon P, Perricaudet M. Canstatin acts on endothelial and tumor cells via mitochondrial damage initiated through interaction with alphavbeta3 and alphavbeta5 integrins. Cancer Res. 2005; 65:4353–61. https://doi.org/10.1158/0008-5472.CAN-04-3536

21. Yeh JR, Mohan R, Crews CM. The antiangiogenic agent TNP-470 requires p53 and p21CIP/WAF for endothelial cell growth arrest. Proc Natl Acad Sci USA. 2000; 97:12782–87. https://doi.org/10.1073/pnas.97.23.12782

22. Assadian S, El-Assaad W, Wang XQ, Gannon PO, Barrès V, Latour M, Mes-Masson AM, Saad F, Sado Y, Dostie J, Teodoro JG. p53 inhibits angiogenesis by inducing the production of Arresten. Cancer Res. 2012; 72:1270–79. https://doi.org/10.1158/0008-5472.CAN-11-2348

23. Kagan VE, Mao G, Qu F, Angeli JP, Doll S, Croix CS, Dar HH, Liu B, Tyurin VA, Ritov VB, Kapralov AA, Amoscato AA, Jiang J, et al. Oxidized arachidonic and adrenic PEs navigate cells to ferroptosis. Nat Chem Biol. 2017; 13:81–90. https://doi.org/10.1038/nchembio.2238

24. Ou Y, Wang SJ, Li D, Chu B, Gu W. Activation of SAT1 engages polyamine metabolism with p53-mediated ferroptotic responses. Proc Natl Acad Sci USA. 2016; 113:E6806–12. https://doi.org/10.1073/pnas.1607152113

25. Chicas A, Wang X, Zhang C, McCurrach M, Zhao Z, Mert O, Dickins RA, Narita M, Zhang M, Lowe SW. Dissecting the unique role of the retinoblastoma tumor suppressor during cellular senescence. Cancer Cell. 2010; 17:376–87. https://doi.org/10.1016/j.ccr.2010.01.023

26. Vernier M, Bourdeau V, Gaumont-Leclerc MF, Moiseeva O, Bégin V, Saad F, Mes-Masson AM, Ferbeyre G. Regulation of E2Fs and senescence by PML nuclear bodies. Genes Dev. 2011; 25:41–50. https://doi.org/10.1101/gad.1975111

27. Sinha VC, Qin L, Li Y. A p53/ARF-dependent anticancer barrier activates senescence and blocks tumorigenesis without impacting apoptosis. Mol Cancer Res. 2015; 13:231–38. https://doi.org/10.1158/1541-7786.MCR-14-0481-T

28. Jiang L, Hickman JH, Wang SJ, Gu W. Dynamic roles of p53-mediated metabolic activities in ROS-induced stress responses. Cell Cycle. 2015; 14:2881–85. https://doi.org/10.1080/15384101.2015.1068479

29. Yang WS, SriRamaratnam R, Welsch ME, Shimada K, Skouta R, Viswanathan VS, Cheah JH, Clemons PA, Shamji AF, Clish CB, Brown LM, Girotti AW, Cornish VW, et al. Regulation of ferroptotic cancer cell death by GPX4. Cell. 2014; 156:317–31. https://doi.org/10.1016/j.cell.2013.12.010

30. Mallette FA, Gaumont-Leclerc MF, Ferbeyre G. The DNA damage signaling pathway is a critical mediator of oncogene-induced senescence. Genes Dev. 2007; 21:43–48. https://doi.org/10.1101/gad.1487307

31. Bartkova J, Rezaei N, Liontos M, Karakaidos P, Kletsas D, Issaeva N, Vassiliou LV, Kolettas E, Niforou K, Zoumpourlis VC, Takaoka M, Nakagawa H, Tort F, et al. Oncogene-induced senescence is part of the tumorigenesis barrier imposed by DNA damage checkpoints. Nature. 2006; 444:633–37. https://doi.org/10.1038/nature05268

32. Di Micco R, Fumagalli M, Cicalese A, Piccinin S, Gasparini P, Luise C, Schurra C, Garre' M, Nuciforo PG, Bensimon A, Maestro R, Pelicci PG, d'Adda di Fagagna F. Oncogene-induced senescence is a DNA damage response triggered by DNA hyper-replication. Nature. 2006; 444:638–42. https://doi.org/10.1038/nature05327

33. Hubackova S, Novakova Z, Krejcikova K, Kosar M, Dobrovolna J, Duskova P, Hanzlikova H, Vancurova M, Barath P, Bartek J, Hodny Z. Regulation of the PML tumor suppressor in drug-induced senescence of human normal and cancer cells by JAK/STAT-mediated signaling. Cell Cycle. 2010; 9:3085–99. https://doi.org/10.4161/cc.9.15.12521

34. Tamiya T, Kashiwagi I, Takahashi R, Yasukawa H, Yoshimura A. Suppressors of cytokine signaling (SOCS) proteins and JAK/STAT pathways: regulation of T-cell inflammation by SOCS1 and SOCS3. Arterioscler Thromb Vasc Biol. 2011; 31:980–85. https://doi.org/10.1161/ATVBAHA.110.207464

35. Bakkenist CJ, Beumer JH, Schmitz JC. ATM serine-1981 phosphorylation is a plausible biomarker. Cell Cycle. 2015; 14:3207–08. https://doi.org/10.1080/15384101.2015.1084205

36. Al Rashid ST, Dellaire G, Cuddihy A, Jalali F, Vaid M, Coackley C, Folkard M, Xu Y, Chen BP, Chen DJ, Lilge L, Prise KM, Bazett Jones DP, Bristow RG. Evidence for the direct binding of phosphorylated p53 to sites of DNA breaks in vivo. Cancer Res. 2005; 65:10810–21. https://doi.org/10.1158/0008-5472.CAN-05-0729

37. Webley K, Bond JA, Jones CJ, Blaydes JP, Craig A, Hupp T, Wynford-Thomas D. Posttranslational modifications of p53 in replicative senescence overlapping but distinct from those induced by DNA damage. Mol Cell Biol. 2000; 20:2803–08. https://doi.org/10.1128/MCB.20.8.2803-2808.2000

38. Zhang XP, Liu F, Wang W. Two-phase dynamics of p53 in the DNA damage response. Proc Natl Acad Sci USA. 2011; 108:8990–95. https://doi.org/10.1073/pnas.1100600108

39. Wang C, Ivanov A, Chen L, Fredericks WJ, Seto E, Rauscher FJ 3rd, Chen J. MDM2 interaction with nuclear corepressor KAP1 contributes to p53 inactivation. EMBO J. 2005; 24:3279–90. https://doi.org/10.1038/sj.emboj.7600791

40. Xue W, Zender L, Miething C, Dickins RA, Hernando E, Krizhanovsky V, Cordon-Cardo C, Lowe SW. Senescence and tumour clearance is triggered by p53 restoration in murine liver carcinomas. Nature. 2007; 445:656–60. https://doi.org/10.1038/nature05529

41. Bouamar H, Jiang D, Wang L, Lin AP, Ortega M, Aguiar RC. MicroRNA 155 control of p53 activity is context dependent and mediated by Aicda and Socs1. Mol Cell Biol. 2015; 35:1329–40. https://doi.org/10.1128/MCB.01446-14

42. Mignacca L, Saint-Germain E, Benoit A, Bourdeau V, Moro A, Ferbeyre G. Sponges against miR-19 and miR-155 reactivate the p53-Socs1 axis in hematopoietic cancers. Cytokine. 2016; 82:80–86. https://doi.org/10.1016/j.cyto.2016.01.015

43. Ron D, Habener JF. CHOP, a novel developmentally regulated nuclear protein that dimerizes with transcription factors C/EBP and LAP and functions as a dominant-negative inhibitor of gene transcription. Genes Dev. 1992; 6:439–53. https://doi.org/10.1101/gad.6.3.439

44. Acosta JC, O'Loghlen A, Banito A, Guijarro MV, Augert A, Raguz S, Fumagalli M, Da Costa M, Brown C, Popov N, Takatsu Y, Melamed J, d'Adda di Fagagna F, et al. Chemokine signaling via the CXCR2 receptor reinforces senescence. Cell. 2008; 133:1006–18. https://doi.org/10.1016/j.cell.2008.03.038

45. Kuilman T, Michaloglou C, Vredeveld LC, Douma S, van Doorn R, Desmet CJ, Aarden LA, Mooi WJ, Peeper DS. Oncogene-induced senescence relayed by an interleukin-dependent inflammatory network. Cell. 2008; 133:1019–31. https://doi.org/10.1016/j.cell.2008.03.039

46. Takekawa M, Tatebayashi K, Itoh F, Adachi M, Imai K, Saito H. Smad-dependent GADD45beta expression mediates delayed activation of p38 MAP kinase by TGF-beta. EMBO J. 2002; 21:6473–82. https://doi.org/10.1093/emboj/cdf643

47. Willers H, McCarthy EE, Wu B, Wunsch H, Tang W, Taghian DG, Xia F, Powell SN. Dissociation of p53-mediated suppression of homologous recombination from G1/S cell cycle checkpoint control. Oncogene. 2000; 19:632–39. https://doi.org/10.1038/sj.onc.1203142

48. Dudenhöffer C, Rohaly G, Will K, Deppert W, Wiesmüller L. Specific mismatch recognition in heteroduplex intermediates by p53 suggests a role in fidelity control of homologous recombination. Mol Cell Biol. 1998; 18:5332–42. https://doi.org/10.1128/MCB.18.9.5332

49. Ferbeyre G, de Stanchina E, Querido E, Baptiste N, Prives C, Lowe SW. PML is induced by oncogenic ras and promotes premature senescence. Genes Dev. 2000; 14:2015–27.

50. Mallette FA, Gaumont-Leclerc MF, Huot G, Ferbeyre G. Myc down-regulation as a mechanism to activate the Rb pathway in STAT5A-induced senescence. J Biol Chem. 2007; 282:34938–44. https://doi.org/10.1074/jbc.M707074200

51. Wang F, Wang R, Li Q, Qu X, Hao Y, Yang J, Zhao H, Wang Q, Li G, Zhang F, Zhang H, Zhou X, Peng X, et al. A transcriptome profile in hepatocellular carcinomas based on integrated analysis of microarray studies. Diagn Pathol. 2017; 12:4. https://doi.org/10.1186/s13000-016-0596-x

52. Gao J, Aksoy BA, Dogrusoz U, Dresdner G, Gross B, Sumer SO, Sun Y, Jacobsen A, Sinha R, Larsson E, Cerami E, Sander C, Schultz N. Integrative analysis of complex cancer genomics and clinical profiles using

the cBioPortal. Sci Signal. 2013; 6:pl1. https://doi.org/10.1126/scisignal.2004088

53. Li B, Dewey CN. RSEM: accurate transcript quantification from RNA-Seq data with or without a reference genome. BMC Bioinformatics. 2011; 12:323. https://doi.org/10.1186/1471-2105-12-323

A

Category	Term	Genes	Count	%	P-Value	Benjamini
SP_PIR_KEY WORDS	Secreted		87	19.7	2.90E-15	1.10E-12
SP_PIR_KEY WORDS	signal		119	26.9	1.70E-10	3.30E-08
SP_PIR_KEY WORDS	glycoprotein		137	31	5.30E-08	7.00E-06
SP_PIR_KEY WORDS	disulfide bond		100	22.6	2.90E-07	2.80E-05
SP_PIR_KEY WORDS	egf-like domain		19	4.3	1.60E-06	1.20E-04
SP_PIR_KEY WORDS	extracellular matrix		18	4.1	1.20E-05	8.10E-04
SP_PIR_KEY WORDS	Growth factor binding		5	1.1	2.70E-04	1.50E-02
SP_PIR_KEY WORDS	cell adhesion		20	4.5	1.40E-03	6.60E-02

B

Genes from "Secreted" group	GENE NAME	Related Genes	Species
Kazal-type serine peptidase inhibitor domain 1	Kazal-type serine peptidase inhibitor domain 1	RG	Homo sapiens
connective tissue growth factor	connective tissue growth factor	RG	Homo sapiens
endothelial cell-specific molecule 1	endothelial cell-specific molecule 1	RG	Homo sapiens
insulin-like growth factor binding protein 3	insulin-like growth factor binding protein 3	RG	Homo sapiens
insulin-like growth factor binding protein 4	insulin-like growth factor binding protein 4	RG	Homo sapiens
insulin-like growth factor binding protein 5	insulin-like growth factor binding protein 5	RG	Homo sapiens
insulin-like growth factor binding protein 6	insulin-like growth factor binding protein 6	RG	Homo sapiens
insulin-like growth factor binding protein 7	insulin-like growth factor binding protein 7	RG	Homo sapiens

C

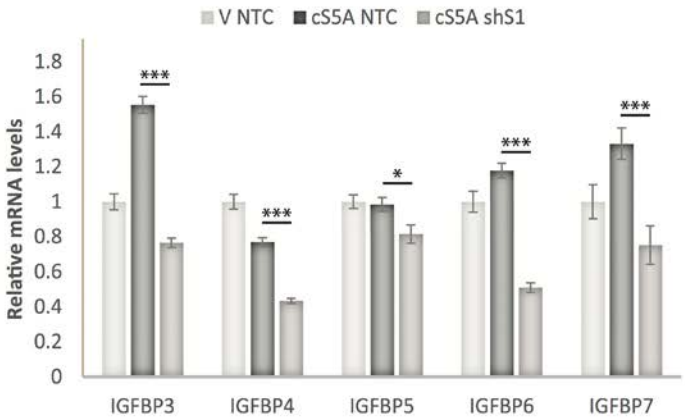

Supplementary Figure S1. David Analysis identifies Secreted proteins as differentially regulated in cells with SOCS1 knockdown. (**A**) DAVID Analysis of Key words category. (**B**) Genes differentially regulated in the "Secreted" category as identified by David Analysis. (**C**) QPCR validation of secreted factors of the IGFBP family identified by David Analysis in IMR90 cells expressing E7 in combination with either an empty vector (V) or with constitutively activated STAT5A (cS5A) and with either a control shRNA (shNTC) or an shRNA against SOCS1 (shS1). All experiments were performed three times, error bars indicate standard errors of triplicates *= p<0.05, using the Student's t test, **=p<0.01, ***=p<0.005.

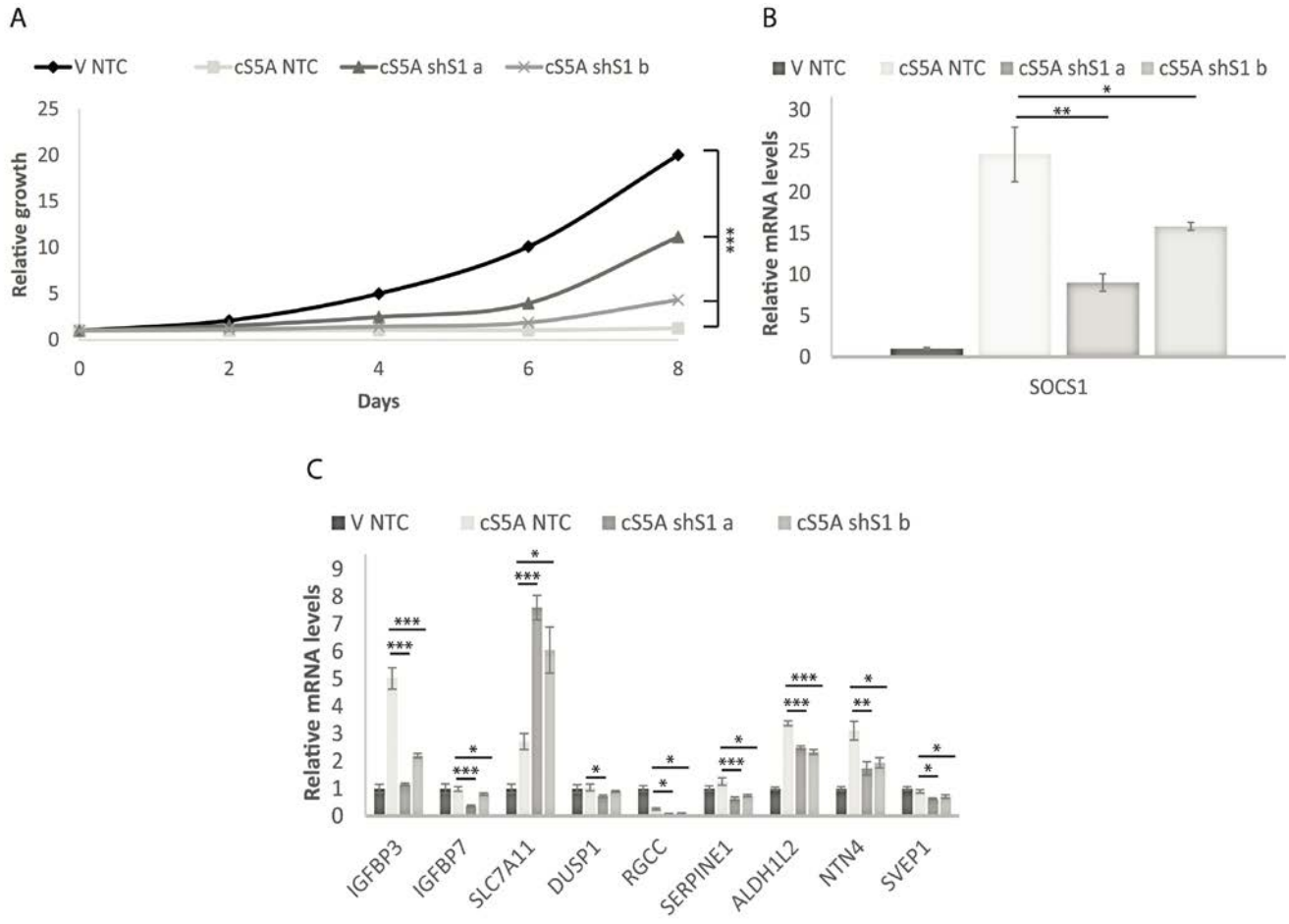

Supplementary Figure S2. Validation of SOCS1-dependent p53 target genes with two shRNAs against SOCS1. (**A**) Growth curves of IMR90 cells expressing E7 with either an empty vector (V) or with constitutively activated STAT5A (cS5A) and with either a control shRNA (NTC) or one of two shRNAs (shS1a or shS1b). (**B**) SOCS1 mRNA levels were measured by qPCR in IMR90 cells expressing the same constructs as described in (A) to assess SOCS1 knockdown efficiency. (**C**) QPCR of SOCS1-dependent p53 target genes in the conditions described previously. All experiments were performed three times, error bars indicate SD of triplicates (growth curves) or standard errors of triplicates (QPCR), *= p<0.05, using the Student's t test, **=p<0.01 and ***=p<0.005.

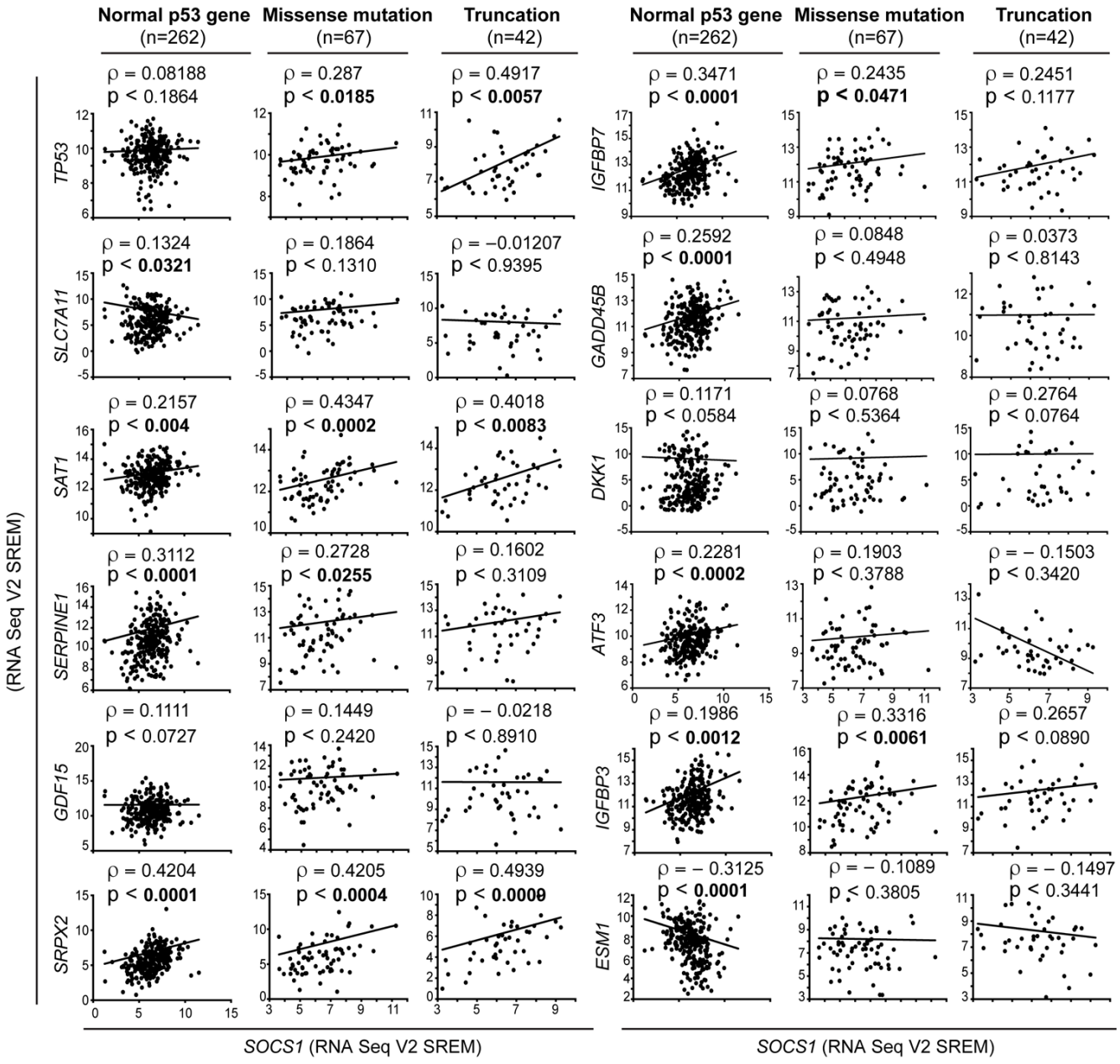

Supplementary Figure S3. Correlation between SOCS1 and p53-target gene expression in hepatocellular carcinoma samples separated according to p53 status. The Spearman correlation (ρ) and the *p* values are given at the top of each plot.

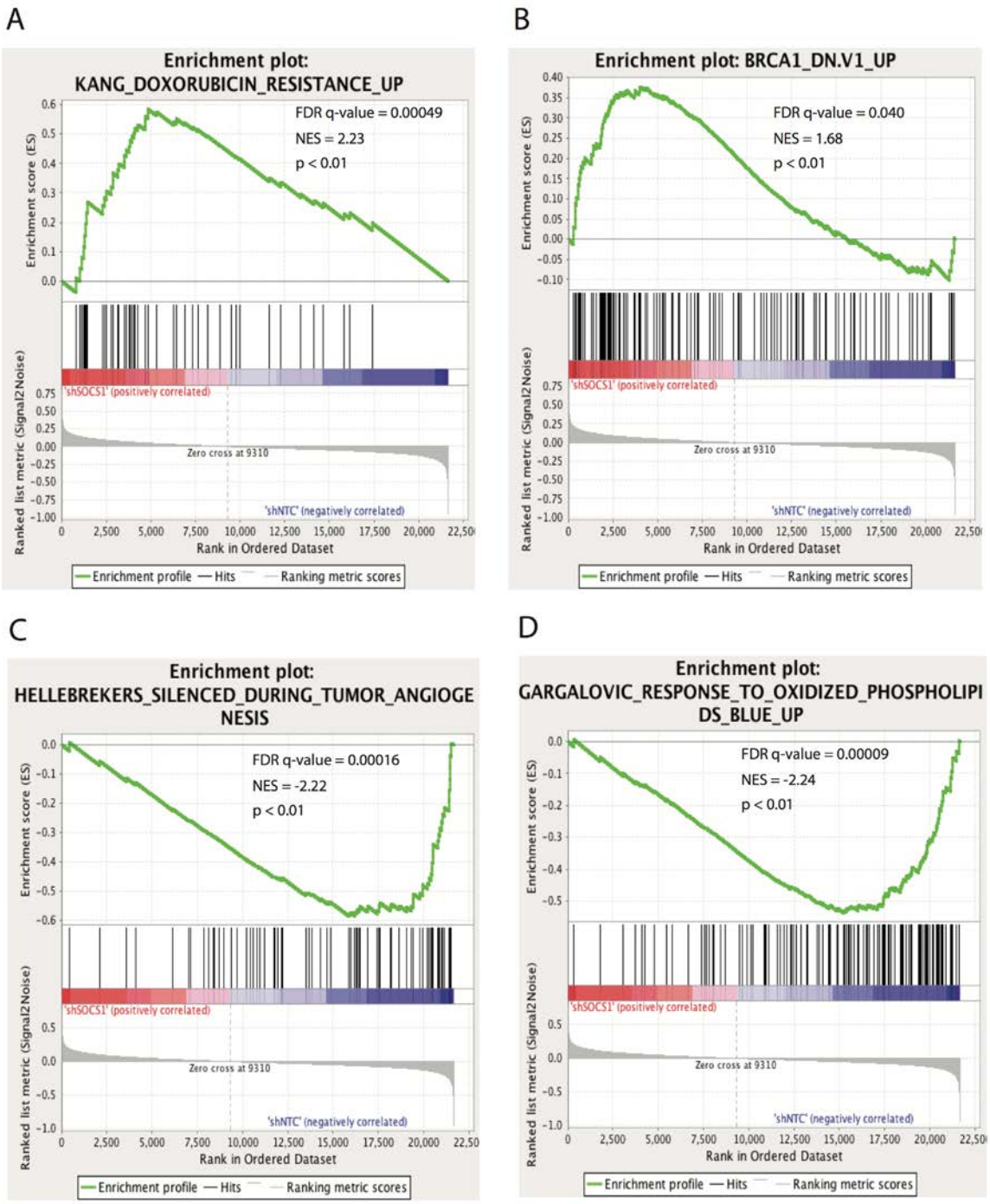

Supplementary Figure S4. GSEA analysis identifies genes sets associated with p53, angiogenesis and lipid oxidation as differentially regulated by SOCS1 knockdown. (**A**) Genes upregulated in a doxorubicin resistance context correlate with genes upregulated in presence of shSOCS1. (**B**) Genes upregulated in a BRCA1 dominant negative context are upregulated in presence of shSOCS1. (**C**) Genes silenced during tumor angiogenesis correlate with genes upregulated in the presence of SOCS1. (**D**) Genes upregulated in response to oxidized phospholipids are enriched in the presence of SOCS1.

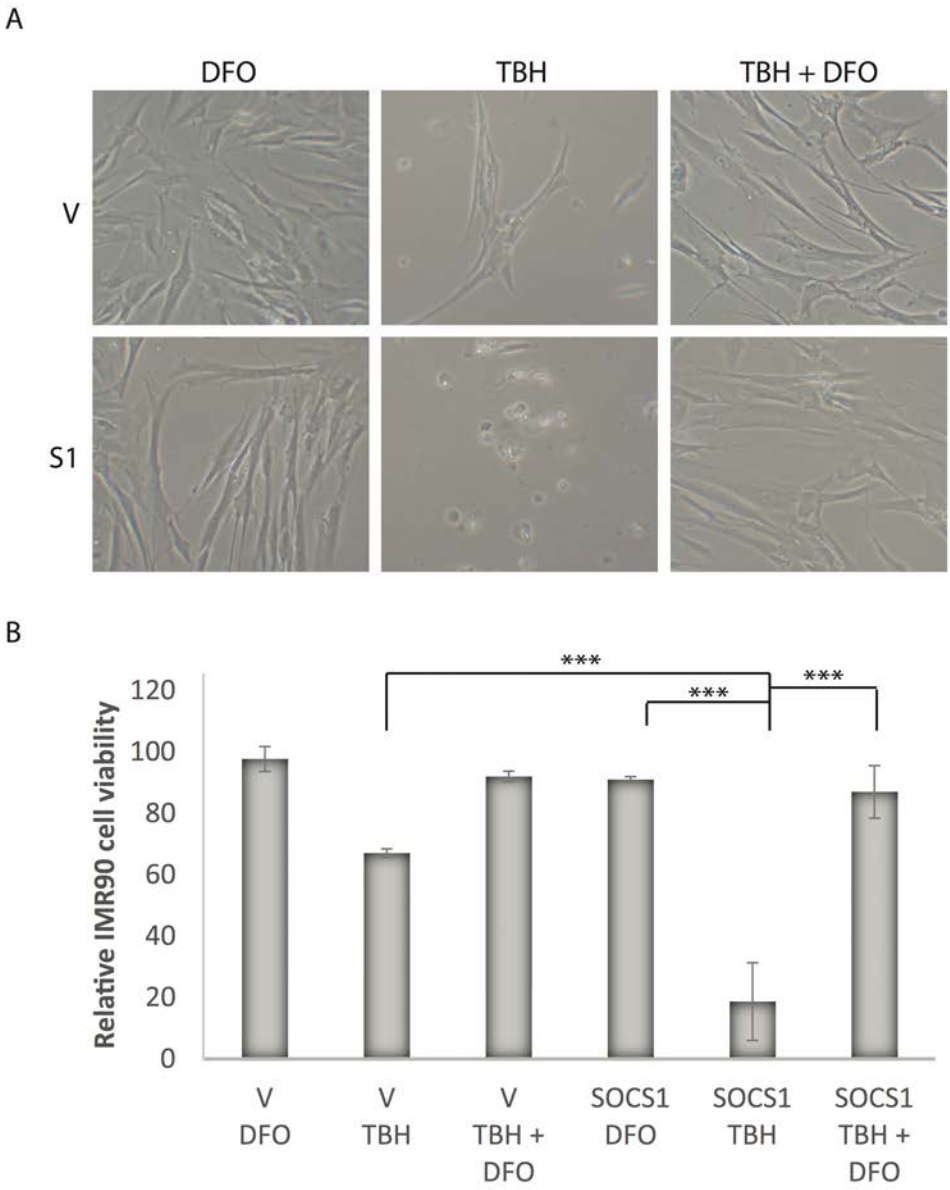

Supplementary Figure S5. DFO rescues TBH-induced ferroptosis in IMR90 cells. (**A**) Representative photos of IMR90 cells expressing either V or S1 by retroviral infection and treated 24 hours after plating with either 88 µM tert-butyl-hydroperoxide (TBH) alone, 100 µM Deferoxamine mesylate (DFO) alone or the combination of both drugs. (**B**) Quantification of cell viability of cells portrayed in A. All experiments were performed three times, error bars indicate SD of triplicates, *= p<0.05, using the Student's t test, **=p<0.01, ***=p<0.005.

Research Paper

Premature aging and cancer development in transgenic mice lacking functional CYLD

Josefa P. Alameda[1,2], Ángel Ramírez[1,2], Rosa A. García-Fernández[3], Manuel Navarro[1,2], Angustias Page[1,2], José C. Segovia[4], Rebeca Sanchez [4], Cristian Suárez-Cabrera[1,2], Jesús M. Paramio[1,2], Ana Bravo[5], M. Jesús Fernández-Aceñero[6], M. Llanos Casanova[1,2]

[1]Molecular Oncology Unit, Centro de Investigaciones Energéticas, Medioambientales y Tecnológicas (CIEMAT)/CIBERONC, 28040 Madrid, Spain
[2]Biomedical Research Institute I+12, 12 de Octubre University Hospital, 28040 Madrid, Spain
[3]Department of Animal Medicine and Surgery, Faculty of Veterinary, UCM, 28040 Madrid, Spain
[4]Division of Hematopoietic Innovative Therapies, CIEMAT/CIBERER/II-FJD, 28040 Madrid, Spain
[5]Department of Anatomy, Animal Production and Veterinary Clinical Sciences, Faculty of Veterinary Medicine, University of Santiago de Compostela, Lugo, Spain
[6]Servicio de Anatomía Patológica Hospital Clínico San Carlos, Departamento de Anatomía Patológica, Facultad de Medicina, UCM, Instituto de Investigación Sanitaria del Hospital Clínico San Carlos (IdISSC), 28040 Madrid, España

Correspondence to: M. Llanos Casanova; **email:** llanos.casanova@ciemat.es
Keywords: CYLD, premature aging, tumor suppressor, NF-κB, keratinocyte differentiation, skin, inflammation.
Received: October 9, 2018 **Accepted:** December 17, 2018 **Published:** January 10, 2019

ABSTRACT

CYLD is a deubiquitinating enzyme known for its role as a tumor suppressor whose mutation leads to skin appendages tumors and other cancers. In this manuscript we report that the tumor suppressor CYLD, similarly to other renowned tumor suppressor genes, protects from premature aging and cancer. We have generated transgenic mice expressing the mutant CYLD$^{C/S}$ protein, lacking its deubiquitinase function, under the control of the keratin 5 promoter, the K5-CYLD$^{C/S}$ mice. These mice express the transgene in different organs, including those considered to be more susceptible to aging, such as skin and thymus. Our results show that K5-CYLD$^{C/S}$ mice exhibit epidermal, hair follicle, and sebaceous gland alterations; and, importantly, they show signs of premature aging from an early age. Typically, 3-month-old K5-CYLD$^{C/S}$ mice exhibit a phenotype characterized by alopecia and kyphosis, and, the histological examination reveals that transgenic mice show signs of accelerated aging in numerous organs such as skin, thymus, pancreas, liver and lung. Additionally, they spontaneously develop tumors of diverse origin. Over-activation of the NF-κB pathway, along with hyperactivation of Akt, JNK and c-Myc, and chronic inflammation, appear as the mechanisms responsible for the premature aging of the K5-CYLD$^{C/S}$ mice.

INTRODUCTION

The *CYLD* gene [1, 2] encodes an enzyme (CYLD) that is ubiquitously expressed and contains a deubiquitinating (DUB) domain at the C-terminus, which removes lysine-63 linked polyubiquitin chains. The first function described for CYLD was the inhibition of the nuclear factor (NF)-κB pathway [1], and mutations that inactivate the carboxyl-terminal deubiquitinating domain of CYLD deregulate the NF-κB activity, leading to the development of skin appendages tumors in patients of familial cylindromatosis [2].

The ubiquitous NF-κB family of transcription factors is composed of dimers of five members, being the predominant dimer in skin p65/p50 [3]. In resting cells NF-κB is maintained inactive and its activation by pro-inflammatory signals (such as cytokines IL-1β and TNF-α in the canonical pathway), results in the phosphorylation and posterior degradation of the inhibitor of NF-κB, IκB, enabling a rapid nuclear entry of the NF-κB dimers, and the consequent activation of specific target genes [3]. NF-κB plays a crucial role in various biological processes, such as immune response and inflammation, and its dysregulated activity leads to the development of various autoimmune disorders, as well as to cancer development [4].

The skin is composed of three layers: epidermis, dermis and hypodermis; and also contains specialized structures, such as hair follicles (HF) and sebaceous and sweat glands. The balance between cell proliferation and differentiation of the epidermis must be maintained in order to preserve their functionality. The HF is a highly sensitive appendage undergoing continuous regeneration throughout life: HFs undergo periodic phases of rapid growth (anagen), apoptosis-driven regression (catagen) and relative quiescence (telogen). HF characteristics associated with each phase are morphologically distinct and distinguishable [5]. Loss of homeostasis of the epidermis and skin appendages leads to numerous skin alterations, such as alopecia, inflammatory diseases and non-melanoma skin cancer (NMSC). Our group and others have described that CYLD acts as a suppressor of the development and progression of the most aggressive form of the NMSC, i.e. skin squamous cell carcinomas (SCC) [6-9]. However, the role that CYLD plays *in vivo* in the epidermis and HF homeostasis has not been fully characterized.

In recent years, several genetic studies have associated the loss of CYLD functionality with the dysregulation of NF-κB, JNK, c-Myc or Akt [10-12] and the development of different types of cancers of high prevalence in the population (multiple myeloma, hepatocarcinomas, lung, breast and gastric cancers, etc.) [13]. Therefore, it seems that CYLD, like other well-known tumor suppressor proteins such as Ink4a, Arf and PTEN, acts as a tumor suppressor in a variety of malignancies. It is interesting that these other renowned tumor suppressors develop important additional roles protecting from aging [14-16]. However, the possible role of CYLD as an aging guard has not been yet investigated.

The dual role of the tumor suppressors protecting from cancer and aging is not surprising, as it has been considered that age is the most significant risk factor for cancer development [17]. It is remarkable that it is widely accepted that the activation of the NF-κB signaling pathway is the driver of aging [18], since the genetic or pharmacological inhibition of NF-κB results in the blocking of aging and even the reversion of tissue characteristics of old mice to those of young mice [19, 20]. Thus, the continuous NF-κB hyperactivation has been directly linked to the aging process [4, 20]; moreover, abnormal NF-κB activation is known to occur in diverse age-associated diseases (diabetes, osteoporosis, neurodegeneration etc.) [4].

It is relevant to mention that although there are many other molecules whose activation have been implicated in pro-aging and longevity processes, such as c-Myc, Akt and JNK, all of them converge in the activation or inhibition of NF-κB signaling pathways respectively [4]. Also, chronic inflammation has been considered as a predominant and recurrent factor that is associated with the process of physiological and pathological aging, and, in this case, NF-κB is also found on the axis of the inflammatory network of aging, since it is activated by innate/inflammatory responses, provoking a host defense mechanism, responsible for the release of SASP (senescence-associated secretory phenotype) molecules, principally IL-6 and TNF-α, which in turn favors the aging process and leads to the activation of many pro-inflammatory signaling pathways, mainly the NF-κB pathway [21, 22].

We reasoned that CYLD, a tumor suppressor that is an inhibitor of NF-κB activation, and consequently of inflammation, could also play an important role against aging. To study this possibility, we have generated a new model of transgenic mice, the K5-CYLD$^{C/S}$ mice, carrying the mutant CYLD$^{C/S}$ construct [6, 9, 23] under the regulatory elements of the keratin 5 (K5). These mice express a mutant CYLD$^{C/S}$ protein defective in its DUB function in the skin and other numerous organs, and our results show that they exhibit signs of accelerated aging from very early ages; they also exhibit inflammation and develop spontaneous tumors in many organs. Therefore, our data indicate that CYLD, like other well-known tumor suppressor genes, also acts as an aging protector. Moreover, we propose that this is an important mechanism through which CYLD exerts its function as a tumor suppressor.

RESULTS

K5-CYLD$^{C/S}$ transgenic mice have an impaired deubiquitination function

We have generated transgenic mice expressing a mutant CYLD protein (defective in the DUB function) under the control of the K5 promoter. The transgenic construct

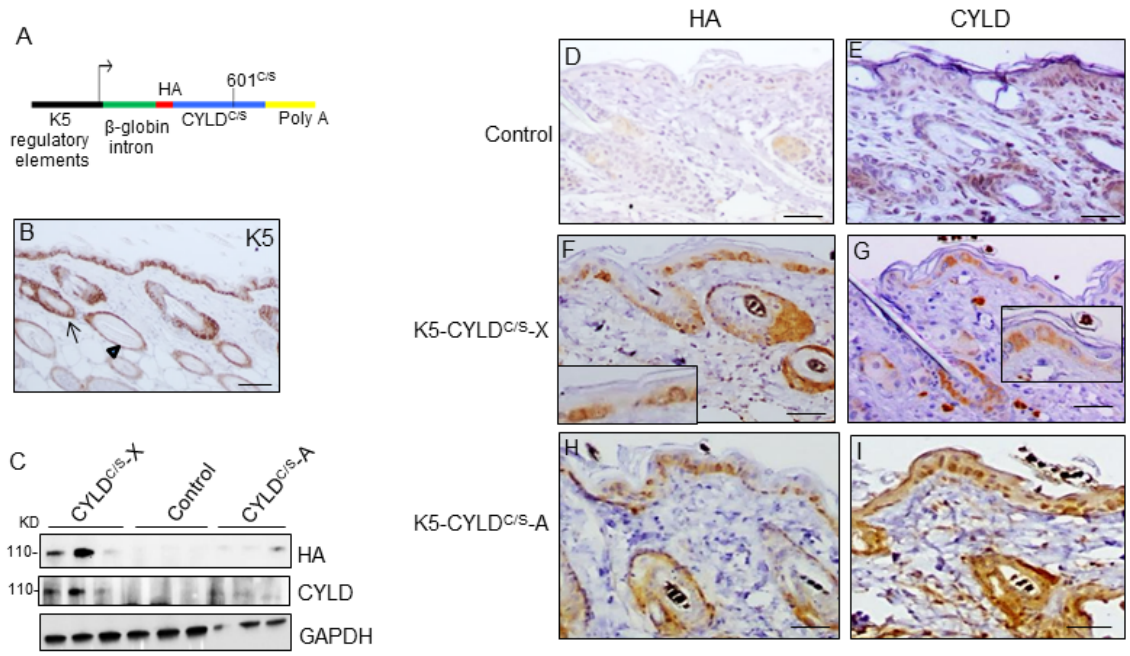

Figure 1. Analysis of the expression of the endogenous and the mutant CYLD protein in the K5-CYLD$^{C/S}$ mice. (**A**) Scheme of the construction used to obtain the K5-CYLD$^{C/S}$ mice. (**B**) Representative image showing the expression of K5 in the back skin of Control mice. Arrow: sebaceous gland; arrow head: ORS. (**C**) Analysis by WB of the expression of HA and CYLD in total protein extracts from the back skin of 30 day-old control and transgenic mice. Both lines of K5-CYLD$^{C/S}$ mice express higher levels of CYLD than Controls. HA was not detected in Control mice. GAPDH was used as a loading control. Immunostaining -with HA (**D, F, H**) and CYLD (**E, G, I**) antibodies- of back skin samples from Control (**D, E**) and transgenic (K5-CYLD$^{C/S}$-X and K5-CYLD$^{C/S}$-A) mice (**F-G, H-I,** respectively). HA is not expressed in Control mice (**D**). In the K5-CYLD$^{C/S}$ mice both, the expression of HA (**F, H)** and CYLD **(G, I)** follows the expression pattern of K5. Scale bars: 250μm (B); 150μm (D-I).

contains a mutant CYLD$^{C/S}$ complementary DNA carrying a 601C/S point mutation in the cysteine box of the DUB domain (Fig. 1A), resulting in a catalytically inactive protein that acts as a dominant negative protein and is able to compete with the endogenous CYLD [2, 6, 9, 23]. The K5 derived sequences included in this construct drive transgene expression to the skin, specially to keratinocytes of the basal layer of the epidermis, the outer root sheath (ORS) of hair follicles, and the mitotically active basal cells of the secretory units that are the source of new secretory sebaceous glands [24] (Fig. 1B). K5 promoter also drives transgenic expression to other organs besides skin, i.e. tongue, palate, thymus, lung, stomach etc. [24] Two independent lines of transgenic mice were obtained, named as K5-CYLD$^{C/S}$-A and K5-CYLD$^{C/S}$-X. We verified by immunoblotting using two different antibodies (against CYLD or against the HA tag contained in the construct), that both lines expressed the transgene, although at different levels (Fig. 1C). The expression of the transgenic protein was also detected *in situ,* by immunohistochemical staining in different tissues (such as back and tail skin and tongue) of both lines of transgenic mice, and we found that it was expressed following the K5 expression pattern (Fig. 1, F-I; Fig. S1). We also checked in both lines of transgenic mice, that, as expected, the CYLD$^{C/S}$ mutant was catalytically inactive and inhibited the DUB function of the endogenous CYLD, as we previously described that occurred in the epidermal HaCaT-CYLD$^{C/S}$ and PDVC57-CYLD$^{C/S}$ cells [6, 9] (Fig. S2). The following analyses were performed in both lines of transgenic mice and obtained similar results.

CYLD controls hair follicle growth cycle

Young transgenic mice appeared normal and healthy; however, they showed an abnormal, untidy hair and patches of diffuse alopecia (Fig. 2A), visible from early age, i.e. 3-month-old mice. In addition, the histology of skin sections showed that while hair follicles in dorsal skin of 1-month-old Control mice had progressed to the anagen phase of the second hair growth cycle (Fig. 2B), as it occurs in normal mice at this age, HF in dorsal skin of 1-month-old transgenic mice remained in the first telogen phase (Fig. 2C). To ascertain whether CYLD had a role in hair follicle homeostasis and/or hair cycling, we depilated the dorsal skin of 7-week-old

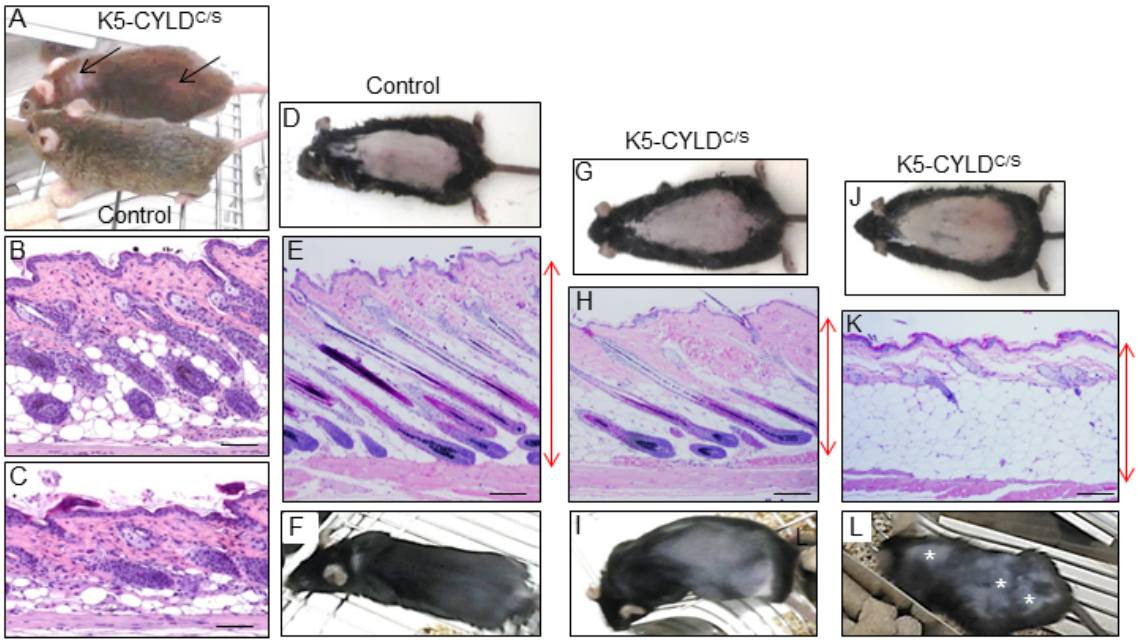

Figure 2. Analysis of the hair regrowth in Control and K5-CYLD$^{C/S}$ mice. (**A**) Representative image of the patches of diffuse alopecia (arrows) of the transgenic mice (7-month-old mice are shown). (**B, C**) Representative images of the skin of 1-month-old mice. (**D-L**) Representative images of a hair growth experiment. The back of 7-week-old mice was shaved and the skin was collected 16 days after depilation. (**D-F**) Hair regrowth in Control mice. (**G-L**) Hair regrowth in the K5-CYLD$^{C/S}$ mice. (**D, G, J**) Representative images of freshly depilated mice of the corresponding phenotypes (day 0 of the experiment). (**E, F**) 16 days after shaving Control HFs were in the anagen-catagen I phase (**E**) and mice exhibited a homogeneous hair regrowth (**F**). (**H**) Histology showing initiation of the anagen phase of the hair cycle 16 days after shaving the back of a transgenic mouse. The macroscopic view of this mouse showed that hair was very short and hardly visible (**I**). (**K**) Histology of a section of the back skin of a K5-CYLD$^{C/S}$ mouse showing a delay in the growth of the new hair, so that 16 days after shaving it still remains in the telogen phase. (**L**) Macroscopically these areas correspond to those lacking hair in the back skin of the transgenic mouse (white asterisks). Red arrows show differences in the thickness of the skin between Control (**E**) and transgenic mice (**H, K**). Scale bars: 280 μm.

mice (depilation allows the study of HF cycle in conditions of fully synchronized anagen [25]). Sixteen days later Control mice exhibited a homogenous short-haired layer (Fig. 2F), corresponding histologically to HF in the anagen-catagen I phase of the hair growth (Fig. 2E), while HFs of K5-CYLD$^{C/S}$ mice had just entered the anagen phase (Fig. 2H) or still remained in the telogen phase (Fig. 2K) and, accordingly, hair was not visible yet or it had grown in a patched form (Fig. 2I and L). These histological differences were also reflected in the decrease in the skin thickness of the transgenic mice. Therefore, these findings indicate that CYLD is a positive stimulator of hair growth and that the DUB function of CYLD is essential for HF anagen induction of the second hair cycle.

K5-CYLD$^{C/S}$ transgenic mice exhibit a premature aging skin phenotype

In addition to diffuse alopecia, young transgenic mice (8-12 months old, and even younger) also showed an abnormal posture, characterized by excessive outward curvature of the spine (kyphosis) (Fig. S3). These features, alopecia and kyphosis in youth, are suggestive of premature aging. To check for the presence of other signs of accelerated aging in the K5-CYLD$^{C/S}$ mice, histological analyses of the skins of mice at different ages were performed, as this organ is one of the first in which the signs of aging manifest (number and age of analyzed mice is showed, Table S1). We observed that at 1 month of age, in addition to the delay in the entry into the second hair growth cycle commented above (Fig. 2C), K5-CYLD$^{C/S}$ mice presented a mild hyperplasia of the sebaceous glands, showing 6-8 mature sebaceous cells (Fig. 3B), versus 3-4 mature sebaceous cells in Control mice (Fig. 3A). Additionally, the interfollicular epidermis tended to be slightly thinner in the transgenic mice (compare Fig. 3D and E), and showed regions of thicker epidermis forming ridges of pyknotic keratinocytes (Fig. 3B and C). At 3 months of age, the skin phenotype of K5-CYLD$^{C/S}$ mice was more obvious, showing a further pronounced thinning

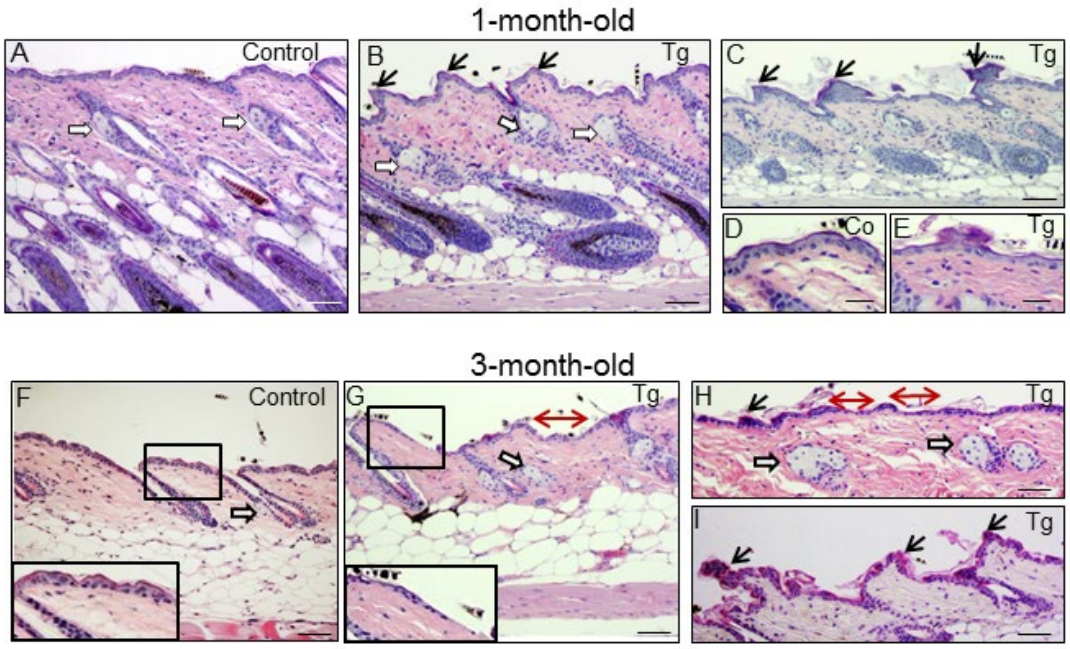

Figure 3. Histological alterations in the back skin of 1 and 3-month-old K5-CYLD$^{C/S}$ mice. (**A-E**) Histology of the back skin of 1-month-old Control (**A, D**) and K5-CYLD$^{C/S}$ mice (**B, C, E**). (**A**) Observe small sebaceous glands (white arrows) and HFs in the anagen phase in Control mice. (**B, C**) Note in transgenic mice the presence of moderately hyperplastic sebaceous glands, epidermal ridges and HFs initiating the anagen phase of the second hair growth cycle. (**D, E**) Slight thinning of the epidermis of K5-CYLD$^{C/S}$ mice. (**F-I**) Histology of the back skin of 3-month-old Control (**F**) and K5-CYLD$^{C/S}$ mice (**G-I**). (**F**) Note small sebaceous glands and telogenic HFs in Control mice. (**G-I**) Observe marked epidermal atrophy; abundant epidermal ridges of pyknotic keratinocytes, increased hyperplasia of the sebaceous glands and areas with orphan sebaceous glands lacking hair follicles in transgenic mice. White arrows: sebaceous glands; black arrows: epidermal ridges of pyknotic keratinocytes; double-headed red arrows: areas of epidermal atrophy. Scale bars: 250 µm (**C, F-H**); 200 µm (**A, B**); 180 µm (**I**); 150 µm (**D, E**).

of the interfollicular epidermis, which presented areas with just one layer of flat keratinocytes, versus the 3 layers usually found in Control mice (compare insets in Fig. 3F and G); the epidermal ridges were more abundant (Fig. 3H and I), and orphan and hyperplasic sebaceous glands, with absence of HF were frequently observed (Fig. 3G and H), being macroscopically coincident with the incipient alopecia observed in the scalp of 3-month-old transgenic mice (not shown). Afterwards, additional young mice of 5- and 8-month-old were analyzed (Fig. 4 A-N; images of both K5-CYLD$^{C/S}$-X and -A mice are shown) and we found that the skin alterations of the transgenic mice were quickly emphasized as the mice grew; thus, 5-month-old K5-CYLD$^{C/S}$ mice exhibited a very prominent phenotype, showing large areas of atrophic interfollicular epidermis in the back skin (Fig. 4B,C,E,I,J) alternating with regions of large epidermal ridges (Fig. 4 E, G) which often form foci of papillomatous hyperplasia, giving the appearance of a thin and wrinkled skin (Fig. 4 C, I, J). Also, transgenic mice showed scarcity of adipose tissue in the hypodermis (compare Fig. 4 F, G), which together with the atrophic epidermis contributes to the thinning of the skin in these mice. In addition, these animals showed an important reduction in the number of hair follicles in the back skin (Fig. 4 B, C, J), as well as abundant hyperplastic and orphan sebaceous glands clustered in the dermis (Fig. 4 C-E; I, L-N). The analysis of the tail skin of the K5-CYLD$^{C/S}$ mice revealed histological alterations similar to those in the back skin, i.e., hyperplasia of sebaceous glands, and thinning of the interfollicular epidermis (Fig. 4 K-N). In addition to these symptoms, the back skin of older transgenic mice (20-month-old) showed a striking lack of adipose tissue and the presence of profuse orphan sebaceous glands (Fig. 5 B-D) which resulted in the development of a severe alopecia of the K5-CYLD$^{C/S}$ mice. Also, aggravation of the phenotypic alterations of the tail skin was detected in the 20-month-old transgenic mice (Fig. 5 F-H); however, 20-month-old Control littermates did not show these alterations neither in the back skin nor in the tail skin (Fig. 5).

Besides back and tail skin, other stratified epithelia of the K5-CYLD$^{C/S}$ mice showed relevant alterations suggestive of early aging; it was the case of the palate,

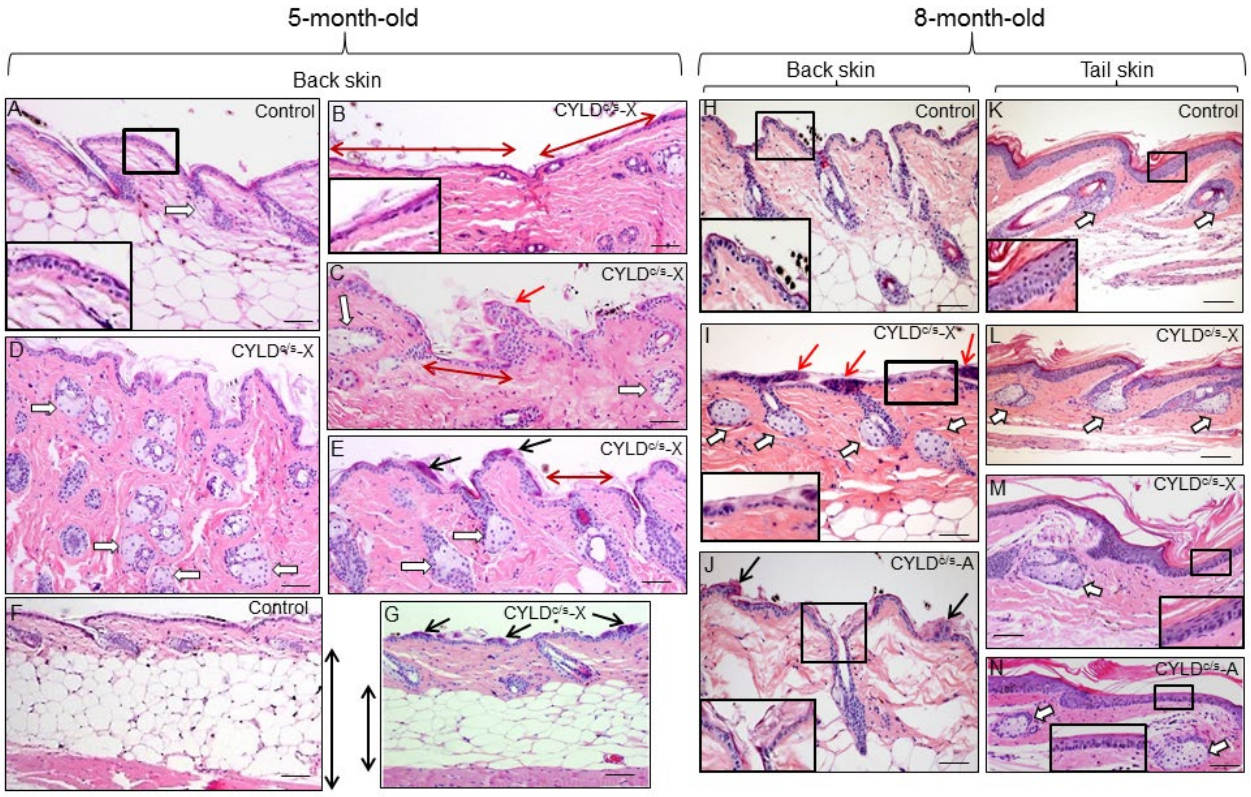

Figure 4. Histopathological signs of premature aging in the back skin of young (5- and 8-month-old) transgenic mice. Representative histology of the back skin of 5-month-old Control and transgenic mice (**A-G**). (**A**) Histology of the back skin of a Control mouse. Observe the presence of small sebaceous glands (white arrow) and 3 layers of keratinocytes in the interfollicular epidermis (higher magnification is showed in the inset). (**B-E**) The epidermis of the K5-CYLD$^{C/S}$ mice shows frequent and extensive areas of atrophy (double-headed red arrows in **B** and **C**; also compare the inset in **B** with that of **A**); as well as papillomatous hyperplasia (red arrow in **C**) and epidermal ridges (black arrows in **E** and **G**). Abundant hyperplastic sebaceous glands -often orphan, were detected (white arrows in **C-E**). (**F-G**) Observe the scarce adipose tissue present in the skin of the transgenic mice (compare the length of the double-headed black arrows). Representative histology of the back skin of Control (**H**) and transgenic mice (**I, J**) of 8-month-old. Observe in the K5-CYLD$^{C/S}$ mice the presence of papillomatous hyperplasia (red arrows in **I**); epidermal ridges (black arrows in **J**); abundant hyperplastic sebaceous glands (white arrows), some of them orphan (without HF) (**I**), and patchy epidermal atrophy associated to moderate hyperkeratosis (compare the inset in **H** with those of **I** and **J**). Representative histological images of the tail skin of Control (**K**) and transgenic mice (**L-N**). Note in the skin of transgenic mice the presence of hyperplastic sebaceous glands, most of them orphan (white arrows), and epidermal atrophy (compare the insets in **K** with those of **M** and **N**). Images of the histology of both K5-CYLD$^{C/S}$-X and K5-CYLD$^{C/S}$-A are shown. White arrows, sebaceous glands; black arrows: epidermal ridges; double-headed red arrows: areas of epidermal atrophy. Scale bars: 150 μm (**C, E**); 180 μm (**A, B, D, I, J, L-N**); 200 μm (**H, K**) and (**F, G**) 350 μm.

tongue and plantar skin; the epithelia of the snout and eyelids; also, the Meibomian glands presented a marked hyperplasia (Fig. S4).

Therefore, the signs of aging found in the skin of the K5-CYLD$^{C/S}$ mice from 1 month of age can be considered characteristics of premature aging, as they were not manifested in the skin of Control mice until they were over 24 or 28 months old, suggesting that CYLD protects from aging. To further reinforce our findings, we analyzed the level of expression of classical molecular markers of aging, i.e., p16 and p19, and found that these were elevated in the skin of the K5-CYLD$^{C/S}$ mice (Fig. 5I); which strengthen our observations about the accelerated aging of the transgenic mice, since the levels of p16INK4a (and, to a lower extent, also p19ARF) increase with aging in almost all tissues analyzed both in mice and humans [26, 27]. Moreover, we analyzed levels of γH2AX, a molecular marker of DSBs, whose elevation has been proposed as a molecular marker of aging [28], and found that levels of γH2AX were also increased in the skin of the K5-CYLD$^{C/S}$ mice (Fig. 5J).

Additionally, we have analyzed the level of expression of CYLD in the skin of Control mice at different ages

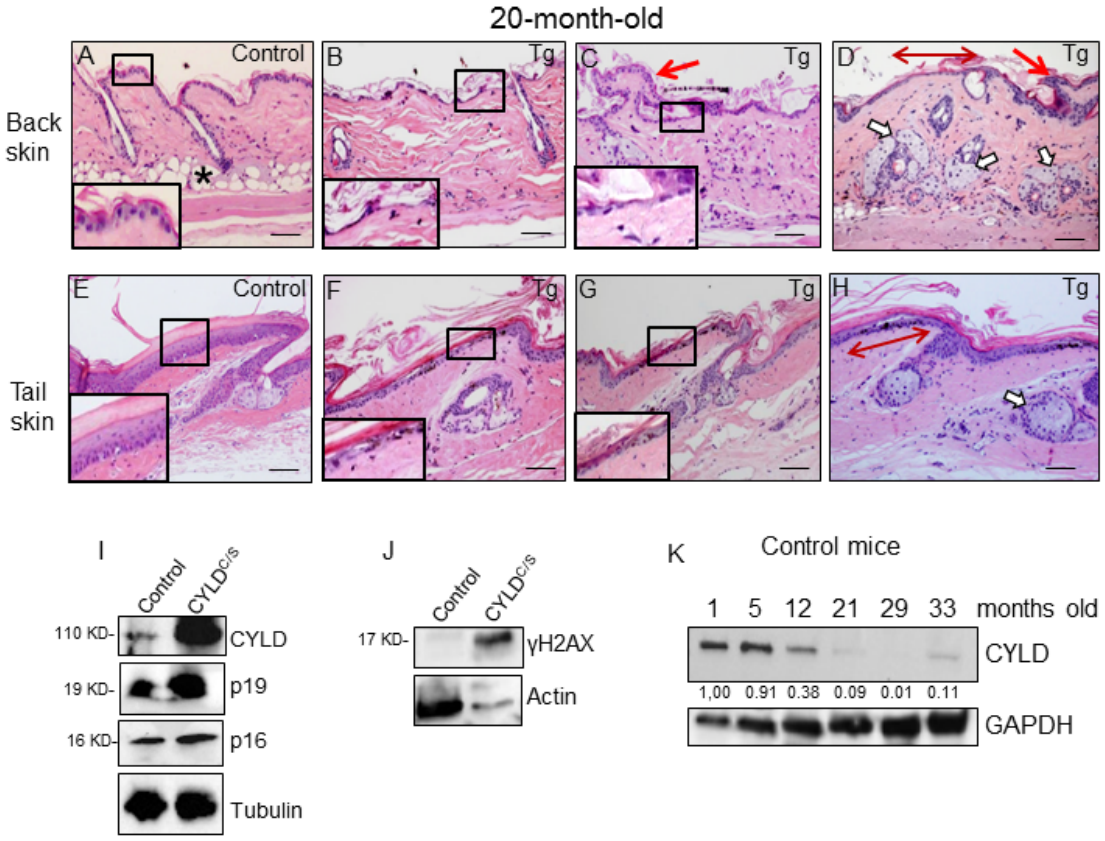

Figure 5. Histological and molecular signs of premature aging in the back skin of transgenic mice. (**A-H**) Representative histological images showing the back skin of 20-month-old Control mice (**A**) and the severe aging phenotype of the back skin of 20-month-old transgenic mice (**B-D**). (**B-D**) Note severe epidermal atrophy (compare insets in **A** with those of **B** and **C**; double-headed red arrow in **D**); foci of papillomatous hyperplasia (red arrows in **C** and **D**); numerous hyperplastic sebaceous glands, most of them orphan and grouped in the dermis (**D**); reduced number of HFs, and scarce or even lack of adipose tissue (compare **A** with **B-D**) in the back skin of the K5-CYLD$^{C/S}$ mice. (**E-H**) Tail skin of Control (**E**) and transgenic (**F-H**) mice. Note the presence of hyperplastic sebaceous glands and extensive epidermal atrophy (compare inset in **E** with those in **F** and **G**) in the tail of the K5-CYLD$^{C/S}$ mice. (**I, J**) WB of total protein extracts from skin of 12-month-old (**I**) and 6-month-old (**J**) showing elevated levels of p16, p19 and γH2AX in the K5-CYLD$^{C/S}$ mice. Tubulin and Actin are used as control loading. (**K**) WB of total protein extracts from the skin of Control mice from 1 to 33 months of age showing the decreased expression of CYLD as mice age. GAPDH is used as a control loading. White arrows: sebaceous glands; red arrows: papillomatous hyperplasia; double-headed red arrows: areas of epidermal atrophy. Scale bars: 250 µm (**A-D**); 200 µm (**E-H**).

and found an important decrease in the amount of CYLD protein with aging, i.e. there was a diminished expression of CYLD in the skin of 12 month-old mice respect to that observed in younger mice (1-month-old); and, in aged mice (from 21-month-old), the expression of CYLD was hardly detected, being observed a decrease of more than 10 fold in the expression levels of CYLD (Fig. 5K). Therefore, all these results support the role of CYLD as a suppressor of aging in the skin.

Impaired differentiation of the epidermis of K5-CYLD$^{C/S}$ mice

The analysis of the proliferation rate in the skin showed increased levels of BrdU and Ki67 staining in the sebaceous glands of K5-CYLD$^{C/S}$ mice (Fig. S5; S6 and S7), which is in accordance with its hyperplastic condition. No differences in apoptosis were found (measured by Caspase 3 cleaved immunostaining; data not shown). We then analyzed whether the differentiation of the epidermis of the K5-CYLD$^{C/S}$ mice was affected by the lack of the DUB function of CYLD. The immunohistochemical examination of the early (K10, involucrin) and late (loricrin and filaggrin) differentiation markers showed a continuous and strong staining for all these markers in the suprabasal layers of the epidermis of Control mice; by contrast, the skin of K5-CYLD$^{C/S}$ mice showed a pattern of discontinuous and scarce staining (Fig. 6 A-H). This deficiency in the epidermal differentiation of the skin of transgenic mice

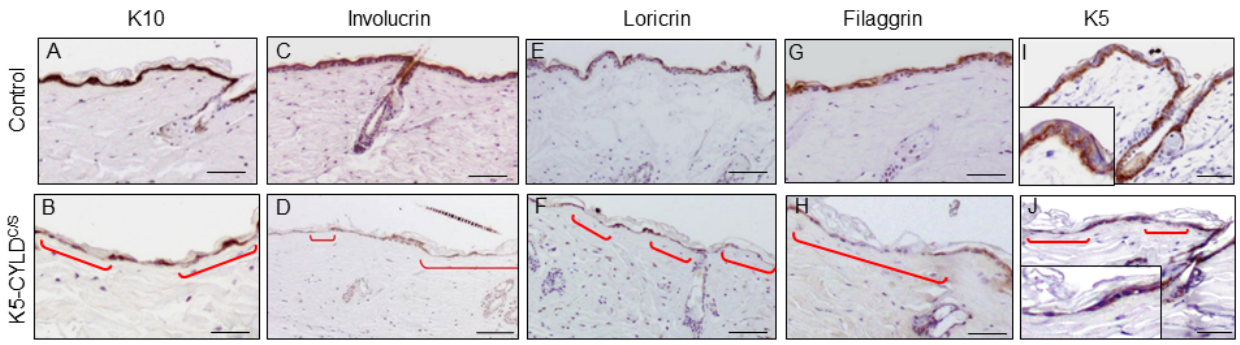

Figure 6. Deficient differentiation in the skin of K5-CYLD$^{C/S}$ mice. Representative immunostainings of the back skin of 20-month-old mice (**A-J**). Observe the strong expression of the epidermal differentiation proteins Involucrin, Loricrin and Filaggrin in the suprabasal layers of the epidermis of Control mice (**A,C,E,G**); and the weak and discontinuous expression of these proteins in the epidermis of K5-CYLD$^{C/S}$ mice (**B,D,F,H**), specially faint in the areas of epidermal atrophy (red brackets). (**I, J**) Representative images corresponding to the immunostaining of the back skin of Control (**I**) and transgenic (**J**) mice with the K5 specific antibody. (**I**) Strong K5 staining in basal keratinocytes of Control mice. A faint and patched expression is detected in the epidermis of the transgenic mice, especially in the regions of atrophic epidermis (indicated by red brackets). Scale bars: 180 μm (**A-H**); 150 μm (**I, J**).

was also confirmed by a semiquantitative analysis of the expression of these differentiation markers (Fig. S8). In addition, K5 staining of the basal layer of the epidermis of transgenic mice was also abnormal, showing areas of positive staining containing flat keratinocytes, with nuclei parallel to the basal membrane, alternating with no-staining skin, in which almost no keratinocytes were detected (Fig. 6J). This K5 staining pattern contrasted greatly with the continuous K5 expression found in the basal layer of the epidermis of Control littermates (Fig. 6I). Therefore, our results suggest that the atrophic skin of the transgenic mice is linked to alterations in the morphology of the basal keratinocytes and the impairment of the early and terminal epidermal differentiation.

The skin of K5-CYLD$^{C/S}$ transgenic mice displays chronic activation of NF-κB and other pro-aging pathways, along with increased inflammation

Searching for the mechanisms responsible for the premature aging of the skin of K5-CYLD$^{C/S}$ mice, we first studied the activation of the NF-κB signaling in the skin of 3-day-old mice and found that in the unstimulated, basal state, transgenic mice showed increased activation of NF-κB (measured as P-p65 levels), as well as a long-lasting activation after 40 minutes of treatment with TNF-α (Fig. 7A). To analyze whether the hyperactivation of NF-κB occurred only in newborn mice, coinciding with a rapid skin growth, we analyzed the activation of NF-κB in the skin of older mice (20-month-old), and found that P-p65 was also increased in these transgenic mice (Fig. 7B). In addition, elevated phosphorylation of the inhibitor of NF-κB, IκBα, was detected (Fig. 7B), which may also contribute to the increased levels of P-p65 observed. Thus, our results indicate that the skin of transgenic mice exhibit a constitutive activation of the NF-κB canonical pathway, from birth to advanced age. Since a relevant mechanism through which NF-κB activation promotes aging is by upregulating the expression of inflammatory cytokines, we analyzed by Western blot the expression of IL-6 and TNF-α in skin and found that they were significantly increased in that of transgenic mice (Fig. 7C); in addition, they were also increased in the serum of the K5-CYLD$^{C/S}$ mice, mainly IL6 (Fig. S9). Although NF-κB activation is the main regulator of aging, it has been described that the activation of other pathways, which in turn feeds the NF-κB activation, such as Akt, JNK and c-Myc, also favors aging. In agreement with the reported negative regulation of JNK and c-Myc activation by CYLD [29], WB analysis of these molecules showed increased Akt, JNK and c-Myc activation (measured as levels of P-Akt, P-JNK and P-c-Myc respectively) in the skin of transgenic mice lacking the DUB function (Fig. 7 D-F).

K5-CYLD$^{C/S}$ transgenic mice exhibit a premature aging of thymus

Together with the skin, other organ that is highly susceptible to premature aging is the thymus [19]. As the K5 promoter also drives transgene expression to this organ [24], we first analyzed whether the transgene was expressed in the thymus of the K5-CYLD$^{C/S}$ mice, and found that it was mainly detected in the epithelial cells of the medullar area (Fig. 8B) of the thymus, coincident with the pattern of expression of K5 in this organ (Fig. 8C); WB also confirmed the expression of the transgene in the thymus of the K5-CYLD$^{C/S}$ mice (Fig. 8D). Then,

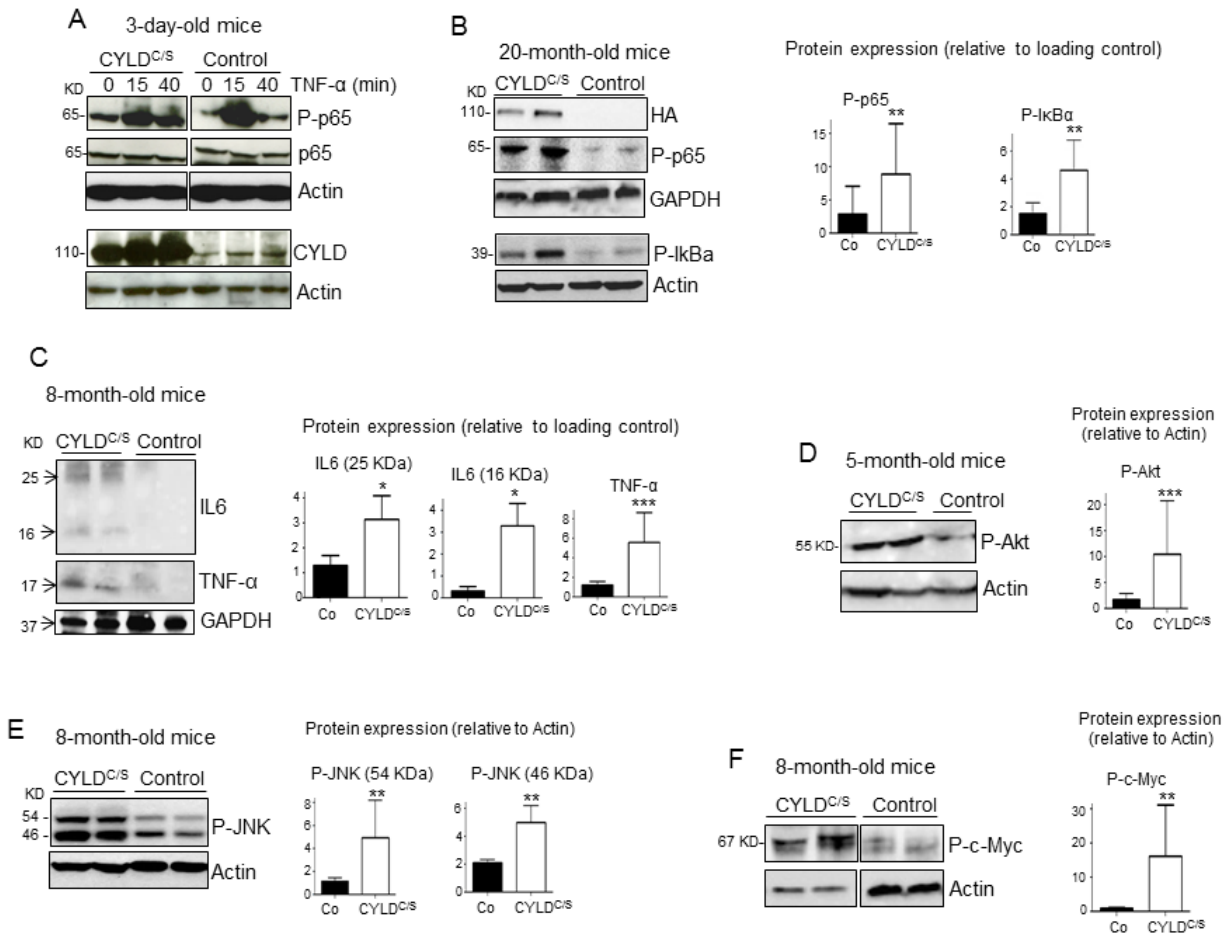

Figure 7. Overactivation of the NF-κB, and other pro-aging pathways, along with increased IL6 and TNF-α expression in the skin of the K5-CYLD$^{C/S}$ mice. (**A**) p65 and IκBα phosphorylation kinetics in the back skin of 3-day-old Control and transgenic mice treated with TNF-α for the indicated times. (**B**) WB showing over-activation of the classical NF-κB signaling pathway (P-p65 and P-IκBα) in the skin of 20-month-old transgenic mice. (**C**) Increased expression of the inflammatory cytokines TNF-α and IL6 in the skin of the K5-CYLD$^{C/S}$ mice. (**D-F**) WB showing the hyperactivation (phosphorylation) of Akt (**D**), JNK (**E**) and c-Myc (**F**) in the skin of adult K5-CYLD$^{C/S}$ mice. Graphic representations of the densitometric analysis of western blots corresponding to extracts from 5-7 animals of each genotype are shown. Mann-Whitney U test was used for statistical analysis. (*p<0.05; **p<0.01; ***p<0.001).

we performed a histological analysis of the thymus at different ages (see Table S2) and found that in very young animals (2.5-months-old) alterations suggestive of premature aging took place. These changes consisted in the expansion of the cortical area, while a reduction of the medullar region occurred (Fig. 8F). Moreover, in 3.5 months-old transgenic mice an involution of the thymus was observed, as reflected by the atrophy of the organ and the infiltration of fat cells at expense of thymic tissue; by contrast, thymic involution was not observed in the thymus of aged-matched Control littermates (Fig. 8G and H), being the involution of the thymus considered as one of the most characteristic changes of the aging immune system [30, 31]. Since the NF-κB pathway has been shown to be critically involved in thymic aging [32], we analyzed NF-κB activation by WB and found that it was overactivated in the thymus of the K5-CYLD$^{C/S}$ mice (Fig. 8D), suggesting that, as in the skin, the overactivation of NF-κB in the thymus could explain the accelerated aging of this organ. To further reinforce our findings, we analyzed the level of expression of CYLD in the thymus of Control mice at different ages and found that it decreases with aging, mainly from 7 months of age (Fig. 8I), reinforcing our finding of the role of CYLD as a protector of aging in the thymus.

K5-CYLD$^{C/S}$ mice exhibit inflammation and other signals of premature aging in further organs

We found that, in addition to skin and thymus, K5-CYLD$^{C/S}$ mice displayed signs of premature aging in

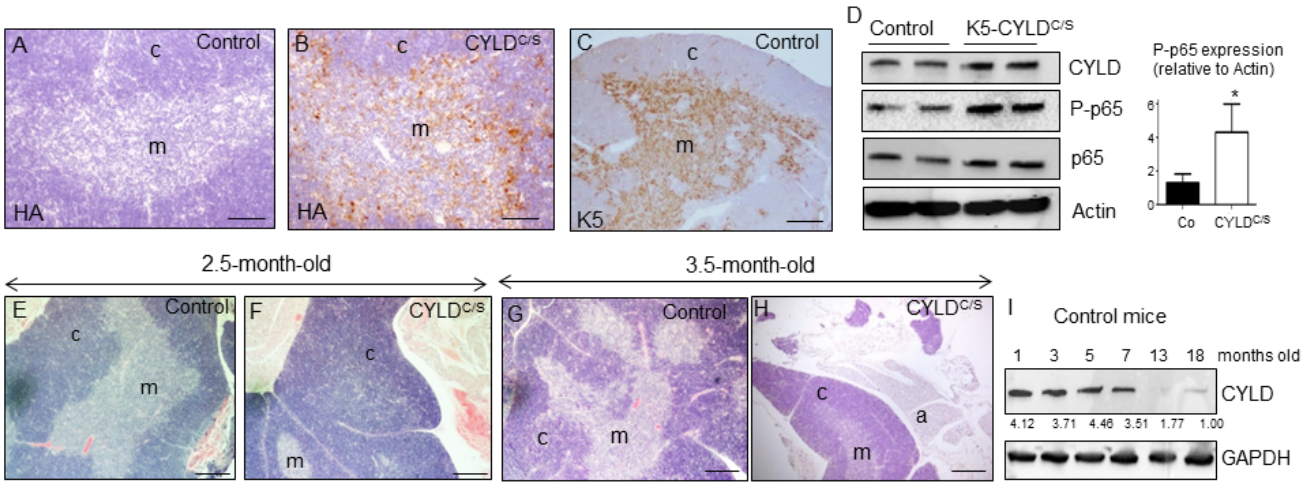

Figure 8. Premature thymic involution and over-activation of NF-κB in the thymus of K5-CYLD$^{C/S}$ mice. (**A-C**) Analysis of the expression of the transgene by immunostaining with a specific antibody against the HA tag. Expression of HA is detected in the medulla of the thymus of the K5-CYLD$^{C/S}$ mice (**B**), following the expression pattern of the K5 (**C**), while it is not detected in the Controls (**A**). (**D**) Analysis by WB of the expression of the transgene in protein extracts from isolated thymic cells of mice of 3.5-month-old. Note the overactivation of NF-κB (increased levels of P-p65) in the K5-CYLD$^{C/S}$ mice. Mann-Whitney U test was used for statistical analysis. (*p<0.05). (**E, F**) Histological analysis of the thymus of 2.5-month-old mice. Observe the expansion of the cortical zone and reduction of the medullar region in the thymus of transgenic mice (**F**). (**G, H**) H&E staining of 3.5-month-old Control (**G**) and K5-CYLD$^{C/S}$ mice (**H**) thymus. A representative image of the thymic atrophy and infiltration of white adipose tissue in the thymus of transgenic mice (**H**) is shown. (**I**) Western blot showing the decreased expression of CYLD with age in the thymus of control mice. M, medulla. C, cortex. a, adipose tissue. Scale bars: 200 µm (**A, B**); 300 µm (**C**); 350 µm (**E-H**).

other organs. Among them, it was remarkable the accelerated aging of the pancreas, liver, lung and stomach (Fig. 9). Features of early aging of the pancreas in the transgenic mice are the presence of huge islets of Langerhans detected in transgenic mice from 5-month-old (Fig. 9B, C and G), often observed in extrapancreatic locations, i.e. in the peripancreatic fat (Fig. 9D), and the mild chronic inflammation detected even in young mice (since 3-months-old) [33] (Fig. 9H). The liver of transgenic mice also exhibited marked aging-related lesions such as anisokaryosis, anisocytosis, karyomegalia, and inter- and- intranuclear eosinophilic inclusions (Fig. 9I-K) as well as mild to moderate inflammation, i.e., multifocal chronic hepatitis (Fig. 9L). These alterations were not found in the liver of aged-matched Control littermates, with the exception of inflammatory cells that were sometimes detected, although in lower numbers than those found in the liver of transgenic mice (data not shown). Lungs of K5-CYLD$^{C/S}$ mice showed moderate inflammation, consisting in BALT (Broncus Associated Lymphoid Tissues) hyperplasia, which is typically found in lung of

Table 1. Number of tumors spontaneously developed in the K5-CYLD$^{C/S}$ mice.

Genotype	Skin and HF Tumors	Lung ADC	Gastric ADC	Gastric Carcinoma *in situ*	HCC	Mammary ADC
Control	0/10	0/6	0/7	0/7	0/6	0/1
K5-CYLD$^{C/S}$	2/10	4/6	3/8	1/8	2/6	1/2

Number of animals that have developed each type of tumor, as well as the number of mice that has been analyzed is shown. Mice of 8-29 months of age were analyzed.

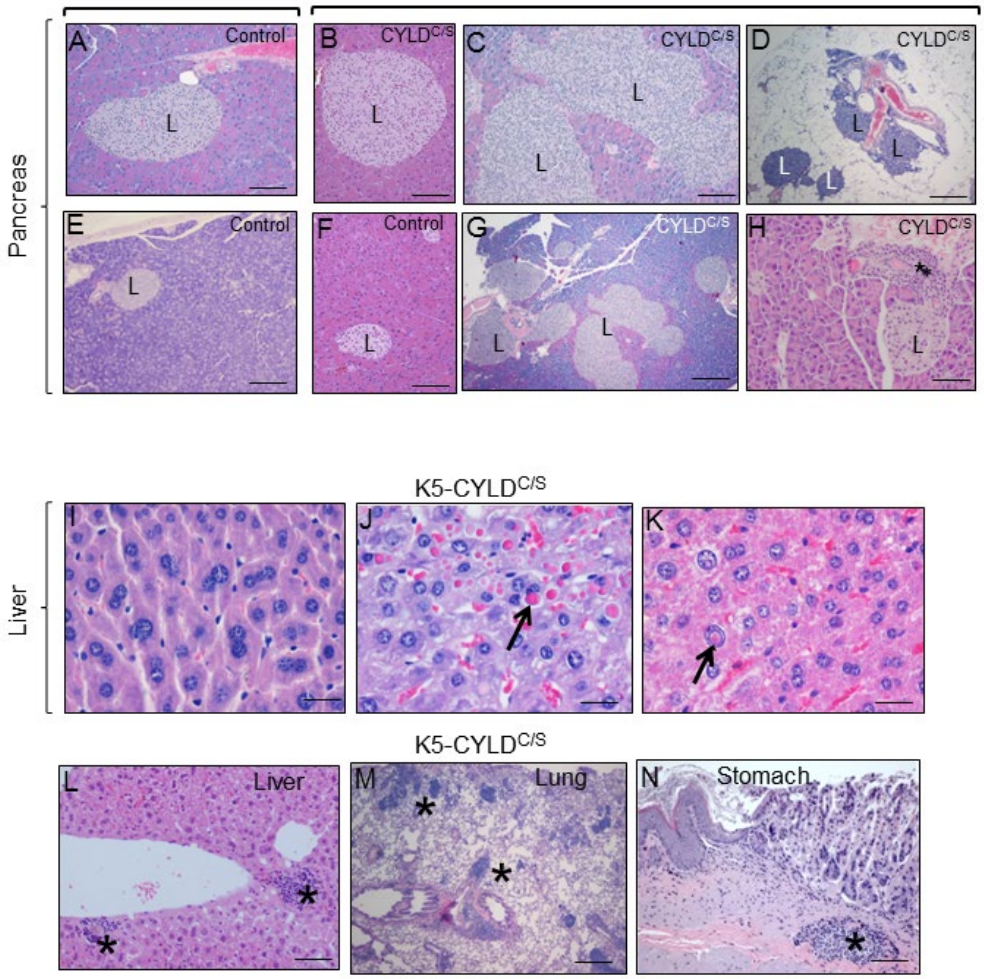

Figure 9. **Alterations found in the pancreas, liver, lung and stomach of the K5-CYLD$^{C/S}$ mice suggestive of early aging of the K5-CYLD$^{C/S}$ mice**. (**A-H**) Histopathologic analysis by H&E staining of pancreas from 5-month-old (**B**, **F**) and 12-month-old Control and transgenic mice. (**A, E, F**) Pancreas from Control mice: note the presence of Islets of Langerhans (L) of heterogeneous but moderate size. (**B-D; G, H**) Histology sections representatives of pancreas from K5-CYLD$^{C/S}$ mice. Note the hyperplasia of the Islets of Langerhans (**B, C, G, H**). (**D**) Extrapancreatic location of the Islets of Langerhans, in the peripancreatic fat, observed in the K5-CYLD$^{C/S}$ mice. (**H**) Foci of inflammation (asterisk) in the pancreas of K5-CYLD$^{C/S}$ mice. (**I-N**) Histopathological analysis of liver, lung and stomach sections from different organs of 20-month-old K5-CYLD$^{C/S}$ mice. (**I-K**) Representative images showing anisokariosis (**I**), eosinophilic intracytoplasmic inclusions (arrow in **J**), intranuclear eosinophilic inclusions (arrow in **K**), and inflammation foci (asterisks in **L**) in the liver. (**M**) Example of inflammation foci observed in the lung. (**N**) Stomach with an inflammation focus. The pancreas of 4 Control and 4 transgenic mice of 5- and 12-month-old were analyzed. Number of animals whose liver, lung and stomach has been analyzed is showed in Table 1. Asterisks: Inflammation. Scale bars: 250 µm (**A, B, D-F**); 350 µm (**C**); 500 µm (**G**); 150 µm (**H; L-N**); 40 µm (**I-K**).

elderly mice, but it was observed in young transgenic mice (Fig. 9M); by contrast, Control age-matched littermates showed only a discrete inflammation in the lungs (not shown). Other organ showing evident lymphocyte infiltration was the stomach of K5-CYLD$^{C/S}$ mice (Fig. 9N). Therefore, our results, showing several histological signs of aging in many organs of the transgenic mice, along with the chronic inflammation detected in those organs suggest that K5-CYLD$^{C/S}$ mice undergo a systemic premature aging.

Aged K5-CYLD$^{C/S}$ transgenic mice develop tumors in many organs

An important consequence of aging is the development of cancer [34]. Thus, a further confirmation of the premature aging of the K5-CYLD$^{C/S}$ mice was the observation that transgenic animals (of both lines) develop spontaneous tumors of diverse origin when they reached about 8 months of age, while tumors were not detected in Control mice of similar age. The number

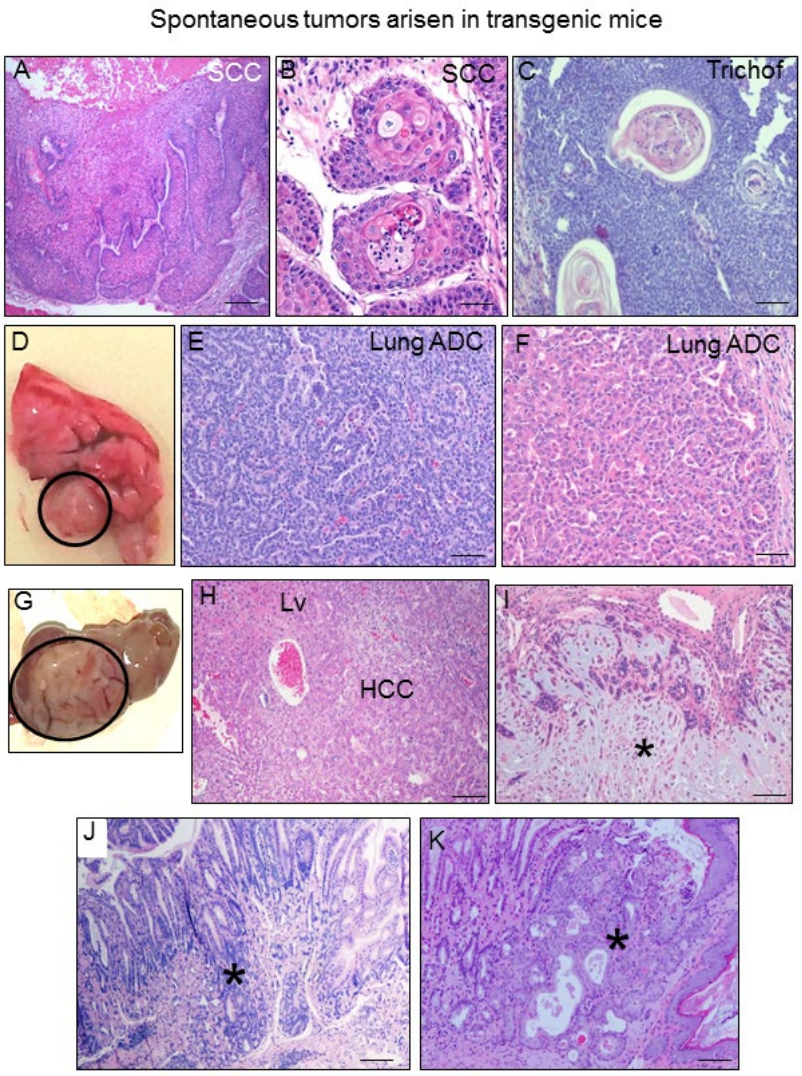

Figure 10. **K5-CYLD$^{C/S}$ mice develop spontaneous tumors in many organs**. (**A-C**) Skin tumors. Infiltrating SCC arisen in the back skin of 8-month-old transgenic mouse (**A, B**). (**C**) Hair follicle derived tumor (trichofolliculoma) developed in the snout of a K5-CYLD$^{C/S}$ mouse. (**D**) Macroscopic appearance of a lung adenocarcinoma. (**E**) Lung acinar adenocarcinoma. (**F**) Lung papillary adenocarcinoma. (**G, H**) Hepatocellular carcinoma (HCC); liver (Lv). (**I**) Mammary adenoepithelioma (asterisk). (**J**) Well differentiated gastric adenocarcinoma (asterisk). (**K**) *In situ* gastric carcinoma (asterisk). Scale bars: 500 µm (**A**); 300 µm (**C, J, K**); 200 µm (**E, F**); 250 µm (**H, J**); 100 µm (**B**).

of tumors originated in K5-CYLD$^{C/S}$ mice is summarized (Table 1). We observed the development of skin tumors, such as a squamous cell carcinoma (Fig. 10A and B) and a hair follicle-derived tumor (trichofolliculoma) (Fig. 10C). Pulmonary adenocarcinomas (acinar ADC and papillary-predominant ADC) were also detected (Fig. 10D-F). A differentiated hepatocellular carcinoma (HCC) and a hepatocellular adenoma were also found in two transgenic mice (Fig. 10G and H). K5-CYLD$^{C/S}$ mice also exhibited well differentiated gastric adenocarcinomas (Fig. 10J) and one *in situ* gastric carcinoma (Fig. 10K). Other tumor less frequently developed in K5-CYLD$^{C/S}$ mice was a mammary adenomyoepithelioma (Fig. 10I). These findings indicate that the lack of the DUB function of CYLD makes transgenic mice more susceptible to the development of tumors, confirming *in vivo* the role of *Cyld* as a tumor suppressor gene in distinct organs.

Next, we performed immunostaining with the specific HA antibody to examine whether the transgene was expressed in these tumors; our data showed that the transgene was expressed in all tumors- as well as in the corresponding non tumoral tissues- except for the HCC, in which the transgene was not detected (Fig. 11).

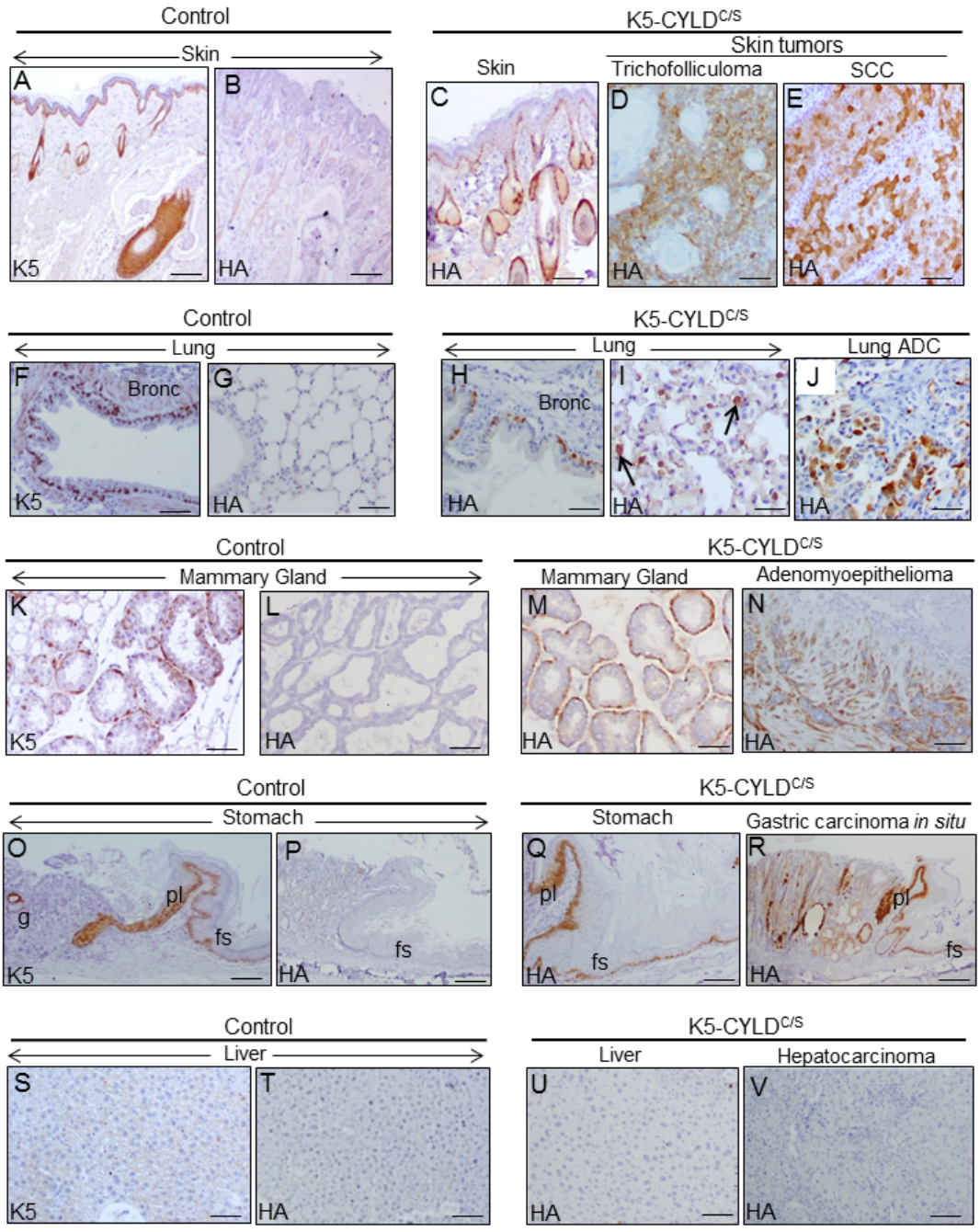

Figure 11. Analysis of the expression of the transgene in the tumors developed in the K5-CYLD$^{C/S}$ mice and in their matched non tumoral tissue. Immunohistochemical staining with K5 and HA antibodies. (**A, B**) Snout sections from Control mice. K5 expression in the basal layer of the epidermis, HF and the immature cells of the sebaceous glands (**A**); HA is not detected (**B**). (**C**) HA expression in the snout of transgenic mice following the K5 expression pattern. HA expression in the tricofolliculoma of the snout (**D**) and in the SCC of the back skin of K5-CYLD$^{C/S}$ mice (**E**). (**F-G**) K5 expression in the basal layer of the epithelium of bronchia and bronchioles of Control mice (**F**); no HA staining was observed (**G**). (**H, I**) HA in bronchia and bronchioles of transgenic mice (**H**) and in alveolar cells (**I**). (**J**) HA expression in the lung ADC. (**K, L**) K5 expression in the myoepithelial cells around the mammary secretory acini of Control mice (**K**); HA is not detected (**L**). (**M**) HA in the mammary secretory acini of lactating transgenic mice following the K5 expression patter. (**N**) HA expression in the mammary adenomyoepithelioma. (**O, P**) Stomach from a Control mice showing K5 expression in the aglandular epithelia (forestomach, fs), plica (pl), and in scattered glands (g) (**O**); HA is not expressed (**P**). (**Q**) Expression of HA in the stomach of transgenic mice following the K5 expression pattern. (**R**) Gastric carcinoma *in situ* expressing HA. (**S, T**) Neither K5 nor HA are expressed in the liver of Control mice. (**U**) HA is not detected in hepatocytes of K5-CYLD$^{C/S}$ mice. (**V**) HA is not expressed in the hepatocarcinomas (HCC) of transgenic animals. Scale bars: 300 μm (**A-C; N, R**); 150 μm (**D, E, I, J**); 70 μm (**K-M**); 250 μm (**G, O, P**); 200 μm (**F, H, Q, V**); 100 μm (**S-U**). ADC: adenocarcinoma.

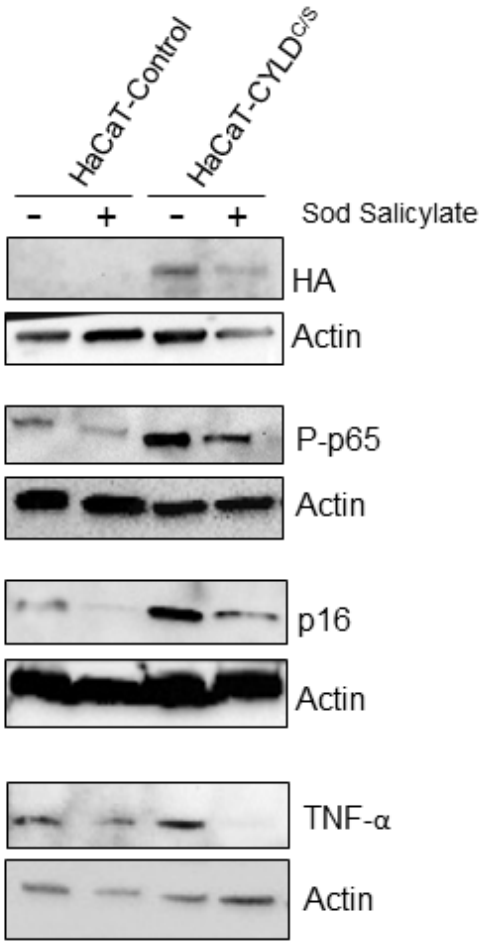

Figure 12. The reduction of the NF-κB overactivation in keratinocytes expressing the CYLD$^{C/S}$ mutant decreases the expression of the biomarker of aging p16 and TNFα. HaCaT (Control and CYLD$^{C/S}$) cells were treated with sodium salicylate for 48h when indicated (+). WB shows that HaCaT-CYLD$^{C/S}$ cells exhibit increased levels of expression of P-p65, p16 and TNFα, but the treatment with sodium salicylate, which reduced P-p65 levels, also decreases p16 and TNF-α levels in these cells. Actin was used as a control loading.

To further reinforce our findings showing the role of CYLD as a protector from aging and tumor development, we analyzed the phenotype of the transgenic mice in a different genetic background (i.e., FVB/N background) and found that K5-CYLD$^{C/S}$ /FVB/N mice develop similar alterations to those described above, i.e., they showed premature aging of skin and other organs (thymus, pancreas, stomach, lung etc.) (Fig. S10 and S11) and develop spontaneous tumors (from 8-10 months onwards), while their age-matched Control littermates do not show tumor development (Fig. S12).

The reduction of NF-κB activity decreases the expression of TNF-α and p16 in keratinocytes

To establish a causal relationship between CYLD lack of function, and NF-κB activation and aging, we studied the properties of the HaCaT keratinocytes expressing the CYLD$^{C/S}$ mutant [6, 9]. We checked that HaCaT-CYLD$^{C/S}$ cells presented overactivation of the NF-κB pathway (Fig. 12) and increased levels of p16 expression, whose increment is considered a biomarker of aging [26]. However, treatment of HaCaT keratinocytes with sodium salicylate reduced NF-κB activation in both, Control and CYLD$^{C/S}$ expressing cells, and reduced the overexpression of p16 found in the mutant HaCaT-CYLD$^{C/S}$ keratinocytes to those levels showed in the HaCaT-Control cells (which contain a functional CYLD) (Fig. 12). In addition, we also found that NF-κB inhibition in the HaCaT-CYLD$^{C/S}$ cells reduces the expression of TNF-α (target of NF-κB). Thus, our results in keratinocytes suggest a causal relationship between the lack of CYLD function, the NF-κB hyperactivation, and the expression of aging hallmarks and inflammatory cytokines.

DISCUSSION

We have generated a new model of transgenic mice, the K5-CYLD$^{C/S}$ mice, carrying the mutant CYLD$^{C/S}$ construct [6] under the control of the keratin 5 (K5) promoter. The resultant CYLD$^{C/S}$ mutant protein lacking the DUB function of CYLD, acts as a dominant negative of the endogenous CYLD. The study of our transgenic mice has allowed us to know that the DUB function of CYLD is essential for the maintenance of the homeostasis of the skin and other organs, including thymus, lung, stomach, etc. preventing the development of cancer. Notably, we have discovered a new function of CYLD as a suppressor of aging.

In the skin, we have found the importance of CYLD for the maintenance of hair follicle homeostasis and for the regulation of the hair growth cycle, showing that the DUB function of CYLD is essential for HF anagen induction of the second hair cycle. Moreover K5-CYLD$^{C/S}$ mice show an early diffuse alopecia, progressive with age, which could be the result of both the constitutive activation of the canonical pathway of NF-κB, and the increased expression of its targets, the pro-inflammatory cytokines TNF-α and IL-6, as inflammation is known to be linked to the development of the most common form of alopecia in humans, the androgenetic alopecia [35]. The K5-CYLD$^{C/S}$ transgenic mice show in addition hyperplastic and orphan sebaceous glands, reminiscent of those found in another model of transgenic mice, the *Cyld*$^{E\Delta 9/\Delta 9}$ mice, also deficient in its DUB function [36]. In both types of

transgenic mice the increased c-Myc activation found in skin could be mediating disorders of the sebaceous glands, as c-Myc has been characterized as a key regulator of homeostasis of these glands [37].

In addition to the skin appendages changes, the K5-CYLD$^{C/S}$ mice show epidermal alterations, mainly impaired keratinocyte differentiation, thus confirming *in vivo* the results that our group have previously described using a model of skin equivalents of human HaCaT keratinocytes [9], in which we demonstrated that the overexpression of the wild-type CYLD (CYLD^{wt}) promoted keratinocyte differentiation, whereas the expression of the mutant CYLD$^{C/S}$ prevented, through the activation of the JNK pathway, the epidermal differentiation [9]. Now our results *in vivo*, ratify the relevance of the DUB function of CYLD for epidermal differentiation, and also show the overactivation of JNK in the skin of transgenic mice.

A very relevant finding of our studies is that CYLD acts as a suppressor of aging, suggesting that CYLD is necessary to maintain the homeostasis of many organs, protecting them from premature aging. The anti-aging function of some well-known tumor suppressor genes (i.e. PTEN, Ink4/Arf) has been previously reported [16, 38], but the role of CYLD as an aging protector is a function not previously described. Supporting our results, CYLD deficiency in *Drosophila melanogaster* shortened life expectancy [39]. In addition, we show that levels of CYLD diminished in the skin and thymus of aged mice, as well as in the mammary gland (Alameda et al, not published) and other group has described it decreased expression in aged lungs [40].

One of the first manifestations of the early aging of the K5-CYLD$^{C/S}$ mice is progressive diffuse alopecia, an alteration usually found in other models of mice exhibiting premature aging [41], and in progeria human diseases, such as Werner syndrome and Hutchinson-Gilford progeria [42]. Likewise, progressive hair loss related to age is also a hallmark of aging in humans [43]; as well as decreased hair growth [41], which we also find in our transgenic mice. Other symptoms of aging in both mice and humans are aging of the skin, mainly characterized by epidermal atrophy [44]; loss of panniculus adipose [45] and sebaceous gland hyperplasia [46]. We have observed all these signs of aging in the skin of young K5-CYLD$^{C/S}$ mice (from 3 to 5 months of age), but they were not found in control mice of the same age; in fact these aging features are characteristics of 24-month-old control mice. Additionally the K5-CYLD$^{C/S}$ mice show increased levels of both p16 and p19 in the skin, having been widely accepted that the expression of these proteins is augmented in aged tissues in both mice and humans [26, 27]. Also, the K5-CYLD$^{C/S}$ mice show increased levels of γH2AX, which is also considered a marker of aging [28]. Therefore, all these changes found in the skin of our transgenic mice lacking a functional CYLD suggest a role for CYLD as a protector of skin aging.

Chronic activation of NF-κB in the skin appears as the key alteration causing the premature aging of this organ in K5-CYLD$^{C/S}$ mice, as it has been described that the main mechanism responsible for both physiological and pathological aging is the activation of NF-κB [18]. Accordingly, transgenic mice deficient in the p50 NF-κB subunit also show hyperactivation of the classical pathway of NF-κB and accelerated aging [47]. Although the skin of K5-CYLD$^{C/S}$ mice show hyperactivation of other molecules, that also may favor aging (as JNK, Akt and c-Myc), it is interesting to note that the mechanism proposed through which the activation of these other pathways promotes aging is by activating NF-κB in turn [4].

Besides the skin, other organs present accelerated aging in our transgenic mice, among them, the early aging of the thymus is very remarkable, appearing also in this case the NF-κB over-activation as the likely mechanism causing the aging, as it has been previously reported that NF-κB is critically involved in the aging of the thymus [19, 32]. The premature aging of other organs of the K5-CYLD$^{C/S}$ mice could be the result of the early thymic involution (since it is considered one of the main regulators of physiological aging) as well as to the overexpression of TNF-α and IL-6, as it is known that these proinflammatory cytokines can affect distant organs causing systemic inflammation, compromising the homeostasis of the tissues and in turn promoting the accelerated aging [22]. Accordingly, elevated expression of TNF-α and IL-6 by the over-activation of NF-κB has been proven to occur in both physiological aging and in progeria human diseases [48]. Our transgenic mice show inflammation and early aging in numerous organs (lung, stomach etc.), which could be due either to a systemic effect of TNF-α and IL-6 in the skin and/or to the expression of the transgene in these organs. These possibilities will be analyzed.

It is interesting that although there are two other models of transgenic mice that, similar to the K5-CYLD$^{C/S}$ mice, express a mutated form of CYLD that causes the lack of DUB activity in the epidermis and other tissues (the CYLD^{m} [7] and the CYLD$^{E\Delta9/\Delta9}$ mice [36]); however, no premature aging has been described in neither of these two models. In the CYLD^{m} mice it was demonstrated the activation of JNK/AP1 in keratinocytes and skin tumors, though no significant increase in NF-κB activation was detected. Activation of c-Myc was observed in the epidermis of the

CYLD$^{E\Delta9/\Delta9}$ mice, and no reference to NF-κB overactivation is mentioned. Thus, it seems that the most likely reason for these other mice to age normally may be the absence of NF-κB hiperactivation. It also suggests that although both JNK and c-Myc activation might contribute to aging, the most important pro-aging pathway is that of NF-κB, as it has been widely demonstrated before [18].

A relevant phenotype of the K5-CYLD$^{C/S}$ mice is also their susceptibility to spontaneously develop different types of tumors from an early age (8 months). Among them it has been shown the growth of skin tumors, which are likely the result of the molecular alterations observed in the skin of the transgenic mice, i.e. the overactivation of NF-κB, JNK, c-Myc and Akt. Different evidences support the role of these proteins in skin cancer development and progression, i.e., the activity of NF-κB increases with the skin tumor progression, supporting the pro-tumoral action of NF-κB in the cutaneous SCC [49]; also, NF-κB and JNK activation cause tumor development in familial cylindromatosis patients [1, 2]. The amplification or deregulation of c-Myc causes the genesis and tumor promotion of cutaneous SCC, and we have described the increased malignancy of cutaneous SCCs overexpressing c-Myc [50]. Our group has also found that the constitutive activation of Akt in the basal keratinocytes of the K5-myrAkt transgenic mice promotes the development and malignancy of cutaneous SCC [51].

But in addition to the skin tumors, other tumor types are found with a high frequency in the K5-CYLD$^{C/S}$ mice, such as those developed in the lung, liver, and stomach. It is known that in addition to keratinocytes, the K5 regulatory elements direct the expression of the transgene to other cell types that express K5, including those in the mammary gland, stomach and lung [24]. Thus, the growth of tumors in these organs may be the direct consequence of the expression of the transgene. In fact, the lack of CYLD function has been detected in many human tumor cells of lung, stomach and breast cancer, in which the activation of NF-κB, JNK and/or c-Myc appears as the mechanisms through which CYLD downregulation promotes tumor development [10-12]. But, in addition, K5-CYLD$^{C/S}$ mice form tumors derived from cells that do not express the transgenic protein, such as the hepatocytes. In these cases, tumors may develop as a consequence of the premature aging of the transgenic mice. In this context, it is remarkable that all types of tumors arise mainly in organs in which premature aging and inflammation has been noticed, such as in the skin, stomach, lung and liver. Therefore, it seems that tumor development could be the consequence of these pathologies, as the relationship between aging, chronic inflammation and tumor development is well established [34, 52].

Thereby, the study of the K5-CYLD$^{C/S}$ mice demonstrates the essential role of CYLD, *in vivo*, as a tumor suppressor of wide spectrum, providing an excellent model for studying, *in vivo*, the signaling pathways throughout CYLD exerts its tumor suppressor role in different types of cancer. In addition, our results suggest that the role of CYLD as an aging suppressor may be a mechanism through which CYLD acts as a tumor suppressor. In support of our hypothesis is the fact that although the function of CYLD as a tumor suppressor has been reported for different types of cancer [53]; however, none of the other two models of mutant CYLD transgenic mice (i.e. the CYLD^{m} and *Cyld*$^{E\Delta9/\Delta9}$ mice) develop cancer spontaneously, strongly suggesting that the reason for this may be that they do not age prematurely. Therefore, the K5-CYLD$^{C/S}$ mice constitute a suitable *in vivo* model for the study of the mechanisms through which NF-κB activation promotes aging, and to test putative targets aimed to delay the devastating effects of progeria syndromes. Moreover, the K5-CYLD$^{C/S}$ mice offer a useful model for the study of the mechanisms involved in the chronological aging of the human skin, as it recapitulates its fundamental alterations.

MATERIALS AND METHODS

Generation of transgenic mice

HA-tagged murine CYLD$^{C/S}$ [6] was placed under the control of a 5.2 kb 5'-upstream fragment of bovine K5 promoter and a rabbit β-globin intron (Figure 1A). Transgenic mice were generated by microinjection of this construct into B6D2F2 embryos using standard techniques. Mice were genotyped by PCR analysis of tail genomic DNA using primers specific for the rabbit β-globin intron. Wild type non-transgenic littermates were used as control animals. Two lines of transgenic mice were established (K5-CYLD$^{C/S}$-A and K5-CYLD$^{C/S}$-X). In addition, transgenic K5-CYLD$^{C/S}$-X mice were derived to FVB/N genetic background and analyzed.

Induced adult hair cycle

The hair parallel to the paravertebral line on the back skin of 7-week-old control and transgenic mice were removed. This procedure leads to synchronized development of anagen hair follicles. Tissues were obtained at days 16 and 21 after depilation and fixed in 10% buffered formalin. The distinct phases of hair follicle development were determined as previously described [5]. Body weight of the two groups of mice

was not significantly different at any point of time during the experiment. Six animals of each genotype were analyzed.

BrdU labeling

Mice received an intraperitoneal injection of BrdU 120 mg/kg body weight 1 h before sample harvesting. BrdU incorporation was detected by immunohistochemistry of paraffin-embedded sections using an anti-BrdU monoclonal antibody (Roche).

Isolation of thymic cells

Thymus from 1year old mice were collected and immersed in PBS, then mechanical disaggregation with syringe and filter system was performed.

Ethics statement

All animal experimental procedures were performed according to European and Spanish laws and regulations (2007/526/CE) and approved by the Ethics Committee for Animal Welfare of CIEMAT and by the legal authority (protocol code PROEX182/15).

Histology and immunohistochemistry

Mouse tissues were dissected and fixed in 10% buffered formalin or 70% ethanol and embedded in paraffin. Five μm-thick sections were used for H&E staining or immunohistochemical preparations. Antibodies used in immunostaining were: antibodies against HA (3724, Cell Signaling Technology); CYLD (SAB4200061), Involucrin (I9018) and Sma (C-6198) (Sigma-Aldrich); K5, K10, Filaggrin and Loricrin (Covance).

Immunoblots and immunoprecipitation

Antibodies used in Western blots were: Actin (sc-1616), GAPDH (sc-25778), IκBα (sc-371), p65 (sc-8008), Bcl-3 (sc-185) and P-c-Myc (sc-8000) (Santa Cruz Biotechnology); HA (3724), Ubiquitin (3936), P-Akt (4068), P-IκBα (2859), P-JNK (4668) and P-p65 (3033) (Cell Signaling Technology); IL-6 (9324) (R&D Systems); CYLD (SAB4200061, Sigma-Aldrich); c-Myc (626802, Biolegend); TNF-α (654250, Calbiochem); IKKγ (IMG-5480-2, Novus Biologicals); K63-Ubiquitin (ab179434), p19 (ab80) and p16 (ab51243) (Abcam) and γH2AX (05-636) (Millipore). For immunoprecipitation 300 μg cell lysate were incubated at 4ºC overnight. Then washed, and performed the immunoblotting.

Determination of TNF-α and IL-6 in serum

Mice were anesthetized and blood were obtained (300μl) by puncture of the vein of the tail. Serum was stored at -20ºC until assay. Serum from Control (n=16) and K5-CYLD$^{C/S}$ (n=16) mice of 15-20 months of age were analyzed for the expression of both TNF-α and IL-6 cytokines (LEGENDplex Multi-Analyte Flow Assays Kit, Biolegend). Cytokines were measured in a Tecan GENios Microplate Reader (Tecan Trading AG, Switzerland).

Cell culture and treatment

HaCaT cell lines of human keratinocytes were cultured in DMEM supplemented with 10% fetal calf serum. HaCaT-Control, HaCaT-CYLD$^{C/S}$ cells have been previously described [54]; briefly, HaCaT-CYLD$^{C/S}$ cells were transfected in a stable manner with the β-Actin-CYLD$^{C/S}$ construct and are deficient in the DUB function of CYLD. Cells were grown in the presence of G418 (0.4mg/ml). When indicated, cells were incubated with 10mM sodium salicylate (S3007, Sigma-Aldrich) in DMEM for 48h.

Abbreviations

ORS: outer root sheath; HF: hair follicle; ADC: adenocarcinoma; HCC: hepatocarcinoma; SCC: squamous cell carcinoma; DUB: deubiquitinase; NMSC: non melanoma skin cancer.

AUTHOR CONTRIBUTIONS

Conception and design were performed by JPA and MLC. Data acquisition was performed by JPA, AR, AP, CS-C, JCS and RS. Data analysis was performed by JPA, AR, MN, JMP, RG-F; AB, MJF-A, Drafting of the manuscript was performed by MLC.

ACKNOWLEDGMENTS

We would like to thank Federico Sánchez-Sierra and Pilar Hernández for their histological processing of the samples; and Edilia de Almeida, Jesús Martínez-Palacio and the personnel of the CIEMAT Animal Unit for mice care.

CONFLICTS OF INTEREST

The authors declare that they have no competing interests.

FUNDING

This research was supported by grants from the Spanish Government and co-financed by Fondo Europeo de

Desarrollo Regional (FEDER): PI16/00161from the Instituto de Salud Carlos III to M.L. Casanova; PI14/01403 from the Instituto de Salud Carlos III to A. Ramírez; PI17/00578 from the Instituto de Salud Carlos III to A. Ramírez and M. Navarro; and FEDER cofounded MINECO grant SAF2015-66015-R, ISCIII-RETIC RD12/0036/0009, PIE 15/00076 and CB/16/00228 to J.M. Paramio.

REFERENCES

1. Trompouki E, Hatzivassiliou E, Tsichritzis T, Farmer H, Ashworth A, Mosialos G. CYLD is a deubiquitinating enzyme that negatively regulates NF-kappaB activation by TNFR family members. Nature. 2003; 424:793–96. https://doi.org/10.1038/nature01803

2. Brummelkamp TR, Nijman SM, Dirac AM, Bernards R. Loss of the cylindromatosis tumour suppressor inhibits apoptosis by activating NF-kappaB. Nature. 2003; 424:797–801. https://doi.org/10.1038/nature01811

3. Ghosh S, Karin M. Missing pieces in the NF-kappaB puzzle. Cell. 2002 (Suppl); 109:S81–96. https://doi.org/10.1016/S0092-8674(02)00703-1

4. Tilstra JS, Clauson CL, Niedernhofer LJ, Robbins PD. NF-κB in aging and disease. Aging Dis. 2011; 2:449–65.

5. Straile WE, Chase HB, Arsenault C. Growth and differentiation of hair follicles between periods of activity and quiescence. J Exp Zool. 1961; 148:205–21. https://doi.org/10.1002/jez.1401480304

6. Alameda JP, Moreno-Maldonado R, Navarro M, Bravo A, Ramírez A, Page A, Jorcano JL, Fernández-Aceñero MJ, Casanova ML. An inactivating CYLD mutation promotes skin tumor progression by conferring enhanced proliferative, survival and angiogenic properties to epidermal cancer cells. Oncogene. 2010; 29:6522–32. https://doi.org/10.1038/onc.2010.378

7. Miliani de Marval P, Lutfeali S, Jin JY, Leshin B, Selim MA, Zhang JY. CYLD inhibits tumorigenesis and metastasis by blocking JNK/AP1 signaling at multiple levels. Cancer Prev Res (Phila). 2011; 4:851–59. https://doi.org/10.1158/1940-6207.CAPR-10-0360

8. Masoumi KC, Shaw-Hallgren G, Massoumi R. Tumor Suppressor Function of CYLD in Nonmelanoma Skin Cancer. J Skin Cancer. 2011; 2011:614097. https://doi.org/10.1155/2011/614097

9. Alameda JP, Fernández-Aceñero MJ, Moreno-Maldonado R, Navarro M, Quintana R, Page A, Ramírez A, Bravo A, Casanova ML. CYLD regulates keratinocyte differentiation and skin cancer progression in humans. Cell Death Dis. 2011; 2:e208. https://doi.org/10.1038/cddis.2011.82

10. Deng LL, Shao YX, Lv HF, Deng HB, Lv FZ. Over-expressing CYLD augments antitumor activity of TRAIL by inhibiting the NF-κB survival signaling in lung cancer cells. Neoplasma. 2012; 59:18–29. https://doi.org/10.4149/neo_2012_003

11. Hayashi M, Jono H, Shinriki S, Nakamura T, Guo J, Sueta A, Tomiguchi M, Fujiwara S, Yamamoto-Ibusuki M, Murakami K, Yamashita S, Yamamoto Y, Li JD, et al. Clinical significance of CYLD downregulation in breast cancer. Breast Cancer Res Treat. 2014; 143:447–57. https://doi.org/10.1007/s10549-013-2824-3

12. Zhu M, Zhou X, Du Y, Huang Z, Zhu J, Xu J, Cheng G, Shu Y, Liu P, Zhu W, Wang T. miR-20a induces cisplatin resistance of a human gastric cancer cell line via targeting CYLD. Mol Med Rep. 2016; 14:1742–50. https://doi.org/10.3892/mmr.2016.5413

13. Mathis BJ, Lai Y, Qu C, Janicki JS, Cui T. CYLD-mediated signaling and diseases. Curr Drug Targets. 2015; 16:284–94. https://doi.org/10.2174/1389450115666141024152421

14. Carrasco-Garcia E, Moreno M, Moreno-Cugnon L, Matheu A. Increased Arf/p53 activity in stem cells, aging and cancer. Aging Cell. 2017; 16:219–25. https://doi.org/10.1111/acel.12574

15. Collado M, Blasco MA, Serrano M. Cellular senescence in cancer and aging. Cell. 2007; 130:223–33. https://doi.org/10.1016/j.cell.2007.07.003

16. Ortega-Molina A, Serrano M. PTEN in cancer, metabolism, and aging. Trends Endocrinol Metab. 2013; 24:184–89. https://doi.org/10.1016/j.tem.2012.11.002

17. Hsu T. Educational initiatives in geriatric oncology - Who, why, and how? J Geriatr Oncol. 2016; 7:390–96. https://doi.org/10.1016/j.jgo.2016.07.013

18. Osorio FG, Soria-Valles C, Santiago-Fernández O, Freije JM, López-Otín C. NF-κB signaling as a driver of ageing. Int Rev Cell Mol Biol. 2016; 326:133–74. https://doi.org/10.1016/bs.ircmb.2016.04.003

19. Osorio FG, Bárcena C, Soria-Valles C, Ramsay AJ, de Carlos F, Cobo J, Fueyo A, Freije JM, López-Otín C. Nuclear lamina defects cause ATM-dependent NF-κB activation and link accelerated aging to a systemic inflammatory response. Genes Dev. 2012; 26:2311–24. https://doi.org/10.1101/gad.197954.112

20. Adler AS, Sinha S, Kawahara TL, Zhang JY, Segal E, Chang HY. Motif module map reveals enforcement of aging by continual NF-kappaB activity. Genes Dev. 2007; 21:3244–57. https://doi.org/10.1101/gad.1588507

21. Chung HY, Cesari M, Anton S, Marzetti E, Giovannini S, Seo AY, Carter C, Yu BP, Leeuwenburgh C. Molecular inflammation: underpinnings of aging and age-related diseases. Ageing Res Rev. 2009; 8:18–30. https://doi.org/10.1016/j.arr.2008.07.002

22. Balistreri CR, Candore G, Accardi G, Colonna-Romano G, Lio D. NF-κB pathway activators as potential ageing biomarkers: targets for new therapeutic strategies. Immun Ageing. 2013; 10:24. https://doi.org/10.1186/1742-4933-10-24

23. Alameda JP, Fernández-Aceñero MJ, Quintana RM, Page A, Ramírez Á, Navarro M, Casanova ML. Functional inactivation of CYLD promotes the metastatic potential of tumor epidermal cells. J Invest Dermatol. 2013; 133:1870–78. https://doi.org/10.1038/jid.2013.76

24. Ramírez A, Bravo A, Jorcano JL, Vidal M. Sequences 5 of the bovine keratin 5 gene direct tissue- and cell-type-specific expression of a lacZ gene in the adult and during development. Differentiation. 1994; 58:53–64.

25. Chase HB. Growth of the hair. Physiol Rev. 1954; 34:113–26. https://doi.org/10.1152/physrev.1954.34.1.113

26. Krishnamurthy J, Torrice C, Ramsey MR, Kovalev GI, Al-Regaiey K, Su L, Sharpless NE. Ink4a/Arf expression is a biomarker of aging. J Clin Invest. 2004; 114:1299–307. https://doi.org/10.1172/JCI22475

27. Ressler S, Bartkova J, Niederegger H, Bartek J, Scharffetter-Kochanek K, Jansen-Dürr P, Wlaschek M. p16INK4A is a robust in vivo biomarker of cellular aging in human skin. Aging Cell. 2006; 5:379–89. https://doi.org/10.1111/j.1474-9726.2006.00231.x

28. Bohr VA. Deficient DNA repair in the human progeroid disorder, Werner syndrome. Mutat Res. 2005; 577:252–59. https://doi.org/10.1016/j.mrfmmm.2005.03.021

29. Reiley W, Zhang M, Sun SC. Negative regulation of JNK signaling by the tumor suppressor CYLD. J Biol Chem. 2004; 279:55161–67. https://doi.org/10.1074/jbc.M411049200

30. Aw D, Palmer DB. The origin and implication of thymic involution. Aging Dis. 2011; 2:437–43.

31. George AJ, Ritter MA. Thymic involution with ageing: obsolescence or good housekeeping? Immunol Today. 1996; 17:267–72. https://doi.org/10.1016/0167-5699(96)80543-3

32. Bektas A, Zhang Y, Lehmann E, Wood WH 3rd, Becker KG, Madara K, Ferrucci L, Sen R. Age-associated changes in basal NF-κB function in human CD4+ T lymphocytes via dysregulation of PI3 kinase. Aging (Albany NY). 2014; 6:957–74. https://doi.org/10.18632/aging.100705

33. Slavin BG, Paaule WJ, Bernick S. Edited by Johnson John E., Jr. Morphological changes in the aging mammalian pancreas. In "Aging and Cell Structure", North Campus Library Plenum Press New York and London. 1945; 2: 198-206.

34. Zinger A, Cho WC, Ben-Yehuda A. Cancer and aging - the inflammatory connection. Aging Dis. 2017; 8:611–27. https://doi.org/10.14336/AD.2016.1230

35. Sueki H, Stoudemayer T, Kligman AM, Murphy GF. Quantitative and ultrastructural analysis of inflammatory infiltrates in male pattern alopecia. Acta Derm Venereol. 1999; 79:347–50. https://doi.org/10.1080/000155599750010238

36. Jin YJ, Wang S, Cho J, Selim MA, Wright T, Mosialos G, Zhang JY. Epidermal CYLD inactivation sensitizes mice to the development of sebaceous and basaloid skin tumors. JCI Insight. 2016; 1:e86548. https://doi.org/10.1172/jci.insight.86548

37. Arnold I, Watt FM. c-Myc activation in transgenic mouse epidermis results in mobilization of stem cells and differentiation of their progeny. Curr Biol. 2001; 11:558–68. https://doi.org/10.1016/S0960-9822(01)00154-3

38. Matheu A, Maraver A, Collado M, García-Cao I, Cañamero M, Borras C, Flores JM, Klatt P, Viña J, Serrano M. Anti-aging activity of the Ink4/Arf locus. Aging Cell. 2009; 8:152–61. https://doi.org/10.1111/j.1474-9726.2009.00458.x

39. Xue L, Igaki T, Kuranaga E, Kanda H, Miura M, Xu T. Tumor suppressor CYLD regulates JNK-induced cell death in Drosophila. Dev Cell. 2007; 13:446–54. https://doi.org/10.1016/j.devcel.2007.07.012

40. Hinojosa CA, Akula Suresh Babu R, Rahman MM, Fernandes G, Boyd AR, Orihuela CJ. Elevated A20 contributes to age-dependent macrophage dysfunction in the lungs. Exp Gerontol. 2014; 54:58–66. https://doi.org/10.1016/j.exger.2014.01.007

41. Tyner SD, Venkatachalam S, Choi J, Jones S, Ghebranious N, Igelmann H, Lu X, Soron G, Cooper B,

Brayton C, Park SH, Thompson T, Karsenty G, et al. p53 mutant mice that display early ageing-associated phenotypes. Nature. 2002; 415:45–53. https://doi.org/10.1038/415045a

42. Kamenisch Y, Berneburg M. Progeroid syndromes and UV-induced oxidative DNA damage. J Investig Dermatol Symp Proc. 2009; 14:8–14. https://doi.org/10.1038/jidsymp.2009.6

43. Trüeb RM. Aging of hair. J Cosmet Dermatol. 2005; 4:60–72. https://doi.org/10.1111/j.1473-2165.2005.40203.x

44. Rittié L, Fisher GJ. Natural and sun-induced aging of human skin. Cold Spring Harb Perspect Med. 2015; 5:a015370. https://doi.org/10.1101/cshperspect.a015370

45. Kondratov RV, Kondratova AA, Gorbacheva VY, Vykhovanets OV, Antoch MP. Early aging and age-related pathologies in mice deficient in BMAL1, the core componentof the circadian clock. Genes Dev. 2006; 20:1868–73. https://doi.org/10.1101/gad.1432206

46. Montagna W, Carlisle K. Structural changes in aging human skin. J Invest Dermatol. 1979; 73:47–53. https://doi.org/10.1111/1523-1747.ep12532761

47. Bernal GM, Wahlstrom JS, Crawley CD, Cahill KE, Pytel P, Liang H, Kang S, Weichselbaum RR, Yamini B. Loss of Nfkb1 leads to early onset aging. Aging (Albany NY). 2014; 6:931–43. https://doi.org/10.18632/aging.100702

48. Freund A, Orjalo AV, Desprez PY, Campisi J. Inflammatory networks during cellular senescence: causes and consequences. Trends Mol Med. 2010; 16:238–46. https://doi.org/10.1016/j.molmed.2010.03.003

49. Budunova IV, Perez P, Vaden VR, Spiegelman VS, Slaga TJ, Jorcano JL. Increased expression of p50-NF-kappaB and constitutive activation of NF-kappaB transcription factors during mouse skin carcinogenesis. Oncogene. 1999; 18:7423–31. https://doi.org/10.1038/sj.onc.1203104

50. Alameda JP, Gaspar M, Ramírez Á, Navarro M, Page A, Suárez-Cabrera C, Fernández MG, Mérida JR, Paramio JM, García-Fernández RA, Fernández-Aceñero MJ, Casanova ML. Deciphering the role of nuclear and cytoplasmic IKKα in skin cancer. Oncotarget. 2016; 7:29531–47. https://doi.org/10.18632/oncotarget.8792

51. Segrelles C, García-Escudero R, Garín MI, Aranda JF, Hernández P, Ariza JM, Santos M, Paramio JM, Lorz C. Akt signaling leads to stem cell activation and promotes tumor development in epidermis. Stem Cells. 2014; 32:1917–28. https://doi.org/10.1002/stem.1669

52. Munn LL. Cancer and inflammation. Wiley Interdiscip Rev Syst Biol Med. 2017; 9:e1370. https://doi.org/10.1002/wsbm.1370

53. Massoumi R. CYLD: a deubiquitination enzyme with multiple roles in cancer. Future Oncol. 2011; 7:285–97. https://doi.org/10.2217/fon.10.187

54. Alameda JP, Fernández-Aceñero MJ, Moreno-Maldonado R, Navarro M, Quintana R, Page A, Ramírez A, Bravo A, Casanova ML. CYLD regulates keratinocyte differentiation and skin cancer progression in humans. Cell Death Dis. 2011; 2:e208. https://doi.org/10.1038/cddis.2011.82

.

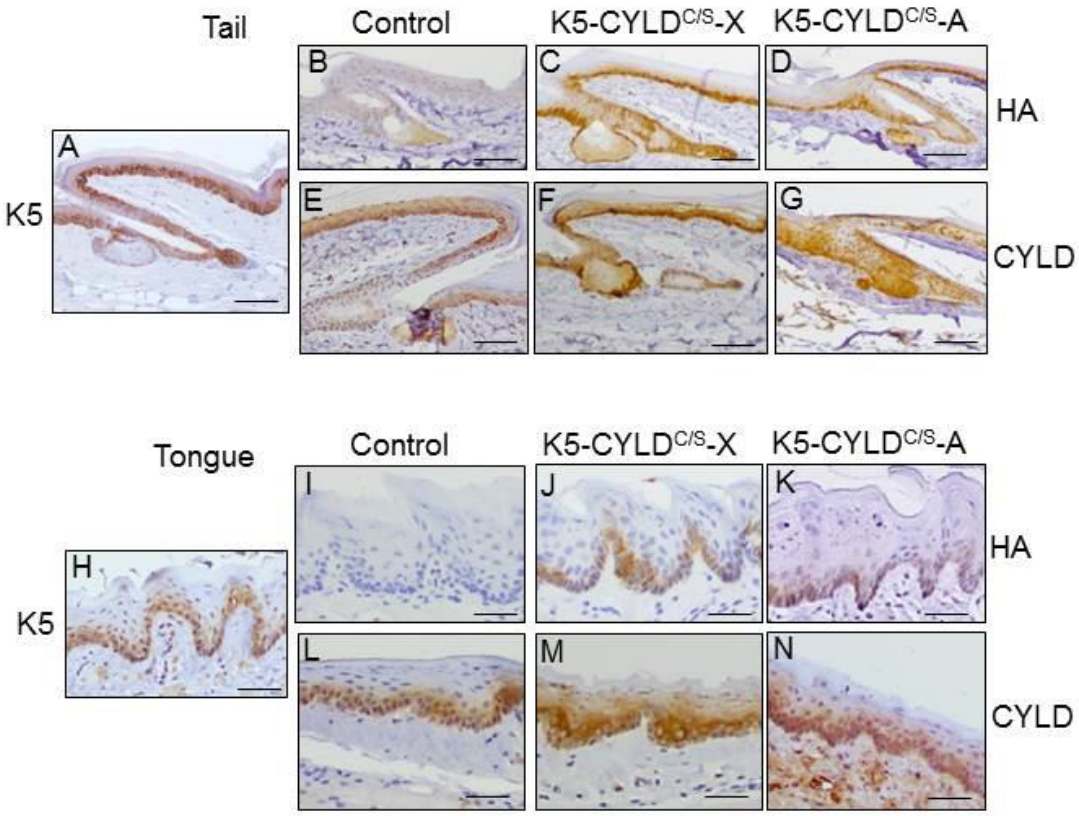

Figure S1. Analysis of the transgene expression in tail skin and tongue. (**A**) Representative staining of K5 in the skin of a control mouse. (**B-D**) HA and (**E-G**) CYLD expression in the tail skin of Control and transgenic mice. Observe that HA is not detected in Control sections (**B**), while HA expression in the tail of K5-CYLD$^{C/S}$ mice follows the K5 expression pattern (**C-D**). (**H**) Representative sections showing the expression of K5 in the tongue of a control mouse. (**I-K**) HA and (l-n) CYLD expression in the tongue of Control and transgenic mice. HA is not expressed in the tongue of Control mice (**I**), while HA expression in the tongue of transgenic mice follows the K5 expression pattern in control mice (**J, K**). Sections correspond to 1-month-old mice. Scale bars: (**A-D**) 220 µm; (**E-G**) 200 µm; (**H, J, K**); 180 µm; (**I, L-N**) 160 µm.

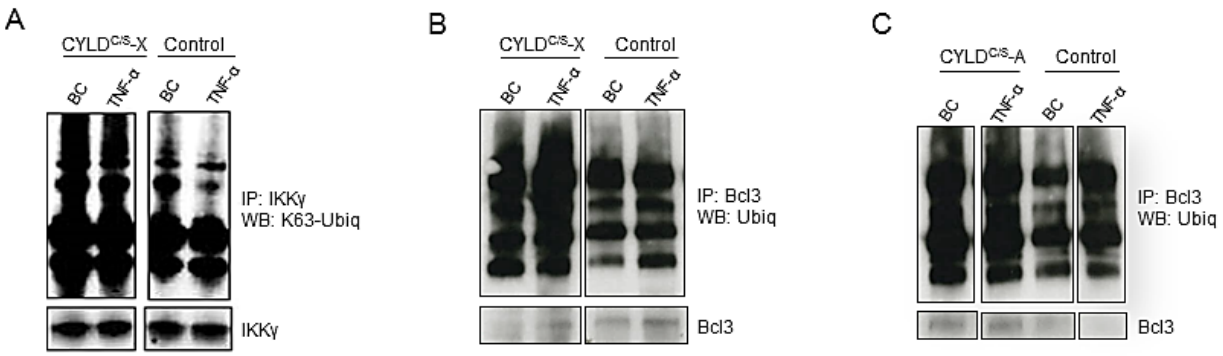

Figure S2. Lack of CYLD DUB function in the K5-CYLD$^{C/S}$ mice. Functional analysis of the CYLD$^{C/S}$ transgene, by IP of back skin protein extracts with an IKKγ or Bcl3 specific antibodies, in the presence and absence of TNF-α. Western blots using Ubiquitin and IKKγ specific antibodies are shown. (**A**) Observe the lack of DUB function in transgenic mice checked as elevated levels of polyubiquitinated IKKγ in both the basal contition (BC) and after TNF-α treatment. (**B, C**) Observe the increased levels of ubiquitinated Bcl3 in the back skin of transgenic mice in both states: without TNF-α stimulation (BC, basal condition), and after TNF-α treatment. Similar results were obtained for both K5-CYLD$^{C/S}$-X (**B**) and K5-CYLD$^{C/S}$-A (**C**) mice. BC: basal condition, i.e., without TNF-α stimulation. (**A, B**) when indicated, cells were incubated for 15 min with TNF-α treatment; (**C**) when indicated cells were incubated 40 min with TNF-α.

Figure S3. External phenotype of the K5-CYLD$^{C/S}$ mice. Representative image showing kyphosis in the back of a transgenic mouse. Both Control and K5-CYLD$^{C/S}$ mice are littermates of 11 months-old.

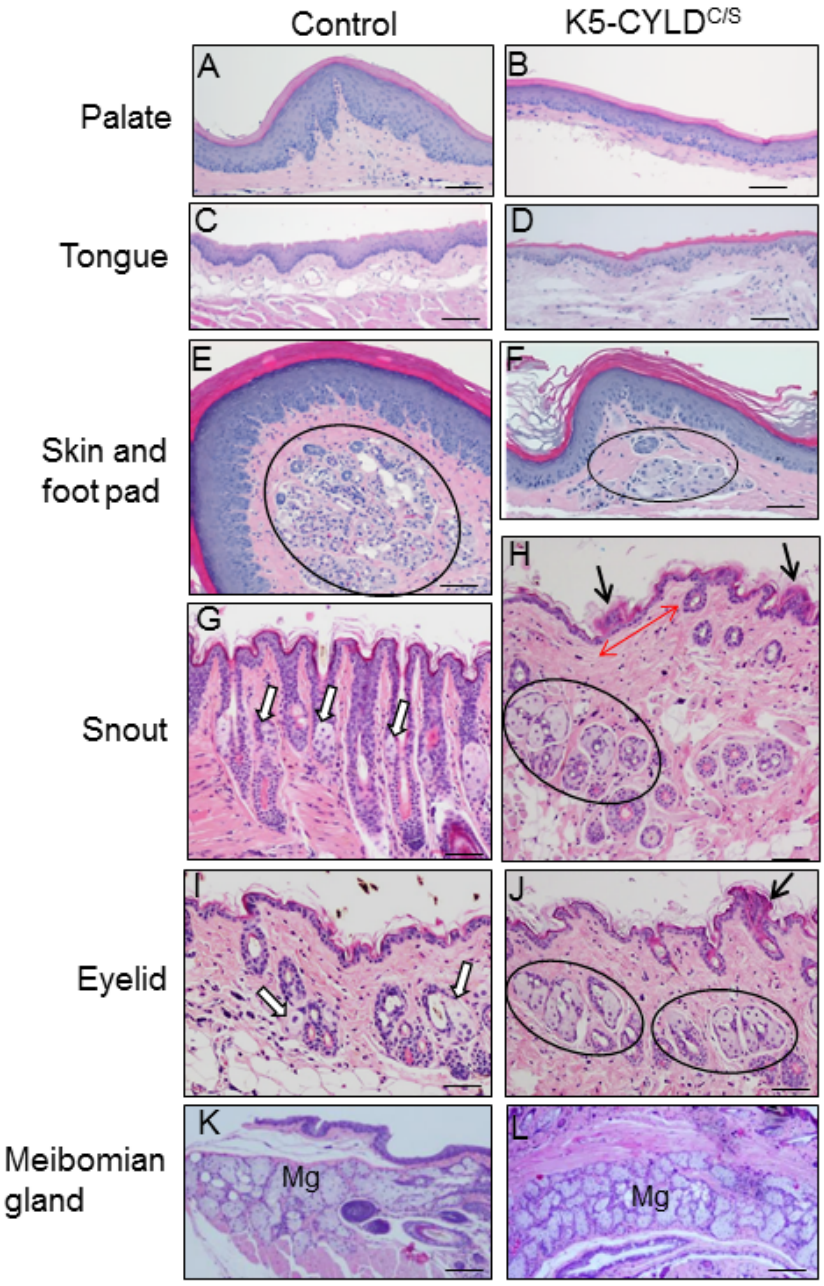

Figure S4. Histological analysis showing the premature aging of different epithelia of the K5-CYLD$^{C/S}$ mice. Sections from both Control (**A, C, E, G, I, K**) and transgenic mice (**B, D, F, H, J, L**) of 5- (**G-J**) and 20-month-old are shown. (**A, B**) Palate epithelium; note the atrophy in that of K5-CYLD$^{C/S}$ mice (**B**). (**C, D**) Stratified epithelium of the tongue. Note the thinning of the epithelium in transgenic mice (**D**). (**E, F**) Scarce eccrine glands in the hind limb foot pads of the K5-CYLD$^{C/S}$ mice are appreciated (circle). (**G, H**) Snout skin of 5-month-old mice. Highly abundant hyperplastic sebaceous glands are observed in the transgenic mice (circles in **H**); additionally, an atrophic epidermal area (double-headed red arrow) and epidermal ridges (black arrows) are shown. Eyelid skin of 5-month-old mice (**I, J**); note the presence of numerous hyperplastic sebaceous glands in the K5-CYLD$^{C/S}$ mice (enclosed in circles), in clear contrast with those found in the corresponding tissue of Control mice (**I**, white arrows). Also note the absence adipose tissue in the eyelid transgenic mice and the presence of epidermal ridges (**J**, black arrows). (**K, L**) Note the abundant hyperplastic Meibomian glands (Mg) found in the eyelids of K5-CYLD$^{C/S}$ mice (**L**) compared to those in Control mice (**K**). Images from 20-month-old mice are showed, although similar alterations are found in young transgenic mice (from 3 months-old). Scale bars: 250 µm (**A-F, K, L**); 150 µm (**G, H**) 230 µm (**I, J**).

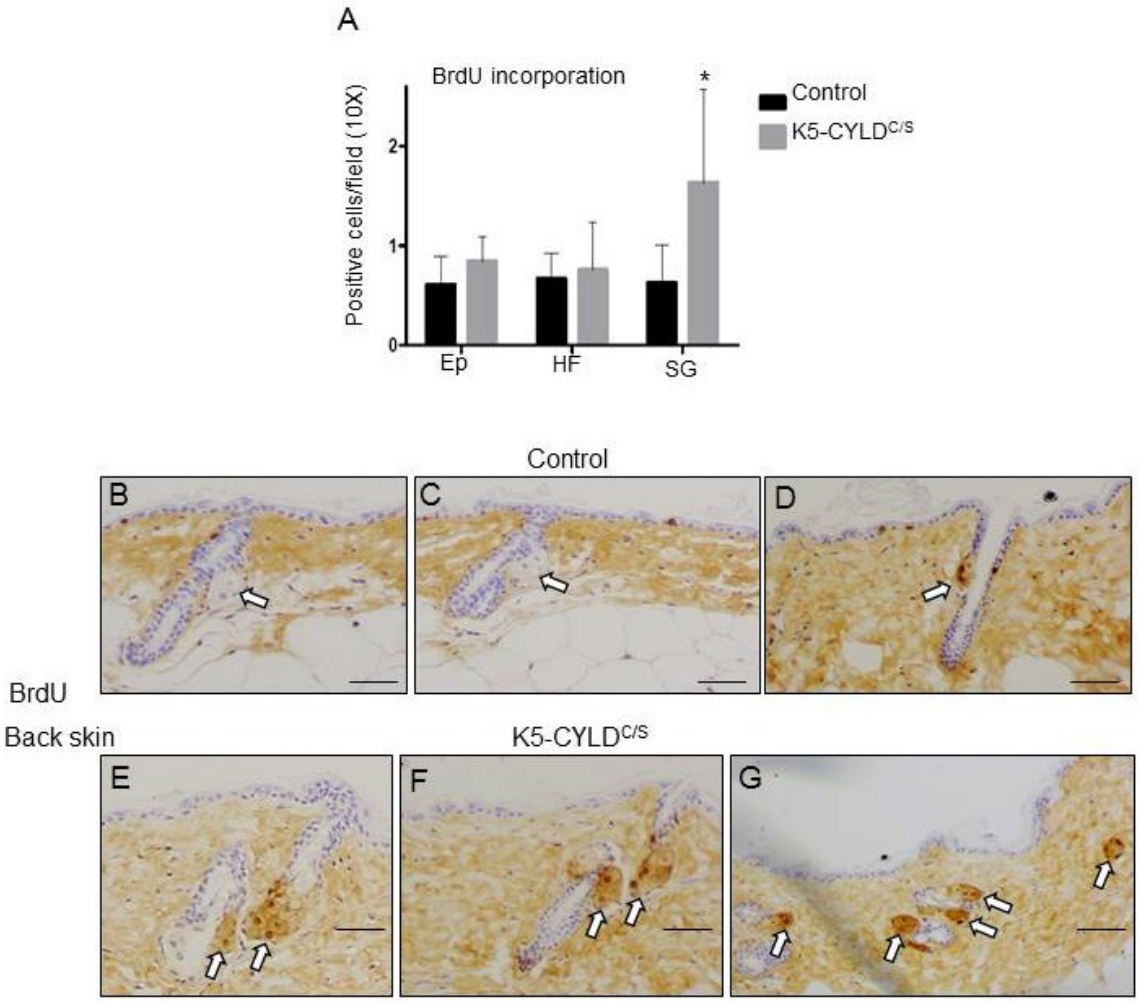

Figure S5. BrdU analysis in the back skin of Control and K5-CYLD$^{C/S}$ mice. (**A**) BrdU incorporation in the back skin of 1-year-old mice. Note the increased proliferation of the sebaceous glands from transgenic mice (4 Control and 5 transgenic mice were analyzed; error bars represent SEM; *P* value by Bonferroni multiple comparisons test: two-way ANOVA). P<0.05. (**B-G**) Representative image showing the BrdU staining in Control (**B-D**) and transgenic (**E-G**) sections of back skin. Observe the increased BrdU incorporation in the sebaceous glands of the K5-CYLD$^{C/S}$ mice. Scale bars: 150 µm. Ep: epidermis; HF: hair follicles; SG: sebaceous glands.

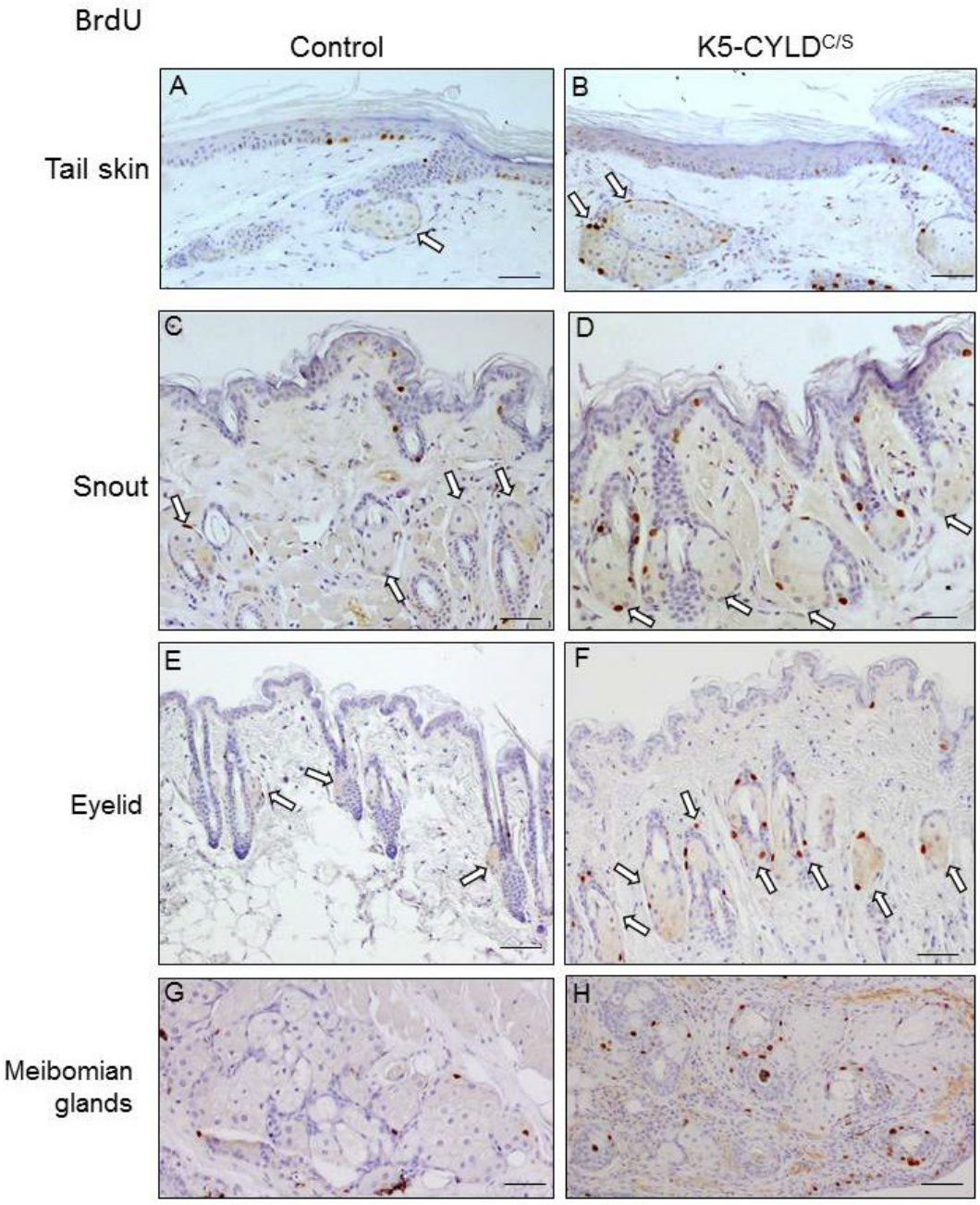

Figure S6. BrdU incorporation in the skin of Control and K5-CYLD$^{C/S}$ mice. BrdU staining in Control (**A, C, E, G**) and transgenic (**B, D, F, H**) sections showing increased signal in the hyperplastic sebaceous glands of the tail, snout and eyelid skin of the K5-CYLD$^{C/S}$ mice (**B, D, F**); as well as in the Meibomian glands (**H**) of the transgenic mice. White arrows point to sebaceous glands. Scale bars: 140 µm (**A-F**); 110 µm (**G, H**).

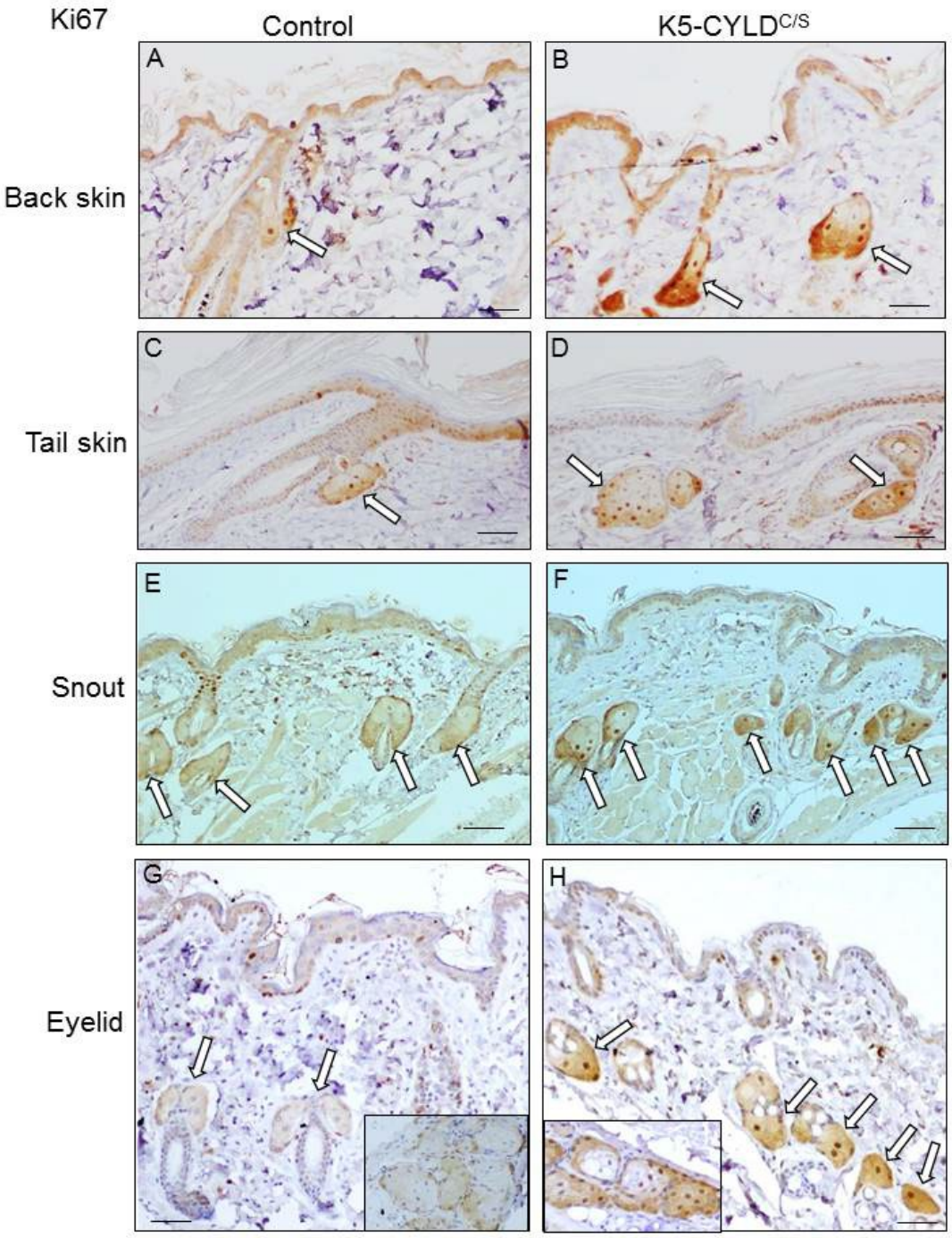

Figure S7. Analysis of cell proliferation in the skin of Control and K5-CYLD$^{C/S}$ mice. Ki67 staining in Control (**A, C, E, G**) and transgenic (**B, D, F, H**) sections showing increased signal in the hyperplastic sebaceous glands of the back, tail, snout and eyelid skin of transgenic mice. Also note that Meibomian glands of the K5-CYLD$^{C/S}$ mice are more proliferative than those of Control mice (compare insets in **G** and **H**). White arrows point to sebaceous glands. Scale bars: 160 µm (**A-F**); 120 µm (**G, H**).

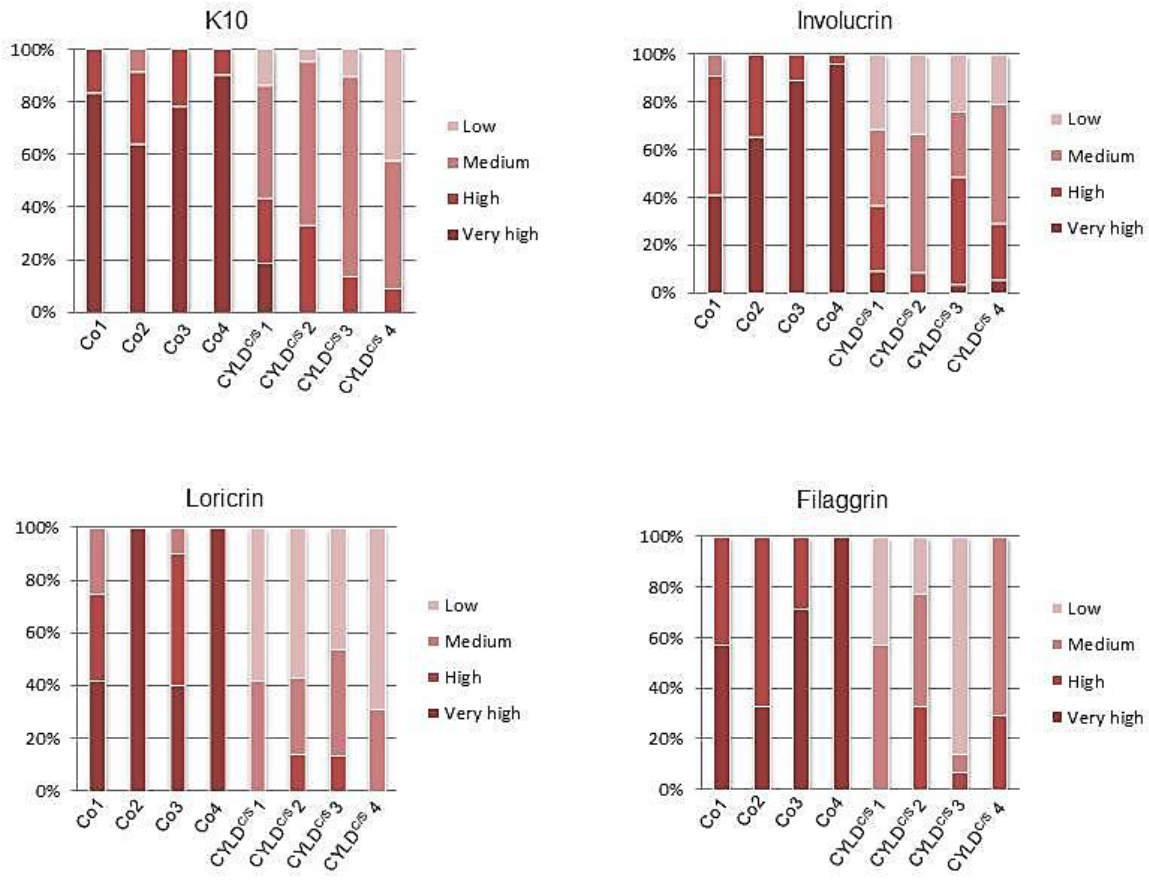

Figure S8. Semiquantitative analysis of the intensity of the expression of epidermal differentiation markers in Control and K5-CYLD$^{C/S}$ mice. 10-15 fields, 10X magnification, corresponding to K10, Involucrin, Loricrin and Filaggrin immunostainings were analyzed and quantified as very high, high, medium or low expression. Analysis of the expression in 4 animals per genotype and staining is showed. Co: Control animals; CYLD$^{C/S}$: K5-CYLD$^{C/S}$ transgenic mice.

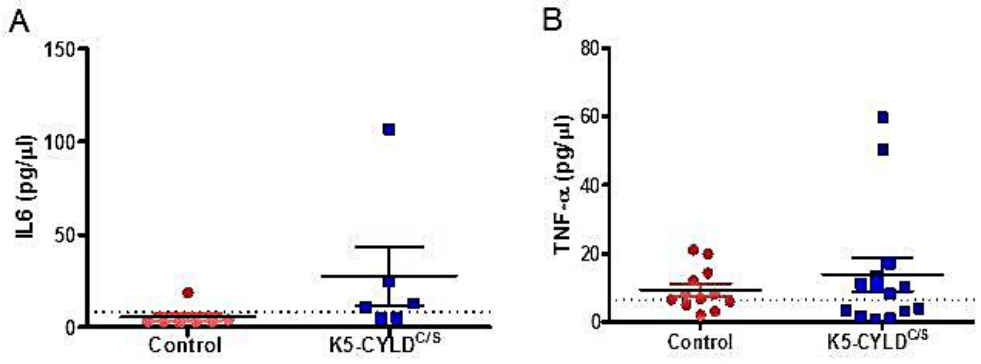

Figure S9. Increased levels of IL6 and TNF-α in the serum of K5-CYLD$^{C/S}$ mice. IL6 (**A**) and TNF-α (**B**) serum levels from 8 Control and 8 transgenic mice of both 16 and 22 months-old (i.e., a total of 16 control and 16 transgenic animals) were analyzed. Results show increased levels of both cytokines in the serum of transgenic mice, mainly of IL-6.

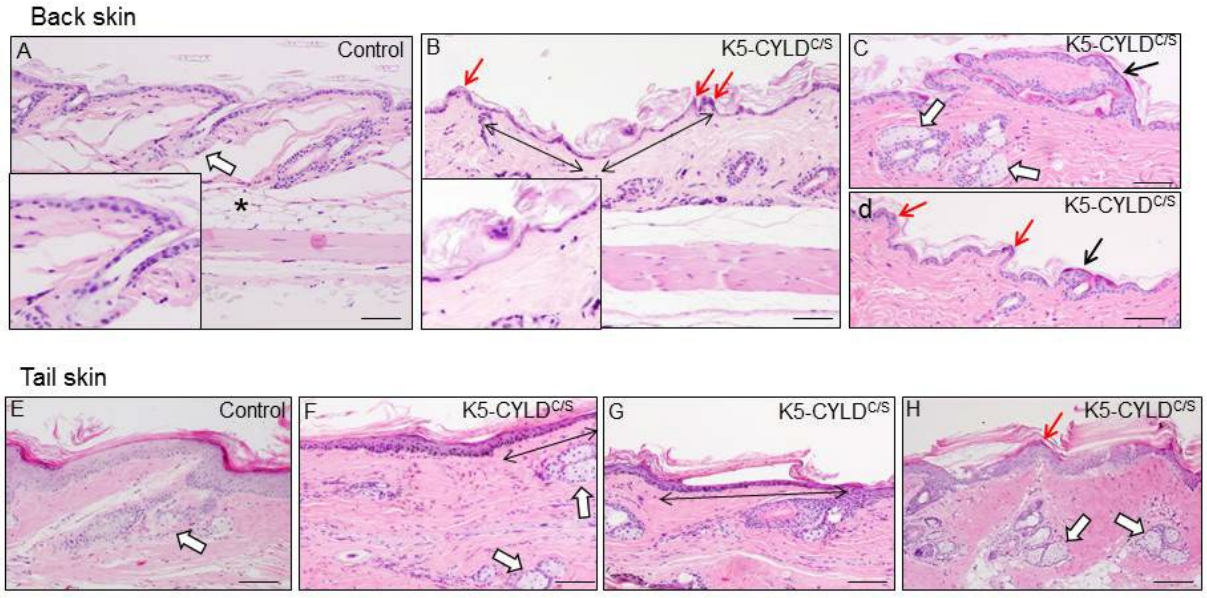

Figure S10. Phenotypic alterations in the skin of FVB/N-K5-CYLD$^{C/S}$ mice indicating that premature aging signs are independent of their genetic background. Representative images showing the main histological alterations presented by K5-CYLD$^{C/S}$ mice developed in a FVB/N genetic background (these are coincident with that observed in B6D2-transgenic mice). (**A-D**) Back skin sections from Control (**A**) and FVB/N-transgenic mice (**B-D**); (**E-H**) tail skin images from Control (**E**) and FVB/N-transgenic (**F-H**) mice. Observe areas of atrophy in the epidermis of the FVB/N-K5-CYLD$^{C/S}$ mice (double-headed arrows in **B,F,G**; compare inserts in **A,B**); epidermal ridges of pyknotic keratinocytes (red arrows in **B,D,H**); papilomatous hyperplasia (black arrows in **C, D**); hyperplasic and orphan sebaceous glands (white arrows in **C,F,H**) compared with normal-size sebaceous glands in Control (white arrows in **A, E**). Reduced number of hair follicles (**C, F, H**), and scarce adipose tissue (**B**) is observed in FVB/N-transgenic mice; asterisk in (**A**) indicates fat tissue in Control mice hypodermis. Five animals of each genotype (18-20-month-old) were analyzed. Scale bars: 250 µm (**A-D**); 300 µm (**E-H**).

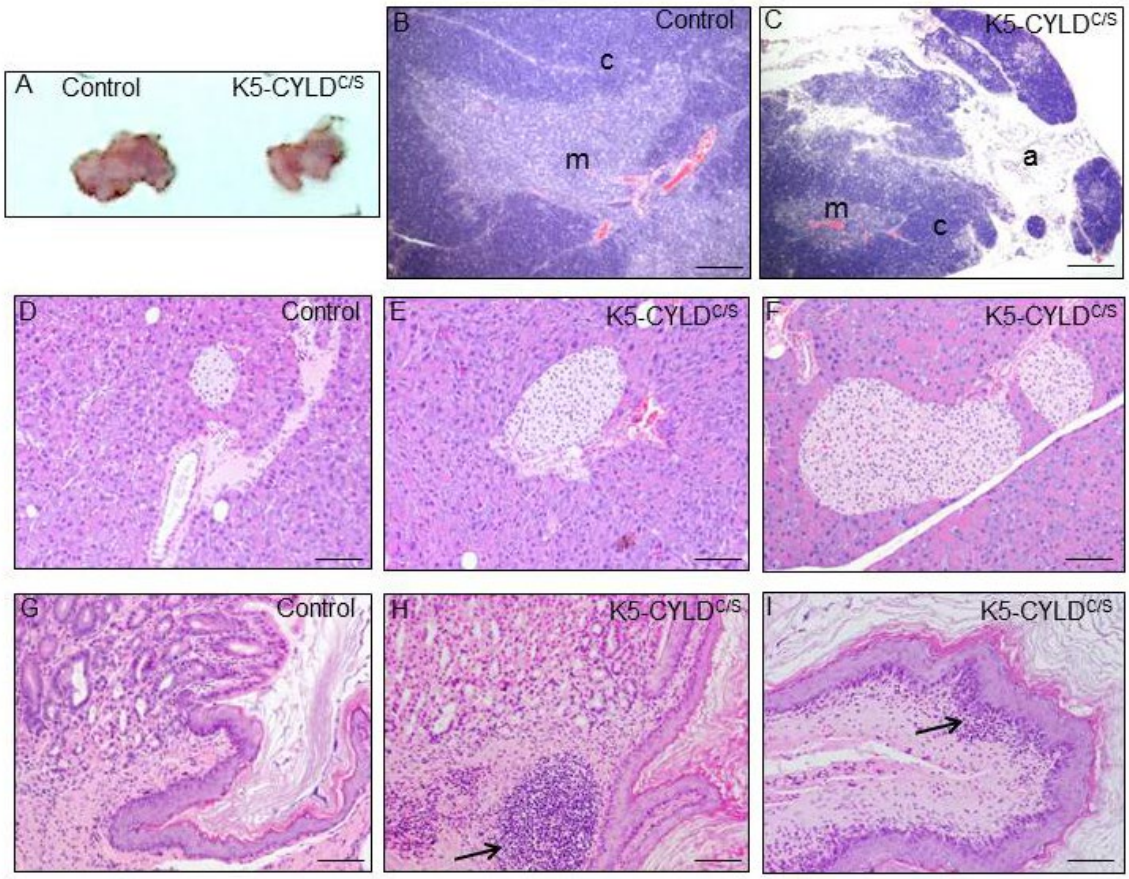

Figure S11. Signs of premature aging in the thymus, pancreas and stomach of FVB/N-K5-CYLD$^{C/S}$ mice. (**A**) Representative images showing the smaller size of the thymus of 3-month-old FVB/N-transgenic mice. (**B, C**) Thymic atrophy and infiltration of white adipose tissue (**A**) in the thymus of FVB/N-transgenic mice (**C**) compared to thymus of age-matched Control mice (b). Histopathologic analysis of pancreas (**D-F**) and stomach (**G-I**) from 18-month-old Control (**D, G**) and FVB/N-transgenic (**E, F, H, I**) mice. Note the hyperplasia of the Islets of Langerhans in the FVB/N-K5-CYLD$^{C/S}$ mice (**E, F**). (**H, I**) Representative images showing foci of inflammation in the stomach of FVB/N-transgenic mice (black arrows). Scale bars: 400 µm (**B, C**); 200 µm (**D-F**); 250 µm (**G-I**).

A

FVB/N-K5-CYLD$^{C/S}$ mice develop spontaneous tumors

FVB/N Mouse genotype	Lung ADC	Mammary ADC
Control	0/5	0/3*
K5-CYLD$^{C/S}$-X	2/5	1/3*

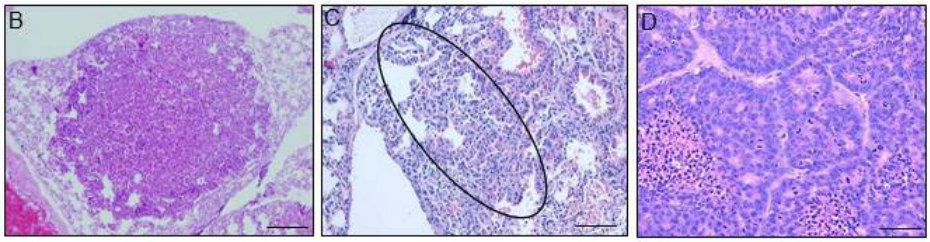

Figure S12. K5-CYLD$^{C/S}$ mice develop spontaneous tumors independently of their genetic background. Control and transgenic mice (FVB/N background) were analyzed (3 females and 2 males). (**A**) Lung and mammary adenocarcinomas were detected in aging FVB/N-K5-CYLD$^{C/S}$ mice. Number of animals that have developed each type of tumor, as well as the number of mice that have been analyzed is shown. (**B**) Image of lepidic lung adenocarcinoma developed in a FVB/-N-transgenic mouse. (**C**) Atypical adenomatous hyperplasia of lung in a FVB/N-K5-CYLD$^{C/S}$ mouse (circle). (**D**) Mammary adenocarcinoma of high grade in a female FVB/N-transgenic mouse. ADC: Adenocarcinoma; (*): female mice. Scale bars: 500 µm (**A**); 150 µm (**B, C**).

Table S1. Number of mice whose skin has been analyzed.

Genotype	Age (months)							
	1 m	3 m	5 m	8 m	12m	20 m	21-24 m	25-30 m
Control	4	6	5	4	4	7	4	8
K5-CYLD$^{C/S}$-X	4	6	5	4	5	10	3	9

The number of animals analyzed at the indicated months of age is showed.

Table S2: Number of mice whose thymus has been analyzed.

Genotype	Age (months)			
	1m	2.5 m	3m	3.5m
Control	3	3	8	3
K5-CYLD$^{C/S}$-X	3	3	8	3

The number of animals analyzed at the indicated months of age is showed.

Editorial and Publishing Office Aging
6666 E. Quaker St., Suite 1B,
Orchard Park, NY 14127
Phone: 1-800-922-0957
Fax: 1-716-508-8254
e-Fax: 1-716-608-1380

Submission
Please submit your manuscript on-line at http://aging.msubmit.net

Editorial
For editorial inquiries, please call us or email editors@impactaging.com

Production
For questions related to preparation of your article for publication, please call us or email krasnova@impactaging.com

Indexing
If you have questions about the indexing status of your paper, please email kurenova@impactaging.com

Billing/Payments
If you have questions about billing/invoicing or would like to make a payment, please call us or email payment@impactaging.com

External & Legal Affairs
If you have questions about post publication promotion, Altmetric, video interviews or social media, please email RyanJamesJessup@impactjournals.com

Printing
Each issue or paper can be printed on demand. To make a printing request, please call us or email printing@impactjournals.com

Publisher's Office
Aging is published by Impact Journals, LLC
To contact the Publisher's Office, please email: publisher@impactjournals.com, visit www.impactjournals.com, or call 1-800-922-0957

Aging (ISSN: 1945 - 4589) is published monthly by Impact Journals, LLC.
6666 East Quaker St., Suite 1B, Orchard Park, NY 14127

Abstracted and/or indexed in: PubMed/Medline (abbreviated as "Aging (Albany NY)"), PubMed Central (abbreviated as "Aging (Albany NY)"), Web of Science/Science Citation Index Expanded (abbreviated as Aging-US) & listed in the Cell Biology-SCIE and Geriatrics & Gerontology category, Scopus /Rank Q1(the highest rank) (abbreviated as Aging) - Aging and Cell Biology category, Biological Abstracts, BIOSIS Previews, EMBASE, META (Chan Zuckerberg Initiative), Dimensions (Digital Science's).